UNIVERSITÀ
DEGLI STUDI
DI PADOVA

Sede Amministrativa: Università degli Studi di Padova
Dipartimento di Istologia, Microbiologia e Biotecnologie Mediche

SCUOLA DI DOTTORATO DI RICERCA IN BIOSCIENZE
INDIRIZZO: GENETICA E BIOLOGIA MOLECOLARE DELLO SVILUPPO
CICLO: XXIII

Role of collagen VI in skeletal muscle homeostasis

Direttore della Scuola: Ch.mo Prof. Giuseppe Zanotti
Coordinatore d'indirizzo: Ch.mo Prof. Paolo Bonaldo
Supervisore: Ch.mo Prof. Paolo Bonaldo

Dottoranda: Anna Urciuolo

Abstract

Collagen VI (ColVI) is an extracellular matrix protein forming a microfilamentous network in various tissues, and composed by three chains, α1(VI), α2(VI) and α3(VI), encoded by separate genes. Mutations of ColVI genes in humans cause various muscle diseases, including Bethlem Myopathy and Ullrich Congenital Muscular Dystrophy (UCMD). Mice lacking ColVI (*Col6a1*$^{-/-}$) display a myopathic phenotype with mitochondrial dysfunction and spontaneous apoptosis of muscle fibers. Analysis of muscle biopsies and primary cultures of UCMD patients revealed a similar phenotype, which could be normalized by treatment with cyclosporin A or its non-immunosuppressive derivatives.

During the first two years of my PhD work, I focused on studies aimed at elucidating collagen VI pathomolecular defects in human disorders, characterizing three novel ColVI chains in humans and mice and understanding molecular pathways underlying the phenotype of *Col6a1*$^{-/-}$ mice.

Considering the remarkable apoptotic phenotype displayed by *Col6a1*$^{-/-}$ and UCMD myoblasts, and persuaded by the regenerative effect of cyclosporin A treatment in UCMD patients, during the second half of my PhD work I started investigating muscle regeneration and satellite cell (SC) activity in the *Col6a1*$^{-/-}$ mouse model. SCs are an adult stem cell population of skeletal muscle, representing the main player in skeletal muscle regeneration. Under physiological condition, I found that *Col6a1*$^{-/-}$ mice display an altered regenerative activity when compared to wild-type mice. In order to investigate further muscle regeneration capability of *Col6a1*$^{-/-}$ mice, I analyzed the regenerative response after muscle injury, induced either by cardiotoxin injection or by muscle training by voluntary exercise on running wheels. Light microscopy showed that after repeated cardiotoxin injury *Col6a1*$^{-/-}$ mice lose the ability to properly regenerate muscles, compared to wild type mice. Further studies, using Pax7 as a marker for SCs, revealed that in *Col6a1*$^{-/-}$ muscles SCs are able to complete muscle regeneration, but are unable to expand and maintain their pool. Interestingly, during the first stages of regeneration wild-type muscles showed a marked increase of ColVI deposition in the regenerating area, where Pax7-positive cells were found to proliferate extensively. In addition, almost all Pax7-positive cells were found in close

contact with ColVI, and some of these cells were totally surrounded by the protein. Moreover, apoptotic nuclei were found to be strongly increased in *Col6a1*$^{-/-}$ muscles during starting events of regeneration, when compared to both untreated *Col6a1*$^{-/-}$ and cardiotoxin-treated wild-type muscles. In order to perform further studies on SC activity, I set up an *in vitro* experimental system with single myofiber cultures derived from wild-type and *Col6a1*$^{-/-}$ EDL muscles. These *in vitro* studies showed that wild-type SCs doubled during myofiber culture and gave origin both to activated cells (Pax7^{+}MyoD^{+}) and cell returned to the quiescence state (Pax7^{+}MyoD^{-}). Conversely, the number of quiescent Pax7-positive cells per fiber was strongly reduced in *Col6a1*$^{-/-}$ cultures compared to both wild-type cultures and freshly isolated *Col6a1*$^{-/-}$ myofibers.

Altogether, these *in vivo* and *in vitro* studies strongly suggest a new role for ColVI in skeletal muscle regeneration and indicate that in *Col6a1*$^{-/-}$ muscles SCs have an impaired ability to expand and maintain the stem cell pool. We are currently investigating the mechanism through which ColVI signals are transduced in SCs *in vivo* and *in vitro*.

1. Introduction

1.1 Skeletal muscle and extracellular matrix.

Skeletal muscle is a tissue composed by highly specialized post-mitotic, multinucleated myofibers that contract to generate force and movement. Thousands of muscle fibers form together an individual skeletal muscle surrounded by connective tissue, called epimysium, from which processes start to form the perimysium that enwrap several myofibers; each single myofiber is further surrounded by the endomysium, composed by a basement membrane in contact with connective tissue characterized by scarce extracellular matrix (ECM), capillaries and nerve terminals (Buckingham 2001). The basement membrane is constituted by the inner basal lamina, in tight connection with the plasma membrane of cells, and the fibroreticular lamina, that bound to the connective tissue (Sanes, 2003). The basal lamina is mainly constituted by two proteins, collagen IV and laminin (Timpl, 1996), which interact each other through nidogen/entactin and perlecan. The importance of these proteins is not only due to the anchoring role between endomysium and basal lamina, but also in the interaction with a number of cell receptors, like $\alpha_7\beta_1$ integrin (Campbell and Stull, 2003). The fibroreticular lamina is characterized by the presence of a microfilament network of collagen VI, which guarantees the connection between the basal lamina and the connective tissue (Kuo et al., 1997). For long time ECM was considered only as a mechanical support to tissues, but in the last years its role in regulating growth factors availability and molecular pathways became evident. In skeletal muscle, the importance of ECM/cell contact and ECM integrity is evident in a number of animal models and human patients where the absence or defects in ECM proteins or in proteins connecting myofibers to ECM lead to muscle diseases (Sanes, 2003).

1.2 Collagen VI.

Collagen VI (ColVI) is an ECM protein forming a microfilamentous network in several organs including skeletal muscle, skin, cornea, lung, blood vessels, intervertebral disks and joints (Knee et al., 1988). It consists of three chains, α1(VI), α2(VI) and

α3(VI), encoded by distinct genes (COL6A1, COL6A2, COL6A3, respectively) (Fig. 1). The α1(VI) and α2(VI) chains are about 140 kDa, while the α3(VI) chain has several alternatively spliced variants with molecular weigh of 250–300 kDa (Bonaldo e tal., 1989; Bonaldo et al., 1990; Chu et al., 1990; Doliana et al., 1990). Each chain contains a short triple helical domain of 335–336 amino acids and two large N– and C–terminal globular ends composed of repeated domains of 200 amino acids sharing similarity with the type A module of von Willebrand factor (vWF–A) (Colombatti and Bonaldo, 1991). The larger α3(VI) chain also shows additional peculiar domains: C3 is a proline rich domain, C4 show similarity with the III module of fibronectin, and C5 is similar to the Kunitz protease inhibitor domain. It was found that C5 domain is cleaved when collagen VI is deposited in the ECM (Nanda et al., 2004), and its function remains to be clarified.

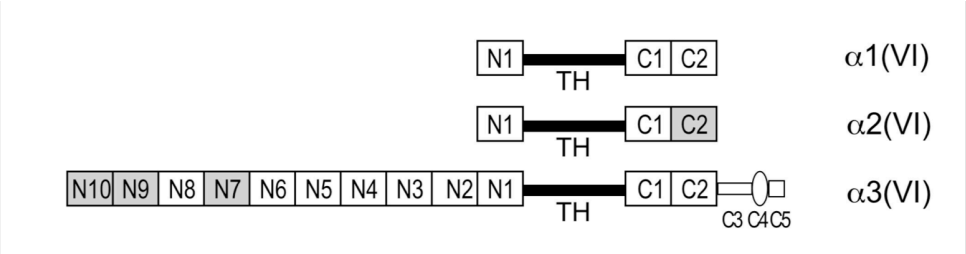

Figure 1. Structural organization of collagen VI alpha chains. In grey are indicated the regions undergoing alternative splicing. TH: triple helix.

ColVI is synthesized and secreted by cells organizing ECM such as skin and muscle fibroblasts and smooth muscle cells, and transcriptional regulation is a key step in its production (Braghetta et al., 2008). In muscle, ColVI is mainly produced by fibroblasts, and is a major component of the endomysium (Zou et al., 2008; Kuo et al., 1997). The assembly of collagen VI require the intracellular interaction of the three alpha chains to form monomers, which are further assembled into dimers and tetramers (Colombatti et al., 1987) (*see also in "Part II: other projects, Studies on patients affected by collagen VI related pathologies"*). Finally, tetramers are secreted from cells in the extracellular space, where they interact each other to form the typical network of beaded microfilaments (Fig. 2).

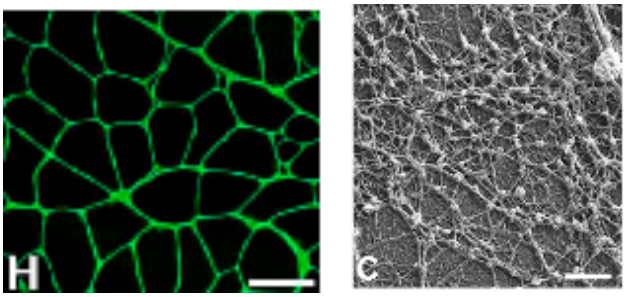

Figure 2. Collagen VI organization. On the left it is shown the localization of collagen VI (green) in human skeletal muscle cross-section. On the right, beaded microfilaments of collagen VI are visualized by rotary-shadowed electron microscopy in a primary skin fibroblast culture. *Images modified from Bovolenta et al., 2010 (reported in section II: other projects).*

ColVI has a wide range of interactions with ECM components (Bonaldo et al., 1990; Kuo et al., 1997; Sabatelli et al., 2001). In particular, the strong interaction between ColVI and collagen IV permits the formation of a physical connection between muscle cells and ECM. Moreover, ColVI have an important role in mediating the adhesion of fibroblast and other cells. ColVI is able to interact with specific cell surface receptors, including $\alpha_1\beta_1$ and $\alpha_2\beta_1$ integrins and NG2 proteoglycan (Pfaff et a., 1993; Burg et al., 1996). Some studies suggested that NG2 has a role in signal transduction, regulating cell adhesion and proliferation and modulating integrin activity (Midwood and Salter, 2001; Stallcup et al., 2002). Even if recent studies demonstrated that the absence of ColVI in skeletal muscle alters molecular signals and cell viability (Irwin et al., 2003; Grumati et al., 2010), the cell receptors responsive to ColVI and mediating its survival effects are still unknown.

1.3 Muscular dystrophies and muscle pathologies linked with collagen VI.

Muscular dystrophies are referred to a wide heterogeneous group of hereditary muscle disorders characterized by progressive muscle weakness and wasting (Durbeej and Campbell, 2002). As previously mentioned, several muscular dystrophies involve the alteration or absence of proteins located in the ECM or

involved in myofiber/ECM connection, and ColVI-related disorders represent a major group of such diseases. One of the most frequent forms of dystrophy in humans are dystrophinopathies, in which mutations occur in proteins composing the dystrophin glycoprotein complex (DGC). This large protein complex is associated with the plasma membrane and shows an important role in regulating signalling pathways and anchoring myofibers to the basal lamina, connecting the laminin-2 of the basement membrane to cytoskeletal actin (Durbeej and Campbell, 2002). Differently, mutations in *LAMA2* gene, encoding for the α chain of laminin-2, are involved in a group of congenital muscular dystrophies named MDC-1A. Laminin-2 is the main component of basal lamina, and it is involved in interaction between DGC, integrins and ECM. Even if DGC represent an anchoring structure belonging to myofibers, and laminin is present outside of cells, it is evident that the connection between myofibers and the basal lamina is of key importance for the normal behaviour of skeletal muscle. This is true also for proteins that are "more distant" from myofibers, such as ColVI. Deficiency or alteration of ColVI in humans, due to mutations in the COL6 genes, causes two main syndromes, Bethlem Myopathy (BM) and the more severe Ullrich Congenital Muscular Dystrophy (UCMD) (Lampe and Bushby, 2005). The wide spectrum of mutation associated to COL6 genes and the related pathologies revealed an important role of the protein in muscle not only on the basis of its quantity, but also depending on qualitatively alterations (*see also in "Part II: other projects, Studies on patients affected by collagen VI related pathologies"*).

1.4 Collagen VI null mouse model.

In 1998 Paolo Bonaldo's laboratory developed the *Col6a1*$^{-/-}$ mouse via targeted mutation of the second exon of *Col6a1* gene. The generated mutation causes an interruption of *Col6a1* gene, which becomes null, leading to the absence of the α1(VI) chain. Even if the other two chains composing ColVI, α2(VI) and α3(VI), are normally transcribed, the absence of α1(VI) chain does not allow the formation of ColVI monomers, thus preventing the assembly and secretion of ColVI, and therefore *Col6a1*$^{-/-}$ mice completely lack ColVI in their tissues. *Col6a1*$^{-/-}$ mice show an early onset myopathic disease, characterized by histological alterations of skeletal muscle

tissue, like necrosis, centrally nucleated fibers and variability of myofibers size (Bonaldo et al., 1998). Moreover, muscle weakness was demonstrated by strength measurements *ex vivo*, underling a significant reduction of tension developed by *Col6a1*$^{-/-}$ muscles compared to wild type (Irwin et al., 2003). Further studies carried out on ColVI null mice allowed to understand the mechanisms underlying BM and UCMD, and these mice represent an excellent model for human ColVI diseases. Ultrastructural and molecular studies performed on *Col6a1*$^{-/-}$ mice revealed novel and unexpected aspects of the pathogenetic mechanisms underlying the myophatic phenotype. By electron microscopy, alterations in mitochondria and sarcoplasmic reticulum (SR) were identified in *Col6a1*$^{-/-}$ muscles. In addition, electrondense nuclei were found in myofibers lacking ColVI, suggesting apoptotic events. Indeed, TUNEL analysis confirmed a seven-fold increase of spontaneous apoptosis in *Col6a1*$^{-/-}$ diaphragm compared to wild type. Further studies carried out on myofibers isolated from *flexor digitorum brevis* (FDB) muscle revealed, in association with apoptosis, the presence of a latent mitochondrial dysfunction, that could be unmasked by oligomycin (Irwin et al., 2003). In these studies, the mitochondrial membrane potential was monitored by fluorescence microscopy using tetramethylrhodamine methyl ester (TMRM), a fluorescent lipophilic cation that is accumulated in energized mitochondria and is released when mitochondria undergo depolarization. The addition of oligomycin, a drug inhibiting the mitochondrial F_1F_0 ATP-synthase, revealed a latent mitochondrial dysfunction in *Col6a1*$^{-/-}$ myofibers, which showed a rapid mitochondrial depolarization, at difference from wild type fibers. The reason why *Col6a1*$^{-/-}$ mitochondria are not able to maintain their membrane potential is to the increased sensibility to opening of the permeability transition pore (PTP), a large pore present in the inner membrane of mitochondria (Irwin et al., 2003). PTP opening not only leads to mitochondria depolarization, but also causes the release of cytochrome *c*, a strong inductor of apoptosis (Bernardi et al., 2001; Forte and Bernardi, 2005; Zamzami et al., 2005). Treatment of *Col6a1*$^{-/-}$ fibers with cyclosporin A (CsA), a drug able to bind mitochondrial cyclophilin D, leads to desensitization of PTP opening and rescues both mitochondrial and apoptotic phenotypes. The same phenotypes could also be rescued by growing *Col6a1*$^{-/-}$ myofibers onto a purified native ColVI substrate. Remarkably, *in vivo* administration of CsA for four days to

Col6a1$^{-/-}$ mice rescued of apoptotic-mitochondrial defects and led to a marked recovery from the myopathic phenotype (Irwin et al., 2003).

The reason why an ECM protein is able to influence in such a manner the activity of mitochondria remains still unknown. However, the scientific impact of these studies on human ColVI diseases was very important, since the cell and molecular features displayed by ColVI deficient mice are similar to those detected in BM and UCMD patients. Indeed, subsequent studies in muscle sections and primary muscle cultures derived from BM/UCMD patients showed spontaneous apoptosis and mitochondria dysfunction that could be normalized by CsA (Angelin et al., 2007). On the basis of these findings, a pilot clinical trial was performed on four UCMD patients and one BM patient by oral treatment for one month with CsA. The endpoint of this study was the evaluation of apoptotic-mitochondrial phenotype in muscles biopsies before and after CsA treatments. Interestingly, one-month CsA treatment led to a strong reduction of apoptotic-mitochondrial phenotype and increased muscle regeneration in the patients (Merlini et al., 2008a).

Recently, other studies carried out in *Col6a1*$^{-/-}$ mice throw further light on the molecular pathways involved in the myopathic disease. These studies have revealed that the AMP-dependent protein kinase (AMPK) is markedly activated in *Col6a1*$^{-/-}$ muscles, suggesting an energetic imbalance in muscles lacking ColVI. Further analysis demonstrated an impaired autophagic flux in *Col6a1*$^{-/-}$ muscles, with persistent activation of the mTOR pathway and decreased levels of Beclin1 and Bnip3, molecules playing a key role in regulating the starting events of autophagy. Although autophagy has been known since many years, it became recently clear that this process is essential for tissue homeostasis by clearing of altered/aged organelles and proteins through the lysosome system. Remarkably, an impairment of the autophagic machinery was also demonstrated in UCMD/BM patients and forced reactivation of autophagic flux in *Col6a1*$^{-/-}$ mice allowed the rescue of myopathic phenotype, indicating that defective autophagy plays a key pathogenic role in ColVI diseases (Grumati el al., 2010) (*see also in "Part II: other projects, Study of autophagy in collagen VI null mice"*).

1.5 Skeletal muscle regeneration.

Skeletal muscle has the great ability to regenerate itself, responding with a highly synchronized process to a number of physiological conditions or injured stimuli. The main players in muscle regeneration are the so-called satellite cells (SCs), a particular population of muscle cells located between the basal lamina and the plasma membrane of muscle fibers (Mauro et al., 1961). SCs are necessary for postnatal muscle growth, and are responsible for maintenance, hypertrophy and repair of adult skeletal muscle (Ono et al., 2009). On the basis on these characteristics and their ability to differentiate and self-renewing, SCs are defined as adult muscle stem cells (Zammit et al., 2006). During physiological growth and maintenance conditions, the myonuclei turnover is a rare event that involves a small number of myonuclei in skeletal muscle (Spalding et al., 2005). In this contest, SCs do not need to migrate away from their position, but they can undergo proliferation and differentiation *in situ* giving their support where new nuclei are specifically needed (Kuang et al., 2008). The context strongly changes when the muscle is subjected to an injury. Indeed, after a muscle injury muscle regeneration can be divided into two distinct phases: *i) degeneration* and *ii) regeneration*. The inital events of *degeneration* is characterized by a rapid necrosis of the injured muscle fibers, with subsequent release of cytosolic proteins, like creatine kinase, in the extracellular space, and accumulation of inflammatory cells (Karalaki et al., 2009). The first inflammatory cells that invade the injured tissue are neutrophils, than the predominant inflammatory cells are macrophages (McClung et al., 2007). After the inflammatory infiltration, macrophages not only remove cell debris, but also release factors to activate myogenic cells, thus enhancing the *regenerative* phase (Lescaudrom et al., 1999). SCs activation concerns not only cells associated with degenerated fibers, but also those present in undamaged fibers and neighboring intact muscles (Kuang et al., 2008). After the activation, myogenic cells start to proliferate and migrate to the damaged site, differentiate into myoblasts and fuse with existing damaged fibers for repair or fuse each other for new myofiber formation (Snow et al., 1977). Only when fusion is completed, myofibers start to increase their size and myonuclei, located in the centre of the fiber, begin to move to the periphery (Karalaki et al., 2009). In humans migration of myonuclei to cell periphery is a relatively fast process, but in

mouse centrally myonuclei are maintained for months. Despite the phases of muscle repair are similar following different types of injury, the amplitude and kinetics of each phase may depend on the type and extent of damage. One of the commonly used experimental models for injury is muscle injection of cardiotoxin, a snake venom that induces myofiber degeneration but preserves basal lamina, thus sparing SCs, vessels and nerves. In this way, basal lamina and SCs act as the scaffold on which muscle regeneration can occur (Kuang el al., 2008).

1.5.1 Adult skeletal muscle stem cells.

Even if SCs are considered the main players in skeletal muscle regeneration, *in vitro* and transplantation experiments have been shown that other progenitor cells located outside the basal lamina, such as pericytes, endothelial and interstitial cells, display a myogenic potential (Tedesco et al., 2010) (Fig. 3).

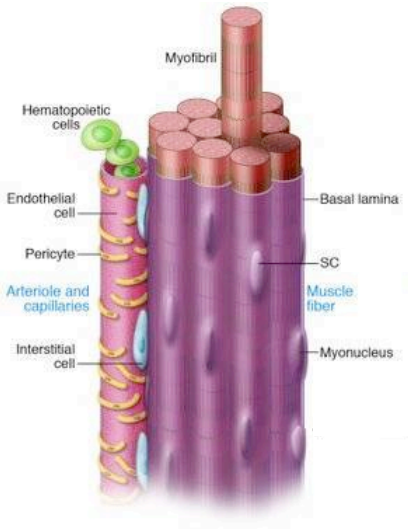

Figure 3. Representation of a muscle fiber and adjacent small vessel, SCs and other myogenic precursors. *Image modified by Tedesco et al., 2010*.

A number of not yet fully characterized subpopulations of hematopoietic stem cells seem to display myogenic potential, even if with low capability. The $CD45^+$ and $CD133^+$ fraction populations of bone morrow have been found to contribute to muscle repair when transplanted in animal models or in DMD patients (McKinney-Freeman et al., 2002; Gussoni et al., 2002; Corbel et al., 2003; Camargo et al., 2003; Torrente et al., 2004; Benchaouir et al., 2007). Other mesoderm-derived cells were shown to exhibit myogenic potential *in vitro*, after genetic modification, drug

treatments or co-culture with SCs or myoblasts, and in some cases this potential was also observed *in vivo*. Mesenchymal stem cells (Gang et al., 2009), multipotent adult progenitor cells, muscle-derived stem cells, mesoangioblasts (Sampaolesi et al., 2003), endothelial progenitors cells and adipose-derived stem cells (Meliga et al., 2007) are all included in this class of myogenic cells (Tedesco et al., 2010). Even if all these adult stem cells are able to differentiate in skeletal muscle cells, it seems that this potential is very low compared to that displayed by SCs.

1.6 Satellite cells.

SCs are determined during the embryonic development of skeletal muscle, when the somites, spheres of paraxial mesoderm, start to generate skeletal muscle (Shi et al., 2006; Sambasivan et al., 2007). However, the exact progenitor from which SCs derive remains to be identified. SCs exist in the mammalian skeletal muscles as a quiescent cell population and represent from 2.5 to 6% of all myonuclei of a skeletal muscle, although their percentage is different and characteristic for each muscle (Tedesco et al., 2010). SCs are unmistakably identified by their anatomic location between the basal lamina and the plasma membrane of myofibers (Mauro et al., 1961). In the last years, a number of characteristic (but not unique) markers for SCs were characterized. The combination of multiple markers is a useful tool to identify SCs in either quiescent, activated or differentiated state (Tab. 1). The most widely used marker is the transcriptional factor paired box 7 (Pax7) (Zammit et al., 2006), which is essential for SC specification and survival (Kuang et al., 2006). Conversely, the SC expression of another paired box, Pax3, is limited to few skeletal muscles, like diaphragm (Relaix et al., 2006).

After muscle injury, SCs becomes activated and start to proliferate. A number of signals, triggered by damaged fibers and inflammatory cells, are necessary to induce SCs activation. These signals include HGF (Tatsumi et al., 1998), FGF (Floss et al., 1997), IGF (Musarò, 2005) and NO (Wozniak et al., 2007). After activation, SCs start to proliferate, differentiate and fuse with either damaged myofibers or each other to form new fibers. In mouse, these events end after 7 days from an acute injury (Zammit et al., 2002). SCs differentiation fate is mainly triggered and controlled by *myogenic regulatory factor 5* (Myf5) and *myogenic regulatory factor 1* (MyoD)

(Tajbakhsh et al., 1996). Indeed, SC fates are determined by MyoD expression: those few cells that are $Pax7^{+}MyoD^{-}$ return to quiescence, thus maintaining the progenitor pool; differently, SC cells expressing both Pax7 and MyoD ($Pax7^{+}MyoD^{+}$) are committed to differentiation (Zammit et al., 2004). To increase the complexity of this regulatory process, experimental data suggest that some $Pax7^{+}MyoD^{+}$ cells can lose MyoD expression and revert back to a SC-like $Pax7^{+}MyoD^{-}$ state (Crosgrove et al., 2009).

Table 1
SC markers

Marker	SC expression	Localization	Function	Prospective isolation[A]	Expression in other tissues/cells	Ref
Pax7	100% of quiescent and activated SCs	Nucleus	Transcription factor	Pax7-GFP	Absent	14
Pax3	Quiescent SCs (only in a subset of muscles)	Nucleus	Transcription factor	Pax3-GFP	Melanocyte stem cells	16
Myf5	Most quiescent SCs and all proliferating SCs and myoblasts	Nucleus	Transcription factor	Myf5-nLacZ	Absent	17
Syndecan-3 and -4	98% of quiescent and activated SCs	Membrane	Transmembrane heparan sulfate proteoglycan	Cell sorting	Brain, dermis, BM, bone, smooth muscle, tumors	18
VCAM-1	Quiescent and activated SCs	Membrane	Adhesion molecule	Cell sorting	Activated endothelial cells	19
c-met	Quiescent and activated SCs	Membrane	HGF receptor	Not used	Many tissues and tumors	20
Foxk1	Quiescent and activated SCs	Nucleus	Nuclear factor	Not used	Neurons	21
Cd34	Quiescent and activated SCs	Membrane	Membrane protein	Cell sorting	Hematopoietic, endothelial, mast, and dendritic cells	13
M-cadherin	Quiescent and activated SCs; myoblasts	Membrane	Adhesion protein	Not used	Absent	22
Caveolin-1	Quiescent and activated SCs; myoblasts	Membrane	Membrane protein	Not used	Endothelial fibrous and adipose tissue	23
α_7 Integrin	Quiescent and activated SCs; myoblasts	Membrane	Adhesion protein	Cell sorting	Vessel-associated cells	24
β_1 Integrin	Quiescent and activated SCs	Membrane	Adhesion protein	Cell sorting	Many tissues	25
Cd56	Quiescent and activated SCs; myoblasts	Membrane	Homophilic binding glycoprotein	Cell sorting	Glia, neurons, and natural killer cells	26
SM/C2.6[B]	Quiescent and activated SCs; myoblasts	Unknown	Unknown	Cell sorting	Unknown	27
Cxcr4	Subset of quiescent SCs	Membrane	SDF1 receptor	Cell sorting	HSCs, vascular endothelial cells, and neuronal cells	28
Nestin	Around 98% of quiescent SCs and myoblasts	Intermediate filament	Intermediate filament protein	Nestin GFP	Neuronal precursor cells	29

[A]Prospective isolation: direct isolation of cells from tissue, usually based upon cytofluorimetric sorting with antibodies directed against cell surface markers.
[B]Novel monoclonal antibody directed against an unknown antigen present on SCs. Foxk1, forkhead box k1.

Table 1. SC markers and their use *(from Tedesco et al., 2010)*.

Generally, the choice of a stem cell to undergo self-renewal is carried out through either *asymmetric* or *symmetric* cell divisions (Cosgrove et al., 2009). These two mechanisms of cell division fulfil two different requests of stem cells in the tissue: *i) asymmetric* self-renewal, in which each stem cell divides into one stem cell and one differentiated cell, allows to maintain a constant number of stem cells, sufficient under physiological conditions; *ii) symmetric* self-renewal, in which each stem cell gives two daughter stem cell, permit to have an expansion of the stem cell pool,

needed after an injury or disease (Morrison and Kimble, 2006). The mechanisms by which SCs undergo self-renewal started to be elucidated in recent years. Several data suggest that both asymmetric and symmetric division are involved in SC self-renewal (Fig. 4).

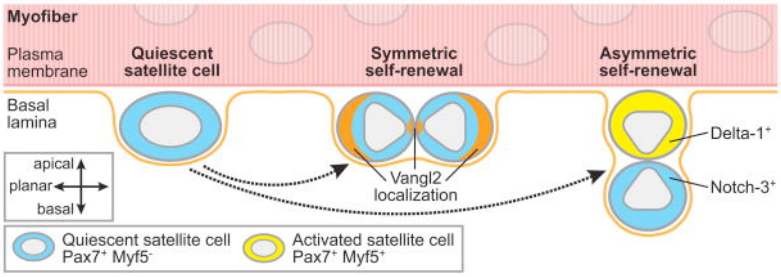

Figure 4. Model of SC self renewal *(from Crosgrove et al., 2009)*.

The so called "immortal DNA strand" hypothesis have demonstrated an asymmetrical cosegregation of older (immortal) and younger DNA strands in daughter cells during SC division, suggesting an asymmetric cell division of SCs. More in detail, it was observed that the older strand is cosegregated in the self-renewing daughter cell, while the younger template is cosegregated in the differentiating daughter cells (Shinin et al., 2006; Conboy et al., 2007). Another evidence of SCsasymmetric division was suggested by the analysis of the cytosolic protein Numb, a repressor of Notch signalling (Conboy and Rando, 2002; Shinin et al., 2006). Notch signals play an important role during muscle regeneration, regulating SC activation and inhibiting myogenic differentiation (Brack et al., 2008; Conboy and Rando, 2002; Conboy et al., 2003). Thus, asymmetric retention of Numb can suggest a different fate of the daughter cells, with cells that retain Numb more differentiated than those that lose Numb. Although it was observed a Numb-mediated asymmetric segregation during SC division and muscle progenitor cell development (Conboy and Rando, 2002), it was also found that high level of Numb are expressed by those daughter cells that retain the old immortal DNA strand, and therefore are stem cells and not differentiated cells (Shinin et al., 2006). These contrasting studies suggest a more complex mechanism underlying SC self-renewal division than the initially proposed model. In addition, other studies have reported that Myf5, a potential target of Notch signalling (Delfini et al., 2000; Kopan at al., 1994), could play a role in SC self-renewal. In mouse only 10% of Pax7-positive SCs never express Myf5 and these cells remain

under the basal lamina during asymmetric division, each generating one $Pax7^{+}Myf5^{-}$ "stem cell", that maintains the contact with the basal lamina, and one $Pax7^{+}Myf5^{+}$ daughter cell that loses the contact with the basal lamina and contact the myofiber plasma membrane (Kuang et al., 2007). This study suggests that the choice between asymmetric and symmetric self-renewal divisions is dictated by the mitotic spindle orientation of SCs. In the asymmetric division, it was observed that the Notch ligand Delta-1 is asymmetrically expressed by the apical and basal daughter cells, with higher expression in apical committed $Pax7^{+}Myf5^{+}$cells, while the basal less differentiated $Pax7^{+}Myf5^{-}$ SCs show increase level of receptor Notch-3. In this scenario the role of Notch signalling seems to be crucial in determining the differentiation state of the two interacting daughter cells. Conversely, symmetric cell division is associated to the formation of two identical daughter cells, both differentiated or both undifferentiated, that are in planar alignment with the myofiber plasma membrane and basal lamina (Kuang et al., 2007). In addition, recent findings demonstrated that the niche factor Wnt7a play an important role in the symmetric self-renewal regulation, controlling planar tissue morphogenesis (Le Grand et al., 2009). To make these events even more complex, some studies demonstrated the possibility of committed cells to go back into a stem cell state (Zammit et al., 2004). Emerging evidence suggests that in skeletal muscle the described models of SC self-renewal are controlled by specific molecular components of the SC niche (Crosgrove et al., 2010).

1.6.1 Niche and extracellular signals regulating satellite cell function.

It is well known that the ability of a stem cell to maintain its properties is strongly determined by the so-called *niche*. Stem cell niche is defined as the local microenvironment that sustains stem cells identity and regulates their function, directing a slow cell division during homeostasis, and assuring the activation and the maintenance of stem cell pool after an injury (Cosgrove et al., 2009; Kuang et al., 2008). Although the exact activity of niche needs to be established for most stem cells, its importance was demonstrated in several stem cells, such as hematopoietic, intestinal crypt, hair follicle and neural stem cells (Fuchs et al., 2004; Moore et al., 2006; Scadden et al., 2006). In skeletal muscle, SC niche, consisting in the surrounding microenvironment, is characterized by asymmetric distribution of its components: *i)*

myofibers that contact SCs through the apical surface, and *ii)* ECM components that lie on their basal surface (Fig. 6).

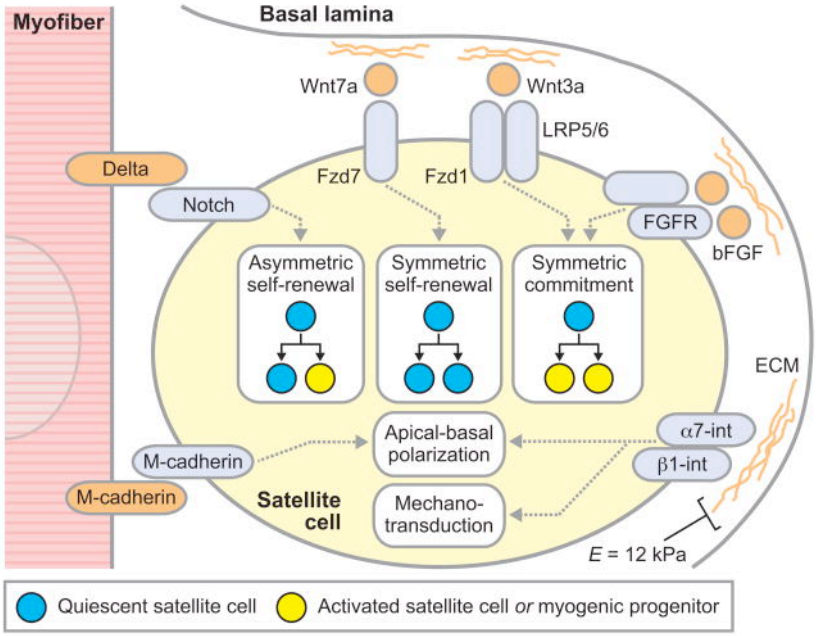

Figure 4. Niche and regulators of SC activity and fate *(from Crosgrove et al., 2009)*.

In this way SCs are subject to a "bipolar signal" system, receiving myofiber signals on their apical surface and ECM signals on their basal surface. In other tissues, asymmetric signals were found to be essential for stem cell polarity and asymmetric self-renewal (Fuchs et al., 2004; Kuang et al., 2008). The myofiber basal membrane is composed by several proteins and proteoglycan able to interact directly or indirectly with SC surface receptors. The scenario is further complicated when considering the role of ECM components in growth factors distribution and function, either sequestering them in an inactive form or presenting them in active signalling state. Indeed, ECM proteoglycans are able to bind a number of growth factors derived from systemic, SCs, interstitial cells, or myofibers sources, including basic fibroblast growth factor (bFGF), hepatocyte growth factor (HGF), epidermal growth factor (EGF), insulin-like growth factor-1 (IGF-1), and the large Wnt family of glycoprotein ligands (Brack et al., 2008; DiMario et al., 1989; Golding et al., 2007; Le Grand et al., 2009; Machida and Booth, 2004; Tatsumi et al., 1998). All these factors can modify the activity, survival and proliferation of SCs (Cornelison et al., 2001; Jenniskens et al., 2006; Langsdorf et al., 2007; Tatsumi et al., 1998). On the other side, myofibers exert

similar effects, secreting a number of factors that influence SC activity. SC migrating response is mediated by myofiber-secreted SDF-1, which in turn is able to bind CXCR4 receptors present on SC surface (Ratajczak et al., 2003; Sherwood et al., 2004). Moreover, M-cadherin expressed on myofibers membrane modulates their interaction with SCs and seems to be important in SC fusion (Irintchev et al., 1994). In addition, SCs display ligands able to regulate their own fate through autocrine and juxtacrine signals, including Notch ligands (Conboy and Rando, 2002; Conboy et al., 2003; Kuang et al., 2007). Recent studied suggested a fundamental role of mechanotransduction in SC differentiation and survival (Gilbert et al., 2010). Indeed, ECM microenvironment can strongly affect proliferation, differentiation, and morphogenesis of a number of different cell types, including muscle cells, through its mechanical properties called the elastic modulus (E) (Guilak et al., 2009; Lopez et al., 2008). Healthy muscle tissue present a particular E value ($E \approx 12$ kPa), that is altered during aging, disease and injury, as revealed in dystrophyn-deficient *mdx* mouse model of Duchenne muscular dystrophy (Engler et al., 2004) and in aged mice (Gao et al., 2008). These studies strongly suggest an important role of biophysical stimuli on SC function.

1.6.2 Satellite cell function and muscular dystrophies.

The involvement of SCs in muscular dystrophies was not an obvious evidence, and only in the recent years studies of human dystrophies and/or mouse models have investigated the correlation between muscle disorders and SC activity. It have been reported that a number of muscle dystrophies not only result in myofiber wasting, but also involve SCs, as pathogenic mutations can directly or indirectly influence the activity of SCs (Morgan and Zammit, 2010). Mutations of dystrophin, one component of DGC, cause Duchenne muscular dystrophy (DMD) and Becker muscular dystrophy (BMD) in humans. Even if dystrophin is only expressed in myofibers and not in SCs, the myofiber wasting due to mutations in this protein indirectly involves also SC activity. Indeed, the compensation response of SCs to muscle wasting is characterized by their continue activation and proliferation associated to repeated cycles of muscle degeneration and regeneration, which at the end lead to ineffective regenerative capabilities in DMD patients. The *mdx* murine model of this pathology also displays cycling events of degeneration and repair, but the inability of SCs to regenerate

muscle is not lost, and with age the dystrophic phenotype is milder than in humans (Morgan and Zammit, 2010). This apparently contrasting feature observed between humans and mice seems to be due to the higher ability of murine SCs to maintain telomeres of proper length during division (Sacco et al., 2010). Differently from DMD, were the mutated protein is expressed only by myofibers, in CMD due to mutations of laminin-2 the pathogenic effects are linked to both myofibers and SCs, since the protein is expressed by both cells. A dystrophic phenotype is present in laminin-2 null mice, which do not compete muscle regeneration in response to injury, with excessive death of cells associated with immature fibers observed during the abortive regenerative response (Kuang et al., 1999). Other types of muscular dystrophies seem to be associated to alteration in SC activity, and more in detail in the perturbation of their ability to activate from quiescence, proliferate to expand the myoblast pool, efficiently differentiate, fuse into existing myofibers or fuse together to produce new myotubes, thus maintaining the stem cell pool by self-renewal (Morgan and Zammit, 2010).

2. Methods

2.1 Mice.

Six and two month, and two week old wild type C57BL/6 and *Col6a1*$^{-/-}$ (Bonaldo et al., 1998) mice were used to perform the studies described in this thesis. Animals were sacrificed by cervical dislocation and all analysis were made comparing almost three wild type and *Col6a1*$^{-/-}$ mice at the same age and sex.

2.2 Muscle injury by cardiotoxin injection.

Wild type and *Col6a1*$^{-/-}$ mice were subject to anesthesia using isofluorane (Merial) and treated with 10 μl subcutaneous injection of anti paining Rymadil (Carprofen, Pfizer). Each TA muscles were injected with 30 μl of cardiotoxin (Naja mossambica mossambica, 10 μM; Sigma). After the needed time, mice were sacrificed by cervical dislocation and TA and EDL muscles were isolated; TA muscles were freezing in liquid nitrogen, and EDL was previously dispose in cryomolds (Tissue tek II) and covered by OCT tissue tek (Sakura) before freezing. For multiple injuries, TA muscles were injected with cardiotoxin one month after the previous injection.

2.3 Mice training.

Two months old wild type and *Col6a1*$^{-/-}$ mice were subject to muscle training by voluntary exercise on running wheels. After one month, exercise was continually monitored for next two months (analysis kindly provided by Dr Alvise Schiavinato). TA and diaphragm muscles were isolated and frozen in liquid nitrogen before starting with next analysis.

2.4 Histological analysis.

TA and EDL muscles were used to obtain cryo-cross sections of 7 μm. Hematoxylin-eosin staining was performed immersing slides in Meyer hematoxylin (Sigma) for 3.5 minutes, which color in blue negative-charged basic cellular components, like nuclei. Next step was the incubation of slides in water for 3.5 minutes, and then stained with 2% eosin-distilled water solution (Sigma) for 3 minutes. Eosin permits the staining of cell structure displaying positive-charged acid characteristics, as cytoplasm, in various shades of red, pink and orange. To dehydrate muscle sections, slides were

subject to sequential immersion in alcoholic solutions: 30 seconds in 50% ethanol-water; 30 seconds in 70% ethanol-water; 30 seconds in 100% ethanol; 10 minutes in 100% ethanol. Before covering slides, sections were treated 3 minutes with 100% xylene solution.

Tricromic Azan staining was performed on cryosections of muscles starting with azocarmine coloration at 56 °C for 30 minutes. After cooling, slides were incubated for 5 minutes with aniline oil at 90 °C, and put in a mordant solution for 1 hour. Next, slides were stained with Mallory solution (aniline blue and orange G mix) for 2 hours at room temperature, dehydrated in crescent alcoholic solutions, washed in xylene for 3 minutes, and covered before analysis. Nuclei, erythrocytes, fibrin, fibrinoid, acidophilic cytoplasm, epithelial hyalin, and so on are stained "red" with azocarmine. Collagen fibers, basophilic cytoplasm, mucus, and so on are counterstained blue with Mollory solution.

Images were acquired by optical microscope (Leica DC500 ZEISS Axioplann); cross sectional area of myofibers (more then 1000 per each experiment) were valued using IM2000 program.

2.5 Single fiber isolation from EDL muscle.

EDL muscles were isolated from wild type and *Col6a1*$^{-/-}$ mice and subject to enzymatic digestion by collagenase I (Gibco) for 80 minutes at 37 °C. Enzymatic digestion was blocked with Dulbecco's Modified Eagle Medium (DMEM, Sigma) added with L-glutamine (0.2 M, Invitrogen), penicillin-streptomicyn (1:100, Invitrogen), fungizone (1:100, Invitrogene), and horse serum (10%, Gibco). Single fibers were genteelly released from the muscle in a petri and, to eliminate other not muscles cells and tissues, were passed for five time in new petri containing fresh media, and maintained at 37 °C in cell incubator almost 15 minutes between each wash cycle. Single fibers not damaged were selected and one part was fixed in 20% PFA-PBS solution and others fibers used to culture.

2.6 Single fiber culture.

Chamber slides (Thermo Scientific) were coated with ECM gel (1:20, Sigma) and used to perform single fiber culture; each well was used for a single fiber culture. Fibers

were grown in Dulbecco's Modified Eagle Medium (DMEM, Sigma) added with L-glutamine (0.2 M, Invitrogen), penicillin-streptomicyn (1:100, Invitrogen), fungizone (1:100, Invitrogene), horse serum (10%, Gibco), fetal bovine serum (20%, Gibco), and chick embryo extract (1%, DBA Italia). This growing media permit the survival of myofibers and SCs division. After 48 hours of culture, single fibers were fixed in 20% PFA-PBS solution before starting with immunofluorescence analysis.

2.7 Fluorescence microscopy.

Analysis performed at fluorescent microscopy had permit the identification and characterization of proteins, cellular markers and apoptotic nuclei in muscle and fibers samples. In this studies were used either epyfluorescence microscope (Leica DC500 ZEISS Axioplann) or confocal microscope (Leica SP5).

Immunofluorescence on muscle sections. Cryosections of TA and EDL muscles were fixed 20 minutes with 20% PFA at room temperature and washed three times in phosphate buffered saline (PBS) buffer. Permeabilization of tissue was performed using cold 100% methanol for 6 minutes at -20 °C, then slides were dry and washed two times in PBS. To unmask nuclear antigens, slides were incubated two times in citric acid (0.1 M, pH 6) for 5 minutes at 70 °C. After washing slides in PBS, samples were incubated with 4% BSA IgG-Free (BBBSA, Jackson) in PBS solution for 2 hours, washed in PBS buffer and treated with for 30 minutes a blocking solution containing the Fab fragment anti-mouse IgG (0,05 mg/ml, Jackson). Slides were washed one time in PBS buffer and three times in 0,1% BSA IgG-Free (Jackson) in PBS (BSA-PBS) solution, and incubated at 4°C over night with primary antibodies diluted in BBBSA solution. The antibody used were mouse anti-Pax7 (1:25; Developmental Studies Hybridoma Bank); rabbit anti-collagene VI (1:100070-XR95, Fitzgerald); rat anti-laminina, (1:250; 4H82, Enzo); rat anti-MOMA2 (1:500; SM065P, Acris). Next step was washing slides three times in BSA-PBS solution before incubation for 45 minutes with secondary antibodies at room temperature. For Pax-7 staining anti-mouse biotynilated (1:1000; 115-007-003, Jackson Immunoresearch) antibody was used, while antibodies anti-mouse CY2 (1:200; 115-226-062, Jackson Immunoresearch) anti-rabbit IRIS5 (1:300; 5WS-08, Cyanine Technologies), anti-rabbit CY2 (1:200; 111-225-144, Jackson Immunoresearch) and anti-rat CY3 (1:300; 112-165-167,

Jackson Immunoresearch) were directed against the others primary antibodies. After washing slides in BSA-PBS solution, when needed samples were incubated for 30 minutes at room temperature with the streptavidin CY5 or CY3 (1:2500; 016-160-084, Jackson Immunoresearch) in BBBSA to reveal Pax-7, and followed by washing passages. All samples are next incubated for three minutes with Hoechst 33258 (1:100; Sigma) for nuclei staining. After washing, slides were covered and ready to analyse at fluorescence microscope.

Immunofluorescence on single myofibers. Single fibers were washed in PBS, permeabilized with 5% Triton-PBS solution for 10 minutes at room temperature, and incubated with the blocking solution of 20% goat serum in PBS for one hour. Primary antibodies were diluted in 1% goat serum in PBS solution and incubated for 2 hours at room temperature or over night at 4° C. For the analysis were used the following antibodies: mouse anti-Pax7 (1:25; Developmental Studies Hybridoma Bank); rabbit anti-collagene VI (1:1000; 70-XR95, Fitzgerald); rat anti-laminina (1:250; 4H82, Enzo), and rabbit anti-MyoD (1:20; Developmental Studies Hybridoma Bank). After three washing step in 1% goat serum in PBS solution, single fibers were incubated one hour with the secondary antibodies diluted in 1% goat serum in PBS solution: anti-mouse CY2 (1:200; 115-226-062, Jackson Immunoresearch) anti-rabbit IRIS5 (1:300; 5WS-08, Cyanine Technologies), anti-rabbit CY2 (1:200; 111-225-144, Jackson Immunoresearch). Single fibers were after washed in 1% goat serum in PBS solution for three times on slides and covered before starting with the analysis at fluorescence microscope.

TUNEL analysis. TUNEL assays were performed with the Dead End Fluorometric in situ apoptosis detection system (Promega). The system measures the fragmented DNA of apoptotic cells by catalytically incorporating fluorescein-12-dUTP at 3´-OH DNA ends using the Terminal Deoxynucleotidyl Transferase, Recombinant, enzyme (rTdT). rTdT forms a polymeric tail using the principle of the TUNEL (TdT-mediated dUTP Nick-End Labeling) assay. The fluorescein-12-dUTP labelled DNA can then be visualized directly by fluorescence microscopy. Muscles cryosections were permeabilized in methanol-acetone 50:50 at -20 °C for 10 minutes. After dried, slides were washed in PBS and treated 5 minutes with proteinase K at room temperature, then washed and incubated with equilibration buffer for 10 minutes. Samples were

further incubated with buffer containing fluorescent nucleotides, rTdT enzyme and hoechst for 1 hour at 37 °C. SSC solution was used to block the activity of rTdT enzyme, before washing and preparing slides for microscopy analysis.

2.8 Statistical analysis.

Data were expressed as means ± s.e.m. Statistical significance was determined by unequal variance Student's t test. A P value of less than 0.05 was considered statistically significant.

3. Results

3.1 *Col6a1*$^{-/-}$ muscles display phenotypic features suggesting abnormal regeneration.

To assess the relative positions of ColVI and SCs in muscle, I first performed immunofluorescence analysis on cross-sections of tibialis anterior (TA) muscle from wild-type mice (Fig. 1A). Under physiological conditions, collagen VI seems to cover SCs (Fig. 1A, *a* and *b*), which are under the basal lamina (Fig. 1A, *c* and *d*). To investigate whether lack of ColVI affects muscle regenerative response, I carried out histological studies on tibialis anterior (TA) and extensor digitorum longus (EDL) muscles of 6-month-old wild type and *Col6a1*$^{-/-}$ mice maintained in standard physiological conditions. Hematoxylin/eosin staining (Fig. 1B, *a*, *b*, *e* and *f*) was used to assess muscle features such as myofiber cross-sectional area (CSA) and centrally nucleated fibers, while Azan staining (Fig. 1B, *c* and *d*) allowed evaluate the amount of fibrillar collagens in the ECM surrounding myofibers. *Col6a1*$^{-/-}$ TA and EDL muscles displayed an increased number of centrally nucleated myofibers, a well-established marker of muscle regeneration (Fig. 1C, *a* and *b*). Immunofluorescence showed that both muscles of *Col6a1*$^{-/-}$ mice had significantly more cells expressing Pax7, a marker for SCs, when compared to the corresponding wild-type muscles (Fig. 1C, *c* and *d*). Despite the increased incidence of SCs and of centrally nucleated myofibers, the mean myofiber CSA was lower in both TA and EDL muscles of *Col6a1*$^{-/-}$ mice, suggesting an alteration of the muscle regenerative response (Fig. 1C, *e* and *f*). To assess whether the muscle alterations observed in adult *Col6a1*$^{-/-}$ mice were also present in youngest animals, hematoxylin-eosin and Pax7 staining were performed on two-week-old mice (Fig. 2A). No significant difference in centrally nucleated myofibers and Pax7-positive cells was observed between two-week-old wild-type and KO mice *Col6a1*$^{-/-}$ (Fig. 2B).

3.2 *Col6a1*$^{-/-}$ mice have an altered regenerative response to muscle injury.

In order to investigate further whether lack of ColVI affects muscle regeneration, I experimentally induced muscle injury in mice, a widely used tool for unmasking regenerative defects (Garry et al., 2000; Tedesco et al., 2010). Towards this aim, wild

type and *Col6a1*$^{-/-}$ TA and EDL muscles were injected with a solution containing cardiotoxin, mice were sacrificed at different times after injury and muscles processed for histology (Fig. 3). Two time points (7 and 30 days) were chosen to check two different phases of muscle regeneration. Indeed, at seven days post-injury, the acute phase of degeneration and inflammatory recruitment is declining and newly forming fibers can be detected. Differently, at one month post-injury the muscle structure is reestablished and SC activity becomes similar to that observed under physiological conditions (Shea et al., 2010). Both TA and EDL muscles showed a slight delay in muscle regeneration at 7 days from cardiotoxin injection in *Col6a1*$^{-/-}$ mice, when compared to the corresponding wild-type samples. Indeed, in *Col6a1*$^{-/-}$ muscles the newly forming fibers were less defined, inflammatory infiltration was more evident and some myofibers were still in degenerative phase (Fig. 3A, *a* and *c*; Fig. 3D, *a* and *c*). Nonetheless, at 30 days post-injury wild type and *Col6a1*$^{-/-}$ muscles became indistinguishable (Fig. 3A, *b* and *d*; Fig. 3D, *b* and *d*). Repeated muscle injury is a well-known tool used to analyze SC self-renewal (Castets et al., 2010). In order to evaluate the self-renewal capability of *Col6a1*$^{-/-}$ SCs, I performed multiple injuries in TA and EDL muscles. One month after the first injury, muscles were subjected to a second injury by cardiotoxin injection and animals were sacrificed at 7 and 30 days from second injury (Fig. 3B and E). Defective muscle regeneration was more evident in *Col6a1*$^{-/-}$ TA and EDL after 7 days from second injury, compared to what displayed by muscle subjected to single injury (Fig. 3B, *a* and *b*; Fig. 3E, *a* and *b*). Despite of this, at one month after second injury *Col6a1*$^{-/-}$ and wild-type muscles showed similar abilities to recover tissue structure (Fig. 3B, *b* and *d*; Fig. 3E, *b* and *d*). I next performed a third injury with cardiotoxin, one month after the second one, in order to push further the muscle regenerative activity (Fig. 3C and F). While wild-type muscles were able to regenerate properly after triple injury, muscle regeneration was strongly decreased in *Col6a1*$^{-/-}$ mice at both 7 and 30 days from the third injury. This was particularly marked in *Col6a1*$^{-/-}$ TA, where muscle tissue was in a large part substituted by fibrous connective tissue (Fig. 3C, *c* and *f*).

The reduced regenerative capability of *Col6a1*$^{-/-}$ muscles was confirmed by analysis of muscle mass before and after cardiotoxin injection (Fig. 4). Indeed, the effect of altered regeneration observed after triple injury was macroscopically evident, with much thinner post-injury muscles in *Col6a1*$^{-/-}$ mice than in wild-type animals (Fig.

4A). These findings were quantified by measurement of TA weight in either non-injured conditions, at 30 days from single, double and triple injury, and at 60 days from double and triple injury (Fig. 4B). In order to allow for a full restoration of the initial tissue conditions, I waited until 60 days from cardiotoxin injection before starting the analysis. Under physiological conditions, the normalized weights of TA from wild-type and *Col6a1*$^{-/-}$ mice were similar. Conversely, normalized TA weights after 30 days from either single or triple injury were significantly lower in *Col6a1*$^{-/-}$ mice compared to wild-type animals. A significantly lower normalized weight was also present after 60 days from cardiotoxin injection in double and triple injured *Col6a1*$^{-/-}$ muscles, when compared to the corresponding wild-type samples (Fig. 4B).

To investigate whether the regenerative defects observed in *Col6a1*$^{-/-}$ mice could involve the early phases of muscle regeneration, I analyzed TA muscles at 4 days from single injury (Fig. 5). Immunofluorescence analysis of wild-type TA muscles showed a strong increase of collagen VI deposition in the endomysial ECM during the early phases of muscle regeneration. In addition, almost all Pax7-positive cells were surrounded by or in contact with ColVI (Fig. 5A, *a* and *b*). Immunofluorescence for MOMA2, a marker for activated monocytes and macrophages, did not show any obvious difference in the recruitment of inflammatory cells between wild type and *Col6a1*$^{-/-}$ muscles at 4 days post-injury (Fig. 5B). TUNEL analysis in regenerating muscles showed a strong increase of apoptotic nuclei in *Col6a1*$^{-/-}$ TA, when compared to both untreated *Col6a1*$^{-/-}$ TA and cardiotoxin-treated wild-type TA (Fig. 5C).

Given the crucial and well-known role of SCs in muscle regeneration, I investigated the incidence of Pax7-positive cells in injured muscles of *Col6a1*$^{-/-}$ and wild-type animals. Pax7 immunofluorescence was performed on regenerated TA muscles after 30 days from single, double and triple injury for the evaluation of SC ratio. At difference from wild-type muscles, where the incidence of Pax7-positive cells was markedly increased at 30 days after single and double injury, *Col6a1*$^{-/-}$ muscles did not show any increase of Pax7-positive cells (Fig. 6A). The incidence of Pax7-positive cells changed in wild-type muscles at 30 days from triple injury, returning to the levels observed under physiological conditions. Conversely, the incidence of SCs was decreased in triple injured *Col6a1*$^{-/-}$ muscle, when compared to either the corresponding wild-type samples and all the other *Col6a1*$^{-/-}$ conditions (Fig. 6A).

Myofiber CSA was measured in TA and EDL muscles at 30 days after single, double and triple injury (Fig. 6B and C). Despite myofiber CSA was significantly lower in *Col6a1*$^{-/-}$ muscles than wild-type under physiological condition, after 30 days from single injury both *Col6a1*$^{-/-}$ TA and EDL muscles showed higher myofiber CSA when compared to the corresponding wild-type samples. Conversely, at 30 days from double injury myofiber CSA of both *Col6a1*$^{-/-}$ muscles decreased when compared to the corresponding wild-type samples, but also in comparison to untreated *Col6a1*$^{-/-}$ muscles. In triple injured TA muscles, CSA differences between wild-type and *Col6a1*$^{-/-}$ were lost at 30 days, but a significant decrease was observed when comparing both genotypes with physiological conditions. Differently from what observed in TA muscles, CSA of EDL muscles at 30 days from triple injury was markedly lower in *Col6a1*$^{-/-}$ when compared to wild-type samples (Fig. 6C).

3.3 Effects of training exercise on muscle phenotype and regeneration in *Col6a1*$^{-/-}$ mice.

In order to induce a chronic muscle injury, we subjected in parallel age- and sex-matched wild-type and *Col6a1*$^{-/-}$mice to muscle training by voluntary exercise on running wheels. Interestingly, *Col6a1*$^{-/-}$ mice were found to cover significantly shorter distances than wild-type littermates, and they also displayed a gradual decline of their locomotory activity (Fig. 7A). Running exercise was continued for three months and at the end of the experiment muscles were analyzed and compared to muscles of non-exercised littermates. Prolonged exercise caused a striking worsening of the myopathic phenotype and a marked increase of muscle fiber death in ColVI null mice, while the wild-type maintained a normal muscle survival (Fig. 7B). In particular, the incidence of myofibers with apoptotic nuclei, which is consistently maintained in the range of about 50-60 TUNEL-positive nuclei/sq.mm in *Col6a1*$^{-/-}$ diaphragms (Irwin et al., 2003; Palma et al., 2009; Tiepolo et al., 2009), was significantly increased in the diaphragms of exercised *Col6a1*$^{-/-}$ mice, with about two-fold higher values than non-exercised *Col6a1*$^{-/-}$ mice (Fig. 7B). Both wild type and *Col6a1*$^{-/-}$ mice showed an increase of centrally nucleated fibers, with a higher rise in *Col6a1*$^{-/-}$ mice (Fig. 7C). Remarkably, long-term exercise led a marked decrease of Pax7-positive cells in *Col6a1*$^{-/-}$ muscles, while it had ho effect on wild type muscles

(Fig. 7D). These findings strengthen the hypothesis that SCs are not able to respond properly to regeneration stimuli in ColVI deficient muscles.

3.4 *Ex vivo* studies reveal altered SC activity in *Col6a1*$^{-/-}$ mice.

In parallel with the *in vivo* studies, and in order to further investigate SC activity, I set up an *ex vivo* approach with single intact myofibers derived from EDL muscles of wild-type and *Col6a1*$^{-/-}$ mice. This experimental model allows not only to study SCs, by maintaining as much as possible their niche, but also to analyze their activity during myofiber culture. Towards this aim, I analyzed freshly isolated myofibers, right after dissection from muscle (time 0) in order to have information about the physiological state of SCs. Moreover, I performed culture of single myofibers to study the activation, proliferation and differentiation of SCs (48-hour culture). Since muscle fibers were cultured singularly, SCs showed a consistent response to culture, miming their activation during *in vivo* muscle regeneration. Immunofluorescence analysis of myofibers derived from wild-type muscle showed that the extracellular network of ColVI was well preserved in the freshly isolated myofibers (Fig. 8A). In particular, ColVI formed a thin microfibrillar network surrounding the myofiber and close to SCs. Pax7 immunofluorescence of freshly isolated myofibers at time 0 showed that SCs were increased in *Col6a1*$^{-/-}$ myofibers compared to wild-type, thus confirming the *in vivo* findings (Fig. 8B). To assess the activation and differentiation of SCs, single myofibers were cultured for 48 hours and subjected to immunofluorescence for Pax7 and MyoD. In these experiments, I divided cells in three subpopulations: *i)* SCs returned to quiescence, classified as cells expressing only Pax7; *ii)* activated and/or committed SCs, corresponding to cells positive to both Pax7 and MyoD; and *iii)* differentiated SCs, corresponding to cells expressing only MyoD (Fig. 8B and C). As expected, wild-type fibers showed an increased number of SCs after 48 hours of culture, maintaining Pax7-positive subpopulation and increasing Pax7- and MyoD-positive cells. Conversely, *Col6a1*$^{-/-}$ SCs did not show any increase, and the SC population was composed of a lower amount of Pax7-positive cells and a similar incidence of Pax7- and MyoD-positive cells (Fig. 8B). Interestingly, the incidence of differentiated SCs, expressing only the MyoD marker, was not different between wild type and *Col6a1*$^{-/-}$ fibers (Fig. 8C).

4. Discussion

Col6a1$^{-/-}$ mice have been revealed a fundamental model for the understanding of the pathomolecular muscle defects caused by lack of ColVI and for the identification of novel therapeutic opportunities for human BM and UCMD patients. Indeed, studies carried out in ColVI null mice revealed a spontaneous apoptosis associated to mitochondrial dysfunction in myofibers and muscle-derived cells, defects that could be normalized by addition of ColVI or treatment with cyclosporin A (Irwin et al., 2003). Moreover, the molecular mechanisms underlying the accumulation of abnormal mitochondria and the ensuing cell death in *Col6a1*$^{-/-}$ muscles were recently elucidated, showing a link between impaired autophagic signaling and the development of the myopathic phenotype (Grumati et al., 2010). Remarkably, the pathogenic mechanisms identified in *Col6a1*$^{-/-}$ mice were also confirmed in UCMD and BM patients (Angelini et al., 2007; Grumati et al., 2010). In addition, the demonstration of the therapeutic efficacy of cyclosporin A in *Col6a1*$^{-/-}$ mice, led to a promising clinical trial with cyclosporin A in UCMD and BM patients, opening new therapeutic perspectives. Interestingly, cyclosporin A treatment not only was found to be able to recover apoptosis and mitochondrial dysfunction, but also promoted muscle regeneration in UCMD pediatric patients (Merlini et al., 2008a).

In some muscular dystrophies, the pathogenic mutation not only results in myofiber wasting, but also directly impairs SC function thus compromising the efficient maintenance and repair of myofibers (Zammit et al., 2010). ColVI is abundantly present in the ECM located in the close periphery of myofibers, thus is can be hypothesized that ColVI may influence the behaviour of either myofibers and/or SCs. Considering the remarkable apoptotic phenotype displayed by *Col6a1*$^{-/-}$ and UCMD myoblasts, and persuaded by the regenerative effect of cyclosporin A treatment in UCMD patients, during the second half of my PhD work I started investigating muscle regeneration and SC activity in the *Col6a1*$^{-/-}$ mouse model.

I found that under physiological conditions TA and EDL muscles of 6-month-old *Col6a1*$^{-/-}$ mice display activation of baseline regeneration, with increased incidence of centrally nucleated myofibers and of Pax7-positive cells ratios. This is in agreement with the myopathic phenotype of these mice, which was demonstrated to cause

muscle defects and myofiber degeneration (Bonaldo et al., 1988; Irwin et al., 2003). Although centrally nucleated myofibers are typically considered a sign of muscle regeneration, they are also representative of a dystrophic condition, since muscle regeneration is often a consequence of muscle damage due to a dystrophic process. For these reasons, it was not surprising to find an increase of centrally nucleated myofibers in ColVI null muscles. In agreement with the need for muscle regeneration, SCs were found increased in number in *Col6a1*$^{-/-}$ mice. Similar features were observed in the dystrophic phase of *mdx* mice, where the absence of dystrophin protein leads to extensive and cycling events of muscle degeneration and regeneration, associated with increased activity of SCs (Morgan and Zammit, 2010). Interestingly, these events were more rare in *Col6a1*$^{-/-}$ muscles, where centrally nucleated myofibers and Pax7-positive cells were respectively four- and two-fold increased compared to wild-type muscles. Furthermore, Pax7-positive cells detected in *Col6a1*$^{-/-}$ muscles seemed to be in a typical 'satellite' position, underneath the basal lamina, both in muscles *in vivo* and in myofibers *ex vivo* (data not shown). The increased number of activated SCs should generate more differentiated myogenic cells able to fuse with pre-existing myofibers, leading to increased myofiber size. Instead, *Col6a1*$^{-/-}$ TA and EDL muscles showed a lower mean cross-section area (CSA) compared to wild-type muscles, suggesting alteration in SC activity. Further experiments are needed to get a better understanding of *Col6a1*$^{-/-}$ SC state under physiological conditions, in terms of quiescence, activation and proliferation. Experiments in this perspective are already ongoing, where *Col6a1*$^{-/-}$ mice are treated *in vivo* with EdU (5-ethynyl-2´-deoxyuridine), a modified nucleoside that is incorporated during DNA synthesis in proliferating cells. This approach will allow us to get detailed information about SC proliferation under physiological conditions in *Col6a1*$^{-/-}$ mice.

Altered activation of SCs represents one of the possible causes of their increased number in *Col6a1*$^{-/-}$ muscles. In addition, modified determination of the SC pool during mouse development could also explain the phenotype observed in adult *Col6a1*$^{-/-}$ mice. In order to test this possibility, I performed SC analysis in young (two-week-old) wild-type and ColVI null TA muscles. It was previously demonstrated that two-week-old mouse muscles display an increased incidence of SCs compared to adult, and they reach SC adult levels after three weeks, with no significant changes

thereafter (White et al., 2010). In the case the observed increased incidence of SCs in ColVI null muscles is of embryological origin, it may be argued that two-week-old mice should have a more evident increase of Pax7-positive cells when compared to wild-type mice of the same age. Differently, I did not observed any significant difference between wild-type and *Col6a1*$^{-/-}$ two-week-old muscles, both in terms of centrally nucleated myofibers and of SC ratios. These findings seem to exclude an involvement of SC embryonic determination in the increased SC ratio observed in 6-month-old *Col6a1*$^{-/-}$ mice, and suggest that this alteration becomes apparent only in adult mice.

In order to investigate further muscle regeneration capability, I subjected 6-month-old wild-type and ColVI null mice to acute muscle injury by cardiotoxin injection. Histological analysis at 7 days from injury showed a slight delay of new myofiber formation in *Col6a1*$^{-/-}$ muscles. In addition, and at difference from the corresponding wild-type samples, myofibers undergoing degradation were still present at this time point in injured *Col6a1*$^{-/-}$ muscles. The importance of the recruitment of cells of the immune system for the elimination of dead myofibers and for the activation of early events of muscle regeneration was demonstrated in a number of studies (Lescaudrom et al., 1999; McClung et al., 2007). Thus, a possible delay or decrease of immune system recruitment may explain the retarded muscle regeneration of *Col6a1*$^{-/-}$ muscles. Detection of active monocytes and macrophages at 4 days from cardiotoxin injury, by immunofluorescence with the MOMA2 marker, did not reveal any obvious difference between wild-type and ColVI null muscles, suggesting that other mechanisms should be responsible for the incomplete elimination of damaged myofibers in *Col6a1*$^{-/-}$ mice. One possibility is the impaired activation of the autophagic degradative process, a major defect recently found in ColVI null mice (Grumati et al., 2010) and which may explain at least in part these features.

Although the histological analysis after 30 days from cardiotoxin-induced injury suggests a rescue of *Col6a1*$^{-/-}$ muscle structure, other parameters reveal an altered progression of muscle regeneration. Indeed, analysis of the incidence of Pax7-positive cells ratio at 30 days from injury showed strong differences between the responses of wild-type and *Col6a1*$^{-/-}$ null TA muscles. Despite the strong increase of Pax7-positive cells in injured wild-type muscles, also reported in another work (Shea et al., 2010),

Pax7-positive cells were reduced in injured *Col6a1*$^{-/-}$ muscles, suggesting that the ability of SCs to maintain their pool after an acute injury was compromised in *Col6a1*$^{-/-}$ mice. Interestingly, although ColVI null myofibers showed an increased mean CSA after 30 days from injury, the weight of TA muscles was decreased when compared to the corresponding wild-type samples. These results suggest that regenerated *Col6a1*$^{-/-}$ muscles were composed by a lower number of larger myofibers compared to regenerated wild-type muscles, highlighting a decreased regenerative capability of ColVI null mice. The observation that regenerated *Col6a1*$^{-/-}$ muscles display an increased mean CSA indicate that SCs are able to correctly differentiate in myoblasts and fuse with myofibers. Altogether, these findings strongly suggest that in *Col6a1*$^{-/-}$ muscles SCs are able to complete muscle regeneration, but are unable to expand and maintain their pool like in wild-type muscles after injury.

Remarkably, similar results were obtained by analyzing wild-type and *Col6a1*$^{-/-}$ mice subjected to muscle training by voluntary exercise on running wheels. It was previously shown that an increased level of physical activity, such as running or resistance training, can also stimulate SC mitotic activity (McCormick and Thomas, 1992) and results in elevated SC numbers (Kadi and Thornell, 2000). Exercise training by progressive treadmill running results in SC activation together with morphological changes indicative of ongoing muscle fibre injury and repair (McCormick and Thomas, 1992). Our data show that, in addition to decreased muscle activity and increased myofiber apoptosis, three months of running wheel exercise results in a strong reduction of Pax7-positive cells in *Col6a1*$^{-/-}$ muscles, when compared to both exercised wild-type mice and non-exercised *Col6a1*$^{-/-}$ mice. At difference from cardiotoxin injection, muscle training represents a more prolonged and less invasive method to induce chronic muscle injury, mimicking in a better way the physiologic damage observed in the human disease. Since two different injury approaches led to similar effects on Pax7-positive cells, we can strongly suppose that SCs are not able to maintain their pool after activation in a muscle lacking ColVI.

It was shown that SCs are capable of both self-renewal and differentiation during skeletal muscle repair (Montarras et al., 2005; Collins et al., 2005; Kuang et al., 2007; Sacco et al., 2008; Cerletti et al., 2008). The mechanism by which this happens is linked to asymmetric and symmetric division of SCs (Crossgrove et al., 2009). Since

Pax7-positive cells were reduced in regenerated *Col6a1*$^{-/-}$ muscles, I decided to perform multiple injuries to test the ability of SCs to self-renew. Indeed, a second injury, carried out in regenerated muscles, activates those SCs that performed self-renewal during the first injury. If SC self-renewal is impaired, repeated injuries determine a progressive loss of SC stem pool with consequent reduction of regenerative capability. Interestingly, the inability of *Col6a1*$^{-/-}$ muscles to regenerate correctly was more evident following multiple muscle injuries. *Col6a1*$^{-/-}$ muscles displayed decreased muscle regeneration at 7 days from a second injury, and this decrease was even more marked at 7 days from a third injury. Moreover, regenerated muscles investigated after 30 days from double cardiotoxin injury showed evident histological alteration with lower mean CSA in *Col6a1*$^{-/-}$ mice compared to wild-type, suggesting a secondary reduction of myogenic cells. Furthermore, *Col6a1*$^{-/-}$ muscles subjected to triple injury were largely unable to regenerate, showing connective tissue substitution and strong decrease in muscle mass. It is interesting to note that also wild-type muscles started to display some problems in muscle regeneration after a triple injury, since mean CSA decreased when compared to untreated condition.

In order to ascertain whether the features displayed by multiple injured *Col6a1*$^{-/-}$ muscles could be only due to a delay in muscle regeneration, muscle mass was also measured after 60 days from double and triple injury. Interestingly, even at 60 days from injury, *Col6a1*$^{-/-}$ muscles were not able to recover muscle mass like wild-type mice, suggesting a decreased regenerative capability rather than a delay of the regeneration process. Looking at the SC ratio in double injured muscles, we found that *Col6a1*$^{-/-}$ ratio was not increased like in wild-type muscle, in agreement to what was observed after the first injury. However, no significant differences in the SC ratio were found between *Col6a1*$^{-/-}$ and wild-type muscles after a triple injury.

Altogether, these results strongly suggest that ColVI plays a role in muscle regeneration and SC maintenance. Similar alterations of SCs were recently described for intracellular proteins involved in muscle homeostasis. Shea and colleagues showed that Sprouty 1 (Spry1), a receptor tyrosine kinase inhibitor, is required for the return to quiescence and homeostasis of the SC pool during repair. When Spry1 is disrupted, muscles display a decreased number of Pax7-positive cells after injury (Shea et al., 2010). In another work, similar effects were observed in mice lacking

selenoprotein N, a protein whose deficiency causes a group of inherited neuromuscular disorders in humans (Castes et al., 2010).

Since the lower regenerative ability of *Col6a1*$^{-/-}$ mice seemed to be due to the inability of SCs to maintain their pool after injury, I decided to analyze ColVI deposition in wild-type muscles during the starting events of muscle regeneration, when SCs are induced to proliferate and expand their pool (Kalaraki et al., 2009). Interestingly, after 4 days from cardiotoxin injection, wild-type TA muscles showed a marked increase of ColVI deposition in the regenerating area, where Pax7-positive cells were found to proliferate extensively. In addition, almost all Pax7-positive cells were found in close contact with ColVI, and some of these cells were totally surrounded by the protein. These data suggest that ColVI may be a component of the SC niche that plays a role during SC activation, and do not exclude a potential role of the protein during the quiescent state of SCs. Various studies demonstrated that the niche is crucial for maintaining the stemness of different kind of stem cells (Fuchs et al., 2004; Moore et al., 2006; Scadden et al., 2006). In skeletal muscle, the ECM surrounding SCs is considered part of their niche and seems to be essential in regulating SC self-renewal (Crossgrove et al., 2009). These evidences strongly support the hypothesis that ColVI is a component of SC niche necessary to induce a correct return to quiescence of SCs. A number of literature data indicate that ECM elasticity regulates the activity of a number of cells, including stem cells, by means of its mechanical properties (Lopez et al., 2008; Guilak et al., 2009). Gilbert and colleagues demonstrated that substrate elasticity regulates SC self-renewal in culture, while other works showed altered muscle elasticity during aging, disease and injury (Gilbert et al., 2010). Therefore, it cannot be excluded that lack of ColVI can alter elasticity in *Col6a1*$^{-/-}$ muscles, leading to improper activity of SCs. It will be very interesting to investigate the ECM mechanical properties of *Col6a1*$^{-/-}$ muscles, and studies were planned towards this aim.

Based on the finding that ColVI is likely needed during the early phases of muscle regeneration, I investigated apoptosis in wild-type and *Col6a1*$^{-/-}$muscles following cardiotoxin-induced injury. Apoptotic nuclei were found to be strongly increased in *Col6a1*$^{-/-}$ muscles after injury, when compared to both untreated *Col6a1*$^{-/-}$ and cardiotoxin-treated wild-type muscles. Since the peak of apoptosis was at 4 days from

injury, it is possible that SCs contributed to the apoptotic increase. It may be speculated that *Col6a1*$^{-/-}$ SCs after activation are not able to properly self-renew and undergo apoptosis. Although this hypothesis needs to be carefully investigated *in vivo*, it remains plausible since Pax7-positive cells, obtained from *Col6a1*$^{-/-}$ muscle cultures, showed increased apoptosis *in vitro* (results not shown). Furthermore, apoptosis occurring in SCs unable to undergo proper self-renewal was reported in different works (Gilbert et al., 2010; Shea et al., 2010), and in more general terms precocious differentiation of stem cells was also associated to apoptosis (Georgia et al., 2006; Liu et al., 2008). It was reported that during the critical phase of stem cell activation from quiescence, anti-apoptotic signals play an important role in preserving the full complement of SCs (Golding et al., 2007). Based on these findings and our data, we can hypothesize that the SC pool is not properly maintained in *Col6a1*$^{-/-}$ muscles because part of SCs that should return to quiescence undergo apoptosis.

In order to perform further studies on SC activity, I set up an *in vitro* experimental system with single fiber cultures derived from wild-type and *Col6a1*$^{-/-}$ EDL muscles. Since SC are maintained in their niche and in contact with host myofibers, single fiber cultures represent one of the best *in vitro* model systems to study SC self-renewal (Zammit et al., 2004). Moreover, I optimized the conditions for muscle dissection and myofiber dissociation, in order to preserve as much as possible the endomysial ECM. Indeed, although myofibers were subjected to enzymatic and mechanic dissociations, the extracellular network of ColVI in wild-type samples was maintained around myofibers and SCs after isolation, thus confirming the appropriateness of the approach. Analysis of Pax7-positive cells in freshly isolated EDL myofibers confirmed the *in vivo* observations, showing about twofold increase of SCs in *Col6a1*$^{-/-}$ compared to wild-type samples. Interestingly, although the total amount of Pax7-positive cells per single fiber was not different between wild-type and *Col6a1*$^{-/-}$ when cultured for 48 hours, *Col6a1*$^{-/-}$ Pax7-positive cells did not expand their pool, as wild-type cells did. More in detail, wild-type SCs doubled during myofiber culture and gave origin both to activated cells (Pax7^{+}MyoD^{+}) and cell returned to the quiescence state (Pax7^{+}MyoD^{-}). Conversely, the number of quiescent Pax7-positive cells per fiber was strongly reduced in *Col6a1*$^{-/-}$ cultures compared to both wild-type cultures and

freshly isolated *Col6a1*$^{-/-}$ myofibers. In agreement with the *in vivo* findings, these data provide evidences that ColVI is required for reversible quiescence of a subpopulation of Pax7-positive cells. Interestingly, differentiated SCs (Pax7^{-}MyoD^{+}) revealed no differences between wild-type and ColVI null cultures, enforcing the hypothesis put forward by the *in vivo* experiments, which showed a normal ability of differentiated myogenic cells to fuse with myofibers and increase their size.

Altogether, our *in vivo* and *in vitro* studies suggest that *Col6a1*$^{-/-}$ SCs have an impaired ability to expand and maintain their stem cell pool. It was reported that Notch and Wnt pathways direct SC proliferation and self-renewal, and alterations in one or both of their players lead to reduced SC self-renewal (Conboy and Rando, 2002; Conboy et al., 2003; Le Grande et al., 2009; Pisconti et al., 2010). In addiction, several growth factors also display the ability to regulate SC proliferation and self-renewal (Machida et al., 2004; Tatsumi et al 2006). Thus, ColVI may either act directly in regulating SC self-renewal, or modulate growth factors and signal molecules involved in this fine process. These different possibilities can be explored by studies in single myofiber cultures, which permit to monitor SC activity in response to different culture conditions, including ECM substrates, addition of growth factors, and modulation of signaling pathways with specific activators and/or inhibitors. In addition, with this model we will also be able to provide purified ColVI to myofiber cultures and analyze its consequences on wild-type and *Col6a1*$^{-/-}$ SCs.

Since *Col6a1*$^{-/-}$ mice display a marked rescue of the myopathic phenotype when treated with cyclosporin A or when autophagy is reactivated (Irwin et al., 2003; Grumati et al., 2010), it will be interesting to study SC activity when the myopathic phenotype of ColVI null mice is rescued by different genetic, pharmacological or dietary means. Along this line, I performed some preliminary studies on muscle regeneration in wild-type and *Col6a1*$^{-/-}$ mice treated for 10 days with either vehicle or 10 mg/kg/day cyclosporin A. However no significant difference could be observed between mice treated with the drug or with vehicle (data not shown). Despite that, studies on the effects of cyclosporin A treatment during the regenerative phases following single and repeated cardiotoxin-induced muscle injury are ongoing. In addition, studies on single myofiber cultures will also help to assess the effects of cyclosporin A or autophagy inducers on SC survival, division and self-renewal. These

experiments will allow determine whether these treatments have any beneficial effect on SC survival, stemness and differentiation. It will be also interesting to study SCs in UCMD and BM patients, before and after cyclosporin A treatment. The identification of a pathogenic contribution of SCs in these human conditions may open new frontiers for therapeutic approaches.

In conclusion, the data reported in this thesis reveal that ColVI plays an important role during skeletal muscle regeneration, and indicate that this ECM protein is necessary for the normal expansion and maintenance of SC stem pool. These findings constitute not only the basis for a better understanding of the pathogenic mechanisms of *Col6a1*$^{-/-}$ mice and human ColVI muscular dystrophies, but they may also open new perspectives for therapeutic approaches.

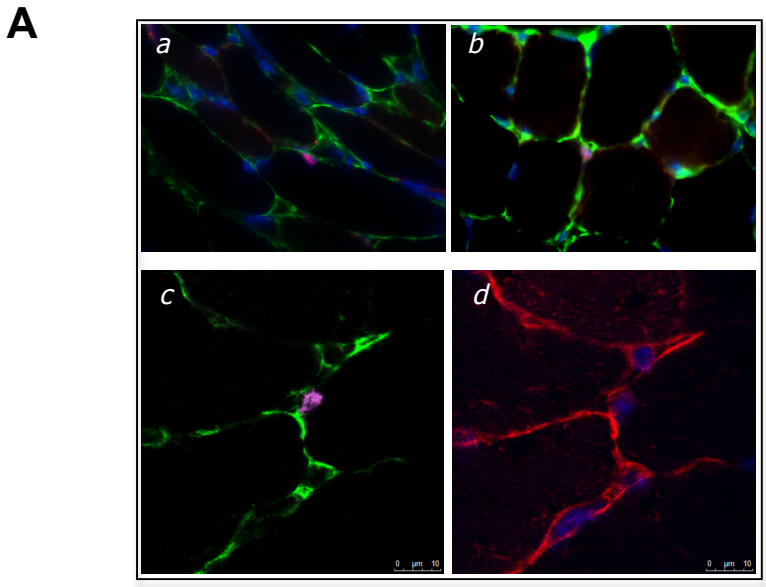
A
a
b
c
d

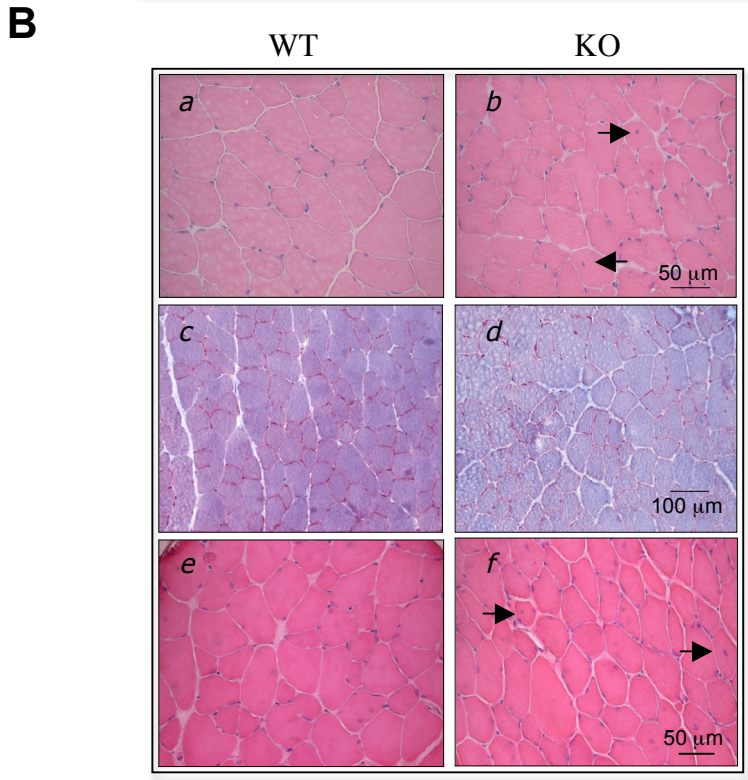
B
WT
KO
a
b
50 µm
c
d
100 µm
e
f
50 µm

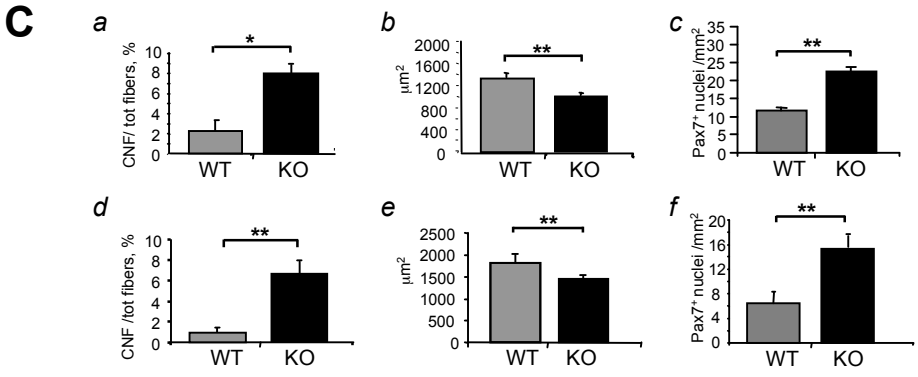
C
a
CNF/ tot fibers, %
WT
KO
b
µm²
c
Pax7⁺ nuclei /mm²
d
CNF /tot fibers, %
e
f

Figure 1. *Col6a1*$^{-/-}$ mice have altered muscle regeneration under physiological condition.

A. Representative images of cross-sections from wild-type TA muscle analyzed by epifluorescence (*a* and *b*) or confocal fluorescence (*c* and *d*) microscopy. ColVI (green) and Pax7-positive cells (violet) are very close (*a* and *b*). Pax7-positive cells (violet) are localized below laminin (red) and ColVI (green) (*c* and *d*). Nuclei were stained with Hoechst (blue).

B. Histological analysis of wild-type (*a*, *c* and *e*) and *Col6a1*$^{-/-}$ (*b*, *d* and *f*) TA (*a*, *b*, *c* and *d*) and EDL (*e* and *f*) cross-sections, after staining with hematoxylin-eosin (*a*, *b*, *e* and *f*) or Azan (*c* and *d*). Arrows indicate centrally nucleated myofibers.

C. Quantification of centrally nucleated myofibers, myofiber cross-sectional area, and Pax7-positive cells in TA (*a*, *b* and *c*) and EDL (*d*, *e* and *f*) muscles from wild-type and *Col6a1*$^{-/-}$ mice. The incidence of centrally nucleated fibers (CNF), calculated on the number of total myofibers, is significantly increased in *Col6a1*$^{-/-}$ muscles, compared to wild-type (*a* and *d*). *Col6a1*$^{-/-}$ muscles display a significantly lower mean cross-sectional area than wild-type (*b* and *e*). The amount of SCs, calculated as Pax7-positive cells per area unit, is significantly increased in *Col6a1*$^{-/-}$ muscles compared to wild-type (*e* and *f*). *: $p<0.05$; **: $p<0.01$.

KO, *Col6a1*$^{-/-}$; WT, wild-type.

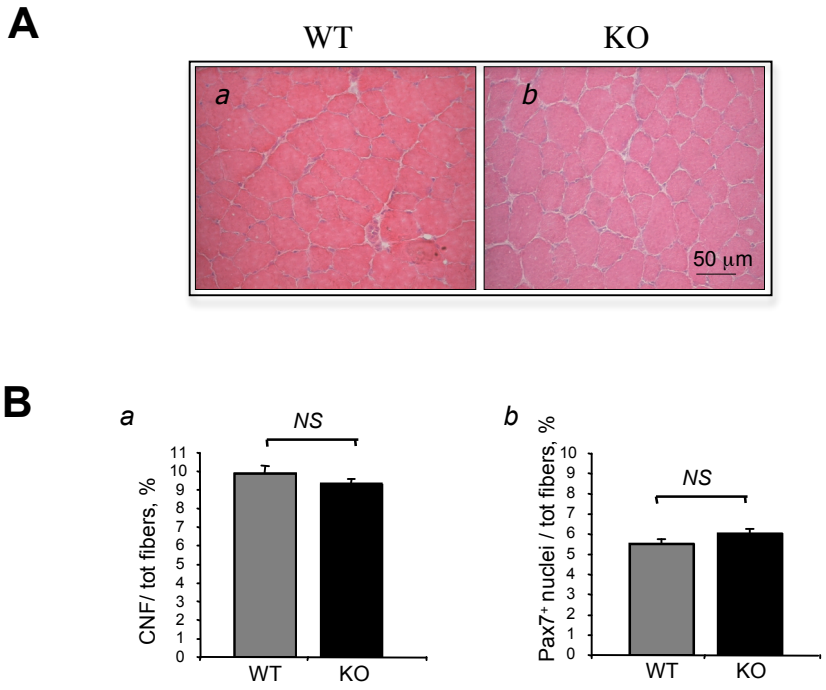

Figure 2. Regenerative defects are not present in two-week old *Col6a1*$^{-/-}$ mice.

A. Hematoxylin-eosin staining of cross-sections of TA muscles from 2-week-old wild-type (*a*) and *Col6a1*$^{-/-}$ (*b*) mice maintained under physiological conditions.

B. Histograms showing quantifications of centrally nucleated myofibers (CNF, *a*) and SCs (*b*), calculated as CNF or Pax7-positive cells on total myofibers, in TA muscles from 2-week-old wild-type and *Col6a1*$^{-/-}$ mice maintained under physiological conditions. *NS*: not statistically significant.

KO, *Col6a1*$^{-/-}$; WT, wild-type.

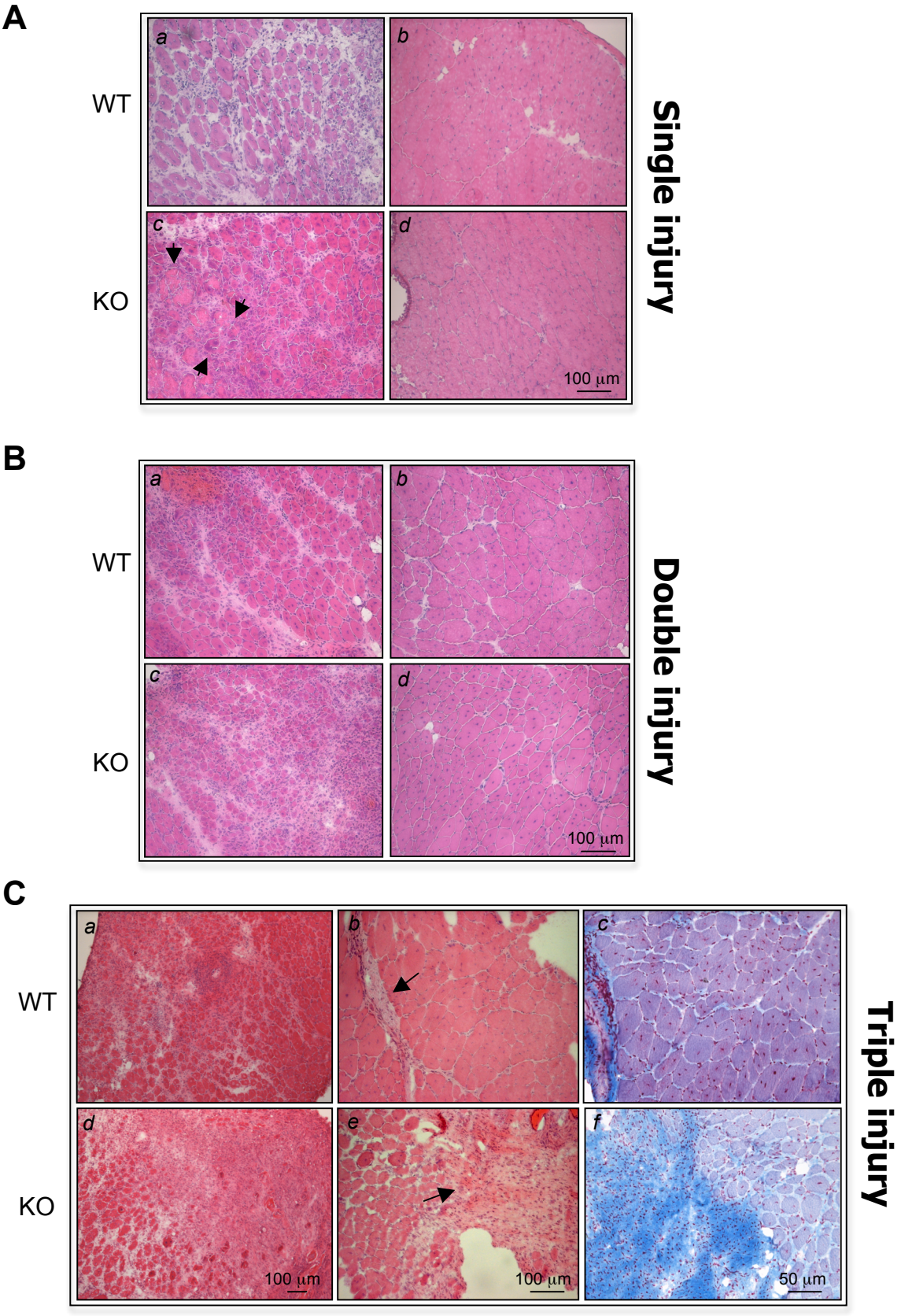
A
WT
KO
a
b
c
d
100 µm
Single injury
B
WT
KO
a
b
c
d
100 µm
Double injury
C
WT
KO
a
b
c
d
e
f
100 µm
100 µm
50 µm
Triple injury

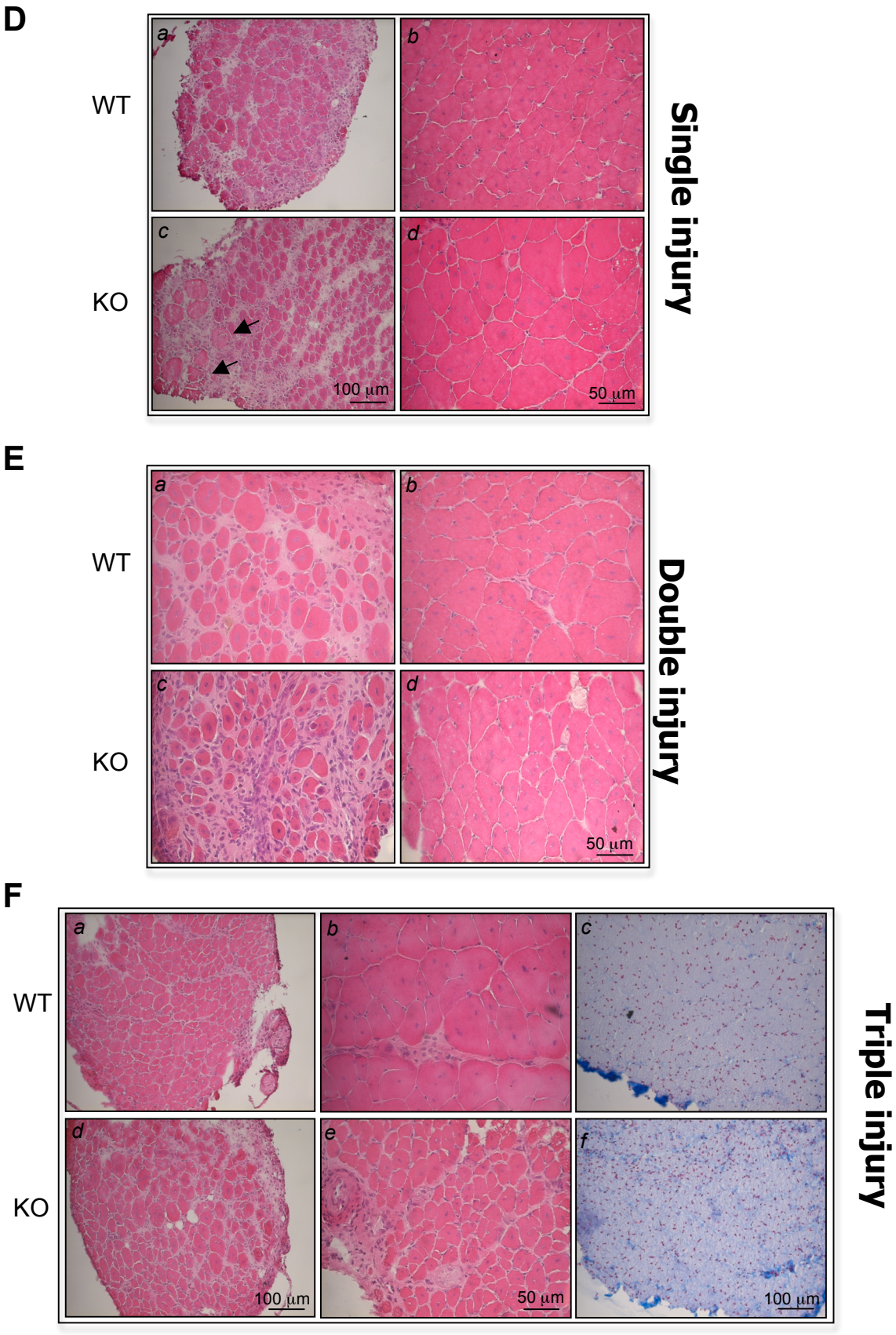
D
WT
KO
a
b
c
d
100 µm
50 µm
Single injury
E
WT
KO
a
b
c
d
50 µm
Double injury
F
WT
KO
a
b
c
d
e
f
100 µm
50 µm
100 µm
Triple injury

Figure 3. Histological analysis of wild type and *Col6a1*$^{-/-}$ TA and EDL muscles after single or multiple cardiotoxin injury.

A. Hematoxylin-eosin staining of cross-sections of TA muscles from wild-type (*a* and *b*) and *Col6a1*$^{-/-}$ (*c* and *d*) mice at 7 days (*a* and *c*) and 30 days (*b* and *d*) after single injection of cardiotoxin. Arrows indicate degenerating myofibers in *Col6a1*$^{-/-}$ muscles.

B. Hematoxylin-eosin staining of cross-sections of TA muscles from wild-type (*a* and *b*) and *Col6a1*$^{-/-}$ (*c* and *d*) mice at 7 days (*a* and *c*) and 30 days (*b* and *d*) days after double injection of cardiotoxin.

C. Cross-sections of TA muscles from wild-type (*a*, *b* and *c*) and *Col6a1*$^{-/-}$ (*d*, *e* and *f*) mice at 7 days (*a* and *d*) and 30 days (*b*, *c*, *e* and *f*) days after triple cardiotoxin injection. Hematoxylin-eosin (*a*, *b*, *d* and *e*) or Azan (*c* and *f*) staining were performed. Arrows indicate substitution of muscle with fibrotic tissue.

D. Hematoxylin-eosin staining of cross-sections of EDL muscles from wild-type (*a* and *b*) and *Col6a1*$^{-/-}$ (*c* and *d*) mice at 7 days (*a* and *c*) and 30 days (*b* and *d*) from single injection of cardiotoxin. Arrows indicate degenerating myofibers in *Col6a1*$^{-/-}$ muscles.

E. Hematoxylin-eosin staining of cross-sections of EDL muscles from wild-type (*a* and *b*) and *Col6a1*$^{-/-}$ (*c* and *d*) mice at 7 days (*a* and *c*) and 30 days (*b* and *d*) from double injection of cardiotoxin.

F. Cross-sections of TA muscles from wild-type (*a*, *b* and *c*) and *Col6a1*$^{-/-}$ (*d*, *e* and *f*) mice at 7 days (*a* and *d*) and 30 days (*b*, *c*, *e* and *f*) days after triple cardiotoxin injection. Hematoxylin-eosin (*a*, *b*, *d* and *e*) or Azan (*c* and *f*) staining were performed.

KO, *Col6a1*$^{-/-}$; WT, wild-type.

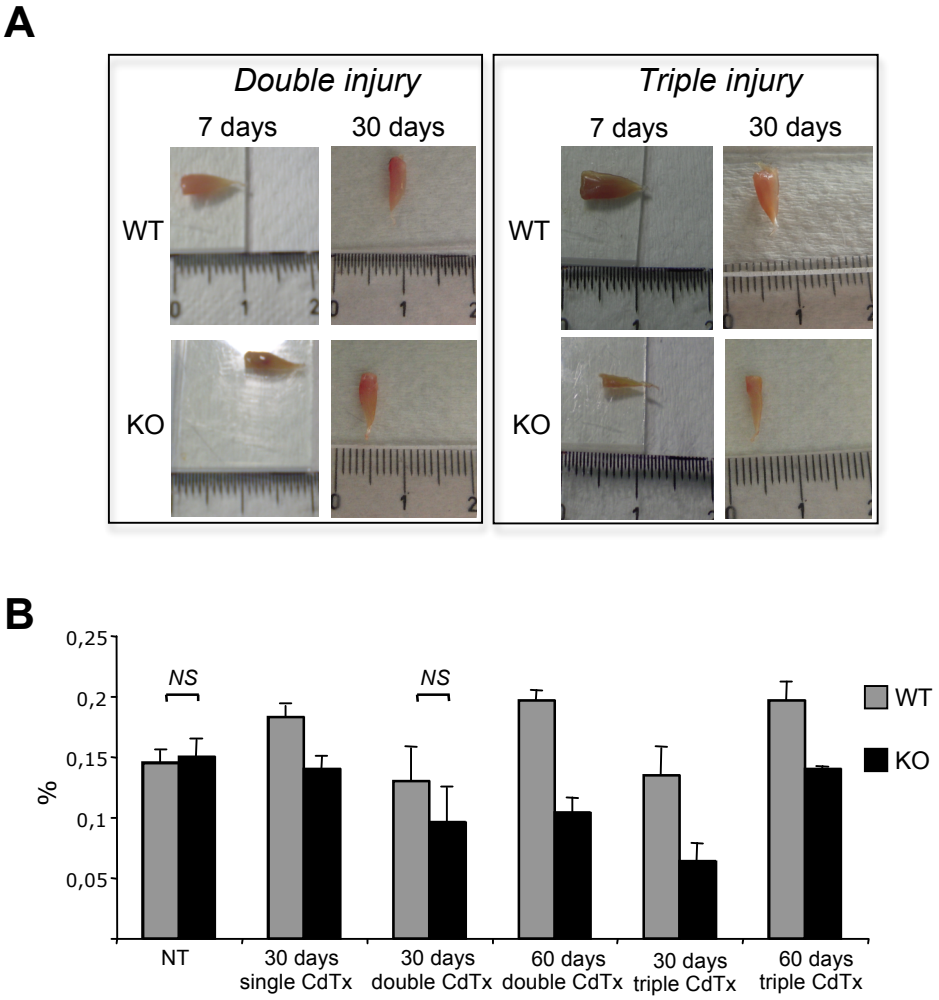

Figure 4. Effects of muscle injury on muscle mass in wild-type and *Col6a1*$^{-/-}$ mice.

A. Images showing representative wild-type and *Col6a1*$^{-/-}$ TA muscles at 7 days and 30 days following double injury or triple cardiotoxin injection. After triple injury, *Col6a1*$^{-/-}$ TA muscles are smaller than WT muscles.

B. Histograms showing quantification of TA muscle weight normalized on mouse weight and expressed in percentage (%). Wild-type and *Col6a1*$^{-/-}$ muscles were analyzed before (NT) and after 30 days from single, double and triple cardiotoxin (CdTx) injection, and 60 days from double and triple cardiotoxin (CdTx) injection. Regenerated *Col6a1*$^{-/-}$ TA muscles display a decreased muscle weight compared to wild-type muscles. All differences are statistically significant with $p<0.01$, expect where noted. *NS,* not significant.

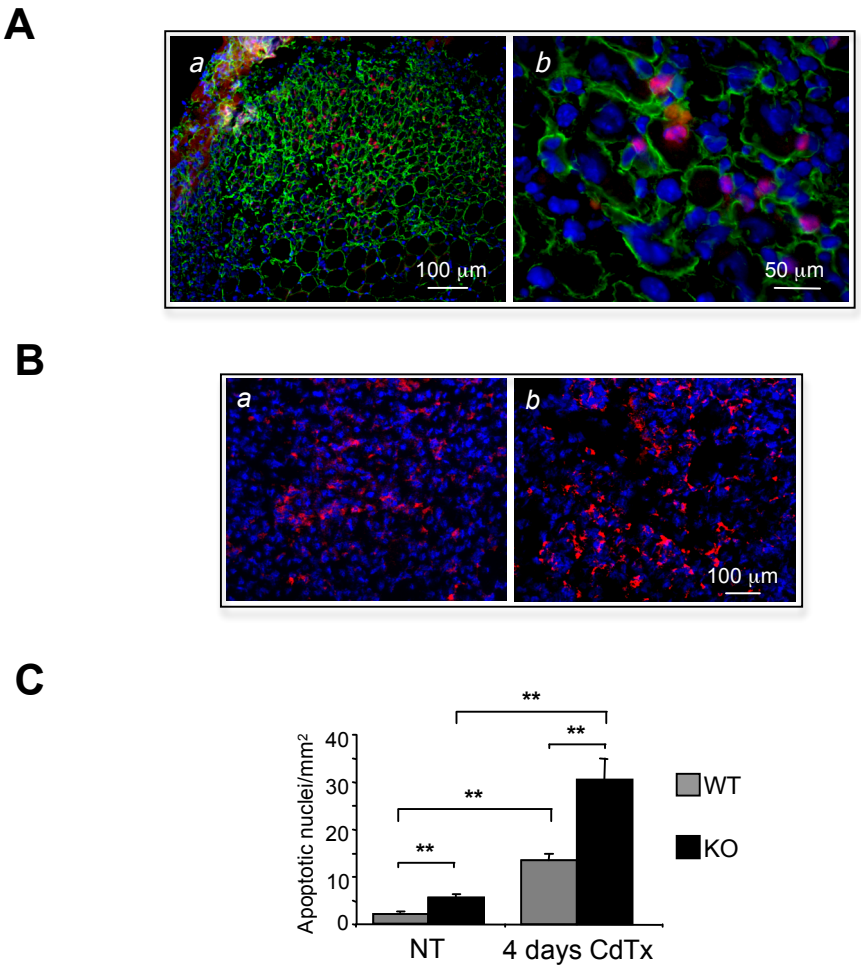

Figure 5. Characterization of early events of muscle regeneration in wild-type and *Col6a1*$^{-/-}$ mice.

A. Immunofluorescence for Pax7 (red) and ColVI (green) in cross-sections of wild-type TA 4 days after CdTx injection. During regeneration, ColVI is abundantly deposited in the endomysial ECM and the protein takes contact with Pax7-positive cells (*a,* low magnification; *b,* high magnification). Hoechst was used to stain all nuclei (blue).

B. Immunofluorescence for MOMA2 (red) in cross-sections of wild-type (*a*) and *Col6a1*$^{-/-}$ (*b*) TA muscles after 4 days from cardiotoxin (CdTx) injection. Nuclei were stained with Hoechst (blue).

C. Histograms showing the incidence of apoptotic nuclei in wild-type and *Col6a1*$^{-/-}$ TA muscles before (NT) and 4 days after cardiotoxin (CdTx) injection by TUNEL analysis. Apoptotic nuclei were calculated on area unit (mm^2). **: $p<0.01$.

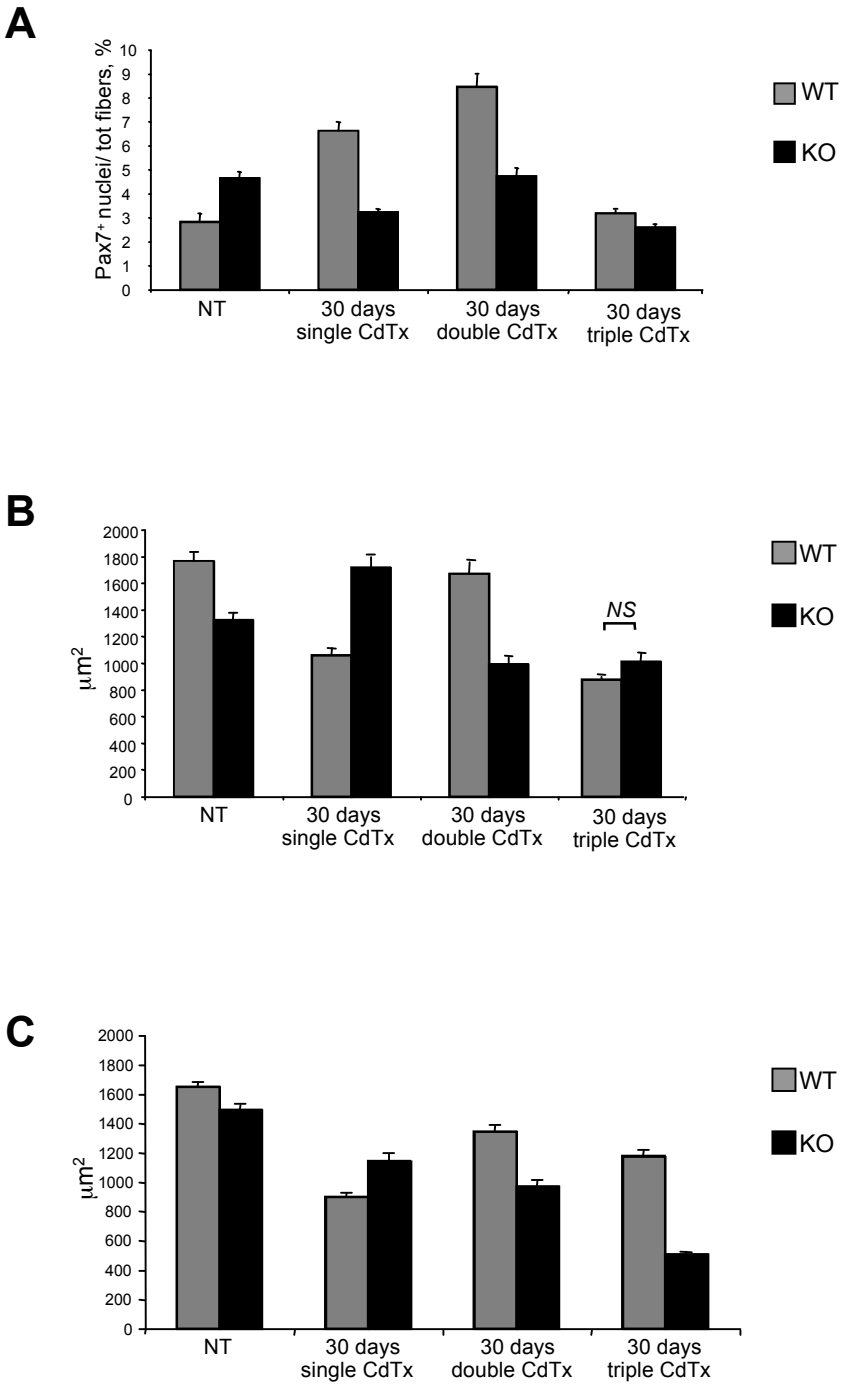
A
Pax7+ nuclei/ tot fibers, %
0
1
2
3
4
5
6
7
8
9
10
NT
30 days single CdTx
30 days double CdTx
30 days triple CdTx
WT
KO
B
µm2
0
200
400
600
800
1000
1200
1400
1600
1800
2000
NS
NT
30 days single CdTx
30 days double CdTx
30 days triple CdTx
WT
KO
C
µm2
0
200
400
600
800
1000
1200
1400
1600
1800
2000
NT
30 days single CdTx
30 days double CdTx
30 days triple CdTx
WT
KO

Figure 6. *Col6a1*$^{-/-}$ muscles display alterations in SCs and myofiber cross-sectional area in response to muscle injury.

A. Histograms showing quantification of Pax7-positive cells in TA muscles from wild-type and *Col6a1*$^{-/-}$ mice in untreated conditions (NT), after 30 days from single, double and triple cardiotoxin (CdTx) injection, and 60 days from double cardiotoxin (CdTx) injection. Pax7-positive nuclei were calculated on the number of total fibers, and the value was expressed in percentage (%). All differences are statistically significant with $p<0.01$.

B. Histograms showing quantification of myofiber cross-sectional area in TA muscles. The analysis was performed in muscles from wild-type and *Col6a1*$^{-/-}$ mice in untreated conditions (NT), after 30 days from single, double and triple cardiotoxin (CdTx) injury, and 60 days from double cardiotoxin (CdTx) injection. Area is expressed in μm^2. All differences are statistically significant with $p<0.01$, expect where noted. *NS,* not significant.

C. Quantification of myofiber cross-sectional area in EDL muscles from wild-type and *Col6a1*$^{-/-}$ mice in untreated conditions (NT), after 30 days from single, double and triple cardiotxin (CdTx) injection. All differences are statistically significant with $p<0.01$.

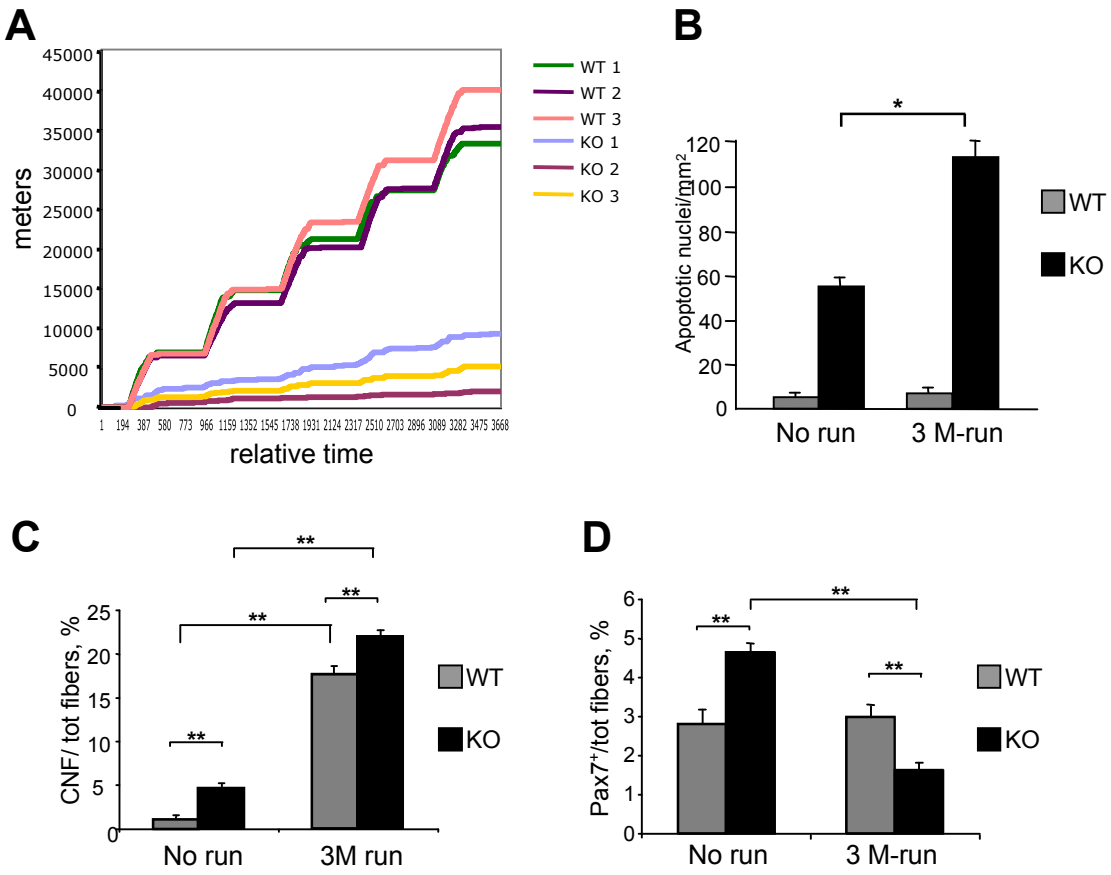

Figure 7. Muscle training affects survival and regeneration in Col6a1$^{-/-}$ muscles.

A. Running activity measured by voluntary running wheel exercise. The diagram plots the distance covered during a period of five days (d1-d5) by sex- and age-matched wild-type (WT, *n*=3) and *Col6a1*$^{-/-}$ (KO, *n*=3) mice. Diagram of wild-type mice show a "stair-step" pattern, reflecting night activity and daily rest.

B. Incidence of TUNEL-positive nuclei in diaphragm of 6-month-old wild-type (WT) and *Col6a1*$^{-/-}$ mice housed either in standard conditions (no run) or after 3 months of running wheel exercise (3M run). * $p<0.05$.

C. Quantification of centrally nucleated myofibers (CNF) in wild-type (WT) and *Col6a1*$^{-/-}$(KO) TA muscles before (no run) and after 3 months (3M run) of voluntary running wheel exercise. ** $p<0.01$.

D. Quantification of Pax7-positive cells in wild-type (WT) and *Col6a1*$^{-/-}$ (KO) TA muscles before (no run) and after 3 months (3M run) of voluntary running wheel exercise. Pax7-positive nuclei were calculated on the number of total fibers, and the value was expressed in percentage (%).** $p<0.01$.

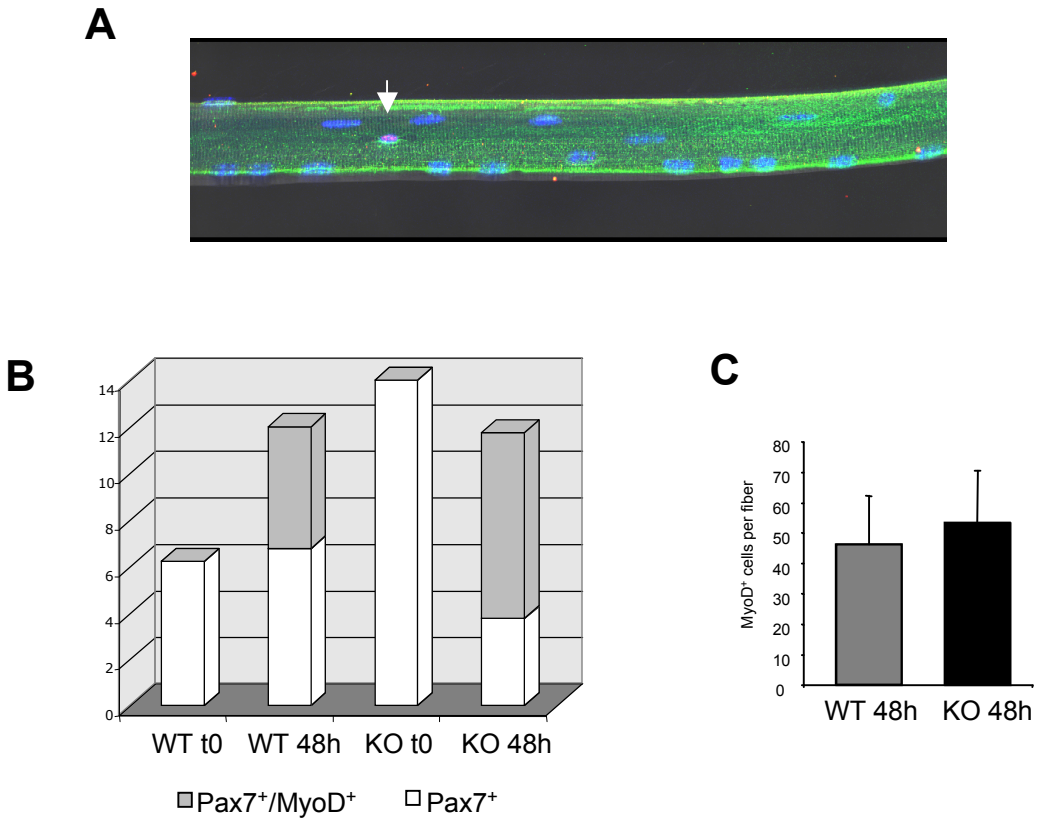

Figure 8. *Ex vivo* analysis revealed altered *Col6a1*$^{-/-}$ SCs activity.

A. Representative image of single fiber immediately after isolation from wild-type EDL muscle and analyzed by immunofluorescence for Pax7 (red, arrow) and ColVI (green). ColVI form a thin microfibrillar network in the ECM around the myofiber and is abundant in the close periphery of Pax7-positive cells.

B. Histograms showing quantification of Pax7- and MyoD-positive cells in myofiber cultures of wild type and *Col6a1*$^{-/-}$ mice. Single myofibers were derived from EDL and analyzed for Pax7 and MyoD nuclear markers by immunofluorescence. For time zero (t0), myofibers were fixed immediately after isolation. Some fibers were cultured for 48 hours (48h) in a medium containing factors stimulating SC proliferation. The ratios of Pax7-positive ($Pax7^+$), and Pax7/MyoD-positive ($Pax7^+MyoD^+$) cells were calculated per single fiber. *, $p<0.05$.

C. Single fibers from wild type and *Col6a1*$^{-/-}$ mice were analyzed after 48 hours culture by immunofluorescence for MyoD, and nuclei expressing the marker were counted per single fiber.

1. Studies on patients affected by collagen VI disorders.

Mutations in one or more COL6 genes cause various types of muscle disorders in humans. More than 70 different mutations were associated with either UCMD and BM (Lampe et al., 2005), and in addition collagen VI mutations were also found in other muscle disorders, such as limb girdle muscular dystrophy (Guglieri et al., 2005) and myosclerosis myopathy (Merlini et al., 2008). Until now, a comprehensive genotype-phenotype correlation could not be established between different COL6 gene mutations and the clinical symptoms and severity of the disorders. It can be predicted that different COL6 gene mutations have different impacts at the protein level, by affecting either collagen VI synthesis, assembly, secretion or function in the ECM.

BM (MIM #158810) is characterized by axial and proximal muscle weakness with finger and joint contractures. The patients have moderate atrophy of trunk and limb muscles (Bethlem & Wijngaarden, 1976). The hallmark of the disease is the presence of contractures of the interphalangeal joints of the last four fingers (Merlini et al., 1994). BM is a very heterogeneous disorder and patients show a wide range of clinical features, from mild myopathy to more severe cases with early onset and features of progressive muscular dystrophy (Jöbsis et al., 1999). The mode of inheritance is autosomal dominant, and mutations can occur in any of the three COL6 genes. Missense mutations in either the triple helical or the vWF–A domains of the three COL6 genes were described for various BM families (Jöbsis et al., 1996; Sasaki et al., 2000; Scacheri et al., 2002). Immunohistochemistry shows apparently normal or mildly reduced levels of ColVI in the endomysium of most BM patients.

UCMD (MIM #254090) is a severe congenital muscular dystrophy characterized by early onset, generalized and rapidly progressive muscle wasting and weakness, proximal joint contractures and distal joint hyperflexibility. Walking ability is rarely achieved or preserved in UCMD patients, and the rapid progression of the clinical symptoms usually leads to early death, due to respiratory failure (Camacho et al., 2001; Demir et al., 2002). Usually, UCMD shows an autosomal recessive inheritance with homozygous or compound heterozygous mutations in the COL6 genes. However, several cases of UCMD with dominant heterozygous mutations were reported (Pan et al., 2003; Baker et al., 2005; Angelin et al., 2007), and patients with a UCMD phenotype but without mutations in COL6 genes were also described. ColVI appears to be strongly reduced or absent in muscle biopsies from UCMD patients, suggesting

that UCMD mutations severely affect the synthesis and secretion of ColVI (Camacho et al., 2001; Zang et al., 2002; Squarzoni et al., 2006).

During the first two years of my PhD, I contributed to a multicentric programme aimed at the characterization of pathomolecular defects of a number of UCMD and BM patients. The final objective of this project was to allow the recruitment of genetically and molecularly characterized patients for clinical trials with cyclosporin A and its derivatives. We also analyzed a family affected by a rare muscle inherited disease, myosclerosis myopathy, and we found a peculiar nonsense mutation in the *COL6A2* gene, demonstrating for the first time a correlation between this rare disorder and collagen VI. The effect of COL6 gene mutations at the protein level was investigated by biochemical and immunohistochemical studies in muscle biopsies and in primary fibroblast cultures from patients. My major contribution to these studies was the elucidation of the effects of COL6 mutations on collagen VI chain synthesis, assembly and secretion by means of biochemical studies.

1.1 Myosclerosis myopathy is a collagen VI disorder.

We studied a family affected by myosclerosis myopathy (MIM 255600), a rare muscle inherited disorder characterised by slender muscles with firm "woody" consistency and severe restriction of movement of all joints. In the two affected siblings, we found that a homozygous nonsense *COL6A2* mutation lead to a peculiar pattern of defects on collagen VI synthesis, assembly, secretion and extracellular organization. These studies indicate, for the first time, that myosclerosis myopathy should be considered a collagen VI disorder allelic to UCMD and BM.

Autosomal recessive myosclerosis myopathy is a collagen VI disorder

L. Merlini, MD
E. Martoni, BS*
P. Grumati, BS*
P. Sabatelli, BS*
S. Squarzoni, MD
A. Urciuolo, BS
A. Ferlini, MD, PhD
F. Gualandi, MD, PhD
P. Bonaldo, PhD

Address correspondence and reprint requests to Dr. Paolo Bonaldo, Dipartimento di Istologia, Microbiologia e Biotecnologie Mediche, Viale Giuseppe Colombo 3, I-35121 Padova, Italy
bonaldo@bio.unipd.it

ABSTRACT

Objective: To determine the clinical and molecular features of a new phenotype related to collagen VI myopathies.

Methods: We examined two patients belonging to a consanguineous family affected by myosclerosis myopathy, screened for mutations of collagen VI genes, and performed a detailed biochemical and morphologic analysis of the muscle biopsy and cultured fibroblasts.

Results: The patients had a novel homozygous nonsense *COL6A2* mutation (Q819X); the mutated messenger RNA escaped nonsense-mediated decay and was translated into a truncated α2(VI) chain, lacking the sole C2 domain. The truncated chain associated with the other two chains, giving rise to secreted collagen VI. Monomers containing the truncated chain were assembled into dimers, but tetramers were almost absent; secreted collagen VI was quantitatively reduced and structurally abnormal in cultured fibroblasts. Mutated collagen did not correctly localize in the basement membrane of muscle fibers and was absent in the capillary wall. Ultrastructural analysis of muscle showed an unusual combination of basement membrane thickening and duplication, and increased number of pericytes.

Conclusions: This familial case has the characteristic features of myosclerosis myopathy and carries a homozygous *COL6A2* mutation responsible for a peculiar pattern of collagen VI defects. Our study demonstrates that myosclerosis myopathy should be considered a collagen VI disorder allelic to Ullrich congenital muscular dystrophy and Bethlem myopathy. ***Neurology*® 2008;71:1245–1253**

GLOSSARY

BM = Bethlem myopathy; **cDNA** = complementary DNA; **ECM** = extracellular matrix; **mRNA** = messenger RNA; **NMD** = nonsense-mediated decay; **UCMD** = Ullrich congenital muscular dystrophy.

The term *myosclerosis* was first introduced by Duchenne. Observation of the needle muscle biopsies obtained from his original case led him to hypothesize that the fundamental anatomic lesion was hyperplasia of the interstitial connective tissue, which prompted him to propose the term *paralysie myosclérosique* as an alternative to *paralysie musculaire pseudohypertrophique*.[1]

Myosclerosis was first considered a new familial degenerative illness of the intermysial connective tissue (myosclerosis, congenital, of Lowenthal; MIM 255600) in a report of six patients in two families presenting a restriction of articular mobility.[2,3] Under the name "syndrome of myosclerosis," a new condition was described in two siblings of a nonconsanguineous family.[4] Difficulty in walking was noted in early childhood, together with toe walking and progressive calf contractures. The clinical picture in the early 30s was characterized by slender muscles with firm "woody" consistency and restriction of movement of many joints because of muscle contractures.

Collagen VI is an extracellular matrix (ECM) protein with a broad distribution and essential for skeletal muscle integrity and function. The protein consists of three distinct α1(VI), α2(VI), and

Supplemental data at www.neurology.org

*These authors contributed equally.

From the Department of Experimental and Diagnostic Medicine (L.M., E.M., A.F., F.G.), Section of Medical Genetics, University of Ferrara; Department of Histology, Microbiology and Medical Biotechnologies (P.G., A.U., P.B.), University of Padova; and IGM-CNR (P.S., S.S.), Unit of Bologna c/o IOR, Italy.

Supported by grants from the Italian Telethon Foundation (GGP04113 and GUP07004), the Italian Ministry for University (PRIN 2005), and the Italian Health Ministry (RF 2005).

Disclosure: The authors report no disclosures.

α3(VI) chains encoded by separate genes (*COL6A1*, *COL6A2*, and *COL6A3*). Mutations of collagen VI genes cause two major phenotypes: Bethlem myopathy (BM; MIM 158810) and Ullrich congenital muscular dystrophy (UCMD; MIM 254090).[5-8] BM is a relatively mild, dominantly inherited disorder and is characterized by proximal muscle weakness with joint contractures mainly involving the fingers, elbows, and ankles.[9] The "scleroatonic" UCMD is a recessive/dominant condition characterized by severe muscle weakness, resulting in limited ability or inability to walk independently, proximal joint contractures and striking hypermobility of distal joints, and early respiratory failure.[10] A pure limb-girdle presentation with absent or mild/late contractures was also recognized in three unrelated families with missense mutations in *COL6A1* and *COL6A2*.[11]

Here we report a family with autosomal recessive myosclerosis myopathy due to *COL6A2* mutation, expanding the spectrum of collagen VI myopathies. The mutation is a novel pathogenic variation of the *COL6A2* gene and represents the first truncating mutation occurring in homozygosity in the C1 domain of the α2(VI) chain.

Figure 1 Clinical features

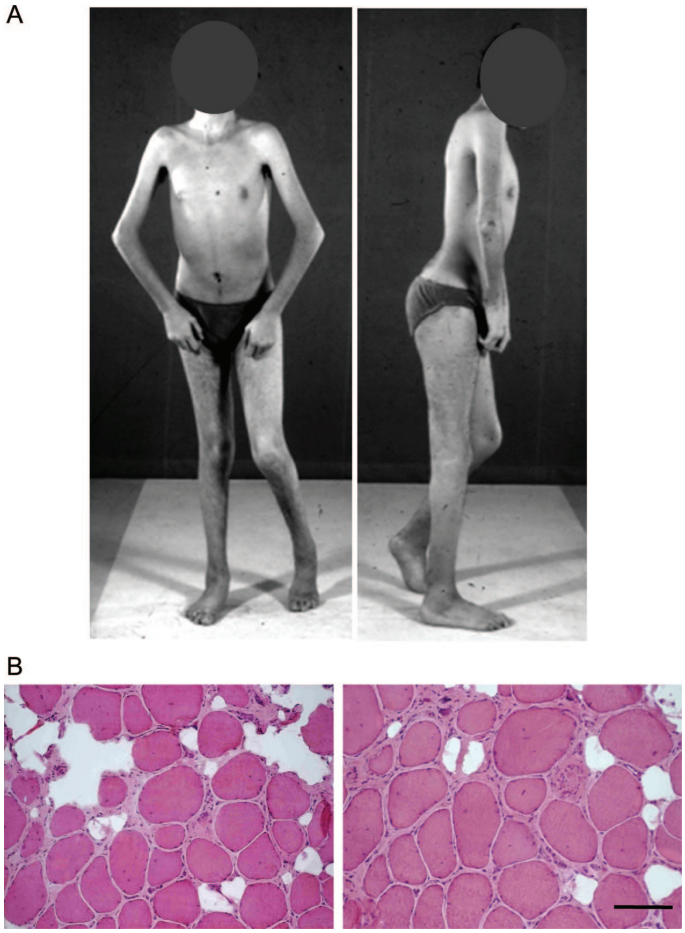

(A) Patient shows diffuse muscle wasting, flexion contractures of both elbows, forward abduction of shoulders, and flexion of fingers. There is fixed flexion of the trunk with lumbar hyperlordosis and marked flexion contractures of the knee and ankle joints in the left lower limb. (B) Transverse section of muscle biopsy from the index case (P1, left) and the affected sibling (P2, right), showing endomysial fibrosis, increased fatty connective tissue, variability of fiber size, and several internal nuclei. Hematoxylin and eosin staining. Bar, 200 μm.

METHODS

Patients. The index case presented at age 21 years for correction of equinus of the feet. Born to consanguineous parents, the patient had one affected and three unaffected siblings. Developmental motor milestones were normal. Slight difficulty in running and climbing stairs and Achilles tendon contractures were noted during early childhood, followed by progressive contractures of all joints, including jaws, spine, shoulders, elbows, wrists, fingers, hips, and knees. Distal joint hypermobility was never noticed. He underwent surgical elongation of Achilles tendons at 5 years and then for relapse at 16 years.

On neurologic examination, he was short with mild thoracolumbar scoliosis and accentuated lumbar lordosis. He had mild facial weakness with inability to completely bury the eyelashes, and a nasal voice. His muscles were thin and "sclerotic" on palpation. There was mild girdle and proximal limb weakness (grade 4/5 upper and 4/5 lower) and moderate distal weakness (grade 3/5 upper and lower). The most striking finding was the diffuse restriction of movements of all joints (figure 1A). Opening of the mouth was only 1.5 cm. Mobility of the cervical spine was limited in all planes and particularly in flexion. Elbows were bent to 120° and limited in further flexion to 30°. Shoulders were limited in abduction and in extrarotation and intrarotation. Hand fingers were flexed and limited in both extension and further flexion, and the wrist was also rigid. The thoracolumbar spine was rigid in both flexion and extension. The patient had flexion of the hips with limitation of passive extension. Knees were bent and restricted in both flexion and extension. He was severely and progressively limited by the contractures, whereas muscle weakness remained relatively mild. He was able to slowly walk and climb stairs. He showed moderate restriction on pulmonary function testing (forced vital capacity 1,820 mL, 44% predicted). Creatine kinase was twice the upper limit of normal.

The 17-year-old affected sibling had normal motor milestones, developed progressive contractures after age 4 years, and had Achilles tendons release bilaterally at 11 years and on the right feet at 17 years. She had stiff walking and climbed stairs slowly with the aid of railing. Contractures were diffuse and severe, involving the jaw, spine with marked limitation in neck flexion and rigid lumbar hyperlordosis, upper and lower girdles, and proximal and distal limb joints. Muscles were thin and of woody consistency on palpation. Forced vital capacity was 52% of predicted. Creatine kinase was 1.5 times the upper limit of normal.

In this family, the disease was linked with *COL6A1–COL6A2* cluster, whereas rigid spine muscular dystrophy 1 in 1p35–36 and *COL6A3* locus were excluded.[12]

The study was approved by the local ethics committee.

Muscle biopsy. Biopsies (tibialis anterior of index case and two age-matched healthy donors; quadriceps of affected sibling)

Figure 2 DNA sequencing and mutation analysis

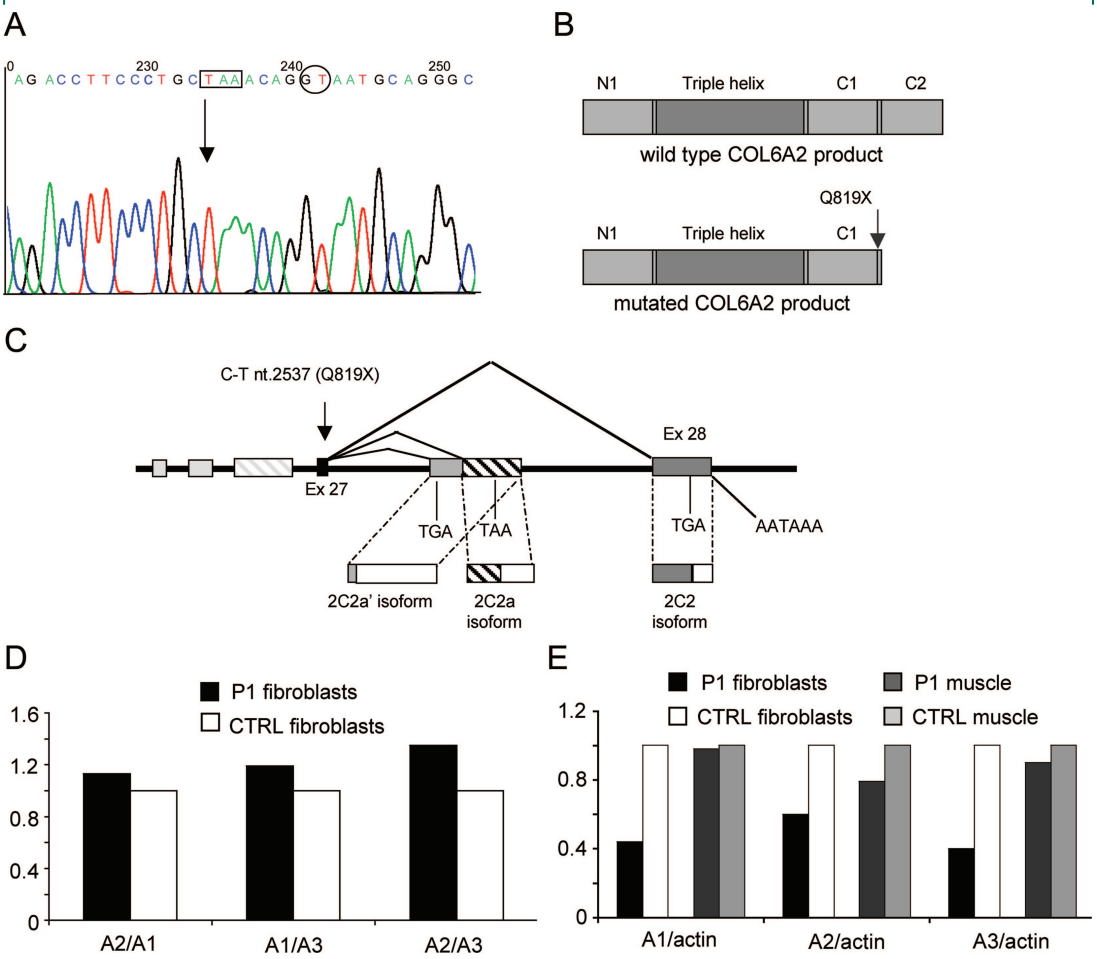

(A) Patient's chromatogram showing a homozygous C >T transition creating a TAA premature termination codon in exon 27 of the *COL6A2* gene. The sequence substitution is located seven nucleotides upstream of the donor splice site of intron 27. (B) Predicted effect of the identified mutation on *COL6A2* protein product. Top: Wild-type α2(VI) chain with N-terminal (N1), triple helical, and C-terminal (C1, C2) domains. Bottom: Truncated α2(VI) chain completely lacking the C2 domain. (C) Position of the identified mutation within exon 27, which represents the last common exon of the three 3′ alternatively spliced isoforms of *COL6A2* messenger RNA (mRNA). (D) Real-time PCR expression analysis in cultured fibroblasts from the patient, showing the absence of nonsense-mediated decay of the mutated *COL6A2* mRNA. The relative ratios of *COL6A2*/*COL6A1* (A2/A1), *COL6A1*/*COL6A3* (A1/A3), and *COL6A2*/*COL6A3* (A2/A3) mRNAs from control fibroblasts were normalized to 1. (E) Real-time PCR expression analysis in cultured fibroblasts and muscle tissue showing a global reduction of *COL6* transcripts in the patient, more marked in fibroblasts. The relative ratios of *COL6*/actin mRNAs in control tissues were normalized to 1.

were snap frozen and stored in liquid nitrogen. Unfixed 7-μm frozen sections were incubated with antibodies for laminin β1 (Chemicon), fibronectin, or collagen IV (both Sigma); double labeling with anti–collagen VI and perlecan (Chemicon) was performed as described.[13] Samples were observed with a Nikon fluorescence microscope. For ultrastructural analysis, biopsies were fixed with 2.5% glutaraldehyde in 0.1 M phosphate buffer for 3 hours and embedded in Epon E812.[14] Ultrathin sections were observed in a Philips EM 400 transmission electron microscope, operated at 100 kV.

Genomic sequence analysis. Genomic DNA was extracted from whole blood by standard methods. Exon 27 of *COL6A2* gene was amplified, including 3′ and 5′ intronic boundaries, and sequenced according to standard procedures. Oligonucleotide sequences were 5′-cagccgctgtctagcgtgag-3′ (A2.27 forward) and 5′-gccatctccctaaggagcagc-3′ (A2.27 reverse).

RNA purification and reverse transcriptase PCR. Total RNA was isolated from cultured fibroblasts and muscle biopsy by RNeasy (Qiagen) following manufacturer instructions. DNase treatment and complementary DNA (cDNA) synthesis were performed as previously described.[15] The 3′ RNA splicing isoforms of *COL6A2* (2C2 NM_001849, 2C2a NM_058174, 2C2a′ NM_058175) were analyzed by using a single forward primer (26F: 5′-gccctcaagtttgcctacgacc-3′) and different isoform-specific reverse primers (2C2R: 5′-ctcgtgcagactgtcgttgcc-3′; 2C2aR: 5′-catgggaagaggctgggagct-3′; 2C2a′R: 5′-cgagtcggtagaggaaatgcag-3′) according to standard PCR and sequencing procedures. To exclude the occurrence of exon 27 skipping, seminested PCR was performed on amplification product of primers 25F (5′-gtcatcgacagctccgagagc-3′) and 2C2R, using 26F as an internal primer.

Real-time PCR. Commercially available TaqMan expression assays (Applied Biosystems) were used for *COL6* genes (*COL6A1*: Hs00242448_m1; *COL6A2*: Hs00365167_m1; *COL6A3*: Hs00915111_m1) and for actin as a reference gene (*ACTB* Endogenous Control). Real-time PCR was performed in triplicate on the

Figure 3 Immunostaining and Western blot of muscle biopsies

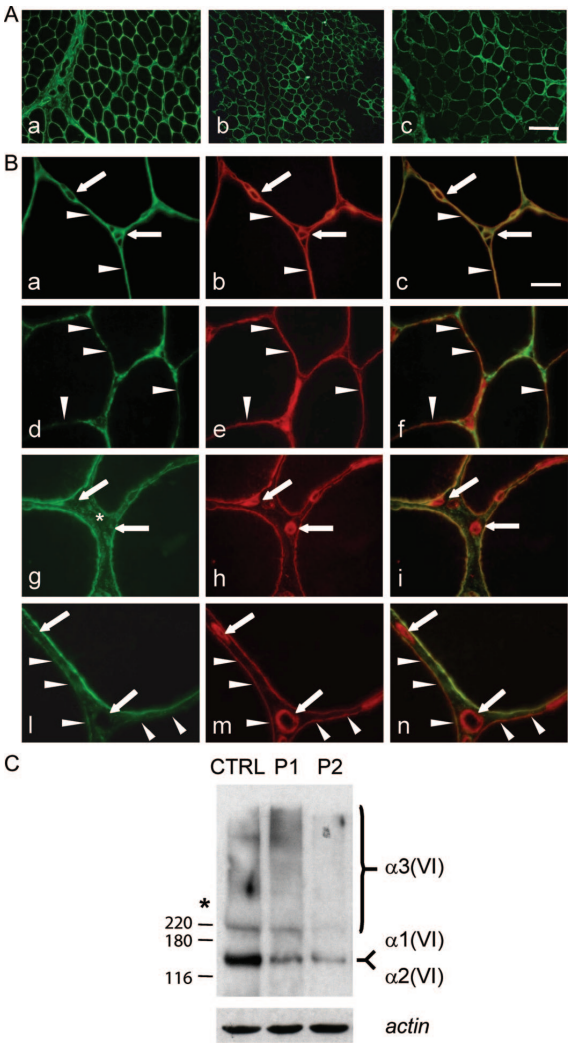

(A) Immunofluorescence of muscle sections from control donor (a) and patients (b, index case; c, affected sister). Collagen VI immunolabeling appears reduced and unevenly distributed in muscle of both patients when compared with control. Bar, 200 μm. (B) Labeling of collagen VI (a, d, g, and l), perlecan (b, e, h, and m), and overlaid images (c, f, i, and n) of control (a–c), index case (d–i), and affected sibling (l–n) muscle biopsies. In normal control, collagen VI and perlecan colocalize at the basement membrane of muscle fibers (arrowheads) and capillary (arrows), as demonstrated by yellow fluorescence in merge (c). In muscle biopsy of both patients, collagen VI labeling is reduced and discontinuous at basal lamina of muscle fibers (d and l, arrowheads) and absent at the basement membrane of capillaries (g and l, arrows), whereas perlecan immunostaining shows an intense and continuous labeling (e, h, and m), as in normal control (b). In overlaid images of the patients (f, i, and n), collagen and perlecan do not colocalize (red fluorescence) in some areas of myofiber basement membrane (f and n, arrowheads) and around capillary vessels (i and n, arrows). Bar, 40 μm. (C) Western blot analysis for collagen VI in muscle biopsies from control (CTRL), index case (P1), and affected sister (P2). Samples (10 μg total protein) were separated by electrophoresis under reducing condition on a 4% to 12% polyacrylamide gradient gel, and immunoblot was performed with an antibody recognizing the three chains. The migration and size in kilodaltons of the protein molecular weight markers are shown on the left. The migration positions of the collagen VI chains are indicated on the right: the α1(VI) and α2(VI) chains comigrate at approximately 140 kd, whereas the α3(VI) chain migrates with multiple bands at approximately 220 to 300 kd. Migration of the α3(VI) chain in muscle samples is distorted by the large amount of myosin heavy chains (asterisk). Control for loading was performed by immunoblot with an antibody for actin.

Applied Biosystems Prism 7300, using 10 ng fibroblast cDNA and default parameters. Evaluation of *COL6* cDNAs compared with actin and relative quantification of the three *COL6* cDNAs were performed by the comparative CT method (ΔΔCT Method; Applied Biosystems User Bulletin #2). cDNAs from control muscle and fibroblasts were used as calibrators.

Immunoblotting and immunoprecipitation of collagen VI. Twenty-micrometer frozen sections were prepared from biopsies and dissolved in a buffer containing protease inhibitors (lysis solution). Dermal fibroblasts were grown until confluence, incubated 24 hours in OPTI-MEM (Invitrogen) containing 0.25 mM L-ascorbic acid, and cell layer solubilized in lysis solution. Western blot was performed under reducing conditions (5% β-mercaptoethanol) by sodium dodecyl sulfate polyacrylamide gel electrophoresis onto 3% to 8% (wt/vol) gradient polyacrylamide gels, followed by transfer to Immobilon membrane (Millipore). Collagen VI was pulled down using a polyclonal antibody (H-200, Santa Cruz) conjugated to protein A-Sepharose, and the immunoprecipitated material was subjected to electrophoresis onto composite 2.4% acrylamide, 0.5% (wt/vol) agarose gels under nonreducing conditions. Collagen VI was detected with a polyclonal antibody recognizing all three chains (70-XR95, Fitzgerald Industries).

Immunoelectron microscopy and rotary shadowing. Fibroblasts were grown onto coverslips until 2 days after confluence in the presence of 0.25 mM L-ascorbic acid. Cells were incubated with a monoclonal anti–collagen VI antibody (Chemicon) diluted 1:25 with Dulbecco's modified Eagle medium and with 5-nm colloidal gold-labeled immunoglobulin G (Amersham). Rotary shadowing electron microscopy was performed as described.[16]

RESULTS

Identification of a homozygous nonsense *COL6A2* mutation. Sequence analysis of the index case revealed a homozygous C >T variation in *COL6A2* exon 27 (nucleotide 2537 of *COL6A2* messenger RNA [mRNA]; NM_001849), lying seven nucleotides upstream of the exon 27–intron 27 junction (figure 2A). This variation introduces a premature termination codon (Q819X) downstream of the C1 domain of the α2(VI) chain (figure 2B). The identified mutation is expected to affect all *COL6A2* splicing isoforms (figure 2C). Sequence analysis of proband family members revealed that the Q819X mutation was present in homozygosity in the affected sibling and in heterozygosity in the consanguineous healthy parents and in the three unaffected siblings.

Transcription analysis, performed on RNA isolated from muscle and fibroblasts of the proband, ruled out an effect of the C >T variation on incorporation of exon 27 into the mRNA and revealed correct amplification of α2C2, α2C2a, and α2C2a′ (data not shown).

Real-time PCR on fibroblast mRNA showed that the mutated *COL6A2* transcript did not undergo nonsense-mediated decay (NMD). When mRNA ratios of control fibroblasts were normalized to 1.0, the *COL6A2*/*COL6A1*, *COL6A2*/*COL6A3*, and *COL6A1*/*COL6A3* mRNA ratios of patient fibroblasts were 1.13,

Figure 4 Ultrastructural analysis

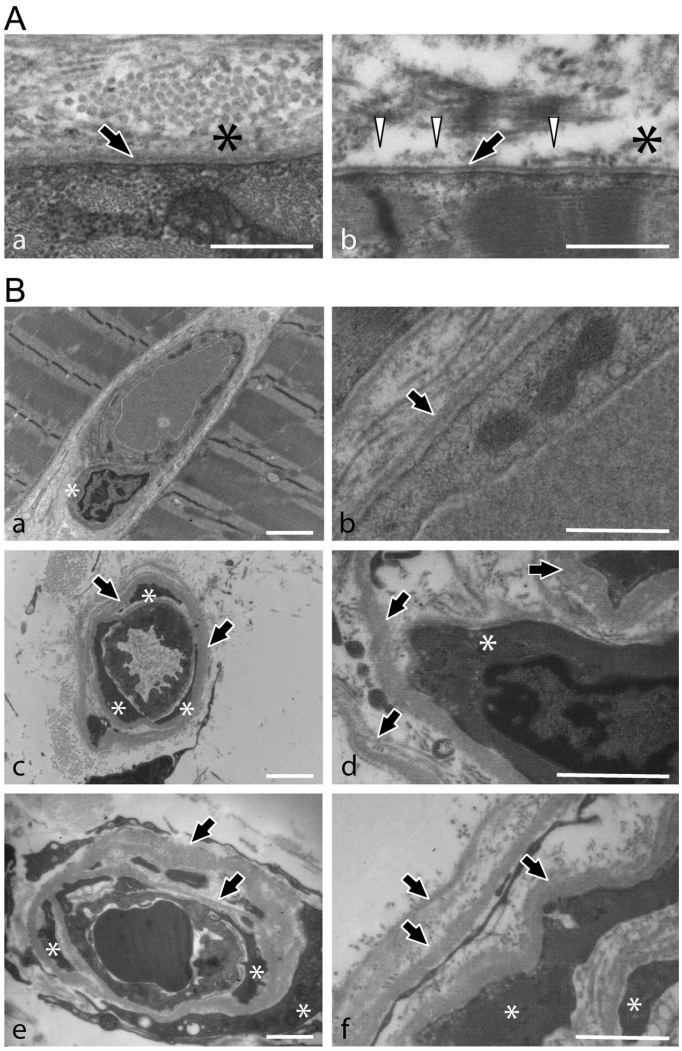

(A) Electron microscopy of muscle biopsy. In unaffected control (a), lamina reticulata (asterisk), made of microfibrils and fibrillar collagen, leans against lamina densa (arrow) of myofibers. In the muscle of patient (b), the lamina reticulata (asterisk) shows focal areas devoid of microfibrillar and fibrillar components, which appear as electron transparent areas (arrowheads). On the contrary, the lamina densa looks normal (arrow). Bar, 400 nm. (B) Electron microscope examination of capillaries in muscle of control (a and b) and patient (c–f). In normal control, capillary wall appears constituted by a single layer of endothelial cells and rare pericytes (asterisk); basement membrane (thickness range: 40–100 nm) is present at the abluminal side of the endothelial cells (b, arrow). Capillary vessels of the patient (c–f) appear encircled by several superimposed layers of basement membrane (arrows) of abnormal thickness (50–300 nm), which enclose several pericytes (asterisks). Bar, 400 nm.

1.35, and 1.19 (figure 2D). Analysis of the global amount of *COL6* transcripts revealed decreased *COL6* mRNA levels in patient samples (figure 2E).

Collagen VI deficiency in muscle biopsy. Muscle of both patients showed a myopathic pattern characterized by fibrosis, with proliferation of endomysial and perimysial connective tissue, variation of myofiber diameter, and internal nuclei (figure 1B). Laminin β1 was reduced in the extrajunctional basal lamina of myofibers, and fibronectin was increased around the capillary wall, whereas collagen IV showed a normal pattern (figure e-1 on the *Neurology*® Web site at www.neurology.org). Collagen VI showed a discontinuous distribution at the basal lamina of myofibers (figure 3A), but it was absent at the basal lamina of most endomysial and perimysial capillaries (figure 3B). Western blot confirmed decreased amounts of collagen VI in the muscle of patients (figure 3C).

At the ultrastructural level, defects were found in the basement membrane of muscle fibers and vessels. In approximately 6% of myofibers, focal areas of lamina reticulata showed a reduced density and were devoid of fibrillar and microfibrillar collagen, whereas lamina densa and plasma membrane appeared normal (figure 4A). Blood vessels showed increased thickness of the basement membrane (figure 4B). In some areas, basement membrane was composed of several layers enclosing pericytes. The number of pericytes was increased, and most of them displayed a phenotype resembling smooth muscle cells, consisting of extended contractile apparatus and long cytoplasmic processes (figure 4B).

Q819X mutation causes defects of collagen VI synthesis in cultured fibroblasts. Immunofluorescence of cultured fibroblasts from the index case revealed a decreased amount of collagen VI deposited in the ECM. The microfibrillar network appeared poorly organized, and abnormal aggregates were detected in the pericellular ECM. Collagen VI secreted by control fibroblasts developed an extensive three-dimensional network, and abnormal aggregates were never detected (figure 5A). Western blot of cell layer and medium samples confirmed a quantitative deficiency of collagen VI in patient cells. Moreover, a band migrating slightly faster than the normal α1(VI)/α2(VI) chains was detected in the patient cell layer. This abnormal band likely corresponded to the mutated α2(VI) chain, thus reflecting the truncating C-terminal mutation, as also confirmed by normal migration of the α1(VI) chain (figure 5B).

Collagen VI monomers and dimers were found in the cell layer of both control and patient cultures. On the contrary, tetramers were abundant in cell layer and medium from control, but they were barely detectable in patient samples. Moreover, monomers and dimers were abnormally detected in the medium of patient fibroblasts, albeit at low levels (figure 5C).

Electron microscope analysis of rotary shadowed fibroblasts revealed the presence of collagen VI microfilaments containing scarcely interconnected tetramers and displaying irregularly shaped globular

Figure 5 **Analysis of collagen VI in fibroblast cultures**

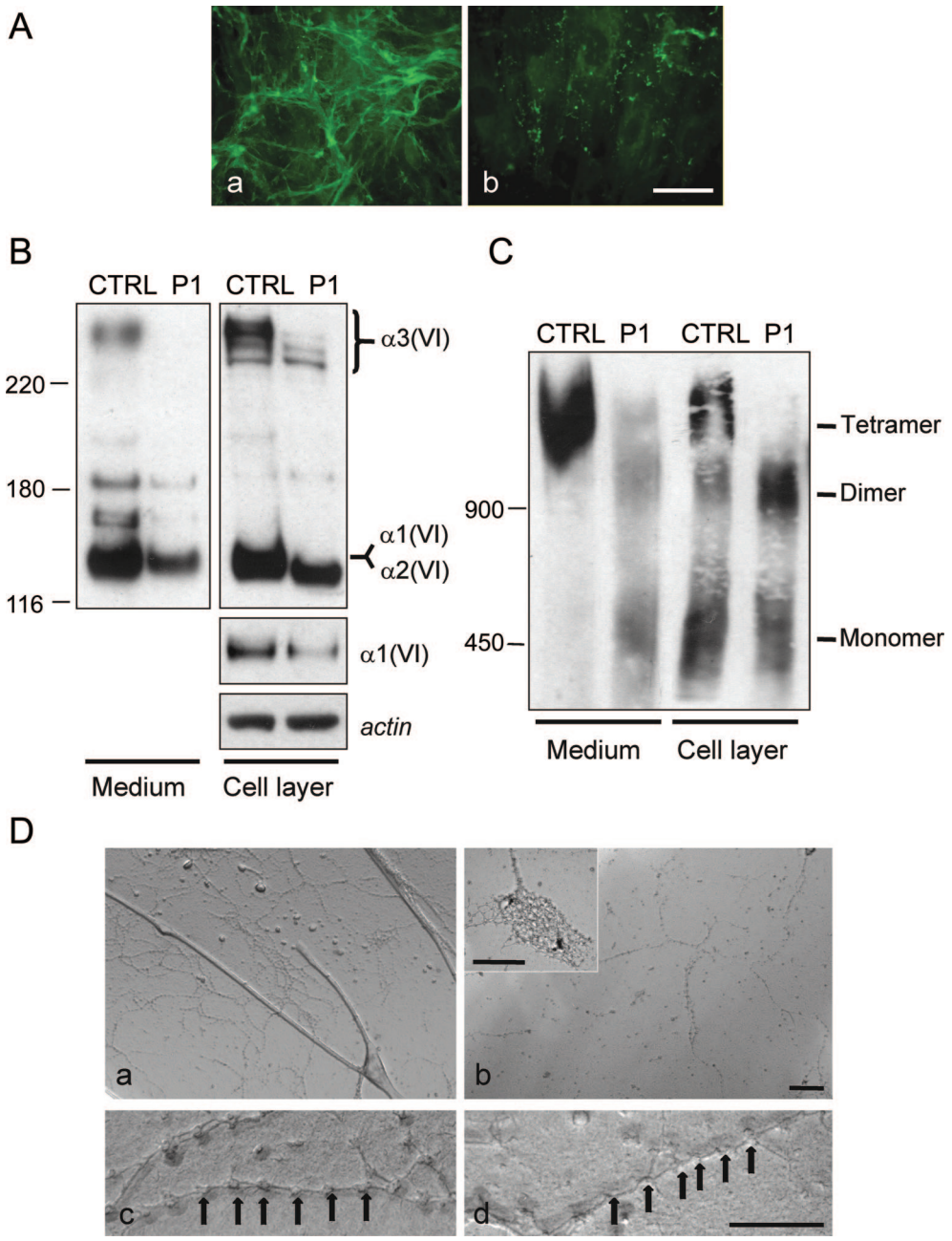

(A) Immunofluorescence of collagen VI on cultured fibroblasts from unaffected control (a) and patient (b) treated for 5 days with 0.25 mM ascorbic acid after confluence. Collagen VI secreted by control fibroblasts develops an extensive three-dimensional network. In the patient, secreted collagen VI appears reduced and abnormally organized with a dotlike appearance. Bar, 20 μm. (B) Electrophoretic analysis of collagen VI produced by cultured fibroblasts from control (CTRL) and patient (P1). Samples corresponding to cell layer (left panel, 10 μg) and culture medium (right panel, 20 μg) were separated by electrophoresis under reducing conditions on a 3% to 8% polyacrylamide gradient gel. Immunoblot was performed with an antibody recognizing the three chains (left and right panels) or with an antibody specific for the α1(VI) chain (middle left panel). The migration and size in kilodaltons of the protein molecular weight markers are shown on the left. The migration positions of the collagen VI chains are indicated on the right. Control for loading in cell extracts was performed by immunoblot with an antibody for actin (lower left panel). (C) Electrophoretic analysis of collagen VI assembly products in cultured fibroblasts from unaffected control (CTRL) and patient (P1). Cell layers and culture media were immunoprecipitated with an antibody against the α1(VI) chain. Samples were resolved by electrophoresis on a composite 0.5% agarose, 2.4% polyacrylamide gel under nonreducing conditions, and analyzed by immunoblot with an antibody recognizing the three chains. The migration and size in kilodaltons of the unreduced forms of fibronectin and laminin are shown on the left. The migration position of disulfide-bonded collagen VI monomers, dimers, and tetramers is indicated on the right. (D) Electron microscope analysis of replicas obtained by rotary shadowed cultured fibroblasts from control (a and c) and patient (b and d). Collagen VI microfilaments produced by patient cells appear constituted by several tetramers scarcely interconnected among themselves. Globular domains (arrows) display an irregular shape when compared with normal control. An abnormal disorganized aggregate of collagen VI microfilaments is shown in the inset of b. Panels a, b and c, d are at the same magnification. Bar, 400 nm.

regions. Typical hexagonal-like structures were absent, and fibrils composed by parallel-aligned microfilaments were barely detected. Additionally, some microfilaments showed an abnormal arrangement into circular arrays (not shown), and numerous disorganized aggregates were found beneath the cell membrane (figure 5D).

DISCUSSION We described two patients from a consanguineous family affected by myosclerosis myopathy due to a novel pathogenic *COL6A2* mutation. Myosclerosis myopathy is the fourth phenotype affecting skeletal muscles and connected with mutations of collagen VI genes. Type and distribution of contractures are distinguishing features of the four disorders. The "scleroatonic" UCMD is characterized by proximal contractures and distal laxity,[12] BM is characterized by distal contractures,[17] limb-girdle phenotype is characterized by late or no contractures,[11] and myosclerosis myopathy is characterized by early, diffuse, and progressive contractures resulting in severe limitation of movement of axial, proximal, and distal joints.

The Q819X substitution represents the first truncating mutation occurring in homozygosity in the C1 domain of the α2(VI) chain. Nonsense or frameshift mutations within *COL6A2* exons 24 through 28, encoding the C-terminal region of the α2(VI) chain, were previously described in UCMD patients, but they were either associated with a nontruncating mutation of the partnering allele (see also http://www.dmd.nl)[18] or predicted to cause a largely abnormal but only slightly shorter C2 domain.[19] In particular, mutations involving the small exon 27 were previously identified in two unrelated UCMD cases, in compound heterozygosity with truncating mutations within other exons.[18] Differently from the myosclerosis family, in both cases the mutation was associated with exon 27 skipping, causing an in-frame deletion of the C1 domain but leaving the C2 domain of the α2(VI) chain unaffected.

Moreover, and at a difference with more proximal mutations, the position of Q819X within exon 27 predicts that the aberrant *COL6A2* transcript is able to escape the NMD pathway, a surveillance mechanism that typically degrades transcripts containing premature termination codons. In fact, the mammalian NMD system cannot distinguish premature termination codons in the penultimate exon and located less than 55 bp from the last intron, as happens for the Q819X mutation.[20] Indeed, we have shown that the Q819X transcript is stable in patient fibroblasts and is translated into a truncated α2(VI) chain, lacking the sole C2 domain.

Exon 27, in which the Q819X mutation lies, represents the last common exon of the 3′ splicing isoforms of *COL6A2* generated by recognition of alternative splice sites within intron 27 and using different polyadenylation sites.[21] Thus, the Q819X mutation is expected to abolish this 3′ variability. Protein data showed that α2C2 is the only isoform detectable in tissue extracts,[21] and the significance of the C-terminal α2(VI) variability, as well as the presence of α2C2a and α2C2a′ isoforms within collagen VI molecules, remains unknown.

The Q819X mutation provided a unique opportunity to investigate the effects of selective loss of α2(VI) C2 domain on collagen VI biosynthesis and assembly. In normal conditions, collagen VI chains associate into triple-helical monomers that are further assembled into disulfide-bonded dimers and tetramers. After secretion, tetramers link together, forming a characteristic network of beaded microfilaments.[22-24] Studies to date indicate that assembly and secretion of collagen VI is possible only if all three chains are present.[22,24,25] The truncated α2(VI) chain of our patient was able to associate with α1(VI) and α3(VI) and form collagen VI molecules, thus implying that the α2(VI) C2 domain is not essential for monomer formation. This is in agreement with previous studies using recombinant constructs, where α2(VI) polypeptides containing the C1 but not the C2 domain were fully capable of forming monomers.[26,27]

Our nonreduced electrophoresis analysis indicates that assembly of collagen VI molecules into higher order structures is impaired in patient cells, with a markedly decreased amount of tetramers matched by an unusual accumulation of dimers. These findings may be the consequence of a defective assembly of dimers into tetramers or a structural instability of tetramers lacking the α2(VI) C2 domain. Electron microscopy confirmed that patient cells secrete structurally abnormal collagen VI products also affecting the three-dimensional organization of microfilaments, which appear scarcely interconnected and have a decreased ability to form extensive networks.

These findings suggest that the α2(VI) C2 domain contributes to supermolecular assembly and organization of collagen VI. Studies on collagen VI biosynthesis in UCMD patients with COL6A2 mutations revealed different scenarios.[16,28,29] A UCMD patient was described who carried two homozygous missense mutations in the α2(VI) C2 domain and had complete absence of collagen VI in the ECM.[28] Another UCMD patient had two compound heterozygous mutations in COL6A2 that caused loss of the entire C-terminal region and part of the triple helical domain of the α2(VI) chain.[16] His mutant α2(VI) chains formed monomers with the other

chains, but further assembly into dimers and tetramers was severely impaired.[16] Interestingly, in this latter UCMD patient, mutated collagen VI did not correctly localize at the myofiber basement membrane.[6] However, this mislocalization is not restricted to COL6A2 mutations,[29] suggesting that different collagen VI chains contribute to the basement membrane–interstitium anchorage.[30,31]

In both myosclerosis patients, muscle biopsy showed a partial collagen VI deficiency at the myofiber basement membrane, as described in some UCMD cases.[13,32] However, collagen VI was absent around most endomysial/perimysial capillaries. This represents a peculiarity of these patients and is consistent with the ultrastructural alterations detected in the biopsy. Electron microscopy showed a peculiar combination of basement membrane and pericyte alterations, with thickening and duplication of capillary basement membrane and proliferation of pericytes. Thickening of capillary basement membrane was reported in UCMD patients with complete lack of collagen VI, whereas alterations of pericytes were never reported in UCMD.[33] Capillary basement membrane thickening was observed in Duchenne muscular dystrophy[34] and inflammatory myopathies,[35] being considered an aspect of vascular regeneration occurring during microcirculation remodelling.[34] Unlike in our patients, in those conditions pericytes appeared relatively unaffected. Pericytes lie in close contact with endothelial cells, contributing to ECM synthesis including basement membrane components, and they may increase the endothelial barrier function, as suggested by in vitro coculture experiments.[36] In the myosclerosis patients, the combination of basement membrane thickening and abnormal pericyte proliferation may affect metabolite and oxygen delivery, thus contributing to myofiber degeneration.

Our results demonstrate that the affected siblings of this consanguineous family have characteristic features of myosclerosis myopathy and carry a homozygous *COL6A2* mutation responsible for a peculiar pattern of collagen VI defects. Based on these findings, myosclerosis myopathy should be considered a collagen VI disorder allelic to UCMD and BM.

ACKNOWLEDGMENT

The authors thank the patients who participated in the study.

Received March 20, 2008. Accepted in final form July 7, 2008.

REFERENCES

1. Duchenne GBA. Recherches sur la paralysie musculaire pseudohypertrophique au paralysie myosclerotique. Arch Gen Med 1868:552–588.
2. Lowenthal A. A new heredodegenerative group: heredofamilial myoscleroses [in French]. Acta Neurol Psychiatr Belg 1954;54:155–165.
3. Lowenthal A. Myositis IV congenital and familial form of generalized muscular sclerosis with blepharoptosis (contribution to the study of congenital diseases of muscles and connective tissue) [in French]. Acta Neurol Psychiatr Belg 1952;52:141–155.
4. Bradley WG, Hudgson P, Gardner-Medwin D, Walton JN. The syndrome of myosclerosis. J Neurol Neurosurg Psychiatry 1973;36:651–660.
5. Jöbsis GJ, Keizers H, Vreijling JP, et al. Type VI collagen mutations in Bethlem myopathy, an autosomal dominant myopathy with contractures. Nat Genet 1996;14:113–115.
6. Camacho Vanegas O, Bertini E, Zhang RZ, et al. Ullrich scleroatonic muscular dystrophy is caused by recessive mutations in collagen type VI. Proc Natl Acad Sci USA 2001; 98:7516–7521.
7. Higuchi I, Shiraishi T, Hashiguchi T, et al. Frameshift mutation in the collagen VI gene causes Ullrich's disease. Ann Neurol 2001;50:261–265.
8. Higuchi I, Suehara M, Iwaki H, et al. Collagen VI deficiency in Ullrich's disease. Ann Neurol 2001;49:544.
9. Bethlem J, Wijngaarden GK. Benign myopathy, with autosomal dominant inheritance: a report on three pedigrees. Brain 1976;99:91–100.
10. Ullrich O. Kongenitale, atonisch-sklerotische Muskeldystrophie. Monatsschr Kinderheilkd 1930;47:502–510.
11. Scacheri PC, Gillanders EM, Subramony SH, et al. Novel mutations in collagen VI genes: expansion of the Bethlem myopathy phenotype. Neurology 2002;58:593–602.
12. Pepe G, Bertini E, Bonaldo P, et al. Bethlem myopathy (BETHLEM) and Ullrich scleroatonic muscular dystrophy: 100th ENMC international workshop, 23–24 November 2001, Naarden, The Netherlands. Neuromuscul Disord 2002;12:984–993.
13. Squarzoni S, Sabatelli P, Bergamin N, et al. Ultrastructural defects of collagen VI filaments in an Ullrich syndrome patient with loss of the alpha3(VI) N10-N7 domains. J Cell Physiol 2006;206:160–166.
14. Sabatelli P, Columbaro M, Mura I, et al. Extracellular matrix and nuclear abnormalities in skeletal muscle of a patient with Walker-Warburg syndrome caused by POMT1 mutation. Biochim Biophys Acta 2003;1638:57–62.
15. Gualandi F, Rimessi P, Trabanelli C, et al. Intronic breakpoint definition and transcription analysis in DMD/BMD patients with deletion/duplication at the 5′ mutation hot spot of the dystrophin gene. Gene 2006;370:26–33.
16. Zhang RZ, Sabatelli P, Pan TC, et al. Effects on collagen VI mRNA stability and microfibrillar assembly of three COL6A2 mutations in two families with Ullrich congenital muscular dystrophy. J Biol Chem 2002;277:43557–43564.
17. Pepe G, de Visser M, Bertini E, et al. Bethlem myopathy (BETHLEM) 86th ENMC international workshop, 10–11 November 2000, Naarden, The Netherlands. Neuromuscul Disord 2002;12:296–305.
18. Lampe AK, Bushby KM. Collagen VI related muscle disorders. J Med Genet 2005;42:673–685.
19. Okada M, Kawahara G, Noguchi S, et al. Primary collagen VI deficiency is the second most common congenital muscular dystrophy in Japan. Neurology 2007;69:1035–1042.

20. Khajavi M, Inoue K, Lupski JR. Nonsense-mediated mRNA decay modulates clinical outcome of genetic disease. Eur J Hum Genet 2006;14:1074–1081.
21. Saitta B, Stokes DG, Vissing H, Timpl R, Chu ML. Alternative splicing of the human alpha 2(VI) collagen gene generates multiple mRNA transcripts which predict three protein variants with distinct carboxyl termini. J Biol Chem 1990;265:6473–6480.
22. Colombatti A, Bonaldo P. Biosynthesis of chick type VI collagen, II: processing and secretion in fibroblasts and smooth muscle cells. J Biol Chem 1987;262:14461–14466.
23. Timpl R, Chu ML. Microfibrillar collagen type VI. In: Yurchenco PD, Birk DE, Mecham RP, eds. Extracellular Matrix Assembly and Structure. Orlando, FL: Academic Press, 1994:208–242.
24. Colombatti A, Mucignat MT, Bonaldo P. Secretion and matrix assembly of recombinant type VI collagen. J Biol Chem 1995;270:13105–13111.
25. Lamande SR, Bateman JF, Hutchison W, et al. Reduced collagen VI causes Bethlem myopathy: a heterozygous COL6A1 nonsense mutation results in mRNA decay and functional haploinsufficiency. Hum Mol Genet 1998;7:981–989.
26. Ball SG, Baldock C, Kielty CM, Shuttleworth CA. The role of the C1 and C2 a-domains in type VI collagen assembly. J Biol Chem 2001;276:7422–7430.
27. Ball S, Bella J, Kielty C, Shuttleworth A. Structural basis of type VI collagen dimer formation. J Biol Chem 2003;278:15326–15332.
28. Baker NL, Morgelin M, Peat R, et al. Dominant collagen VI mutations are a common cause of Ullrich congenital muscular dystrophy. Hum Mol Genet 2005;14:279–293.
29. Pan TC, Zhang RZ, Sudano DG, et al. New molecular mechanism for Ullrich congenital muscular dystrophy: a heterozygous in-frame deletion in the COL6A1 gene causes a severe phenotype. Am J Hum Genet 2003;73:355–369.
30. Ishikawa H, Sugie K, Murayama K, et al. Ullrich disease due to deficiency of collagen VI in the sarcolemma. Neurology 2004;62:620–623.
31. Kawahara G, Okada M, Morone N, et al. Reduced cell anchorage may cause sarcolemma-specific collagen VI deficiency in Ullrich disease. Neurology 2007;69:1043–1049.
32. Petrini S, D'Amico A, Sale P, et al. Ullrich myopathy phenotype with secondary ColVI defect identified by confocal imaging and electron microscopy analysis. Neuromuscul Disord 2007;17:587–596.
33. Niiyama T, Higuchi I, Hashiguchi T, et al. Capillary changes in skeletal muscle of patients with Ullrich's disease with collagen VI deficiency. Acta Neuropathol 2003;106:137–142.
34. Hudlicka O, Brown MD, Egginton S. Microcirculation in muscle. In: Engel AG, Franzini-Armstrong C, eds. Myology. Vol 1. New York: McGraw-Hill, 2003:525.
35. Vlodavsky EA, Ludatscher RM, Sabo E, Kerner H. Evaluation of muscle capillary basement membrane in inflammatory myopathy: a morphometric ultrastructural study. Virchows Arch 1999;435:58–61.
36. Balabanov R, Dore-Duffy P. Role of the CNS microvascular pericyte in the blood-brain barrier. J Neurosci Res 1998;53:637–644.

1.2 Novel splicing mutations in UCMD patients.

We studied four UCMD patients carrying unusual mutations of COL6 genes affecting RNA splicing. Our data showed a strict correlation between transcript and protein levels, indicating that the decreased level of a single collagen VI chain, perturbing the stoichiometric balance of triple helical monomers, is followed by a proportional decrease of the global amount of collagen VI secreted into the extracellular matrix.

HUMAN MUTATION Mutation in Brief #1065, 30:E662-E672 (2009) Online

MUTATION IN BRIEF HUMAN MUTATION

OFFICIAL JOURNAL HGVS HUMAN GENOME VARIATION SOCIETY www.hgvs.org

Identification and Characterization of Novel Collagen VI Non-Canonical Splicing Mutations Causing Ullrich Congenital Muscular Dystrophy

Elena Martoni[1]*, Anna Urciuolo[2]*, Patrizia Sabatelli[3], Marina Fabris[1], Matteo Bovolenta[1], Marcella Neri[1], Paolo Grumati[2], Adele D'Amico[4], Marika Pane[5], Eugenio Mercuri[5], Enrico Bertini[4], Luciano Merlini[1-6], Paolo Bonaldo[2], Alessandra Ferlini[1], and Francesca Gualandi[1]

* these authors equally contributed to the work

[1] Department of Experimental and Diagnostic Medicine, Section of Medical Genetics, University of Ferrara; [2] Department of Histology, Microbiology and Medical Biotechnologies, University of Padova; [3] IGM-CNR, Unit of Bologna c/o IOR, Bologna;[4] Unit of Molecular Medicine, Department of Laboratory Medicine, Bambino Gesu' Hospital, Rome; [5] Department of Child Neurology and Psychiatry, Catholic University, Rome; [6] Laboratory of Biology, IOR, Bologna

*Correspondence to: Francesca Gualandi, Department of Experimental and Diagnostic Medicine, Section of Medical Genetics, University of Ferrara, Italy Tel; + 39 0532 974497 Fax: + 39 0532236157 E-mail: gdf@unife.

Contract grant sponsor: Telethon Foundation Italia; Contract grant number: GGP07004 (to FG)

Communicated by Peter K. Rogan

ABSTRACT: Splicing mutations occurring outside the invariant GT and AG dinucleotides are frequent in disease genes and the definition of their pathogenic potential is often challenging. We have identified four patients affected by Ullrich congenital muscular dystrophy and carrying unusual mutations of COL6 genes affecting RNA splicing. In three cases the mutations occurred in the COL6A2 gene and consisted of nucleotide substitutions within the degenerated sequences flanking the canonical dinucleotides. In the fourth case, a genomic deletion occurred which removed the exon8-intron8 junction of the COL6A1 gene. These mutations induced variable splicing phenotypes, consisting of exon skipping, intron retention and cryptic splice site activation/usage. A quantitative RNA assay revealed a reduced level of transcription of the mutated in-frame mRNA originating from a COL6A2 point mutation at intronic position +3. At variance, the transcription level of the mutated in-frame mRNA originating from a genomic deletion which removed the splicing sequences of COL6A1 exon 8 was normal. These findings suggest a different transcriptional efficiency of a regulatory splicing mutation compared to a genomic deletion causing a splicing defect. ©2009 Wiley-Liss, Inc.

KEY WORDS: Ullrich congenital muscular dystrophy, collagen VI, COL6A1, COL6A2, non-canonical splicing mutations

INTRODUCTION

Ullrich congenital muscular dystrophy (UCMD; MIM# 254090) is a severe disorder, featured by early-onset profound muscle weakness, proximal joint contractures and striking distal hyperlaxity (Bertini and Pepe, 2002). Both recessively inherited and *de novo* mutations of collagen VI genes lead to UCMD (Baker et al., 2005). The milder Bethlem myopathy (BM; MIM# 158810) is invariably associated to dominant mutations. Starting from the

original reports describing BM and UCMD (Jöbsis et al., 1996; Camacho Vanegas et al., 2001), more than 100 pathogenic variations have been described in COL6 genes, highlighting a great allelic heterogeneity and delineating some recurrent mutational mechanisms. Missense substitutions disrupting the Gly-Xaa-Yaa motif of the highly conserved triple helical domain represent a frequent pathogenic mechanism for both UCMD and BM patients (Lampe et al., 2005a, 2005b; Pace et al., 2008). Besides this, splice site mutations causing exon skipping have emerged as particularly common in COL6 genes. Skipping of exon 14 in the COL6A1 gene and of exon 16 in the COL6A3 gene were reported as the most common mutational mechanisms in BM and UCMD patients, respectively (Lampe et al., 2008).

Splicing-relevant base pair substitutions constitute about 9.5% of all mutations causing human inherited diseases (Human Gene Mutation Database at www.hgmd.org; Stenson et al., 2003). Variations affecting the obligate GT and AG dinucleotides are obviously pathogenic and comprise 64% of mutations at donor splice-sites and 77.4% of mutations at acceptor splice-sites. Mutations affecting the consensus sequences flanking the almost invariant GT and AG dinucleotides are equally frequent, but much less obvious in term of associated splicing impairment (Krawczak et al., 2007). In fact, these intronic cis elements are weakly conserved and their degenerated nature implies that the distinction between SNPs and disease-associated mutations can be challenging, especially for highly polymorphic genes (Baralle and Baralle, 2005).

In the recent years, high-throughput genomic sequencing was performed by different groups for all three COL6 genes and in large cohorts of BM and UCMD patients (Lampe et al., 2005a, 2005b; Okada et al., 2007). These extensive approaches have revealed the extremely high frequency of polymorphic changes both within exons and in the intronic regions of COL6 genes. Stringent criteria for the definition of pathogenicity have been adopted and intronic variations located at position +/-4 or more nucleotides away from the splice sites were provisionally classified as probable polymorphisms (Lampe et al., 2005b).

We have identified and finely characterized four non-canonical mutations of COL6 genes, occurring in UCMD patients and affecting splicing. In three cases the mutations occurred in the COL6A2 gene and were localized within degenerated sequences flanking the obligate GT-AG dinucleotides. In the fourth case a genomic deletion occurred, exactly removing the exon8-intron8 splicing border of the COL6A1 gene.

MATERIALS AND METHODS

Genomic analysis

Genomic DNA from UCMD patients and unaffected parents was extracted from peripheral lymphocytes after informed consent by standard methods. PCR primers (sequences are available upon request) were designed to amplify all the 107 exons of COL6 genes and their flanking intronic regions. Amplified fragments were directly sequenced using BigDye Terminator v3.1 Cycle sequencing system on ABI 3130 automated Genetic Analyzer (Applied Biosystems, Foster City, CA). Bioinformatic analysis of mutated splice sites was performed by different tools: BDGP available at http.//www.fruitfly.org/seq_tools/splice.html; Maxent available at http.//genes.mit.edu/burgelab/maxent/Xmaxentscan_scoreseq.html and ASSA available at https://splice.uwo.ca.

RNA analysis

Total RNA was isolated from confluent fibroblasts by using RNeasy Kit (QIAGEN, Chatsworth, CA) and reverse transcribed by using High Capacity cDNA Reverse Transcription Kit (Applied Biosystem, Foster City, CA). RT-PCR was performed as previously described (Merlini et al., 2008). Sequence of primers is available upon request. All RT-PCR products, corresponding to wild-type and aberrant splicing products, were gel purified and sequenced either directly or after cloning into pCRII -TOPO vector (Invitrogen).

In order to quantify the steady state level of transcripts, commercially available TaqMan expression assays (Applied Biosystems) were used for COL6 genes (*COL6A1*: Hs00242448_m1 Ex20/21; *COL6A2*: Hs00242484_m1 (ex 27-28) and for beta actin (*ACTB* Endogenous Control). Real-time PCR was performed in triplicate on the Applied Biosystems Prism 7300 system, using 10 ng of cDNA and default parameters. For relative quantification the ΔΔCT Method (Applied Biosystems User Bullettin #2) was utilized. cDNAs from control fibroblasts served as calibrator.

The relative proportion among different splicing variants induced by the identified mutations was assessed by fluorescent RT-PCR (primer sequences are available upon request) on an ABI 3130 denaturing capillary system

(Applied Biosystems). The fragments size, values of peak height and area were determined by using the GeneScan software.

Immunostaining of fibroblasts

Skin fibroblasts from UCMD patients and control were grown onto coverslips in Dulbecco's modified Eagles medium supplemented with 20% fetal calf serum and antibiotics. When confluent, the medium was enriched with 0.25 mM L-ascorbic acid (SIGMA) and changed every two days. After 48h and 10 days of ascorbic acid treatment, coverslips were incubated with a mouse monoclonal anti-collagen VI antibody (MAB1944, Chemicon). The immunoreaction was detected by incubation for 1 h with a secondary FITC-conjugated anti-mouse antibody (DAKO). All samples were double-labeled with a rat anti-perlecan antibody (Chemicon), followed by incubation with a TRITC-conjugated anti-rat antibody (SIGMA).

Protein analysis by western blot

Dermal fibroblasts were grown to confluence and incubated 24 h in OPTI-MEM (Invitrogen) in the presence of 0.25 mM L-ascorbic acid (Sigma). Medium was collected; cell layer was solubilized in a lysis solution containing protease inhibitors and collected with a scraper. The cell layer and media fractions were quantified with BCA Protein Assay Kit (Pierce). Western blot was performed under reducing conditions (5% β-mercaptoethanol) by SDS-PAGE onto 6% polyacrylamide gels, followed by transfer to Immobilon membrane (Millipore). Collagen VI was detected with a polyclonal antibody recognizing all three chains (70-XR95, Fitzgerald Industries).

RESULTS

The four enrolled patients fulfilled clinical criteria for the diagnosis of UCMD (Pepe et al., 2002). Clinical and molecular data are summarized in Table 1.

UCMD1 carries a heterozygous de novo A>C variation at position +3 of COL6A2 intron 5

Bioinformatic analysis indicated an effect of the +3 intronic COL6A2 variation in weakening the intron 5 donor splice site (wild-type: BDGP score 0.99, Maxent score 10.57, ASSA Ri 10.5; mutated: BDGP score 0.82, Maxent score 6.80, ASSA Ri 5.7). cDNA sequencing revealed the occurrence of the in-frame exon 5 skipping in part of COL6A2 transcript. PCR amplification with a forward primer within exon 5 and a reverse primer within exon 16, followed by sequencing, showed a monoallelic expression of an exon 14 common polymorphism (Ser399Asn), found to be heterozygous at the genomic level. This result implies that transcripts including exon 5 originate only from the wild-type allele and that mRNAs originating from the +3 mutated allele invariably skips exon 5. Fragment analysis showed that the two alleles are unequally represented with a 2.5:1 ratio between the wild type transcript and the one with exon 5 skipping (Fig 1A).

UCMD 2 is a compound heterozygous for a G>A variation at position +5 of COL6A2 intron 8 and the nonsense mutation R366X in COL6A2 exon 12

Bioinformatic analysis showed that the COL6A2 intron 8 +5 G>A substitution either abolished the canonical donor site (BDGP program) or strongly reduced the site score (Maxent score from 9.16 to 5.73; ASSA Ri from 10.7 to 7.2). Two COL6A2 transcripts were detected by RT-PCR and sequencing, one with normal exon 8-exon 9 splice junction and the other with retention of the entire intron 8 and containing an in-frame premature stop codon at nucleotide c.927+16. cDNA sequencing showed pseudo-homozygosity for the wild-type exon 12 sequence, indicating that the Arg366X mutated transcript (c. 1096 C>T) undergoes non-sense mediated decay. Consequently, both COL6A2 splicing variants, with correct exon8-exon9 junction and with intron 8 retention, originate from the +5 mutated allele. Fragment analysis showed a 5.7:1 ratio between the correctly joined transcript and the one retaining intron 8 (Fig 1A).

Table 1: Clinical features of the UCMD patients and summary of molecular data

Features	Patient			
	UCMD1	**UCMD2**	**UCMD3**	**UCMD4**
Sex	M	M	F	M
Age at review, yr	3	8	13	5
Presentation	Birth, arthrogryposis, distal laxity	Birth, floppiness, distal laxity, elbow and knee contractures	Birth, hip dislocation, floppiness	Birth, talipes, floppiness
Max motor ability	Walked 18 mo-present	Walked 15 mo-present	Walked 20 mo-6 yrs	Never walked
Contractures	Elbows, ankles	Elbows, ankles	Elbows, knees, ankles, spine	Jaw, elbows, knees, ankles, spine
Distal laxity	Moderate	Moderate	Mild	Mild
Skin phenotype	Follicular hyperplasia	None	Follicular hyperplasia	Follicular hyperplasia
Spine involvement	None	Lumbar lordosis	Scoliosis, kyphosis	None
Creatine kinase level*	2 x	2.5 x	3 x	1.5 x
Mechanical ventilation	None	None	11 yrs-present	None
Genomic Sequencing	Het COL6A2 intron 5 c.801+3A>C	Het COL6A2 exon 12 c.1096 C>T; Het COL6A2 intron 8 c.927+5 G>A	Het COL6A1 exon8 c.798_804+8del 15	Hom COL6A2 intron25 c.1961-9 G>A
Inheritance	*De novo*	N/A	*De novo*	Heterozygous parents
cDNA Sequencing	Het deletion of exon 5	Pseudo-het retention intron 8	Het deletion of exon8	Pseudo-het ins of 7nt ex25-26
Quantification of COL6 transcripts	COL6A2 reduced (65%)	COL6A2 strongly reduced (6%)	COL6A1 normal levels	COL6A2 reduced (20%)
Predicted Protein Consequence	p.Cys246_Lys 267del (N-terminal domain)	p. Arg366X, NMD; p. Lys 318 fsX6 (N-terminal domain)	p.Pro 254_Glu268 del (N-terminal TH domain)	p. Thr 656fsX18 (C1 domain)
Collagen VI (WB)	Mild decrease in cell layer and medium	Marked decrease in cell layer and medium	Mild decrease in cell layer, marked decrease in medium	Marked decrease in cell layer, mild decrease in medium
Collagen VI (IF)	Mildly reduced	Severely reduced	Mildly reduced	Significantly reduced

*Creatine kinase level: times the upper normal value. The DNA mutation numbering is based on cDNA sequence with a "c." symbol before the number with +1 corresponding to the A of the ATG translation initiation codon in the respective reference sequence (COL6A1 GenBank Refseq NM_001848.2; COL6A2 GenBank Refseq NM_001849.3); hom, homozygous; het, heterozygous; IF immunofluorescence; mo, months; N/A, not available; NMD, nonsense mediated decay; TH, triple helix; WB, western blot; yr, year.

UCMD 3 carries a heterozygous de novo 15 nucleotides deletion involving COL6A1 exon 8-intron 8 junction

The COL6A1 deletion identified in UCMD 3 patient involves 7 exonic and 8 intronic nucleotides. cDNA sequencing showed the in-frame deletion of exon 8 in part of COL6A1 transcript. The relative amount of wild-type and deleted transcript was 1:1.04 at fragment analysis (Fig 1A).

UCMD 4 carries a homozygous G>A variation at position -9 of COL6A2 intron 25, inherited from healthy heterozygous parents

Bioinformatic analysis showed a decreased score of the intron 25 canonical acceptor site in the presence of the intronic COL6A2 variation (wild-type: BDGP score 0.76, Maxent score 6.60, ASSA Ri 5.1; mutated: BDGP score 0.65, Maxent score -0.01, ASSA Ri 4.8). Furthermore, the G>A variation creates an AG dinucleotide which is recognized both by Maxent (4.61 score) and ASSA tools (final Ri 1.3). This novel site is predicted (by ASSA tool) as much weaker than the natural site. Nevertheless, sequence analysis of COL6A2 transcript revealed that the splicing machinery indeed partially recognize this acceptor site, with the insertion of 7 intronic nucleotides and frameshifting. Part of the transcript retains a correct exon 25 -exon 26 junction. Fragment analysis showed a 5.5:1 ratio between the normally spliced transcript and the aberrant out-of-frame messenger (Fig 1A).

Effects of non-canonical splicing mutations on the steady state levels of COL6A1 and COL6A2 mRNAs

The ratio between steady state levels of COL6A2 and COL6A1 messengers in the four UCMD patients is reported in Fig 1B. COL6A2 transcript was reduced to 65% of COL6A1 in UCMD1, to 6% in UCMD2 and to 20% in UCMD4. In UCMD 3, carrying a genomic deletion instead of a regulatory splicing mutation, the ratio between the levels of COL6A2 and COL6A1 transcripts in fibroblasts was similar to control (1:1.06).

Immunofluorescence analysis of collagen VI in fibroblast cultures

After 48h of treatment with ascorbic acid, the amount of collagen VI secreted and assembled in the extracellular matrix was variable, ranging from mildly reduced in patients UCMD1 and UCMD3, to significantly decreased in UCMD4 and severely reduced in UCMD2 (Fig 2A). In all four UCMD cultures, the organization of collagen VI network appeared coarse and several spot-like collagen VI abnormal aggregates could be detected in the extracellular matrix. Moreover, in UCMD1 and UCMD3 cultures, several fibroblasts showed intracellular labeling, suggesting a possible impairment of collagen VI secretion (Fig 2A). To exclude artifacts related to culture conditions and passage number, cultures were double labeled for perlecan and collagen VI after 10 days of ascorbate treatment. Perlecan labeling showed a normal pattern in all UCMD patients; collagen VI appeared reduced in UCMD2 and UCMD4, while UCMD1 and UCMD3 showed a pattern similar to normal control (data not shown).

Western blot analysis of collagen VI in fibroblast cultures

Western blot was performed under reducing conditions in dermal fibroblasts of UCMD patients and control. Cell layers contained both intracellular and matrix deposited collagen VI, while medium samples were analyzed to determine a possible alteration in collagen VI secretion. In cell layer samples, bands corresponding to α1(VI), α2(VI) and the α3(VI) products were detected in control and UCMD patients (Fig. 2B left). However, the amounts of collagen VI in cell layer samples were different. In particular, UCMD2 showed a pronounced deficiency, UCMD4 had significantly decreased levels of collagen VI, while a minor decrease was found in UCMD1 and UCMD3. Moreover, both UCMD1 and UCMD4 displayed markedly decreased amounts of α2(VI) when compared to control. In agreement with the cell layer, the medium of UCMD2 cells showed a marked deficiency of collagen VI secretion. A significant decreased amount of collagen VI was also found in the medium of UCMD3 cells, while this decrease was weak, albeit still detectable, in the medium of UCMD1 and UCMD4 fibroblasts (Fig. 2B right).

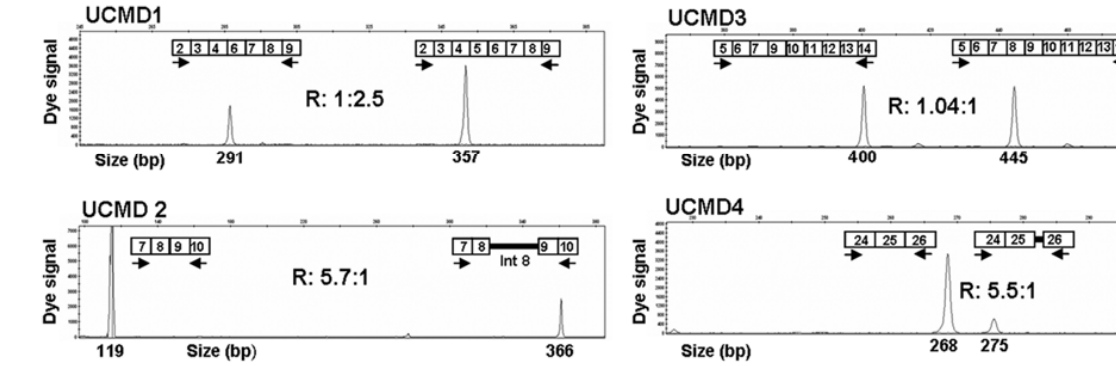

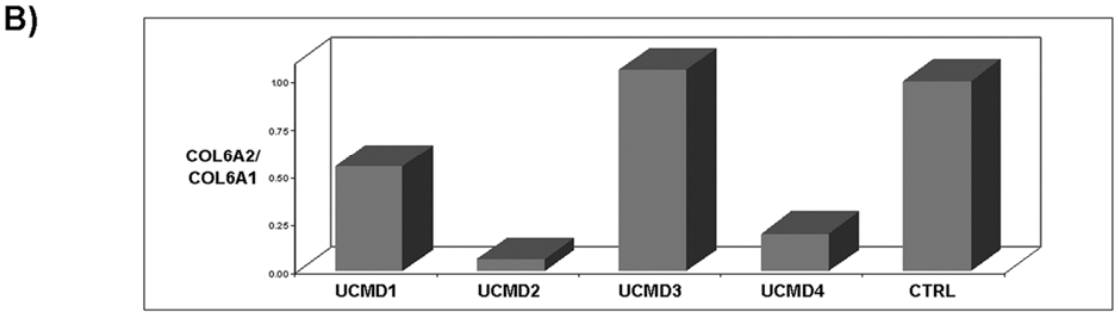

Figure 1. **Transcriptional analysis of COL6 mRNAs in UCMD patients**. A) RT-PCR analysis with a fluorescent prim upstream the splicing mutation coupled with an unlabelled reverse oligonucleotide (arrows). A schematic drawing of the confi splicing products, as determined by cDNA sequencing, is shown. The relative proportion among different splicing variants was by assessing the ratio (R) between peak height and area (GeneScan software – Applied Biosystems). B) Real-time PCR quanti the ratio between the steady state levels of COL6A2 and COL6A1 messengers in the four UCMD patients. The COL6A2/COL6 the control fibroblast is referred as 1. The COL6A2 transcripts resulted reduced to 0.65, 0.06 and 0.20 in UCMD1, UCMD2 an respectively. In UCMD3, the level of COL6A2/COL6A1 ratio is similar to control.

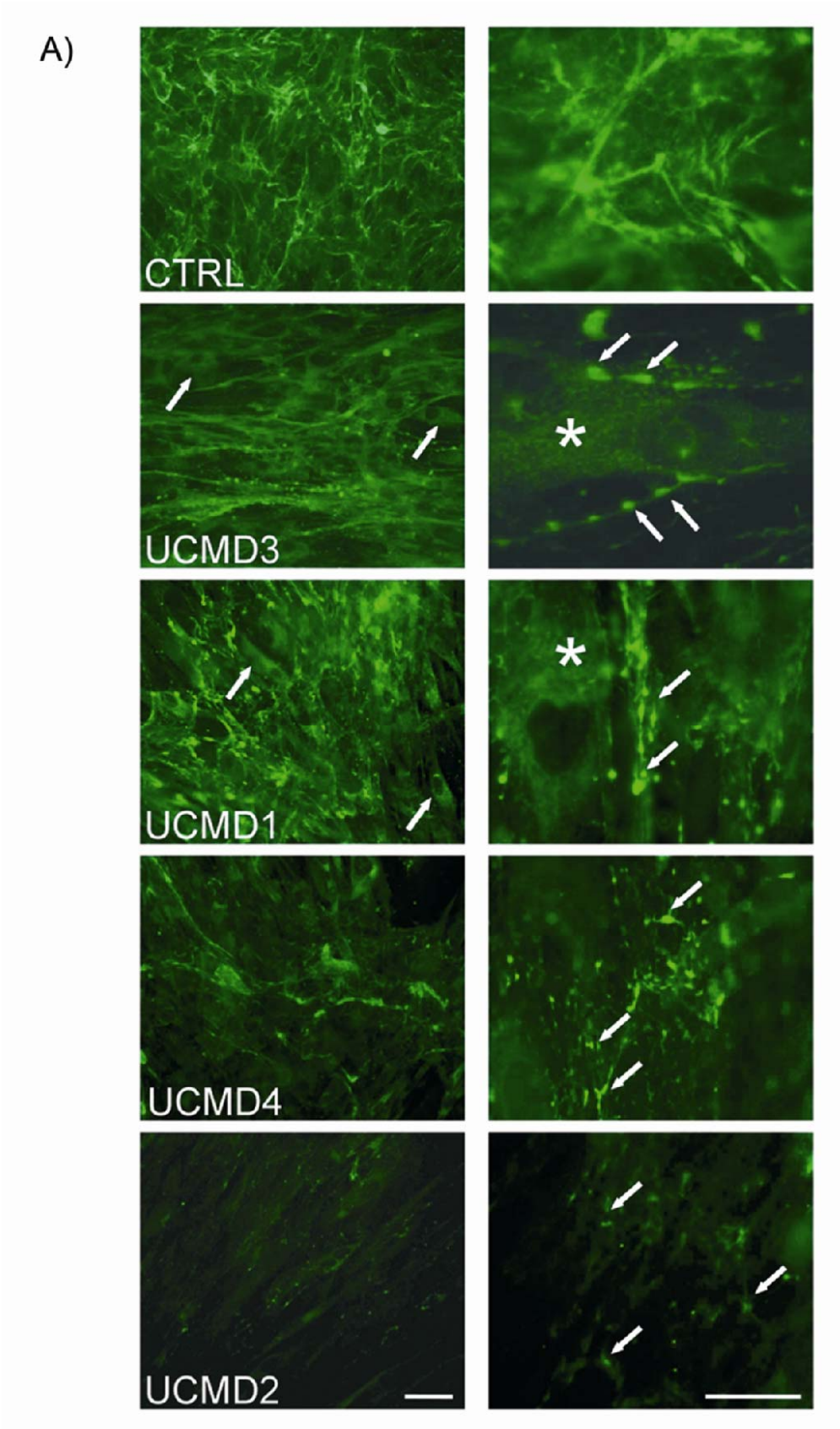
A)
CTRL
UCMD3
UCMD1
UCMD4
UCMD2

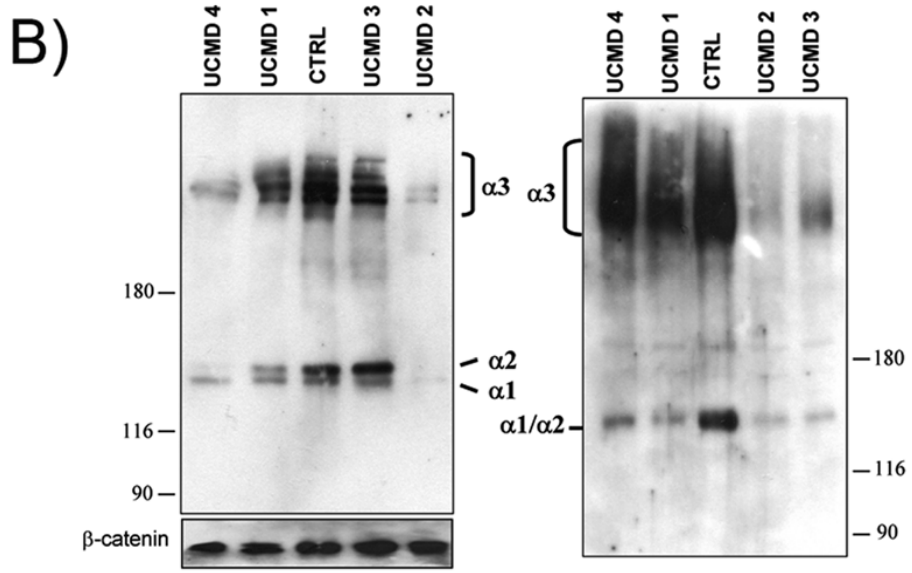

Figure 2: Immunofluorescence and Immunoblot analysis of collagen VI in control and UCMD patients. A) The amount of collagen VI deposited in the extracellular matrix was variable ranging from mildly reduced in patient UCMD1 and UCMD3, to significantly decreased in UCMD4 and severely reduced in UCMD2 (left panels). In UCMD1 and UCMD3 cultures, several fibroblasts showed intracellular retention of collagen VI also after ascorbate treatment (left panels, arrows; right panels, asterisk). The organization of collagen VI network was altered in all UCMD patients when compared with normal fibroblasts. High magnification (right panels) clearly shows the presence of anomalous collagen VI aggregates in all UCMD patients (arrows). Bar, 20 μm. **B)** Samples corresponding to cell layers (30 μg, left) and culture media (50 μg, right), derived from skin fibroblasts of patients (UCMD1-4) and healthy donor (CTRL), were separated by SDS-PAGE onto 6% polyacrylamide gels under reducing conditions. Collagen VI was detected with an antibody recognizing all three alpha-chains, whose migration positions are indicated. The migration of molecular weight marker is shown in kDa. Loading control of cell layer extracts was performed with an antibody for β-catenin (left, lower panel). In culture media, the different α3(VI) splicing products, as well as α1(VI) and α2(VI), could not be well separated from each other likely due to the glycosylation occurring before secretion (Colombatti and Bonaldo, 1987).

DISCUSSION

About 1/3 of disease-causing splicing mutations affect the consensus sequences flanking the obligate GT and AG dinucleotides (Krawczak et al., 2007). The fairly degenerated nature of these sequences makes often challenging the distinction between SNPs and pathogenic mutations and the prediction of their consequences on RNA processing. Nucleotide substitutions at the intronic position +5 have been described in 3 UCMD patients affecting COL6A2 intron 23 (Ishikawa et al., 2004), COL6A3 introns 16 (Lampe et al., 2008) and COL6A3 intron 29 (Demir at al., 2002). In the two cases that were analyzed at the RNA level (COL6A2 intron 23 +5 and COL6A3 intron 16 +5), the intronic mutation caused skipping of the adjacent exon. In the present study, the +5 nucleotide substitution of patient UCMD2 caused intron 8 retention in part of COL6A2 transcript, without evidence of exon 8 skipping. This variable behavior among +5 mutations, seems not to be predictable by comparing either the strength of wild type and mutated sites, or the size of the involved exons or introns, which are known relevant factors for determining the consequences of splicing mutations (Roca et al., 2005; Krawczak et al., 2007). Substitutions at intronic position +3 have never been detected in COL6 genes. In our UCMD1 patient, the +3 variation completely abolishes the recognition of the COL6A2 intron 5 donor splice site, resulting in a constitutive exon 5 skipping in the mutated messenger.

Mutations affecting acceptor splice site consensus sequences have been reported in 3 BM and 2 UCMD patients (Ishikawa et al., 2002; Lampe et al., 2005a, 2005b, 2008). In two cases (COL6A1 intron 13, position -3 and

COL6A2 intron 23, position -3) RNA analysis showed skipping of the adjacent exons. An homozygous variation at position -10 of COL6A2 intron 12, identified in a UCMD patient, caused exon 13 skipping as well as the activation of cryptic splice sites (Lucarini et al., 2005). The COL6A2 intron 25 -9 variation we identified in UCMD4, was previously reported as a possible polymorphism (Lampe et al., 2005b). This substitution creates a cryptic acceptor splice site which is partially recognized by the splicing machinery, leading to frameshifting and premature termination. We demonstrated by real-time PCR a substantial reduction of the COL6A2 mRNA steady state level in patient UCMD4 (20% of normal level), suggesting the diminished COL6A2 mRNA expression due to non-sense mediated decay (NMD) as the primary pathogenic mechanism in this patient. Similarly, NMD is most likely the cause of the very low level of COL6A2 transcript (6% of normal level) in UCMD2 patient. Nevertheless, a substantial decrease of COL6A2 transcript level (65% of normal level), affecting the exon 5 skipped allele, was also present in UCMD1 patient. This behavior is unexpected since the transcript deriving from exon 5 skipping of UCMD1 is in-frame and thus predicted to be stable. The in-frame COL6A1 transcript lacking exon 8 in UCMD3 is indeed normally produced, suggesting a different effect on transcription of a small regulatory splicing mutation (+3 substitution in UCMD1) in respect to a genomic deletion causing a splicing defect (del 15nt in UCMD3).

Being based on single patients, this observation warrants further investigation to be validated. Nevertheless, increasing evidence has established that a reciprocal and mutually beneficial coupling exists between transcription and RNA processing. Promoter strength may influence alternative splicing ("forward coupling") and splicing can stimulate transcription ("reverse coupling") (Damgaard et al., 2008; Pandit et al., 2008). The influence that the splicing process exerts on transcription seems not to be restricted only to transcription initiation, but also involves the elongation phase (Pandit et al., 2008). This observation implies that, besides mutations involving promoter proximal splice sites, known to influence transcription (Damgaard et al., 2008), also splicing mutations involving distal splice sites could theoretically affect transcriptional efficiency. This mechanism might represent a relevant modifier of pathogenic consequences of regulatory splicing mutations.

The identified gene mutations show different consequences on collagen VI synthesis, secretion and extracellular matrix deposition. Both UCMD1 and UCMD3 have a deletion involving few residues in the junctional region between the N-terminal domain and the triple helix. The deletion of UCMD1 causes the loss of two highly conserved cysteine residues located upstream the triple helical domain of α2(VI) and suggested to be involved in intermolecular connections and/or in extracellular assembly processes. In both UCMD1 and UCMD3, the deleted portion of the triple helix includes two residues that were shown to be glycosylated and/or hydroxylated (Chu et al., 1988). The mutant chains contain a small deletion of the N-terminal part of the triple helical domain, therefore they are likely to be incorporated into monomers (Pan et al., 2003), and they may affect collagen VI secretion. Interestingly, UCMD1 and UCMD3 cultured fibroblasts showed intracellular protein retention, suggesting that mutations could impair assembly and secretion. Western blot analysis of medium samples showed that collagen VI secretion was more affected in UCMD3 than UCMD1. This likely reflects the different levels of the mutant polypeptide chains in these two patients. In UCMD1, less mRNA from the mutant allele than from the normal COL6A2 allele was detected, and less than 50% of the α2(VI) chain is expected to be mutant. In contrast, UCMD3 had similar levels of normal and mutant COL6A1 mRNAs, and 50% of the α1(VI) chain is expected to be mutant. Considering the multi-step assembly of collagen VI occurring before secretion (Pan et al., 2003; Lucarini et al., 2005) the defects caused by a mutant chain are likely to be amplified during the assembly process and may severely impair collagen VI secretion, as observed in UCMD3.

Different truncating mutations of the C-terminal part of the α2(VI) chain were previously reported in some patients affected by either UCMD or myosclerosis myopathy (Zhang et al., 2002; Merlini et al., 2008).

Although the mutation of our UCMD4 patient is predicted to produce a truncated α2(VI) chain with a large deletion of the C-terminal region, western blot did not reveal any faster migrating band. A likely explanation is that the truncated chain is unstable and/or present in very low amounts. Moreover, collagen VI shows a marked quantitative decrease in the cell layer of UCMD4, while the medium is less affected. Taken as a whole these data suggest that the mutation of UCMD4 affects the deposition and organization of collagen VI in the extracellular matrix.

UCMD2 patient shows the most severe decrease of collagen VI synthesis and secretion. Both mutated COL6A2 transcripts undergo prevalent degradation via NMD and only the small fraction of the correctly spliced mRNA is probably transcribed into a stable protein, thus allowing the synthesis and secretion of low amount of collagen VI, as described for other UCMD patients (Giusti et al., 2005).

The phenotype of the four reported patients is typical for UCMD (Pepe et al., 2002). No clear genotype/phenotype correlations can be drawn by comparing disease severity in each patient with the mutation effects on both RNA level and protein amount. Motor ability is still preserved in UCMD2 patient at 8 years of age, whereas UCMD4 never acquired walking despite of a less severe collagen VI reduction. As discussed above, the UCMD1 and UCMD3 mutations affect the same protein domains, but their RNA and protein effects are significantly different. Nevertheless, the young age at examination of UCMD1 hampers conclusion regarding possible phenotypic consequences of this different molecular behavior.

In conclusion, our results highlight the complexity and unpredictability of the transcriptional behavior of uncommon splicing mutations. Furthermore we propose a *cis* effect on the transcriptional efficiency as a possible modifier of the pathogenic consequences of regulatory splicing mutations.

ACKNOWLEDGMENTS

This study was supported by the Italian Telethon Foundation grants GUP07004 (to FG) and GGP08197 (to AF and PB), by Italian Ministry for University and Research (to PB). The TREAT-NMD Network of Excellence of EU FP7 (036825 to LM and Telethon-Italy), NMD-Chip (EU Grant Agreement n°223026 to AF) are also acknowledged.

REFERENCES

Baker NL, Mörgelin M, Pace RA, Peat RA, Adams NE, Gardner RJ, Rowland LP,Miller G, De Jonghe P, Ceulemans B, Hannibal MC, Edwards M, Thompson EM, Jacobson R, Quinlivan RC, Aftimos S, Kornberg AJ, North KN, Bateman JF, Lamandé SR. 2005. Dominant collagen VI mutations are a common cause of Ullrich congenital muscular dystrophy. Hum Mol Genet 14:279-293.

Baralle D, Baralle M. 2005. Splicing in action: assessing disease causing sequence changes. J Med Genet 42 (10):737-748. Review.

Bertini E, Pepe G. 2002. Collagen type VI and related disorders: Bethlem myopathy and Ullrich scleroatonic muscular dystrophy. Eur J Paediatr Neurol 6(4):193-198.

Camacho Vanegas O, Bertini E, Zhang RZ, Petrini S, Minosse C, Sabatelli P, Giusti B, Chu ML, Pepe G. 2001. Ullrich scleroatonic muscular dystrophy is caused by recessive mutations in collagen type VI. Proc Natl Acad Sci U S A 98(13):7516-7521.

Chu ML, Conway D, Pan TC, Baldwin C, Mann K, Deutzmann R, Timpl R. 1988. Amino acid sequence of the triple-helical domain of human collagen type VI J Biol Chem. 263(35):18601-18606.

Colombatti A, Bonaldo P.1987. Biosynthesis of chick type VI collagen. II: Processing and secretion in fibroblasts and smooth muscle cells. J.Biol.Chem. 262, 14461-14466.

Damgaard CK, Kahns S, Lykke-Andersen S, Nielsen AL, Jensen TH, Kjems J. 2008. A 5' splice site enhances the recruitment of basal transcription initiation factors in vivo. Mol Cell 29(2): 271-278.

Demir E, Sabatelli P, Allamand V, Ferreiro A, Moghadaszadeh B, Makrelouf M, Topaloglu H, Echenne B, Merlini L, Guicheney P. 2002. Mutations in COL6A3 cause severe and mild phenotypes of Ullrich congenital muscular dystrophy. Am J Hum Genet 70(6):1446-1458

Giusti B, Lucarini L, Pietroni V, Lucioli S, Bandinelli B, Sabatelli P, Squarzoni S, Petrini S, Gartioux C, Talim B, Roelens F, Merlini L, Topaloglu H, Bertini E, Guicheney P, Pepe G. 2005. Dominant and recessive COL6A1 mutations in Ullrich scleroatonic muscular dystrophy. Ann Neurol 58(3): 400-410.

Ishikawa H, Sugie K, Murayama K, Awaya A, Suzuki Y, Noguchi S, Hayashi YK, Nonaka I, Nishino I. 2004. Ullrich disease due to deficiency of collagen VI in the sarcolemma. Neurology 62(4):620-623.

Ishikawa H, Sugie K, Murayama K, Ito M, Minami N, Nishino I, Nonaka I. 2002. Ullrich disease: collagen VI deficiency: EM suggests a new basis for muscular weakness. Neurology 59(6):920-923.

Jöbsis GJ, Keizers H, Vreijling JP, de Visser M, Speer MC, Wolterman RA, Baas F, Bolhuis PA. 1996. Type VI collagen mutations in Bethlem myopathy, an autosomal dominant myopathy with contractures. Nat Genet 14(1):113-115.

Krawczak M, Thomas NS, Hundrieser B, Mort M, Wittig M, Hampe J, Cooper DN. 2007. Single base-pair substitutions in exon-intron junctions of human genes: nature, distribution, and consequences for mRNA splicing. Hum Mutat 28(2):150-158.

Lampe AK, Bushby KM. 2005a. Collagen VI related muscle disorders. J Med Genet 42: 673-685.

Lampe AK, Dunn DM, von Niederhausern AC, Hamil C, Aoyagi A, Laval SH, Marie SK, Chu ML, Swoboda K, Muntoni F, Bonnemann CG, Flanigan KM, Bushby KM, Weiss RB. 2005b. Automated genomic sequence analysis of the three collagen VI genes: applications to Ullrich congenital muscular dystrophy and Bethlem myopathy. J Med Genet 42(2):108-120.

Lampe AK, Zou Y, Sudano D, O'Brien KK, Hicks D, Laval SH, Charlton R, Jimenez-Mallebrera C, Zhang RZ, Finkel RS, Tennekoon G, Schreiber G, van der Knaap MS, Marks H, Straub V, Flanigan KM, Chu ML, Muntoni F, Bushby KM, Bönnemann CG. 2008. Exon skipping mutations in collagen VI are common and are predictive for severity and inheritance. Hum Mutat 29(6):809-822.

Lucarini L, Giusti B, Zhang RZ, Pan TC, Jimenez-Mallebrera C, Mercuri E, Muntoni F, Pepe G, Chu ML. 2005. A homozygous COL6A2 intron mutation causes in-frame triple-helical deletion and nonsense-mediated mRNA decay in a patient with Ullrich congenital muscular dystrophy. Hum Genet 117(5): 460-466.

Merlini L, Martoni E, Grumati P, Sabatelli P, Squarzoni S, Urciuolo A, Ferlini A, Gualandi F, Bonaldo P. 2008. Autosomal recessive myosclerosis myopathy is a collagen VI disorder. Neurology 71(16):1245-1253.

Okada M, Kawahara G, Noguchi S, Sugie K, Murayama K, Nonaka I, Hayashi YK, Nishino I. 2007. Primary collagen VI deficiency is the second most common congenital muscular dystrophy in Japan. Neurology 69:1035-1042.

Pace RA, Peat RA, Baker NL, Zamurs L, Mörgelin M, Irving M, Adams NE, Bateman JF, Mowat D, Smith NJ, Lamont PJ, Moore SA, Mathews KD, North KN, Lamandé SR. 2008. Collagen VI glycine mutations: perturbed assembly and a spectrum of clinical severity. Ann Neurol 64(3):294-303.

Pan TC, Zhang RZ, Sudano DG, Marie SK, Bönnemann CG, Chu ML. 2003. New molecular mechanism for Ullrich congenital muscular dystrophy: a heterozygous in-frame deletion in the COL6A1 gene causes a severe phenotype. Am J Hum Genet.73(2):355-369.

Pandit S, Wang D, Fu XD. 2008. Functional integration of transcriptional and RNA processing machineries. Curr Opin Cell Biol 20(3):260-265. Review

Pepe G, Bertini E, Bonaldo P, Bushby K, Giusti B, de Visser M, Guicheney P, Lattanzi G, Merlini L, Muntoni F, Nishino I, Nonaka I, Yaou RB, Sabatelli P, Sewry C, Topaloglu H, van der Kooi A. 2002. Bethlem myopathy (BETHLEM) and Ullrich scleroatonic muscular dystrophy: 100th ENMC international workshop, 23-24 November 2001, Naarden, The Netherlands. Neuromuscul Disord 12(10): 984-993.

Roca X, Sachidanandam R, Krainer AR. 2005. Determinants of the inherent strength of human 5' splice sites. RNA 11(5): 683-698.

Stenson PD, Ball EV, Mort M, Phillips AD, Shiel JA, Thomas NS, Abeysinghe S, Krawczak M, Cooper DN. 2003. Human Gene Mutation Database (HGMD): 2003 update. Hum Mutat 21(6):577-581.

Zhang RZ, Sabatelli P, Pan TC, Squarzoni S, Mattioli E, Bertini E, Pepe G, Chu ML. 2002. Effects on collagen VI mRNA stability and microfibrillar assembly of three COL6A2 mutations in two families with Ullrich congenital muscular dystrophy. J Biol Chem 277(46): 43557-43564.

1.3 Recessive mutations in BM patients.

A group of BM patients, who unusually carry recessive mutations of COL6 genes, was studied. Molecular data indicate collagen VI protein defects in these patients, confirming the pathogenic nature of mutations. Therefore, this study is the first demonstration that a BM phenotype may be caused by recessively inherited COL6 mutations.

Autosomal recessive Bethlem myopathy

F. Gualandi, MD
A. Urciuolo, BSc
E. Martoni, PhD
P. Sabatelli, BSc
S. Squarzoni, MD
M. Bovolenta, PhD
S. Messina, MD
E. Mercuri, MD
A. Franchella, MD
A. Ferlini, MD
P. Bonaldo, PhD
L. Merlini, MD

Address correspondence and reprint requests to Dr. Francesca Gualandi, Dipartimento di Medicina Sperimentale e Diagnostica, Sezione di Genetica Medica, Università di Ferrara, Ferrara, Italia 44100
gdf@unife.it

ABSTRACT

Background: Bethlem myopathy is a well-defined clinical entity among collagen VI disorders, featuring proximal muscle weakness and contractures of the fingers, wrists, and ankles. It is an early-onset, slowly progressive, and relatively mild disease, invariably associated to date with heterozygous dominant mutations in the 3 collagen VI genes. We have characterized the clinical, laboratory, and genetic features of autosomal recessive Bethlem myopathy in 2 unrelated patients.

Methods: This study is based on clinical, histochemical, immunocytochemical, and electron microscope evaluation of the muscle and dermal fibroblasts, CT imaging of the muscles, and biochemical and molecular analysis.

Results: Both patients carry a truncating *COL6A2* mutation (Q819X; R366X) associated with missense changes in the partnering allele lying within the C2 domain of the α2(VI) chain (D871N; R843W-R830Q). They show decreased amounts of collagen VI in the basal lamina of muscle fibers and in dermal fibroblast cultures and altered behavior of collagen VI tetramers. Biochemical studies supported the pathogenic effect of identified amino acid substitutions, which involve strictly conserved residues.

Conclusions: The reported patients illustrate the occurrence of Bethlem myopathy with a recessive mode of inheritance. This observation completes the hereditary pattern in collagen VI myopathies with both Ullrich congenital muscular dystrophy and Bethlem myopathy underlined by either recessive or dominant effecting mutations. This finding has relevant implications for genetic counseling and molecular characterization of patients with Bethlem myopathy, as well as for genotype-phenotype correlations in collagen VI disorders. ***Neurology*® 2009;73:1883–1891**

GLOSSARY

BM = Bethlem myopathy; **cDNA** = complementary DNA; **MIM** = Mendelian Inheritance in Man; **mRNA** = messenger RNA; **NMD** = nonsense mediated decay; **nNOS** = neuronal nitric oxide synthase; **UCMD** = Ullrich congenital muscular dystrophy.

Ullrich congenital muscular dystrophy (UCMD; Mendelian Inheritance in Man [MIM] 254090) and Bethlem myopathy (BM; MIM 158810) were originally described as separate entities with distinct clinical hallmarks and inheritance patterns.[1,2] The demonstration that both diseases are caused by mutations in collagen VI genes[3,4] has led to the concept of collagen VI–related myopathies as a group of conditions covering a broad spectrum of clinical severity.[5-7] Classic UCMD and BM represent the 2 major clinical forms at the opposite ends of this spectrum, which also includes limb-girdle and myosclerosis variants.[8,9]

UCMD is a congenital disorder characterized by severe muscle weakness resulting in the limitation or loss of independent walking, with proximal joint contractures and striking hypermobility of distal joints and early respiratory failure.[1,10,11] BM is a benign myopathy with onset in early infancy, characteristic distal contractures, and slow progression.[7,12] In the original and in genetically proven families, most of the patients exhibited weakness or contractures during the

Supplemental data at www.neurology.org

From the Dipartimento di Medicina Sperimentale e Diagnostica (F.G., E. Martoni, M.B., A. Ferlini, L.M.), Sezione di Genetica Medica, Università di Ferrara; Dipartimento di Istologia, Microbiologia e Biotecnologie Mediche (A.U., P.B.), Università di Padova; IGM-CNR (P.S., S.S.), Unità di Bologna c/o IOR; Dipartimento di Neuroscienze (S.M.), Psichiatria e Anestesiologia, Policlinico Universitario G. Martino, Università di Messina; Istituto di Neurologia (E. Mercuri), Università Cattolica, Roma; Dipartimento di Riproduzione e Accrescimento (A. Franchella), Ospedale S. Anna, Ferrara; and Laboratorio di Biologia Cellulare (L.M.), IOR, Bologna, Italia.

Supported by Telethon Grants GUPO7004 (to F.G.) and GGP08197 (to A. Ferlini and P.B.) and Fondazione CaRisBo.

Disclosure: The authors report no disclosures.

first 2 years of life, including diminished fetal movements, neonatal hypotonia, congenital contractures, and hypermobility of the wrist and fingers slowly evolving to flexion contractures.[2,12,13] In addition to the early onset and the characteristic contractures of the fingers, the hallmark of the disease is its benign course. Patients with BM remain ambulant in adulthood; some affected individuals older than 50 years need aids for mobility outdoors.[13] Mild or moderate respiratory involvement has been reported in 16% of ambulatory adult patients with BM, whereas the necessity of mechanical ventilation at night was rarely reported and only during later life.[2,14-16]

BM has been invariably associated with heterozygous, dominant mutations in *COL6A1*, *COL6A2*, or *COL6A3* genes, either inherited from an affected parent or occurring de novo[3,5,6] (see also http://www.dmd.nl/). Homozygous or compound heterozygous mutations were initially found in patients with UCMD, supporting recessive inheritance.[4,17] More recently, an increasing number of patients with UCMD have been found to carry heterozygous de novo mutations, increasing the puzzle of the inheritance models of collagen VI disorders.[18,19] UCMD-associated heterozygous de novo mutations are generally considered to have a dominant negative effect, where the heterozygous mutations interfere with collagen VI assembly.[18]

We have identified 2 patients with classic BM with compound heterozygous *COL6A2* mutations, inherited from healthy heterozygous parents. In both patients, a nonsense mutation in *COL6A2* gene (Q819X and R366X) is associated with 1 or 2 missense changes on the partnering allele (D871N; R830Q-R843W), resulting in an allelic configuration not previously reported in collagen VI–related myopathies. This finding illustrates a previously unrecognized category of recessive BM cases.

METHODS

Standard protocol approvals, registrations, and patient consents. We received approval from the institutional ethical committee on human experimentation for genetic and clinical studies. Written informed consent was obtained from all patients participating in the study. We obtained authorization for disclosure of patient BM2's picture.

Genomic and RNA analysis. Genomic DNA was extracted from peripheral lymphocytes by standard methods. The coding sequence of all 3 collagen VI genes was sequenced (primers sequences are available on request) on ABI 3130 Genetic Analyzer (Applied Biosystems, Foster City, CA). Sequence data were compared with genomic and complementary DNA (cDNA) sequences of collagen VI genes in Genbank databases (*COL6A1*: NW_927384, NM_001848; *COL6A2*: NW_927384, NM_001849; *COL6A3*: NW_921618, NM_004369).

Total RNA was isolated from fibroblasts using RNeasy (QIAGEN, Chatsworth, CA) and reverse transcribed by using a High Capacity cDNA Reverse Transcription Kit (Applied Biosystems). To explore nonsense mediated decay (NMD), cDNA was used as a template for PCR amplification of the mutated region of *COL6A2* transcript, according to previously reported cycling conditions.[9] Utilized primers are available on request. PCR products were purified and directly sequenced.

Muscle biopsy. Morphologic and histochemical analyses were performed following standard methods. Unfixed 7-μm-thick frozen sections were labeled with antibodies against caveolin 3 (BD-Transduction, Franklin Lakes, NJ), laminin α2 and β1 (Chemicon, now part of Millipore, Billerica, MA), telethonin, neuronal nitric oxide synthase (nNOS; Santa Cruz, Santa Cruz, CA), emerin, lamin A/C, dystrophin (Novocastra, Newcastle upon Tyne, UK), and α-dystroglycan (Upstate Biotechnologies, now part of Millipore). Double labeling with anti–collagen VI and perlecan (both Chemicon) or nidogen (Calbiochem, Merck Group, Darmstadt, Germany) was performed as previously described.[20,21] Samples were observed with a Nikon Eclipse 80i fluorescence microscope.

Western blot analysis of collagen VI produced by skin fibroblasts. Skin fibroblasts were grown to confluence in OPTI-MEM medium (Invitrogen, Carlsbad, CA) in the presence or absence of 0.25 mM L-ascorbic acid (Sigma, St. Louis, MO). Medium was collected and cell layer was solubilized in lysis solution. Western blotting was performed under reducing conditions in 3% to 8% polyacrylamide gradient gels and transferring to Immobilon membrane (Millipore). Collagen VI was pulled down using an antibody recognizing α1(VI) chain conjugated to protein A-Sepharose (Santa Cruz). Immunoprecipitated samples were separated by electrophoresis in a composite 0.5% agarose–2.4% polyacrylamide gel. Collagen VI was detected with an antibody recognizing all collagen VI chains (Fitzgerald, North Acton, MA).

Immunofluorescence and rotary shadowing analysis of collagen VI on cultured fibroblasts. Fibroblasts were grown on coverslips to 2 days postconfluence in the presence of 0.25 mM L-ascorbic acid. For immunofluorescence analysis, fibroblasts were fixed with cold methanol for 7 minutes, washed with phosphate-buffered saline, and incubated with anti–collagen VI antibody (Chemicon) diluted 1/100 for 1 hour. After washing, samples were incubated with a fluorescein isothiocyanate–conjugated secondary antibody (DAKO, Carpinteria, CA) and mounted with antifade medium (Molecular Probes, Invitrogen).

For immunoelectron microscopy, cells were incubated with a monoclonal anti–collagen VI antibody (Chemicon) diluted 1:25 with Dulbecco's modified Eagle medium and with 5- or 15-nm colloidal gold–labeled immunoglobulin G (Amersham, GE Healthcare, Little Chalfont, UK). Rotary shadowing electron microscopy was performed as described.[22]

RESULTS

Patients. Patient BM1 is a 25-year-old woman, the only child of nonconsanguineous parents with a negative family history. Early motor milestones were normal. From age 2 years, she showed

toe walking and experienced difficulty getting up from the floor and climbing stairs. She underwent Achilles tendon release at ages 6 and 8 years. At age 25 years, she was unable to walk further than half a mile, needed to use a rail to climb stairs, and was unable to get up from the floor. She had mild weakness in the shoulder girdle and upper limb muscles, and moderate weakness in the axial and hip girdle muscles. Moderate rigidity of the spine; prominent contractures of the shoulders, elbows, finger flexors, knees, and Achilles tendons; and hypermobility of the distal joints were noted. Forced vital capacity was 65% of predicted. Creatine kinase was normal. Pelvic and lower limb muscle MRI showed mild to moderate diffuse fibrous substitution of muscle tissue with a nonspecific pattern. Her parents, at ages 52 and 47 years, were normal on clinical examination.

Patient BM2 had bilateral talipes equinovarus at birth. He walked at age 14 months. At age 4 years, he underwent bilateral Achilles tendon lengthening. At ages 7 and 12 years, he had repeated Achilles surgery for marked relapse. Examination at age 19 years revealed a tall man with marked bilateral equinus deformity. He was able to walk and climb stairs without support, but not to run. There was a mild limb-girdle weakness together with a moderate axial involvement, inability to fully close the eyes, and marked digitorum extension weakness. There were contractures at the elbows, knees, and fingers. A mild distal joint hypermobility was present. Creatine kinase was 2.5 times the upper value of normal. Forced vital capacity was 64% of predicted. Muscle CT revealed a mild to moderate diffuse hypodensity particularly in the legs, more pronounced at the periphery of the muscle. At age 19 years, he underwent a bilateral triple arthrodesis with some improvement in stance and balance. He remained stable until age 45 years, when after a fall he reported a femoral neck fracture and was treated with a prosthesis. Examination at age 47 years (figure 1) showed marked long finger flexion contractures without distal hypermobility. He was no longer able to rise from the floor and needed support to get up from a chair. He walked slowly with the aid of a stick. His parents, at ages 69 and 72 years, were normal on clinical examination.

Mutational analysis. Genomic analysis showed that patient BM1 carries a paternal heterozygous C2537T variation within exon 27 of the *COL6A2* gene resulting in the nonsense mutation Q819X, and 2 maternally inherited heterozygous missense mutations in exon 28 (G2571A-R830Q; C2609T- R843W). RNA analysis from cultured fibroblasts showed biallelic expression of *COL6A2* messenger RNA (mRNA), confirming that the Q819X nonsense mutation escapes NMD, as previously reported[9] (figure 2A). Patient

Figure 1 Clinical features

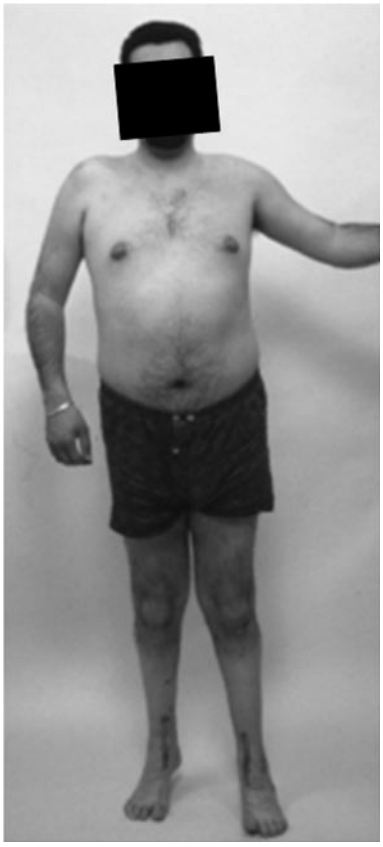

Patient BM2 at age 47 years showing marked finger contractures, equinus of the feet, and mild atrophy of thigh and leg muscles.

BM2 carries a maternally inherited heterozygous C1178T variation within exon 12 of the *COL6A2* gene, resulting in the nonsense mutation R366X, and a de novo heterozygous missense variation in exon 28 (G2693A-D871N). Reverse transcription PCR analysis on cDNA from fibroblasts showed pseudohomozygosity of the G2693A variation, attesting NMD of the R366X allele and also demonstrating that the 2 mutations are in trans (figure 2A). The predicted effects of identified mutations on α2(VI) C2 domain are reported in figure 2B.

All the identified missense variations are novel. Sequencing of 200 control chromosomes excluded common polymorphisms. Sequence comparison by Blast analysis shows that R830Q, R843W, and D871N mutations involve strictly conserved residues within the α2(VI) sequences of all species present in the Genbank databases (figure 2C).

Muscle biopsy. In patient BM1, a muscle biopsy performed at age 3 years showed a myopathic pattern with moderate to marked fibrosis, increased variation in fiber size, type 1 fiber predominance, and increased number of type 2C fibers. Collagen VI im-

Figure 2 Mutation analysis

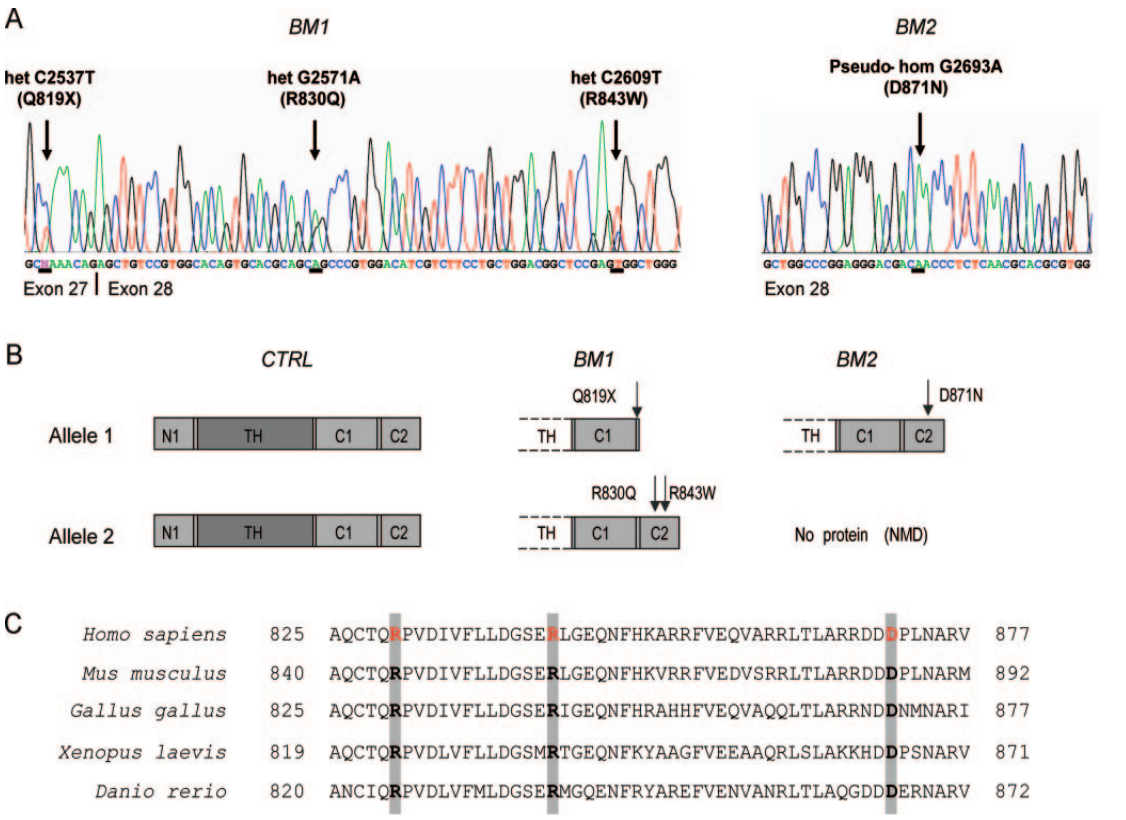

(A) Complementary DNA sequence chromatograms demonstrating balanced transcription of Q819X and R830Q-R843W mutated alleles in BM1 and pseudohomozygosity of D871N allele in BM2. (B) Schematic representation of the predicted effect of BM1 and BM2 mutations on the C-terminal end of α2(VI) chain. On the left, the complete structure of α2(VI) chain produced by unaffected control (CTRL) is shown. NMD = nonsense mediated decay; TH = triple-helical domain. (C) Sequence alignment showing strict conservation of R830, R843, and D871 residues in the α2(VI) protein sequences of distant species.

munofluorescence showed a reduced staining and only a partial colocalization with basement membrane markers (data not shown). Biopsy from patient BM2, taken at age 19 years, showed a dystrophic pattern, with proliferation of endomysial and perimysial connective tissue, variation in muscle fiber diameter, and numerous internal nuclei. Several hypertrophic fibers showed splitting and abnormal distribution of oxidative enzyme activity (figure e-1 on the *Neurology*® Web site at www.neurology.org). Immunofluorescence showed a moderate reduction of collagen VI (figure 3A); several muscle fibers showed a selective reduction of collagen VI expression at the basal lamina, as revealed by double labeling with nidogen (figure 3B). Laminin β1 was also reduced at the basal lamina of muscle fibers, whereas laminin γ1 and α2 chain, dystrophin, caveolin 3, α-dystroglycan, integrin α7b, nNOS, emerin, and perlecan were normal (data not shown).

Collagen VI in skin fibroblasts. Western blot analysis under reducing conditions and immunofluorescence analysis revealed a reduced amount of secreted collagen VI in patient BM2 and, to a lesser extent, also in patient BM1 (figures 4A and 5A).

A band migrating faster than the normal α1/α2 chains was detected in both cell layer and medium of patient BM1 (figure 4A), likely corresponding to the truncated α2(VI) chain, whose predicted molecular weight is approximately 105 kd. To understand whether the truncated protein may affect collagen VI biosynthesis and assembly, we analyzed these aspects in more detail. Western blot analysis of BM1 cultures in nonreducing conditions showed absence of tetramers in cell layer. In medium, a marked decrease of collagen VI tetramers was observed, with increased abundance of monomers and dimers when compared with control (figure 4B). When analyzed under high magnification, immunofluorescence of BM1 fibro-

Figure 3 **Immunofluorescence analysis of collagen VI in muscle**

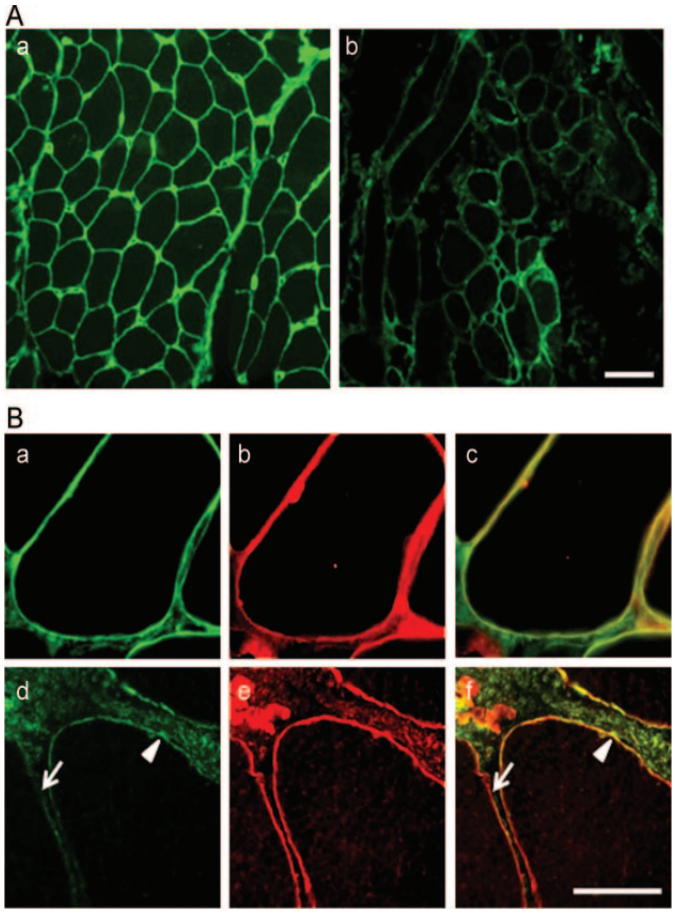

(A) Collagen VI appears reduced and unevenly distributed in muscle of BM2 (b) when compared with control (a). Bar, 200 μm. (B) Double labeling of collagen VI (a and d) and nidogen (b and e) and overlaid images (c and f) of control (a–c) and BM2 (d–f) muscle biopsies. In unaffected control, collagen VI and nidogen colocalize at the basement membrane of muscle fibers as demonstrated by yellow fluorescence in merge (c). In muscle biopsy of BM2, collagen VI labeling is discontinuously distributed in the basal lamina of muscle fibers (d) as demonstrated by red staining in overlaid image (f). Some areas of the basement membrane show a complete absence of collagen VI labeling (d, arrow), also visible as red staining in the overlaid image (f, arrow). However, focal areas of the basement membrane show normal protein expression and localization (d and f, arrowhead). Nidogen immunostaining shows an intense and continuous labeling (e), as in normal control (b).

blasts showed a filamentous arrangement of collagen VI, and 3-dimensional networks could be also detected (figure 5A, b). Electron microscope examination confirmed the presence of collagen VI microfilaments, which appeared correctly assembled and interconnected. Hexagonal-like structures were frequent, whereas parallel-aligned microfilaments were scarcely detected (figure 5B, c and d).

In BM2 cultures, Western blot analysis under nonreducing conditions revealed that collagen VI monomers and dimers were barely detectable in cell layer, and tetramers were strongly decreased in the medium (figure 4B). Immunofluorescence showed that the protein was secreted and assembled in the extracellular matrix, with a spotlike organization (figure 5A, c). Ultrastructural analysis confirmed the presence of collagen VI microfilaments, which appeared composed of several tetramers (ranging from 10 to 30). However, globular domains displayed an irregular shape, and the microfilaments appeared scarcely interconnected. Typical network and hexagonal-like structures were absent, whereas few parallel-aligned microfilaments could be detected in the pericellular matrix (figure 5B, e and f).

DISCUSSION It is increasingly recognized that clinical overlap exists within the spectrum of collagen VI–related myopathies, complicating the classification of intermediate phenotypes[23]; nevertheless, BM and UCMD as originally described remain readily distinguishable clinical entities. The patients we described were still ambulant at ages 25 and 47 years, with a preserved respiratory function and thus clearly belong to the classic BM presentation. Both patients carried compound heterozygous *COL6A2* mutations.

Our observation points out the occurrence, besides dominant and recessive UCMD and dominant BM, of previously unrecognized recessive BM cases. The finding of compound heterozygous genotypes in patients with BM further complicates the interpretation of genotype-phenotype relationship in collagen VI disorders. Recessive collagen VI myopathies reported so far were found to be caused by the combination of 2 truncating mutations, 1 truncating and 1 in-frame deletion, 2 in-frame deletions, or 2 missense changes (see also http://www.dmd.nl/).[5,6,24] In our patients with BM, a truncating mutation either causing NMD (R266X) or removing the α2(VI) C2 domain (Q819X) is partnered by missense changes within the α2(VI) C2 region. This allelic combination (truncating plus missense) was not previously reported in collagen VI disorders.

The identified nonsense mutations were previously described in homozygosity in a recessive myosclerosis myopathy family (Q819X)[9] and in compound heterozygosity with a null allele in a patient with UCMD (R366X/K318fsX6).[25] The interpretation of the 3 missense changes (R830Q, R843W, and D871N) requires caution. Nevertheless, their pathogenic meaning is strongly supported by the association with bona fide recessive mutations in affected subjects and by the strict conservation of the involved residues in the protein sequence from distant species, suggesting a key role in the C2 domain of α2(VI) chain. Moreover, we have provided evidence of their ability to interfere with collagen VI assembly and molecular interactions. In fact, analysis of collagen VI synthesis, assembly, and secretion re-

Figure 4 Western blot analysis of collagen VI in cultured fibroblasts

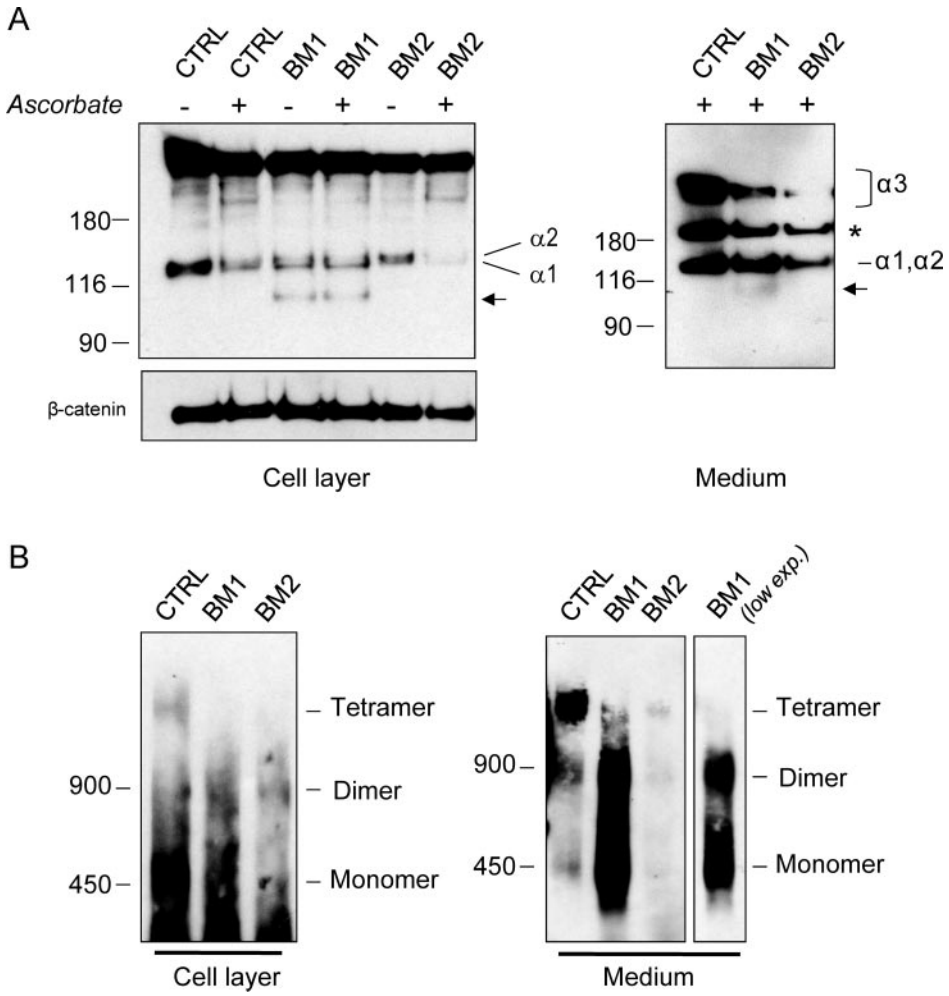

(A) Skin fibroblasts from control (CTRL), BM1, and BM2 were grown in either the presence (+) or the absence (−) of ascorbic acid. Cell layer (20 μg) and medium (30 μg) were separated by electrophoresis under reducing conditions in 3% to 8% polyacrylamide gradient gel, and collagen VI was detected by an antibody recognizing all chains. The migration and size (in kilodaltons) of the protein molecular weight markers are shown on the left, and migration positions of the 3 α(VI) chains are indicated on the right. An additional faster migrating band (arrow) is detected in the cell layer and medium of BM1. *Unspecific band detected by the antibody in all medium samples. Control for loading in cell layer samples was performed by an antibody for β-catenin. (B) Cell layer and medium were immunoprecipitated with an antibody recognizing the α1(VI) chain. Samples were separated by electrophoresis under nonreducing conditions in a composite 0.5% agarose–2.4% polyacrylamide gel. Collagen VI was detected with an antibody recognizing all chains. The expected migration positions of collagen VI monomers, dimers, and tetramers are indicated on the right. The migration and size (in kilodaltons) of molecular weight markers (laminin and fibronectin) are shown on the left. The last lane is a lower exposure of BM1 medium.

vealed qualitative and/or quantitative protein defects in both patients. In patient BM1, the truncated α2(VI) chain was able to participate in collagen VI synthesis and it was secreted, and the amounts of collagen VI were slightly decreased when compared with control. Analysis under nonreducing conditions showed that the assembly or stability of collagen VI tetramers was impaired. The presence of the Q819X mutation in heterozygosity does not seem to cause any pathogenic consequence, as indicated by the normal phenotype of the 2 parents of myosclerosis-affected siblings[9] as well as of the father of patient BM1. Consequently, it is reasonable that in patient BM1 the 2 missense mutations partnering Q819X allele also contribute to the collagen VI defects. Ultrastructural data suggest that these mutations may interfere with protein interactions, thus compromising the integrity of the muscle cell-matrix link. Interestingly, in muscle biopsy of patient BM1, mutated collagen VI showed only partial colocalization with myofiber basal lamina, thus supporting the hypothesis of an altered binding with extracellular matrix components.

The D871N mutated chain is the only α2(VI) polypeptide produced by patient BM2, because the mRNA transcribed by the other allele undergoes

Figure 5 **Immunofluorescence and electron microscope analysis of collagen VI**

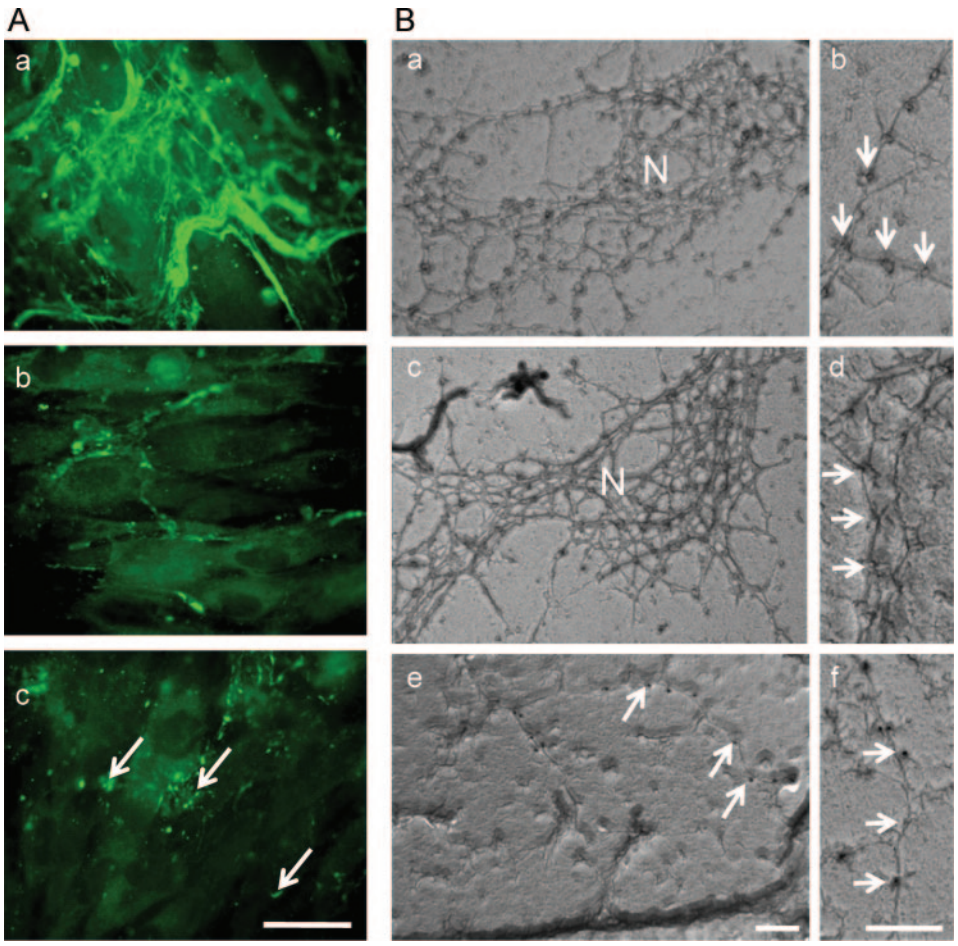

(A) Immunofluorescence analysis of collagen VI on cultured fibroblasts from control (a), BM1 (b), and BM2 (c), treated for 2 days with 0.25 mM ascorbic acid postconfluence. BM1 (b) and BM2 (c) fibroblasts show a reduced amount of collagen VI secreted in the extracellular matrix when compared with the extensive 3-dimensional networks developed by control fibroblasts (a). The organization of collagen VI microfilaments shows a typical filamentous arrangement in BM1 fibroblasts (b), whereas a dotlike appearance is detected in BM2 culture (c, arrows). Bar, 20 μm. (B) Electron microscope examination of rotary shadowed cultured fibroblasts from control (a and b), BM1 (c and d), and BM2 (e and f) labeled with anti–collagen VI and revealed with a secondary antibody conjugated with 5 nm (a–e) and 15 nm (b, d, e, and f) colloidal gold particles. In control fibroblasts, collagen VI microfilaments develop a well-interconnected network (a, N), with a regular distance between globular domains (b, arrows). In BM1 culture, collagen VI microfilaments appear well interconnected (c, N) and composed by regular tetramers (d, arrows). In BM2 culture, the microfilaments appeared scarcely developed and interconnected (e, arrows), and globular domains displayed an irregular shape (f, arrows). Panels a, c, and e are at the same magnification, as well as b, d, and f. Bar, 200 nm.

NMD, and the amounts of collagen VI are markedly decreased in both cell layer and medium of this patient. Considering that the R366X mutation is present in heterozygosity in the healthy mother of patient BM2, the clinical phenotype cannot be ascribed to the sole quantitative decrease of collagen VI. The very low amount of tetramers in the medium of BM2 cells and the presence of dimers in cell samples indicate that the single D871N substitution of the α2(VI) C2 domain affects the synthesis and organization of collagen VI tetramers. Indeed, when investigated by rotary shadowing, secreted tetramers showed altered globular domains and did not develop extensive networks, suggesting that this mutation also affects the 3-dimensional organization of collagen VI microfilaments.

Supporting our observation, several studies indicate that the α2(VI) C2 domain has a crucial role for the correct assembly of collagen VI.[9,22,26,27] A patient with BM carrying a heterozygous P932L mutation showed a defect in the incorporation of the mutated α2(VI) chain within triple-helical monomers, leading to reduced secretion of tetramers.[28] In a patient with UCMD, compound heterozygous *COL6A2* mutations (L837P and delN897) were found to cause a severe decrease of collagen VI assembly and secretion.[28]

The identification of patients with BM with a compound heterozygous genotype for recessive *COL6* mutations has relevant implication for molecular diagnosis of collagen VI–related diseases, emphasizing the importance of a full screening of *COL6* genes irrespectively of the clinical phenotype. Recessive inheritance needs to be considered on a par with dominant transmission when counseling patients with BM, and this implies that a 50% recurrence risk is no longer the rule in BM sporadic cases, even when they are molecularly characterized. The peculiar allelic combination (truncating plus missense) underlying the BM phenotype in our patients does not support pure haploinsufficiency as a causative mechanism for BM and suggests that the existence of missed recessive mutations could explain the rare patients with BM with heterozygous null mutations. These patients represent an intriguing and still unsolved matter when weighed against heterozygous parents of patients with UCMD, carrying equally null collagen VI alleles, but showing no obvious phenotype.[5]

Another peculiar aspect characterizing patients BM1 and BM2 resides in the presence of collagen VI abnormalities both in skeletal muscle and cultured fibroblasts at conventional immunohistochemical analysis. In fact, genetically characterized BM patients usually show normal collagen VI in muscle biopsy,[19,29-31] whereas cultured fibroblasts display a variable amount of protein and/or abnormalities of microfilament organization in the extracellular matrix.[31] The coexistence of collagen VI abnormalities in both fibroblasts and muscle was previously described in only 2 BM cases showing atypical features: one patient, carrying a heterozygous *COL6A3* de novo mutation, had a BM borderline phenotype with restrictive pulmonary function[19]; the other, with an intermediate BM/UCMD phenotype, inherited the heterozygous *COL6A2* mutation from the healthy mother,[31] suggesting that this mutation may not be the only one contributing to the clinical phenotype. These observations further support the hypothesis that recessive mutations could have been missed in some patients with BM, and that BM recessive mutations may affect collagen VI expression both in muscle and fibroblasts.

Received April 29, 2009. Accepted in final form August 25, 2009.

REFERENCES

1. Ullrich O. Kongenitale, atonisch-sklerotische Muskeldystrophie. Monatsschr Kinderheilkd 1930;47:502–510.
2. Bethlem J, Wijngaarden GK. Benign myopathy, with autosomal dominant inheritance: a report on three pedigrees. Brain 1976;99:91–100.
3. Jöbsis GJ, Keizers H, Vreijling JP, et al. Type VI collagen mutations in Bethlem myopathy, an autosomal dominant myopathy with contractures. Nat Genet 1996;14:113–115.
4. Camacho Vanegas O, Bertini E, Zhang RZ, et al. Ullrich scleroatonic muscular dystrophy is caused by recessive mutations in collagen type VI. Proc Natl Acad Sci USA 2001; 98:7516–7521.
5. Lampe AK, Bushby KM. Collagen VI related muscle disorders. J Med Genet 2005;42:673–685.
6. Lampe AK, Dunn DM, von Niederhausern AC, et al. Automated genomic sequence analysis of the three collagen VI genes: applications to Ullrich congenital muscular dystrophy and Bethlem myopathy. J Med Genet 2005;42: 108–120.
7. Merlini L, Bernardi P. Therapy of collagen VI-related myopathies (Bethlem and Ullrich). Neurotherapeutics 2008; 5:613–618.
8. Scacheri PC, Gillanders EM, Subramony SH, et al. Novel mutations in collagen VI genes: expansion of the Bethlem myopathy phenotype. Neurology 2002;58:593–602.
9. Merlini L, Martoni E, Grumati P, et al. Autosomal recessive myosclerosis myopathy is a collagen VI disorder. Neurology 2008;71:1245–1253.
10. Furukawa T, Toyokura Y. Congenital, hypotonic-sclerotic muscular dystrophy. J Med Genet 1977;14:426–429.
11. Nonaka I, Une Y, Ishihara T, Miyoshino S, Nakashima T, Sugita H. A clinical and histological study of Ullrich's disease (congenital atonic-sclerotic muscular dystrophy). Neuropediatrics 1981;12:197–208.
12. Arts WF, Bethlem J, Volkers WS. Further investigations on benign myopathy with autosomal dominant inheritance. J Neurol 1978;217:201–206.
13. Jöbsis GJ, Boers JM, Barth PG, de Visser M. Bethlem myopathy: a slowly progressive congenital muscular dystrophy with contractures. Brain 1999;122:649–655.
14. Pepe G, Giusti B, Bertini E, et al. A heterozygous splice site mutation in *COL6A1* leading to an in-frame deletion of the alpha1(VI) collagen chain in an Italian family affected by Bethlem myopathy. Biochem Biophys Res Commun 1999;258:802–807.
15. Merlini L, Morandi L, Granata C, Ballestrazzi A. Bethlem myopathy: early-onset benign autosomal dominant myopathy with contractures—description of two new families. Neuromuscul Disord 1994;4:503–511.
16. van der Kooi AJ, de Voogt WG, Bertini E, et al. Cardiac and pulmonary investigations in Bethlem myopathy. Arch Neurol 2006;63:1617–1621.
17. Higuchi I, Shiraishi T, Hashiguchi T, et al. Frameshift mutation in the collagen VI gene causes Ullrich's disease. Ann Neurol 2001;50:261–265.
18. Baker NL, Mörgelin M, Peat R, et al. Dominant collagen VI mutations are a common cause of Ullrich congenital muscular dystrophy. Hum Mol Genet 2005;14:279–293.
19. Lampe AK, Zou Y, Sudano D, et al. Exon skipping mutations in collagen VI are common and are predictive for severity and inheritance. Hum Mutat 2008;29:809–822.
20. Sabatelli P, Columbaro M, Mura I, et al. Extracellular matrix and nuclear abnormalities in skeletal muscle of a patient with Walker-Warburg syndrome caused by POMT1 mutation. Biochim Biophys Acta 2003;1638:57–62.
21. Squarzoni S, Sabatelli P, Bergamin N, et al. Ultrastructural defects of collagen VI filaments in an Ullrich syndrome patient with loss of the alpha3(VI) N10-N7 domains. J Cell Physiol 2006;206:160–166.

22. Zhang RZ, Sabatelli P, Pan TC, et al. Effects on collagen VI mRNA stability and microfibrillar assembly of three *COL6A2* mutations in two families with Ullrich congenital muscular dystrophy. J Biol Chem 2002;277:43557–43564.
23. Pace RA, Peat RA, Baker NL, et al. Collagen VI glycine mutations: perturbed assembly and a spectrum of clinical severity. Ann Neurol 2008;64:294–303.
24. Okada M, Kawahara G, Noguchi S, et al. Primary collagen VI deficiency is the second most common congenital muscular dystrophy in Japan. Neurology 2007;69:1035–1042.
25. Martoni E, Urciuolo A, Sabatelli P, et al. Identification and characterization of novel collagen VI non-canonical splicing mutations causing Ullrich congenital muscular dystrophy. Hum Mutat 2009;30:E662–E672.
26. Ball SG, Baldock C, Kielty CM, Shuttleworth CA. The role of the C1 and C2 a-domains in type VI collagen assembly. J Biol Chem 2001;276:7422–7430.
27. Ball S, Bella J, Kielty C, Shuttleworth A. Structural basis of type VI collagen dimer formation. J Biol Chem 2003;278:15326–15332.
28. Baker NL, Mörgelin M, Pace RA, et al. Molecular consequences of dominant Bethlem myopathy collagen VI mutations. Ann Neurol 2007;62:390–405.
29. Merlini L, Villanova M, Sabatelli P, Malandrini A, Maraldi NM. Decreased expression of laminin beta 1 in chromosome 21-linked Bethlem myopathy. Neuromuscul Disord 1999;9:326–329.
30. Merlini L, Angelin A, Tiepolo T, et al. Cyclosporin A corrects mitochondrial dysfunction and muscle apoptosis in patients with collagen VI myopathies. Proc Natl Acad Sci USA 2008;105:5225–5229.
31. Hicks D, Lampe AK, Barresi R, et al. A refined diagnostic algorithm for Bethlem myopathy. Neurology 2008;70:1192–1199.

1.4 BM and UCMD analysis by CGH array.

We studied a group of UCMD and BM patients for the evaluation and validation of CGH as a new diagnostic approach.

Bovolenta *et al. BMC Medical Genetics* 2010, **11**:44
http://www.biomedcentral.com/1471-2350/11/44

BMC Medical Genetics

RESEARCH ARTICLE Open Access

Identification of a deep intronic mutation in the COL6A2 gene by a novel custom oligonucleotide CGH array designed to explore allelic and genetic heterogeneity in collagen VI-related myopathies

Matteo Bovolenta[1†], Marcella Neri[1†], Elena Martoni[1], Anna Urciuolo[2], Patrizia Sabatelli[3], Marina Fabris[1], Paolo Grumati[2], Eugenio Mercuri[4], Enrico Bertini[5], Luciano Merlini[1,6], Paolo Bonaldo[2], Alessandra Ferlini[1], Francesca Gualandi[1*]

Abstract

Background: Molecular characterization of collagen-VI related myopathies currently relies on standard sequencing, which yields a detection rate approximating 75-79% in Ullrich congenital muscular dystrophy (UCMD) and 60-65% in Bethlem myopathy (BM) patients as PCR-based techniques tend to miss gross genomic rearrangements as well as copy number variations (CNVs) in both the coding sequence and intronic regions.

Methods: We have designed a custom oligonucleotide CGH array in order to investigate the presence of CNVs in the coding and non-coding regions of *COL6A1, A2, A3, A5* and *A6* genes and a group of genes functionally related to collagen VI. A cohort of 12 patients with UCMD/BM negative at sequencing analysis and 2 subjects carrying a single *COL6* mutation whose clinical phenotype was not explicable by inheritance were selected and the occurrence of allelic and genetic heterogeneity explored.

Results: A deletion within intron 1A of the *COL6A2* gene, occurring in compound heterozygosity with a small deletion in exon 28, previously detected by routine sequencing, was identified in a BM patient. RNA studies showed monoallelic transcription of the *COL6A2* gene, thus elucidating the functional effect of the intronic deletion. No pathogenic mutations were identified in the remaining analyzed patients, either within COL6A genes, or in genes functionally related to collagen VI.

Conclusions: Our custom CGH array may represent a useful complementary diagnostic tool, especially in recessive forms of the disease, when only one mutant allele is detected by standard sequencing. The intronic deletion we identified represents the first example of a pure intronic mutation in *COL6A* genes.

Background

Mutations in the genes encoding collagen VI (*COL6A1, COL6A2* and *COL6A3*) result in two major phenotypes: Bethlem myopathy [BM, OMIM #158810] and Ullrich congenital muscular dystrophy [UCMD, OMIM #254090]. Despite BM being classically reported as an autosomal dominant condition due to heterozygous COL6 mutations [1,2], we and others have recently described autosomal recessive BM patients [3,4]. In contrast, the allelic form UCMD was initially considered to be an autosomal recessive disorder, with homozygous or compound heterozygous mutations occurring in all three *COL6* genes [2], although a few double heterozygous mutations in two different *COL6* genes have also been described [5]. Recently, however, up to 50% of UCMD cases have been found to carry only one mutated allele, indicating autosomal dominant inheritance [5-7]. Thus far, roughly 100 different mutations in *COL6* genes have been associated with either UCMD or

* Correspondence: gdf@unife.it
† Contributed equally
[1]Department of Experimental and Diagnostic Medicine - Section of Medical Genetics, University of Ferrara, Ferrara, Italy

BM and most of them are confined to single families [5,8].

The distribution of mutations along *COL6* genes is rather uniform and lacks mutation hot spots, therefore these patients require extensive genotyping, which is currently performed by genomic or cDNA sequencing [1,5]. Nevertheless, a relevant proportion of patients clinically diagnosed as having a collagen-VI related myopathy still lack molecular characterization. In fact, with currently available diagnostic tools, the detection rate of mutations of *COL6* genes varies from 60-65% in BM cases and 75-79% in UCMD patients [5]. The majority of these mutations are small variations like missense, frame-shifting, ins-del or point mutations which lead to a splicing defect. Large, multi-exon deletions of the *COL6A1* gene, involving both exonic and intronic regions and thus detectable by mRNA analysis, have been reported as causative mutations in three patients [9,10]. One limitation of PCR-based genome analysis techniques is their inability to detect gross CNVs, as well as atypical mutations, which could account for a significant proportion of undetected *COL6* mutations. On the other hand, the relatively low rate of mutation detection in *COL6* genes could be due to the genetic heterogeneity of these diseases. Thus, mutations in genes functionally related to collagen VI could theoretically underlie UCMD and BM phenocopies and/or be responsible for secondary collagen VI defects [11]. In order to test this hypothesis, we selected 12 UCMD/BM patients who were found to be negative upon extensive sequence analysis of the three *COL6* genes, and two patients carrying only one mutation, deemed insufficient to explain the clinical phenotype, it being inherited from a healthy parent.

The occurrence of both allelic and genetic heterogeneity was explored in these patients by using an innovative oligonucleotide array-based comparative genomic hybridization (CGH) approach able to detect CNVs in *COL6* genes, as well as in other genes functionally related to collagen VI.

A deep intronic deletion in the *COL6A2* gene was discovered in one BM patient, with a single mutation inherited from the healthy mother identified at sequencing analysis. Subsequently, the functional effect of the identified mutation was demonstrated via RNA studies. In the remaining patients, only non pathogenic CNVs were identified.

Methods

Genome sequence analysis

Patients' genomic DNA was extracted from peripheral blood lymphocytes after informed consent and approval by the local ethics committee was obtained (approval number 7/2009). PCR primers (sequences are available upon request) were designed to amplify all the 107 exons of the *COL6* genes, as well as their flanking intronic regions. Amplified fragments were directly sequenced using a BigDye Terminator v3.1 Cycle sequencing system on the automated ABI 3130 Genetic Analyzer (Applied Biosystems, Foster City, CA).

In order to try to attempt amplification across the deletion within COL6A2 intron 1A, identified by the CGH-array, the following oligonucleotides were positioned outside the maximum theoretical deleted region: F1 CCCTGAATTCCTGGACATGAT; R1 GAACGTCCATCCTCCCTGAT; and flanking the region identified by the two deleted probes (F2 AGATCCACAGCCACGACTT; R2 GGCCTCACTGTGCTGCTG) (Figure 1). Long-range PCR was performed using LA-Taq polymerase and 40 cycles at 64°C.

Micro-array design, hybridization and data analysis

COL6-CGH array design was performed using the high-density aCGH search function of the web-based Agilent eArray database, version 4.5 [12].

The genomic regions corresponding to *COL6A1-A2-A3-A5* and *-A6* genes as well as a group of genes functionally related to collagen VI (Table 1) [13-21] were masked for repetitive elements and converted into a 10.197 probe set by selecting the maximum number of exonic and intronic 60 mer oligonucleotide probes available in the Agilent database. This probe set was enriched with 377 probes in triplicate, covering the regions of *COL6A1, 2* and *3* genes not investigated by the Agilent CGH probe database. The final mean resolution for these genes was one probe every 320 bp. In order to reach the 15K array format, each array was filled with control probes from all the chromosomes (2851).

The array format utilized was 8 × 15K, made up of eight identical 15K arrays on a single slide, thereby permitting simultaneous analysis of eight different samples. Genomic DNA was extracted from the patients' whole blood or cultured fibroblasts by a Nucleon™ BACC Genomic DNA Extraction Kit (GE Healthcare). Labeling and hybridization were performed following the protocols provided by Agilent (Agilent Oligonucleotide Array-Based CGH for Genomic DNA Analysis protocol v5.0). The array was analyzed with the Agilent scanner and the Feature Extraction software (v9.1). A graphical overview and analysis of the data were obtained using the CGH analytics software (v3.5). For identifying duplications and deletions we used the statistical calculations based on ADM-2 algorithm provided by the CGH analytics software. According to this set-up and in the case of autosomal genes, deletions are visualized with values of -1 if in heterozygosity and with values of minus infinite (-4 in CGH analytics) if in homozygosity. For three

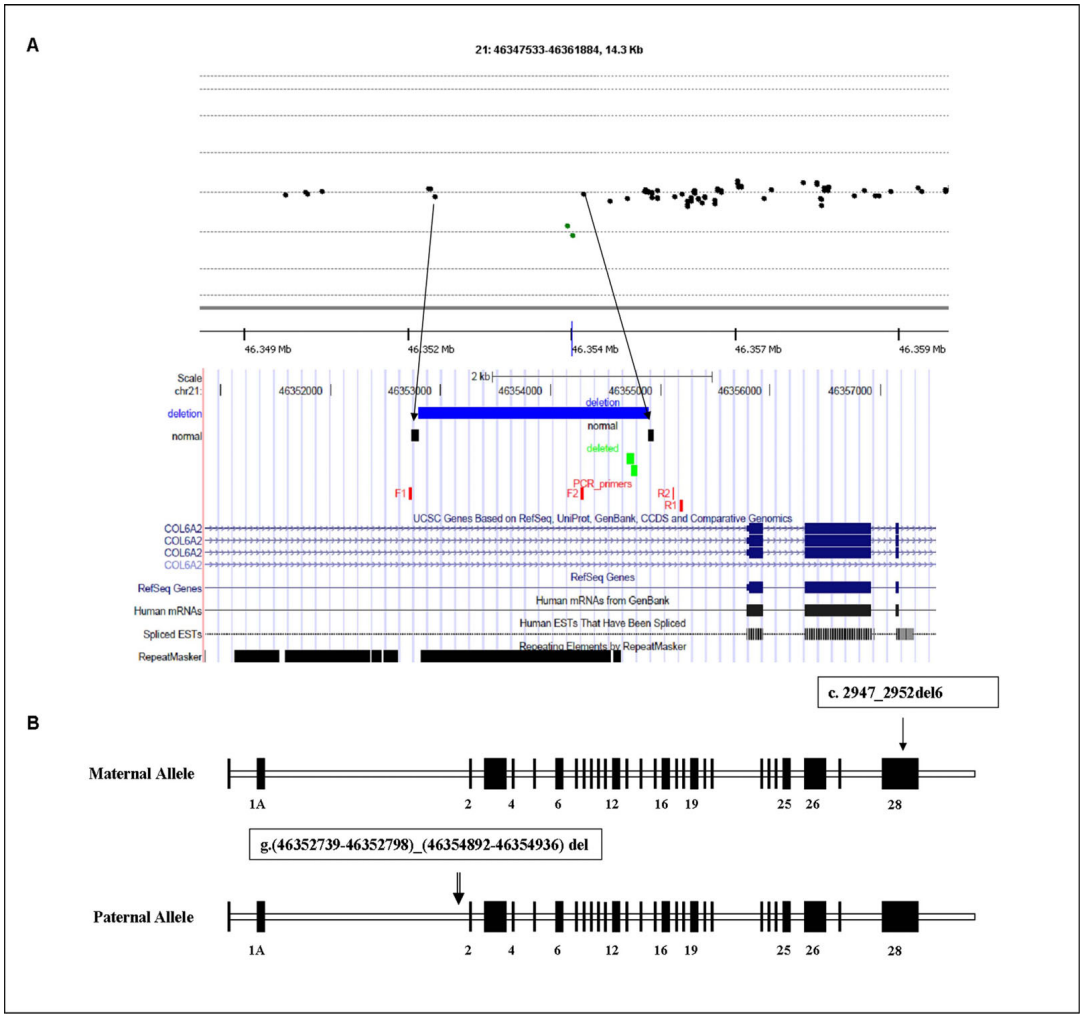

Figure 1 CGH-array profile and *COL6A2* gene allelic configuration. **A)**. CGH-array profile of the *COL6A2* intron 1A deletion and its schematic representation in the context of the entire *COL6A2* gene. A custom track containing the maximum theoretical deleted region spanning 2094 bp (blue bar), derived from the closest normal probes (black bars), the two deleted probes (green bars) and PCR primers pairs (red bars), was created on UCSC Genome Browser. The two deleted probes lay at 1054 bp from exon 2. The region between the 5'-normal probe and the first-deleted probe is covered by repetitive elements (black bar at the bottom). The two probes identifying the deletion lye within unique sequences. **B)** Schematic representation of the *COL6A2* gene allelic configuration in BM Patient 1, with the maternal allele (allele 1) carrying the 6-nucleotide deletion within exon 28 and the paternal allele (allele 2) carrying the intronic deletion within intron 1A.

copies, the value would be approximately +0.6 and for four copies the value would be +1.

The platform informations have been submitted to the online data repository Gene Expression Omnibus (GEO) [22], under accession number GPL9972.

Real-Time PCR

Ad hoc Real-Time PCR assays were designed for the *COL6A2* intron 1A deletion and the CNVs identified within the ITGB1 and ITGA5/ITGA genomic regions (Table 1 and Additional file 1). For confirming *COL6A2* intron 1A deletion, a TaqMan assay was firstly used; MGB probe and primer design was performed by Primer Express Software 2.0 (Applied Biosystems) (FW TTGGTCACAGGTTATGCAACA, Rev GGTGAGTTTCACAGCTTCAAGGA; Probe 6-FAM-AACAAGTTAAATAGCATGAAGTG) (see Additional file 2).

Real-Time PCR was performed in triplicate in 96-well plates using 50 ng genomic DNA and default parameters on the Applied Biosystems Prism 7300 system. For relative quantification, the ΔΔCT Method (Applied Biosystems User Bulletin #2) was utilized. *CFTR* exon 15 was

Table 1 Genes, corresponding genomic regions and protein products included in the *COL6*-CGH micro-array design

Genes	Chromosomal Coordinates (NCBI Build 35)	Proteins
HSPG2	chr1:21894043-22010053	Heparan sulfate proteoglycan 2
COL6A3	Chr2:237914662-238204820	Collagen, type VI, alpha-3 chain
COL29A1; COL6A6	Chr3:131447049-131978580	Collagen, type XXIX, alpha 1 Collagen type VI alpha 6
ITGA1; ITGA2	chr5:52019893-52526365	Integrin, alpha 1 Integrin, alpha 2
TNXB	chr6:32116611-32186183	Tenascin XB
ITGB1	chr10:33130501-33364492	Integrin, beta 1
DCN	chr12:90041504-90075827	Decorin
ITGA5; ITGA7	chr12:52975314-54487894	Integrin, alpha 5; Integrin, alpha 7
CSPG4	chr15:73654019-73892151	Chondroitin sulfate proteoglycan 4
COL6A1; COL6A2	chr21:46126091-46474147	Collagen, type VI, alpha 1 chain Collagen, type VI, alpha 2 chain
BGN	chrX:152181258-152395851	Biglycan

employed as a reference gene, and three control DNAs were used as calibrators for each experiment. Specific assays based on SYBR-green chemistry were also employed in order to further verify the intron 1A deletion and to confirm the CNVs identified in the ITGB1 and ITGA5/ITGA7 genomic regions, (Chr10_FW CGTGGAGATGGGATTAGTGTG, Chr10_Rev TTTGT TGGGAATTTACTTGGTG; Chr12_FW AATTTG CTGTTGCTGGGTCT, Chr12_Rev TCCCATACTCTC-CATTGTCC; Chr21_FW GCCTGTCTGCCTCTTCCA, Chr21_Rev TGTTGCATAACCTGTGACCAA) (see Table 1 and Additional file 2).

Transcript analysis in BM Patient 1

Total RNA was isolated from confluent fibroblasts by using an RNeasy Kit (QIAGEN, Chatsworth, CA), and reverse transcribed using a High Capacity cDNA Reverse Transcription Kit (Applied Biosystem, Foster City CA). RT-PCR was performed with a forward primer within *COL6A2* exon 25 and a reverse primer within the 5' of exon 28, as well as with a forward primer within exon 26 and a reverse within the 3' of exon 28, as previously described [23]. The sequence of primers employed is available upon request.

Immunohistochemistry, electron microscopy and Western Blot in BM Patient 1

Unfixed frozen sections of the *tibialis anterior* muscle from BM Patient 1 and control were labeled with anti-collagen VI antibody (Chemicon MAB1944) diluted 1:100, followed by FITC-conjugated anti-mouse antibody (DAKO); sections were double-labeled with anti-perlecan antibody (Chemicon) diluted 1:100, and revealed with a TRITC conjugated anti-rat antibody (SIGMA). Muscle sections were also labeled with anti-caveolin 3 (BD-Transduction), collagen IV, laminin α2 and laminin β1 chains (Chemicon), followed by FITC-conjugated secondary antibody, while fibronectin (Sigma) and alpha-dystroglycan (Upstate Biotechnologies) were followed by TRITC-conjugated antibody (Sigma, MO). The fibroblast cultures from Patient 1 and from a control were obtained by mechanical means from bioptic skin fragments and set up as previously described [24]. A mouse monoclonal anti-collagen VI antibody (MAB1944, Chemicon) was employed, and the resulting immunoreaction was detected with a secondary FITC-conjugated anti-mouse antibody (DAKO). For immunoelectron microscopy analysis, cells were incubated with a monoclonal anti-collagen VI antibody (Chemicon) diluted 1:25 with Dulbecco's modified Eagle's medium and with 5 or 15-nm colloidal gold-labeled IgG (Amersham). Rotary shadowing electron microscopy was performed as described [25].

Samples derived from skin fibroblast cultures and muscle biopsies were prepared for Western Blot analysis as previously described [23]. Collagen VI was detected by immunoblotting with antibodies recognizing either all collagen VI chains (Fitzgerald 70XR95) or the α1(VI) chain (Santa Cruz sc-20649) alone. Antibodies recognizing AKT (Cell Signaling) and myosin (Sigma) were used for cell culture loading and muscle samples.

Results

Patient selection and COL6-CGH array validation

Twelve patients clinically diagnosed as possessing UCMD (6 patients) or BM (6 patients) phenotypes negative at genomic sequence analysis, and 2 patients (1 UCMD, 1 BM) in whom a sequence analysis positive for *COL6* mutations failed to fully explain the clinical phenotype were selected (Table 2).

Table 2 Summary of clinical and genomic data in the analyzed BM/UCMD patients

SAMPLE ID	COL6A1-A2-A3 Genomic Sequencing	Inheritance	Sex	Presentation	Age at review, yr	Max motor ability (Power Grade)	Contractures	Distal laxity	Skin phenotype	Creatine kinase level*	Respiratory function (% of predicted)	Cardiac evaluation	Collagen VI SKM	Array Results
1 (BM) [26]	COL6A2 c.2947_2952del 6 het (mat)	Sporadic	F	3 yrs, difficulty in running & climbing stairs	20	Walked 15 mo-present	Neck, elbows, fingers, knees, ankles	Fingers	Rough skin, dystrophic nails, cheloids	3.5	52%	normal	Mildly reduced at BM of several muscle fibers	chr21 g.(46352739-46352798) _ (46354892-46354936) del
2 (UCMD)	COL6A1 c.350 C>T het p.V117A (pat)	Sporadic	M	Birth, hip dislocation	4	Able to walk 4 UL and 3,4 LL	Knees, ankles	Fingers	none	1.5	89%	normal	ND	-
3 (BM)	-	Familial	F	3 yrs, difficulty in running & climbing stairs	48	Walked 13 mo-present	Neck, elbows, fingers, ankles	none	none	2	58%	normal	ND	-
4 (BM)	-	Familial AD	M	3 yrs, unable to collect objects from the floor	24	Walked 12 mo-present	Neck, elbows, fingers, knees, ankles	Fingers	Hypertrophic scars	1.5	74%	normal	Mildly reduced at BM of some muscle fibers	chr10 g: (33176784_33176843) _ (33178291_33178350) del
5 (BM) [45]	-	Familial AD	M	18 yrs, reduced stamina	36	Walked 12 mo-present	Neck, fingers, knees, ankles	none	none	4	95%	normal	Normal amount and localization	chr12 g: (54068784_54068843) _ (54070617_54070676) dup
6 (BM)	-	Sporadic	M	5 yrs, difficulty in bending forward	15	Walked 12 mo-14 yrs	Neck, trunk, elbows, fingers, hips, knees, ankles	Fingers	none	18	44%	normal	Normal amount and localization	-
7 (BM)	-	Familial AD	M	30 yrs, easily fatigued, falls	60	Walked 12 mo-present	Fingers, ankles	Fingers	none	2.5	ND	normal	Normal amount and localization	-
8 (BM)	-	Familial AD	F	5 yrs, contractures	39	Walked 12 mo-present	Shoulders, elbows, fingers, hips	None	none	0.8	ND	Sinus tachycardia	ND	-
9 (UCMD)	-	Sporadic	F	Birth with pes talus	3	Walked 14 mo-present	none	Fingers	none	2	ND	ND	Reduced at BM of muscle fibers	-

Table 2: Summary of clinical and genomic data in the analyzed BM/UCMD patients *(Continued)*

10 (UCMD) [11]	-	Sporadic	F	Birth with delay in motor milestones	8	Able to walk 4 UL and LL	none	Fingers	Follicular hyperplasia	normal	85%	normal	Reduced at BM of muscle fibers	-
11 (UCMD)	-	Sporadic	M	2 yrs, hyperlaxity and hyperCK	8	Able to walk 1 hip flex - 3 knees ext	Fingers, hip, knees, ankles	None	none	2	33%	normal	ND	-
12 (UCMD)	-	Sporadic	F	18 mo, unable to walk	31	Able to walk 24 mo-12 yrs	Neck, trunk, elbows, fingers, hips, knees, ankles	None	none	1.5	62%	normal	Normal amount and localization	-
13 (UCMD)	-	Sporadic	F	Birth, floppiness	3	Walked 18 mo-present	Fingers, knees, ankles	Fingers	Follicular hyperplasia	2	ND	ND	Reduced at the BM of muscle fibers	-
14 (UCMD)	-	Sporadic	M	Birth	4	Able to walk at 3 yrs	Congenital kyphosis	Fingers	Follicular hyperplasia	normal	ND	normal	ND	-

*Creatine kinase level: times the upper value of normal.

UL: upper limbs; LL: lower limbs; AD: autosomal dominant; yrs: years; mo: months; ND: not done; SkM: skeletal muscle; BM: basement membrane

One BM patient (Patient 1) had previously been described by Demir *et al*. (# 10, Family 8), who linked the disease in this family to chromosome 21q22.3 [26]. This patient carries a heterozygous small deletion in exon 28 of the *COL6A2* gene (NM_001849, c. 2947_2952del6, p.Asp983_Val984del) inherited from the healthy mother. Patient 2 (UCMD) bears a heterozygous missense alteration (NM_001848, c.350 C>T, V117A) within *COL6A1* exon 3, inherited from the unaffected father. The V117A substitution noted in this patient had not previously been described, so in order to evaluate the pathogenic effect of this missense variation, polymorphism phenotyping predictions were obtained by PolyPhen [27] and SIFT [28] with contrasting results: PolyPhen predicted a benign variation whereas SIFT foresaw a harmful effect of the V117A substitution. Subsequently, amino acid conservation of V117 was analyzed, and sequence alignment between distant species showed high conservation of the residue in the VWFA1 domain (data not shown). The screening of 200 control chromosomes excluded it as a common polymorphism.

The COL6-CGH array was designed to cover the regions of genes *COL6A1-A2-A3-A5* and *-A6* and a group of genes functionally related to collagen VI (Table 1). Ten possible candidate genes were considered on the basis of the following criteria: either i) their direct interaction with collagen VI, as in the case of HSPG2 [13], ITGA1, ITGA2, ITGB1 [14], DNC and BGN [15]; ii) their secondary involvement in collagen VI-deficient tissues, as in NG2-proteoglycan [16,17], ITGA5 and ITGA7 [18,19], or iii) their mutations causing an overlapping phenotype with collagen VI-related myopathies, as in TNXB [20]. COL6A5 (COL29A1) and COL6A6, which are expressed in skeletal muscle, were also included since collagen VI alpha1-deficient mice do not express collagen VI alpha 5 or alpha 6 chains [21].

The full coding region of all selected genes was included, together with intronic sequences and 100 kb at the 5' and 3' of the first and last exons, respectively. The array was technically validated before commencing by using DNA from 8 normal controls; no CNVs were detected.

Two novel CNVs were identified in BM patients 4 and 5 (Table 1 and Additional File 2). The first was a 1.4 Kb deletion, located 35 Kb downstream the ITGB1 gene and the second was a 1.7 Kb duplication in the intergenic region between ITGA5 and ITGA7. Both CNVs were confirmed by Real-Time PCR analysis (data not shown), but the occurrence of both variations in unaffected family members and healthy controls from the general population permitted exclusion of their pathogenic significance (see Additional File 2).

The complete CGH datasets have been submitted to the online data repository Gene Expression Omnibus [22], under accession number GSE20025.

Identification of a pure intronic deletion in intron 1A of the COL6A2 gene in BM patient 1

In early infancy, Patient 1 (BM) (Table 2) attained normal motor milestones and walked at 15 months of age. However, aged 3 and a half, she began to have difficulty running. Creatine kinase was 3.5 times the upper limit of normal, and examination at age 21 revealed a short stature, excessive weight and bilateral club foot. The patient was able to walk and climb stairs without support, but was unable to run. Mild facial and limb/girdle weakness and moderate axial and distal weakness were noted. The patient was unable to bury the eyelashes completely or to flex neck against gravity, and digitorum extension weakness was evident. The patient suffered contractures of the neck, elbows, fingers, knees and ankles, combined with finger extension hypermobility when the wrist was flexed. Her skin was rough and cheloidal, and nails were dystrophic. Forced vital capacity was 52%, and cardiac examination evidenced no abnormality. Examination at age 30 years revealed a relatively stable condition, with only the ability to get up from the floor having been further compromised.

In BM Patient 1, CGH analysis revealed the presence of a deletion within intron 1A of the *COL6A2* gene (NM_001849). This deletion was detected by two overlapping probes which covered 95 base pairs: the 5'-deleted probe lying 12.237 nucleotides from exon 1A, and the 3'-deleted probe located 999 nucleotides from exon 2. The two flanking probes, which showed normal hybridization levels, were localized respectively, 1900 nucleotides from the proximal 5'-deleted probe and 194 nucleotides from the distal 3'-deleted probe. Thus, the identified deletion spans a maximum theoretical region of 2094 bp, and is located 1 kb upstream of the first *COL6A2* coding exon (exon 2). Comparative sequence analysis using the two deleted probes identified a genomic region lying adjacent to a cluster of repetitive elements (Figure 1A) [29].

Real-Time PCR analysis performed using two different assays, one based on SYBR-green and the other on TaqMan chemistries, confirmed the occurrence of the deletion, which was inherited from the healthy father (see Additional File 3). Analysis of 100 control subjects from the normal population by Real-Time PCR failed to identify the *COL6A2* intron deletion.

Genotypic analysis of the proband's parents showed the intronic deletion and the exon 28 small mutations in *trans*, denoting autosomal recessive transmission.

An attempt to amplify by junction PCR the deletion breakpoint with primers outside the maximum theoretical deleted region was unsuccessful, and sequencing analysis of the PCR products obtained using different sets of primers failed to identify the mutated allele. This suggests the possibility of a complex rearrangement/inversion of the involved genomic region (Figure 1A).

Occurrence of monoallelic COL6A2 transcription in BM Patient 1 fibroblasts

In order to assess the pathogenic meaning of the identified intronic deletion found in BM Patient 1, fibroblasts were harvested and cultured prior to RNA analysis. This analysis was focused on the terminal region of the *COL6A2* transcript, from exon 26 (harboring two common polymorphisms (Ala698Ala and Gly699Gly), heterozygous at the genomic analysis) to exon 28 (the site of the maternal heterozygous 6-nucleotide deletion). Direct sequencing of the amplified fragments revealed the presence of a pseudo-homozygosity for the exon-28 deletion, as well as

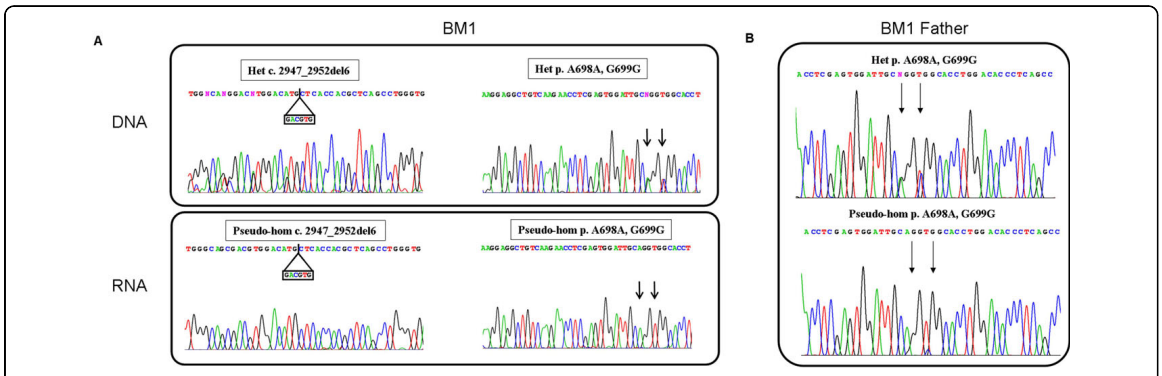

Figure 2 ***COL6A2*** **genomic and transcript analysis in BM Patient 1 and his father**. **A)** Sequence chromatograms of BM Patient 1 showing the maternal deletion within exon 28 (GACGTG) (left) and two polymorphisms (c.2094 G>A - A698A; C.2097 C>T - G699G) within exon 26 (black vertical arrows) (right) occurring heterozygously at the DNA level (upper panel) and pseudo-homozygously at the RNA level (lower panel). **B)** Sequence chromatograms in the BM Patient 1 father showing that the exon 26 polymorphisms (c.2094 G>A - A698A; C.2097 C>T - G699G) occur heterozygously at the DNA level (upper panel). At the RNA level (lower panel) the nucleotide variants that are undetectable in the BM Patient 1 (c.2094 G and c.2097 C), are only barely visible in the father.

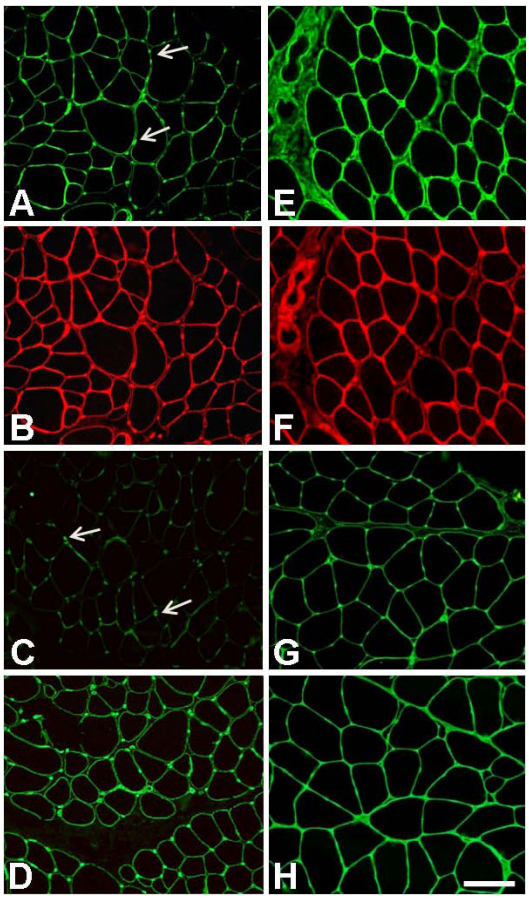

Figure 3 Immunohistochemical analysis on muscle biopsy from BM patient 1. Immunofluorescence analysis on muscle sections of BM Patient 1 (**A-D**) and control (**E-H**) of collagen VI (**A, E**), perlecan (**B, F**), laminin β1 (**C, G**) and collagen IV (**D, H**). A small reduction in collagen VI in the patient's endomysium (**A**) was observed in comparison with control (**E**). However, collagen VI was expressed normally around the blood vessels (arrows, **A**). Double-labeling with anti-perlecan antibody revealed a normal pattern (**B**) as well in the control section (**F**). Laminin β1 expression was reduced at the basal lamina of muscle fibers, while being expressed normally around the capillary walls (arrows, **C**). Collagen IV labeling showed a normal pattern around both vessels and muscle fibers (**D**). Bar, 40 μm.

for the polymorphisms within exon 26 (Figure 2). This implies that the allele carrying the intronic deletion is not transcribed at appreciable levels.

In order to strengthen the case for a relationship between the identified intronic deletion and the transcriptional behavior, RNA analysis was performed on cultured skin fibroblasts from the patient's father. The two exon 26 polymorphisms (Ala698Ala; Gly699Gly) were found to be heterozygous at the genomic level, although their transcription was strongly imbalanced. The nucleotide variant of the polymorphisms (c.2094 G>A - A698A; C.2097 C>T - G699G) that was completely undetectable in the proband's RNA (G and C, respectively), was only barely visible in cells from the father (Figure 2).

Collagen VI expression in muscle and cell cultures from BM Patient 1

Muscle biopsy of Patient 1 revealed a mild reduction in collagen VI in the endomysium (Figure 3A) in comparison with control (Figure 3E). Double labeling with anti-perlecan antibody showed a normal pattern, attesting the integrity of the basement membrane. Alpha-dystroglycan, caveolin 3, fibronectin, and laminin α2 chains (data not shown) were normally expressed, as was collagen IV (Figure 3D), while laminin β1 chain labeling was reduced around the muscle fibers and preserved at the basement membrane of blood capillary vessels (Figure 3C). In cultured skin fibroblasts, a mildly reduced expression of collagen VI protein was associated with an altered organization of the microfibrillar network: the immunofluorescence pattern was characterized by a coarser texture than normal with fewer thinner fibrils (Figure 4A). A finely structured collagen VI network was no longer visible, while thicker fibers were still present. Electron microscopy analysis of rotary-shadowed replicas of patient's *in vivo*-labeled fibroblasts showed the presence of thick collagen VI fibrils, constituted by several parallel microfilaments, while regularly developed webs of interconnected and cross-linked filaments like those seen in control fibroblasts were absent (Figure 4C-E). Western blot of fibroblast cultures and muscle biopsy samples using two different antibodies recognizing either all collagen VI chains or the α1(VI) chain alone revealed a quantitative deficiency of collagen VI in the patient, as compared to an unaffected control (Figure 5). The reduced amount of collagen VI in skeletal muscle was confirmed by immunoblotting for myosin, used as a loading control for normalizing the amount of muscle tissue.

Discussion

Molecular genotyping of UCMD and BM patients is currently performed by extensive sequencing of *COL6A1, A2* and *A3* genes. Unfortunately, however, the PCR-based techniques used in routine screening miss gross rearrangements as well as CNVs which exceed the dimensional limitations of PCR amplification. Furthermore, molecular analysis fails to identify the causative mutation in a significant percentage of patients, ranging from 20-25% in UCMD to 35-40% in BM [5]. This relatively low detection rate of current molecular approaches in collagen VI myopathies could be ascribed to allelic heterogeneity (linked to the abovementioned limitations of PCR-based techniques) and/or genetic heterogeneity. This latter hypothesis implies that UCMD/BM phenocopies

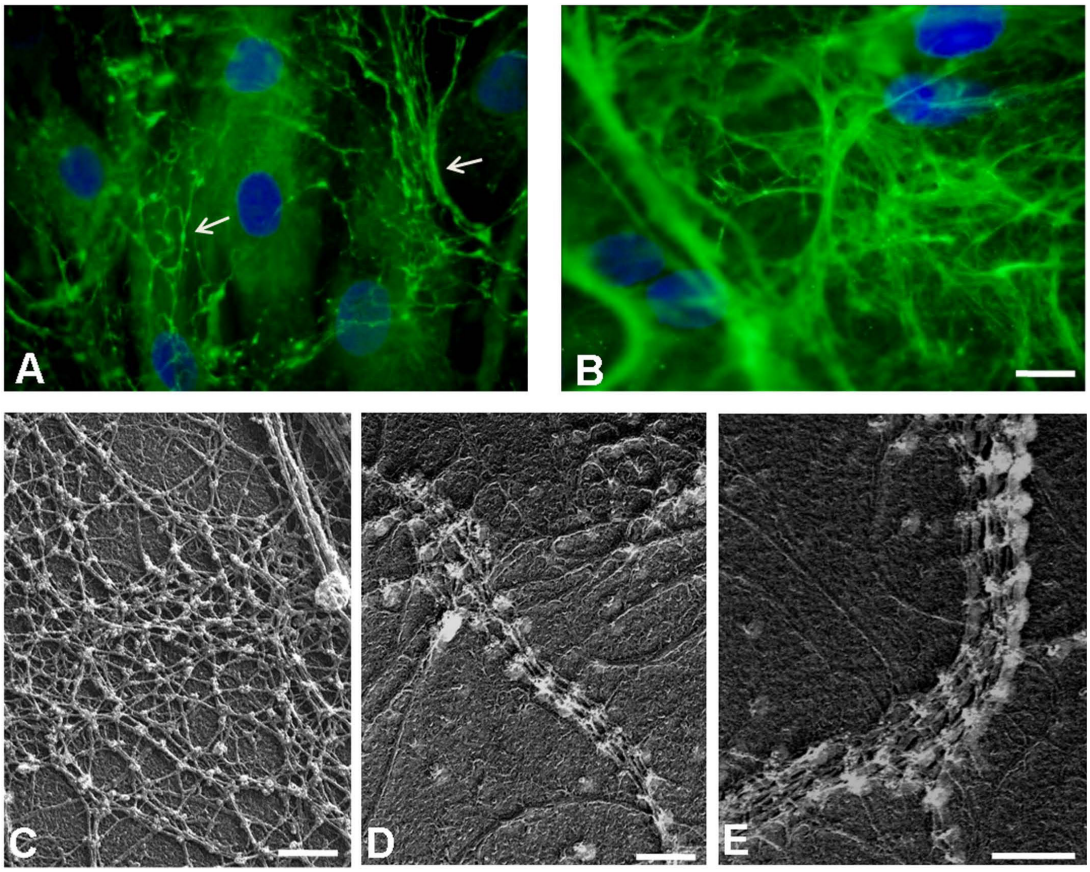

Figure 4 Immunohistochemical analysis and electron microscopy on fibroblasts. Reduced amount of collagen VI microfilamentous network was detected in the extracellular matrix secreted by fibroblasts of BM Patient 1 (**A**) as compared to control fibroblasts (**B**). The microfibrillar network in the patient's fibroblasts showed an altered organization, characterized by a coarser texture than normal (**A**, Arrows) Fibroblast density was monitored by DAPI staining of the nuclei. Bar, 20 μm. Electron microscope examination of rotary-shadowed cultured fibroblasts from control (**C**) and BM Patient 1 (**D-E**), labeled with anti-collagen VI and revealed with a secondary antibody conjugated with 5-nm colloidal gold particles. Ultra-structural analysis of the rotary-shadowed fibroblasts revealed the presence of collagen VI fibrils constituted by several parallel running microfilaments in BM Patient 1 (**D, E**), while regular webs of interconnected microfilaments, like those shown in control fibroblasts (**C**), were absent. Bar, 200 nm.

could occur, due to mutations in different, still unidentified genes.

In the last few years, novel genomic-based technologies have been reported as an efficient and improved alternative to PCR in molecular diagnosis. Oligonucleotide array-based CGH was initially developed to detect major changes in chromosomal copy number [30], and since then both commercial and custom arrays have been also used to discern these changes in selected genomic regions of interest [31,32]. The *DMD* gene was a perfect candidate to test the validity of this approach, due to the large size and high number of gross copy number variations apparent in this condition. Moreover, different custom arrays have already been validated for the exploration of both coding [33] and non-coding regions of the gene [34-36]. For *COL6* genes, the possibility that genomic dosage imbalance or large CNVs occur with significant frequency in UCMD/BM patients still remains untested.

With the aim of increasing the sensitivity of molecular diagnosis in collagen VI-related disorders, a custom oligonucleotide-based CGH array able to detect CNVs in coding and non-coding regions of the *COL6A1, A2, A3*, and the *A5* and *A6* genes recently discovered to encode novel collagen VI chains [21,37] was designed. Moreover, in order to investigate genetic heterogeneity, the genomic regions of other genes selected on the basis of their known or hypothetical functional relationship with

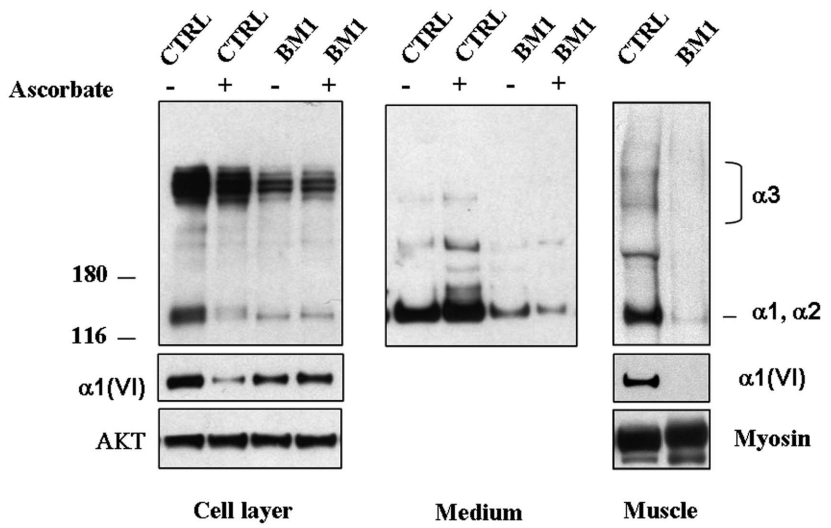

Figure 5 Western Blot analysis of fibroblasts. Western blot analysis of collagen VI in cultured skin fibroblasts and in muscle biopsies from control (CTRL) and BM Patient 1 (BM1) was performed. Samples corresponding to the cell layer (left panel, 20 μg) and medium (middle panel, 30 μg) in the presence or absence of L-ascorbate, and muscle extracts (right panel, 15 μg), were separated by electrophoresis under reducing conditions in 3-8% polyacrylamide-gradient gel. Collagen VI was detected by immunoblotting with antibodies recognizing either all collagen VI chains (Fitzgerald 70XR95) or the α1(VI) chain (Santa Cruz sc-20649). Migration of the collagen VI chains is indicated on the right and molecular weight markers (kDa) are shown on the left. Control for loading was performed by antibodies against AKT (cell layers) or myosin (muscle biopsies).

collagen VI were also included in the design, as all these genes potentially represent candidates for mutations that could underlie phenocopies of collagen VI-related diseases [38,39,13,15,40-42].

By testing our array in 14 selected UCMD/BM patients, we identified a deep intronic deletion in the *COL6A2* gene in a BM patient occurring in compound heterozygosity with a small exonic mutation previously detected by sequencing. Despite not definitively proven, due to the failure to amplify the deletion breakpoint, nevertheless the pathogenic potential of this intronic mutation is supported by the transcriptional impairment of the mutated allele that was demonstrated both in the proband and in her healthy carrier father. The *COL6A2* gene is characterized by a first-coding exon (exon 2) separated from two alternatively spliced 5'-untranslated exons (exon 1 and 1a) by a huge 12 kb intron (intron 1A) [43].

Deletion of this intron may abolish *cis*-acting elements and/or the binding of *trans*-acting factors involved in the regulation of *COL6A2* gene expression. Alternatively, the deletion itself might be the marker for a complex genomic rearrangement occurring in the *COL6A2* gene that inverts or scrambles the entire genomic configuration. The failure of PCR to amplify the deletion junction seems to support this hypothesis.

This study documents an additional case of a BM patient with a compound heterozygous genotype for recessive *COL6A2* mutations. Interestingly, both of the autosomal recessive BM cases we previously described carried a peculiar allele combination consisting of a truncating mutation partnered by missense changes within the α2(VI) C2 region [3]. Despite different (null mutation/in-frame deletion), the allelic configuration of BM Patient 1 also indicates the presence of a mutated α2(VI) C2 domain, derived from a single allele, similar to the recessive BM cases previously described [3]. The findings in this patient also substantiate the observation that recessive BM mutations, unlike the classical dominant cases, affect collagen VI expression in skeletal muscle [3], as attested by immunohistochemical and biochemical analyses showing a decreased amount of this protein.

In the twelve patients who tested negative upon genomic sequence analysis, no CNVs were identified in *COL6* genes using the CGH array. Even though the limited size of the analyzed patient cohort hampered definitive estimations, our results did exclude a relevant incidence of CNVs within *COL6* genes, thereby supporting UCMD/BM genetic heterogeneity. Likewise, no pathogenic CNVs were identified among the other genomic regions potentially harboring candidate BM/UCMD genes that were explored in the array. Nevertheless, these results do not rule out the possibility that genetic heterogeneity could account for some *COL6A1-3*-negative patients and suggest that high-throughput sequencing technologies could

represent more appropriate future approaches for detection of point mutations. In fact, these innovative tools could allow significant enlargement of the spectrum of functionally related collagen VI genes to be explored sequentially via CNV identification and re-sequencing for detection of point mutations.

Conclusions

The described COL6-CGH array could represent a useful complementary diagnostic test, useful for increasing the sensitivity of molecular analysis in patients with a clinical diagnosis of collagen VI-related disorders. The limited size of the patient cohort we analyzed hampered estimation of copy number variation frequency, but analysis of larger populations could well permit conclusions to be drawn. In fact, this novel tool allowed us for the first time to identify a *COL6A2* mutation affecting gene transcription deeply located within an intronic region, and thus undetectable with all other techniques currently available. Furthermore, in recent years specific genetic diagnosis has become mandatory for a patient to be eligible for upcoming therapeutic trials [44], and thus the lack of molecular diagnosis in a large percentage of patients with collagen-VI related phenotypes makes the search and the validation of novel diagnostic tools an ever-more pressing issue.

Additional file 1: Gene Symbols, chromosomal coordinates, transcript and protein identifiers for the genes included in the *COL6*-CGH microarray design.

Additional file 2: CNVs identified in BM Patients 4 and 5. **A)** *COL6*-CGH array result in BM Patient 4, showing the deletion of about 1.4 kb identified on chromosome 10, 35 Kb downstream of the ITGB1 gene. **B)** The CNV on chromosome 10 was validated by Real-Time PCR, and its segregation was analyzed in Patient 4's family; the deletion was present in three unaffected subjects (2-ΔΔCT values of 0.44, 0.41, 0.45) and absent in the symptomatic proband's mother and cousin (2-ΔΔCT values of 0.99 and 0.86), thus not linked to the disease. **C)** *COL6*-CGH array result in BM Patient 5, showing the 1.7 Kb duplication occurring in the intergenic region between ITGA5 and ITGA7 on chromosome 12.

Additional file 3: Real Time PCR experiments confirming COL6A2 intron 1A deletion in BM Patient 1 and in the father. In the upper panel, the results obtained with an intron 1A specific TaqMan assay are shown. Red plots correspond to utilized reference gene (CFTR exon 15) whereas green plots refer to target sequence within intron 1A. The Ct (threshold cycle) values of the target sequence are in line with the reference in control sample (unaffected subject) and in proband's mother, whereas the target Ct values are higher than reference in BM Patient 1 and in the father, attesting the deletion (2-ΔΔCT values were 0.47 and 0.53 in BM Patient 1 and in the father respectively, whereas the 2-ΔΔCT value was 0.97 in the proband's mother). In the lower panel the position of the primers utilized in the SYBR green assay (blu) and of primers and probe utilized in the TaqMan assay (pink), are shown in respect to the deleted region (in bold).

Acknowledgements
This study was supported by the Italian Telethon Foundation grants GUP07004 (to GF). The Telethon grant GGP08107 (awarded to AF and PB) and the TREAT-NMD Network of Excellence of EU FP7 (awarded 036825 to LM and Telethon-Italy), are also acknowledged.

Author details
[1]Department of Experimental and Diagnostic Medicine - Section of Medical Genetics, University of Ferrara, Ferrara, Italy. [2]Department of Histology, Microbiology and Medical Biotechnologies, University of Padua, Padua, Italy. [3]IGM-CNR, Unit of Bologna c/o IOR, Bologna, Italy. [4]Department of Child Neurology and Psychiatry, Catholic University, Rome, Italy. [5]Unit of Molecular Medicine, Department of Laboratory Medicine, Bambino Gesu' Hospital, Rome, Italy. [6]Laboratory of Biology, IOR, Bologna, Italy.

Authors' contributions
MB designed the array and carried out DNA extraction and hybridization of samples, Real-time PCR experiments, and analysis and interpretation of data; MN performed DNA extraction and hybridization of samples, Real-time PCR experiments, and contributed to preparation of the manuscript; EM performed genomic and transcript analyses; MF prepared fibroblasts cell cultures; AU and PG carried out Western Blotting; PS performed ICC analysis; EM and EB carried out clinical evaluation of the patients; LM clinically evaluated the patients and participated in revision of the manuscript; PB assisted in the interpretation of data and revision of the manuscript; AF contributed to conception of the study and preparation of the manuscript; FG conceived and designed the study, prepared and revised the manuscript and approved the final version.

Competing interests
The authors declare that they have no competing interests.

Received: 4 September 2009 Accepted: 19 March 2010
Published: 19 March 2010

References

1. Lampe AK, Bushby KM: **Collagen VI related muscle disorders.** *J Med Genet* 2005, **42**:673-85.
2. Bertini E, Pepe G: **Collagen type VI and related disorders: Bethlem myopathy and Ullrich scleroatonic muscular dystrophy.** *Eur J Paediatr Neurol* 2002, **6**:193-198.
3. Gualandi F, Urciuolo A, Martoni E, Sabatelli P, Squarzoni S, Bovolenta M, Messina S, Mercuri E, Franchella A, Ferlini A, Bonaldo P, Merlini L: **Autosomal recessive Bethlem myopathy.** *Neurology* 2009, **73(22)**:1883-91.
4. Foley AR, Hu Y, Zou Y, Columbus A, Shoffner J, Dunn DM, Weiss RB, Bönnemann CG: **Autosomal recessive inheritance of classic Bethlem myopathy.** *Neuromuscul Disord* 2009, **19**:813-7.
5. Lampe AK, Dunn DM, von Niederhausern AC, Hamil C, Aoyagi A, Laval SH, Marie SK, Chu ML, Swoboda K, Muntoni F, Bonnemann CG, Flanigan KM, Bushby KM, Weiss RB: **Automated genomic sequence analysis of the three collagen VI genes: applications to Ullrich congenital muscular dystrophy and Bethlem myopathy.** *J Med Genet* 2005, **42**:108-20.
6. Baker NL, Morgelin M, Peat R, Goemans N, North KN, Bateman JF, Lamande SR: **Dominant collagen VI mutations are a common cause of Ullrich congenital muscular dystrophy.** *Hum Mol Genet* 2005, **14**:279-93.
7. Giusti B, Lucarini L, Pietroni V, Lucioli S, Bandinelli B, Sabatelli P, Squarzoni S, Petrini S, Gartioux C, Talim B, Roelens F, Merlini L, Topaloglu H, Bertini E, Guicheney P, Pepe G: **Dominant and recessive COL6A1 mutations in Ullrich scleroatonic muscular dystrophy.** *Ann Neurol* 2005, **58**:400-10.
8. **Leiden Pages.** [http://www.dmd.nl/].
9. Pepe G, Lucarini L, Zhang RZ, Pan TC, Giusti B, Quijano-Roy S, Gartioux C, Bushby KM, Guicheney P, Chu ML: **COL6A1 genomic deletions in Bethlem myopathy and Ullrich muscular dystrophy.** *Ann Neurol* 2006, **59**:190-5.
10. Pan TC, Zhang RZ, Sudano DG, Marie SK, Bonnemann CG, Chu ML: **New molecular mechanism for Ullrich congenital muscular dystrophy: a heterozygous in-frame deletion in the COL6A1 gene causes a severe phenotype.** *Am J Hum Genet* 2003, **73**:355-69.
11. Petrini S, D'Amico A, Sale P, Lucarini L, Sabatelli P, Tessa A, Giusti B, Verardo M, Carrozzo R, Mattioli E, Scarpelli M, Chu ML, Pepe G, Russo MA, Bertini E: **Ullrich myopathy phenotype with secondary ColVI defect identified by confocal imaging and electron microscopy analysis.** *Neuromuscul Disord* 2007, **17**:587-96.
12. **Agilent Technologies eArray.** [https://earray.chem.agilent.com/earray].

13. Tillet E, Wiedemann H, Golbik R, Pan TC, Zhang RZ, Mann K, Chu ML, Timpl R: **Recombinant expression and structural and binding properties of alpha 1(VI) and alpha 2(VI) chains of human collagen type VI.** *Eur J Biochem* 1994, **221**:177-85.
14. Pfaff M, Aumailley M, Specks U, Knolle J, Zerwes HG, Timpl R: **Integrin and Arg-Gly-Asp dependence of cell adhesion to the native and unfolded triple helix of collagen type VI.** *Exp Cell Res* 1993, **206**:167-76.
15. Wiberg C, Hedbom E, Khairullina A, Lamandé SR, Oldberg A, Timpl R, Mörgelin M, Heinegård D: **Biglycan and decorin bind close to the n-terminal region of the collagen VI triple helix.** *J Biol Chem* 2001, **276**:18947-52.
16. Petrini S, Tessa A, Stallcup WB, Sabatelli P, Pescatori M, Giusti B, Carrozzo R, Verardo M, Bergamin N, Columbaro M, Bernardini C, Merlini L, Pepe G, Bonaldo P, Bertini E: **Altered expression of the MCSP/NG2 chondroitin sulfate proteoglycan in collagen VI deficiency.** *Mol Cell Neurosci* 2005, **30**:408-17.
17. Higashi K, Higuchi I, Niiyama T, Uchida Y, Shiraishi T, Hashiguchi A, Saito A, Horikiri T, Suehara M, Arimura K, Osame M: **Abnormal expression of proteoglycans in Ullrich's disease with collagen VI deficiency.** *Muscle Nerve* 2006, **33**:120-6.
18. Hu J, Higuchi I, Shiraishi T, Suehara M, Niiyama T, Horikiri T, Uchida Y, Saito A, Osame M: **Fibronectin receptor reduction in skin and fibroblasts of patients with Ullrich's disease.** *Muscle Nerve* 2002, **26**:696-701.
19. Pepe G, Bertini E, Bonaldo P, Bushby K, Giusti B, de Visser M, Guicheney P, Lattanzi G, Merlini L, Muntoni F, Nishino I, Nonaka I, Yaou RB, Sabatelli P, Sewry C, Topaloglu H, Kooi van der A: **Bethlem myopathy (BETHLEM) and Ullrich scleroatonic muscular dystrophy: 100th ENMC international workshop 2001, 23-24 November Naarden, The Netherlands.** *Neuromuscul Disord* 2002, **12**:984-93.
20. Voermans NC, Jenniskens GJ, Hamel BC, Schalkwijk J, Guicheney P, van Engelen BG: **Ehlers-Danlos syndrome due to tenascin-X deficiency: muscle weakness and contractures support overlap with collagen VI myopathies.** *Am J Med Genet A* 2007, **143A**:2215-9.
21. Gara SK, Grumati P, Urciuolo A, Bonaldo P, Kobbe B, Koch M, Paulsson M, Wagener R: **Three novel collagen VI chains with high homology to the alpha3 chain.** *J Biol Chem* 2008, **283**:10658-70.
22. **Gene Expression Omnibus.** [http://www.ncbi.nlm.nih.gov/geo/].
23. Merlini L, Martoni E, Grumati P, Sabatelli P, Squarzoni S, Urciuolo A, Ferlini A, Gualandi F, Bonaldo P: **Autosomal recessive myosclerosis myopathy is a collagen VI disorder.** *Neurology* 2008, **71**:1245-53.
24. Martoni E, Urciuolo A, Sabatelli P, Fabris M, Bovolenta M, Neri M, Grumati P, D'Amico A, Pane M, Mercuri E, Bertini E, Merlini L, Bonaldo P, Ferlini A, Gualandi F: **Identification and characterization of novel collagen VI non-canonical splicing mutations causing ullrich congenital muscular dystrophy.** *Hum Mutat* 2009, **30**:E662-72.
25. Zhang RZ, Sabatelli P, Pan TC, Squarzoni S, Mattioli E, Bertini E, Pepe G, Chu ML: **Effects on collagen VI mRNA stability and microfibrillar assembly of three COL6A2 mutations in two families with Ullrich congenital muscular dystrophy.** *J Biol Chem* 2002, **277**:43557-64.
26. Demir E, Ferreiro A, Sabatelli P, Allamand V, Makri S, Echenne B, Maraldi M, Merlini L, Topaloglu H, Guicheney P: **Collagen VI status and clinical severity in Ullrich congenital muscular dystrophy: phenotype analysis of 11 families linked to the COL6 loci.** *Neuropediatrics* 2004, **35**:103-12.
27. **Polyphen.** [http://genetics.bwh.harvard.edu/pph/].
28. **SIFT.** [http://sift.jcvi.org/www/SIFT_chr_coords_submit.html].
29. **Repeat Masker.** [http://www.repeatmasker.org/].
30. Lu X, Shaw CA, Patel A, Li J, Cooper ML, Wells WR, Sullivan CM, Sahoo T, Yatsenko SA, Bacino CA, Stankiewicz P, Ou Z, Chinault AC, Beaudet AL, Lupski JR, Cheung SW, Ward PA: **Clinical implementation of chromosomal microarray analysis: summary of 2513 postnatal cases.** *PLoS One* 2007, **2**:e327.
31. Wong LJ, Dimmock D, Geraghty MT, Quan R, Lichter-Konecki U, Wang J, Brundage EK, Scaglia F, Chinault AC: **Utility of oligonucleotide array-based comparative genomic hybridization for detection of target gene deletions.** *Clin Chem* 2008, **54**:1141-8.
32. Gunn SR, Robetorye RS, Mohammed MS: **Comparative genomic hybridization arrays in clinical pathology: progress and challenges.** *Mol Diagn Ther* 2007, **11**:73-7.
33. Dhami P, Coffey AJ, Abbs S, Vermeesch JR, Dumanski JP, Woodward KJ, Andrews RM, Langford C, Vetrie D: **Exon array CGH: detection of copy-number changes at the resolution of individual exons in the human genome.** *Am J Hum Genet* 2005, **76**:750-762.
34. Hegde MR, Chin EL, Mulle JG, Okou DT, Warren ST, Zwick ME: **Microarray-based mutation detection in the dystrophin gene.** *Human mutation* 2008, **29**:1091-9.
35. Saillour Y, Cossée M, Leturcq F, Vasson A, Beugnet C, Poirier K, Commere V, Sublemontier S, Viel M, Letourneur F, Barbot JC, Deburgrave N, Chelly J, Bienvenu T: **Detection of exonic copy-number changes using a highly efficient oligonucleotide-based comparative genomic hybridization-array method.** *Human mutation* 2008, **29**:1083-90.
36. Bovolenta M, Neri M, Fini S, Fabris M, Trabanelli C, Venturoli A, Martoni E, Bassi E, Spitali P, Brioschi S, Falzarano MS, Rimessi P, Ciccone R, Ashton E, McCauley J, Yau S, Abbs S, Muntoni F, Merlini L, Gualandi F, Ferlini A: **A novel custom high density-comparative genomic hybridization array detects common copy number variations as well as deep intronic mutations in dystrophinopathies.** *BMC genomics* 2008, **9**:572.
37. Fitzgerald J, Rich C, Zhou FH, Hansen U: **Three novel collagen VI chains, alpha4(VI), alpha5(VI), and alpha6(VI).** *J Biol Chem* 2008, **283**:20170-80.
38. Bonaldo P, Russo V, Bucciotti F, Doliana R, Colombatti A: **Structural and functional features of the alpha 3 chain indicate a bridging role for chicken collagen VI in connective tissues.** *Biochemistry* 1990, **29**:1245-54.
39. Bidanset DJ, Guidry C, Rosenberg LC, Choi HU, Timpl R, Hook M: **Binding of the proteoglycan decorin to collagen type VI.** *J Biol Chem* 1992, **267**:5250-6.
40. Merlini L, Villanova M, Sabatelli P, Malandrini A, Maraldi NM: **Decreased expression of laminin beta 1 in chromosome 21-linked Bethlem myopathy.** *Neuromuscul Disord* 1999, **9**:326-9.
41. Sabatelli P, Bonaldo P, Lattanzi G, Braghetta P, Bergamin N, Capanni C, Mattioli E, Columbaro M, Ognibene A, Pepe G, Bertini E, Merlini L, Maraldi NM, Squarzoni S: **Collagen VI deficiency affects the organization of fibronectin in the extracellular matrix of cultured fibroblasts.** *Matrix Biol* 2001, **20**:475-86.
42. Scacheri PC, Gillanders EM, Subramony SH, Vedanarayanan V, Crowe CA, Thakore N, Bingler M, Hoffman EP: **Novel mutations in collagen VI genes: expansion of the Bethlem myopathy phenotype.** *Neurology* 2002, **58**:593-602.
43. Saitta B, Timpl R, Chu ML: **Human alpha 2(VI) collagen gene. Heterogeneity at the 5'-untranslated region generated by an alternate exon.** *J Biol Chem* 1992, **267**:6188-96.
44. Merlini L, Angelin A, Tiepolo T, Braghetta P, Sabatelli P, Zamparelli A, Ferlini A, Maraldi NM, Bonaldo P, Bernardi P: **Cyclosporin A corrects mitochondrial dysfunction and muscle apoptosis in patients with collagen VI myopathies.** *Proc Natl Acad Sci USA* 2008, **105**:5225-9.
45. Merlini L, Morandi L, Granata C, Ballestrazzi A: **Bethlem myopathy: early-onset benign autosomal dominant myopathy with contractures. Description of two new families.** *Neuromuscul Disord* 1994, **4**:503-11.

Pre-publication history

The pre-publication history for this paper can be accessed here: [http://www.biomedcentral.com/1471-2350/11/44/prepub]

doi:10.1186/1471-2350-11-44
Cite this article as: Bovolenta *et al.*: Identification of a deep intronic mutation in the COL6A2 gene by a novel custom oligonucleotide CGH array designed to explore allelic and genetic heterogeneity in collagen VI-related myopathies. *BMC Medical Genetics* 2010 **11**:44.

2. New collagen VI chains.

The identification of collagen VI in the '80s led to the demonstration that the protein is made of three distinct polypeptide chains, named α1(VI), α2(VI) and α3(VI). A number of biosynthetic studies in different systems allowed elucidate the assembly of the three collagen VI chains, showing the necessity of their equimolar association before collagen VI secretion, which was further proven by the complete absence of collagen VI in *Col6a1*$^{-/-}$ mice (Colombatti and Bonaldo, 1987; Colombatti et al., 1995; Bonaldo et al., 1998). It was found that biosynthesis of collagen VI is a peculiar multistep process (Fig. 1), requiring the equimolar association of the three alpha–chains into a triple helical [α1(VI)α2(VI)α3(VI)] monomer, which is followed by formation of disulfide-bonded dimers and tetramers within the cell. After secretion, the tetramers form a network of microfilaments with a typical 100–nm periodicity that bridges the surface of cells with the connective tissue (Colombatti et al., 1987; Keene et al., 1988; Bonaldo et al., 1990; Colombatti and Bonaldo, 1991).

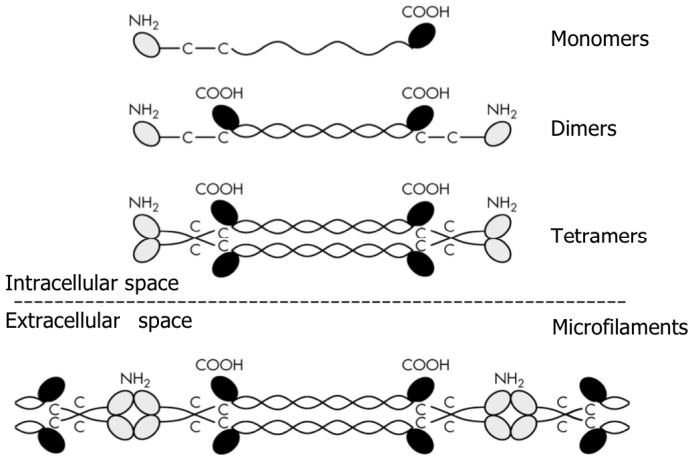

Figure 1. Collagen VI biosynthesis.

In the last years I collaborate with other research groups in a project focused on the During my PhD project, I have been involved in a collaborative project with the group of Mats Paulsson and Raimund Wagener (Department of Biochemistry, University of Cologne, Germany), aimed at the characterization of newly discovered collagen VI chains. In a database mining with collagen VI sequences, three novel collagen VI chains were found in the mouse genome, and named α4(VI), α5(VI) and α6(VI).

These additional chains show a high degree of similarity with the α3(VI) chain and are encoded by distinct genes, *Col6a4*, *Col6a5* and *Col6a6* (Gara et al., 2008). Orthologue genes were also found in humans, but due to a chromosomic inversion of primates, the human *COL6A4* gene is split into two parts and became a pseudogene. Interestingly, genetic studies by other groups have linked human *COL6A5* gene with atopic dermatitis (Söderhäll et al., 2007). Within the above project, I performed a number of biochemical experiments in cells and tissues from wild type and *Col6a1*$^{-/-}$ mice, showing that lack of α1(VI) chain in *Col6a1*$^{-/-}$ mice leads to a parallel absence of the novel collagen VI chains. These findings strongly suggest that the additional chains interact with α1(VI), likely forming additional heterotrimers. Additional studies in human skin biopsies of healthy donors and UCMD and BM patients also support the hypothesis that these chains may substitute for α3(VI), forming α1α2α5 or α1α2α6 heterotrimers. These findings provide novel information for the understanding of atopic dermatitis and BM and UCMD muscle diseases. In these studies, my contributions were focused on the characterization of the novel chains *in vivo* and in purified collagen VI.

2.1 Characterization of three novel collagen VI chains.

Three Novel Collagen VI Chains with High Homology to the α3 Chain*[S]

Received for publication, November 20, 2007, and in revised form, February 11, 2008 Published, JBC Papers in Press, February 13, 2008, DOI 10.1074/jbc.M709540200

Sudheer Kumar Gara[‡1], Paolo Grumati[§], Anna Urciuolo[§], Paolo Bonaldo[§], Birgit Kobbe[‡], Manuel Koch[‡¶‖], Mats Paulsson[‡¶], and Raimund Wagener[‡2]

From the [‡]Center for Biochemistry, [¶]Center for Molecular Medicine, and [‖]Department of Dermatology, Medical Faculty, University of Cologne, D-50931 Cologne, Germany and the [§]Department of Histology, Microbiology and Medical Biotechnologies, University of Padova, 35121 Padova, Italy

Here we describe three novel collagen VI chains, α4, α5, and α6. The corresponding genes are arranged in tandem on mouse chromosome 9. The new chains structurally resemble the collagen VI α3 chain. Each chain consists of seven von Willebrand factor A domains followed by a collagenous domain, two C-terminal von Willebrand factor A domains, and a unique domain. In addition, the collagen VI α4 chain carries a Kunitz domain at the C terminus, whereas the collagen VI α5 chain contains an additional von Willebrand factor A domain and a unique domain. The size of the collagenous domains and the position of the structurally important cysteine residues within these domains are identical between the collagen VI α3, α4, α5, and α6 chains. In mouse, the new chains are found in or close to basement membranes. Collagen VI α1 chain-deficient mice lack expression of the new collagen VI chains implicating that the new chains may substitute for the α3 chain, probably forming α1α2α4, α1α2α5, or α1α2α6 heterotrimers. Due to a large scale pericentric inversion, the human *COL6A4* gene on chromosome 3 was broken into two pieces and became a non-processed pseudogene. Recently *COL6A5* was linked to atopic dermatitis and designated *COL29A1*. The identification of novel collagen VI chains carries implications for the etiology of atopic dermatitis as well as Bethlem myopathy and Ullrich congenital muscular dystrophy.

Members of the collagen protein superfamily play important roles in maintaining extracellular matrix structure and function. To date 28 family members are known (1, 2), among which the fibril-forming collagens and the FACIT collagens form large subgroups. In addition, several collagens exist that have highly specific functions. Among these, collagen VI forms a distinct network of microfibrils in most connective tissues. Electron microscopy revealed a beaded filament structure of the microfibrils (3). The α1, α2, and α3 chains of collagen VI form heterotrimeric monomers that already intracellularly assemble to dimers and tetramers (4, 5). After secretion, filaments are formed by end to end interactions of the preassembled tetramers.

The three previously known collagen VI chains contain a relatively short collagenous domain of about 335 residues together with VWA[3] domains, which are the characteristic non-collagenous domains of collagen VI. A common feature of VWA domains is their involvement in the formation of multiprotein complexes (6). Whereas all three collagen VI chains contain two C-terminal VWA domains, the α1 and α2 chains carry only one and the α3 chain ten VWA domains at the N terminus (7, 8). In addition, the α3 chain contains a unique domain with similarities to salivary gland proteins, a fibronectin type III repeat, and a bovine pancreatic trypsin inhibitor/Kunitz family of serine protease inhibitor domain (Kunitz domain) at the C terminus (8). It was suggested that the VWA domains play a role in the assembly of collagen VI (9–11). However, recently the analysis of lysyl hydroxylase 3-deficient mouse embryos indicated that also the loss of potentially glycosylated hydroxylysine residues prevents the intracellular formation of collagen VI tetramers and leads to impaired secretion of collagen VI (12).

It has been shown that collagen VI interacts with several other extracellular matrix components, including collagen I (13), II (14), and XIV (15), perlecan (16), and the microfibril-associated glycoprotein MAGP1 (17). The N-terminal globular domains of the collagen VI molecules bind the small leucine-rich repeat proteoglycans decorin and biglycan, which in turn interact with matrilins, mediating contacts to further binding partners (18).

Studies on collagen VI have often focused on its function in skeletal muscle because of the patient phenotypes, Beth-

* This work was supported by grants from the Deutsche Forschungsgemeinschaft (WA 1338/2-6, SFB 589), grants from the Köln Fortune program of the Medical Faculty of the University of Cologne, the Maria Pesch Foundation, and the Imhoff Foundation, and Grant GGP04113 from the Italian Telethon Foundation. The costs of publication of this article were defrayed in part by the payment of page charges. This article must therefore be hereby marked "*advertisement*" in accordance with 18 U.S.C. Section 1734 solely to indicate this fact.

[S] The on-line version of this article (available at http://www.jbc.org) contains supplemental Tables 1–4 and supplemental Figs. 1–3.

The nucleotide sequence(s) reported in this paper has been submitted to the GenBank™/EBI Data Bank with accession number(s) AM231151–AM231153, AM748256–AM748258, AM748259–AM748262, AM774225–AM774227, and AM906078–AM906084.

[1] Member of the International Graduate School in Genetics and Functional Genomics at the University of Cologne.

[2] To whom correspondence should be addressed: Institute for Biochemistry II, Medical Faculty, University of Cologne, Joseph-Stelzmann-Str. 52, D-50931 Cologne, Germany. Fax: 49-221-478-6977; E-mail: raimund.wagener@uni-koeln.de.

[3] The abbreviations used are: are: VWA, von Willebrand factor A; RT, reverse transcription; EST, expressed sequence tag; ELISA, enzyme-linked immunosorbent assay; SNP, single nucleotide polymorphism; UTR, untranslated region.

lem myopathy, and Ullrich congenital muscular dystrophy, observed when the α1, α2, or α3 chain carries a mutation (for review see Ref. 19). In mice where the gene coding for the collagen VI α1 chain has been inactivated also the α2 and α3 chains are not secreted, showing that a heterotrimeric assembly is required (20). The mice show a muscular weakness and histological signs of muscle fiber necrosis. Recent studies indicate that the myopathy is due to a mitochondrial dysfunction (21, 22). A possible explanation could be a decreased integrin-mediated signaling from collagen VI to the cells (23), but details of the downstream events are still not known.

Here we describe three new collagen VI chains that have the potential to replace the collagen VI α3 chain in collagen VI assemblies and thereby to increase the structural and functional versatility of collagen VI.

MATERIALS AND METHODS

RT-PCR—RT-PCR was used to clone the mouse and human collagen VI cDNAs. Primers were designed according to EST and genomic sequences that are deposited in the data bases (supplemental Table 1). To prevent mutations in the RT-PCR we used the Expand high fidelity PCR system (Roche Applied Science). The cDNAs for the α4 chain were amplified from mRNA isolated from adult mouse uterus and newborn mouse brain, and cDNAs for the α5 and α6 chains were amplified from mRNA from newborn mouse lung. The human cDNAs for the α5 chain were cloned from mRNA prepared from HT1080 or HEK293-EBNA cells, and the cDNAs for the α6 chain were cloned from mRNA prepared from fetal brain using the primer pairs indicated in supplemental Table 1.

Northern Blot Analysis—Total RNA was extracted from various tissues of newborn and adult C57BL/6J mice by the guanidinium-thiocyanate method. mRNA was prepared by using the Oligotex® mRNA Mini Kit (Qiagen). Aliquots were electrophoresed on a 0.8% denaturing agarose-formaldehyde gel, blotted, and hybridized with digoxigenin-labeled RNA probes. The conditions in the last two wash steps were: 0.1 × SSC, 0.1% SDS at 68 °C for 15 min each. The blots were developed using CDP-Star (Roche) according to the manufacturer's instructions.

Bioinformatic Analysis—The non-redundant NCBI genomic data bases for mouse (Build 37.1) and human (Build 36.2) were scanned for new genes using collagen and matrilin sequences as queries. The exon-intron boundaries of each of the new genes were carefully interpreted using the NCBI Evidence Viewer together with the cloned cDNA sequences. The potential signal peptide and domain structure of each protein was predicted by SignalP v3.1 and SMART, respectively. However, the N1 domain of the α5 chain was manually assigned based on sequence signature motifs because none of the available domain prediction programs could locate it. Multiple sequence alignments were performed using CLUSTAL X (v1.81) and figures were prepared with the BOXSHADE v3.2 program. The protein sequence identities of the new chains were calculated using BOXSHADE. The phylogenetic analysis was done by protein distance and protein parsimony as described in PHYLIP v3.66.

Expression and Purification of Recombinant N-terminal Collagen VI α4, α5, and α6 Chain VWA Domains—cDNA constructs were generated by RT-PCR on mRNA. For the collagen VI α4, α5, and α6 chains, the domains N3–N6, N3, and N1–N7 were chosen, respectively. Suitable primers introduced 5′-terminal NheI and 3′-terminal BamHI, BglII, or XhoI restriction sites (supplemental Table 1). The amplified PCR products were inserted into a modified pCEP-Pu vector (16) containing an N-terminal BM-40 signal peptide and a C-terminal His_8-tag or a C-terminal tandem strepII-tag (17) downstream of the restriction sites. The recombinant plasmids were introduced into HEK293-EBNA cells (Invitrogen) using FuGENE 6 transfection reagents (Roche). The cells were selected with puromycin (1 μg/ml), and the His_8-tagged protein-producing cells were transferred to serum-free medium for harvest of the recombinant protein. The C-terminal tandem strepII-tagged protein was directly purified from serum-containing cell culture medium. After filtration and centrifugation (1 h, 10,000 × *g*), the cell culture supernatants were applied either to a streptactin column (1.5 ml, IBA GmbH) and eluted with 2.5 mM desthiobiotin, 10 mM Tris-HCl, pH 8.0, or to a TALON metal affinity column (Clontech) and eluted following the supplier's protocol.

Preparation of Antibodies against the New Collagen Chains—The purified recombinant collagen VI fragments were used to immunize rabbits and guinea pigs. The antisera obtained were purified by affinity chromatography on a column with antigen coupled to CNBr-activated Sepharose (GE Healthcare). The specific antibodies were eluted with 0.1 M glycine, pH 2.5, and the eluate was neutralized with 1 M Tris-HCl, pH 8.8. The antiserum raised against the domains N1–N7 of the collagen VI α6 chain were affinity-purified on a column coupled with the collagen VI α6 chain N2–N6 domains to prevent cross-reactivity due to the highly identical N7 domains of collagen VI α5 and α6. The lack of extensive cross-reactivity between the new chains was demonstrated by ELISA.

Immunohistochemistry—Immunohistochemistry was performed on frozen embedded sections of adult wild type and collagen VI α1 chain-deficient mice (20). The frozen sections were preincubated in ice-cold methanol for 2 min, blocked for 1 h with 5% normal goat serum in phosphate-buffered saline containing 0.2% Tween 20, and incubated with the primary antibodies overnight at 4 °C followed by AlexaFluor 488-conjugated goat anti-rabbit IgG (Molecular Probes), AlexaFluor 546-conjugated goat anti-rabbit IgG (Molecular Probes), or AlexaFluor 488-conjugated goat anti-guinea pig IgG (Molecular Probes). Collagen VI α1, α2, and α3 chains were detected using a polyclonal antibody (AB7821, Chemicon). A polyclonal antibody against the human native laminin-332 (24) was kindly given by R. E. Burgeson.

Preparation of Muscle Extracts—Frozen mouse skeletal muscle was pulverized by pestle and mortar and lysed with a solution containing 50 mM Tris, pH 7.5, 150 mM NaCl, 10 mM $MgCl_2$, 0.5 mM dithiothreitol, 1 mM EDTA, 10% glycerol, 2% SDS, 1% Triton X-100, 1 mM phenylmethylsulfonyl fluoride, 1

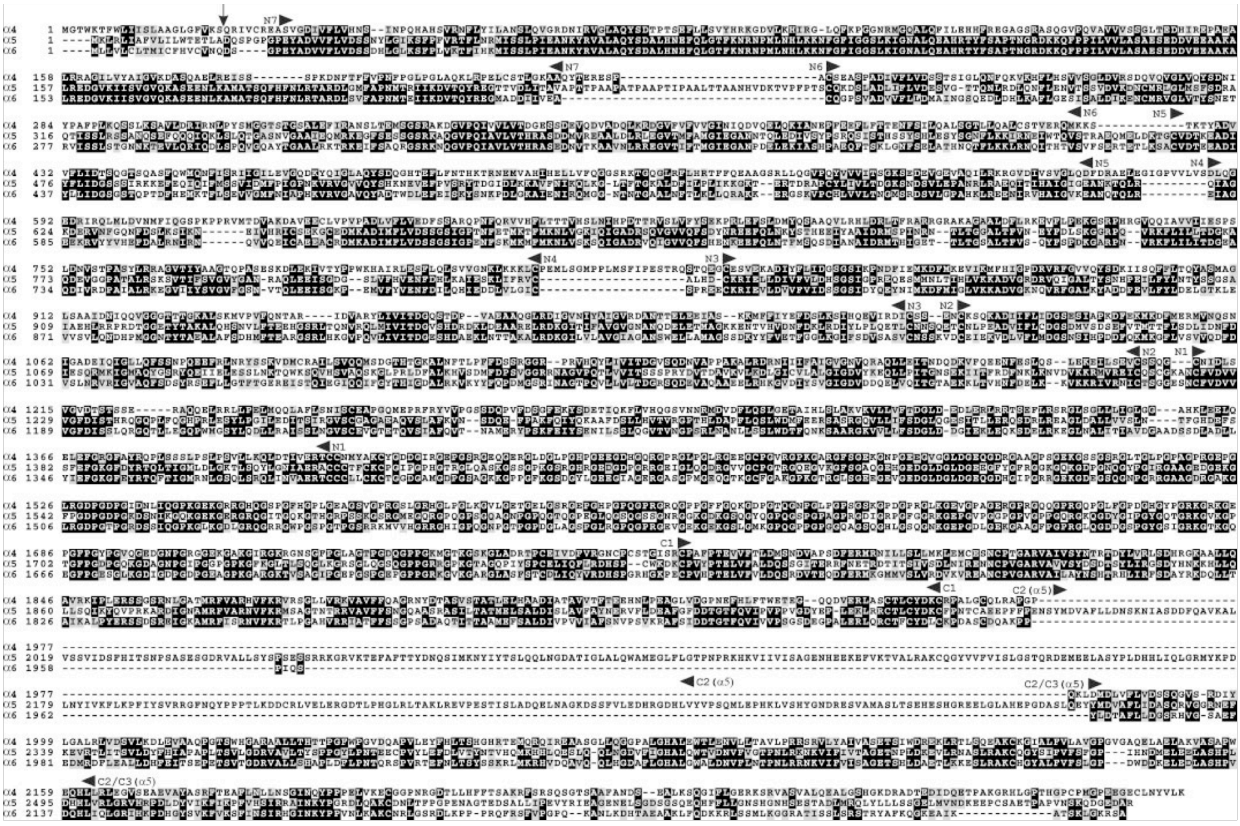

FIGURE 1. **Alignment of amino acid sequences of murine collagen VI α4, α5, and α6 chains.** The amino acid sequences were deduced from the cDNA sequences deposited in the data base under accession numbers AM231151–AM231153, AM748256–AM748258, and AM748259–AM748262, respectively. The *arrow* marks the potential signal peptide cleavage sites. *Arrowheads* indicate the boundaries of the domains depicted in Fig. 2.

mM sodium orthovanadate, 5 mM sodium fluoride, 3 mM glycerol 2-phosphate, and protease inhibitors (Complete, Roche). Proteins were solubilized by heating at 70 °C for 10 min. Samples were clarified by centrifugation at 4 °C.

Purification of Collagen VI—Native collagen VI was purified from newborn mice. Proteins were extracted by urea treatment, and collagen VI was isolated by molecular sieve column chromatography as described previously (25).

Gel Electrophoresis and Immunoblot—Samples were reduced with 5% β-mercaptoethanol and subjected to SDS-PAGE on 4–12% (w/v) gradient polyacrylamide gels. Proteins were electrophoretically transferred to Immobilon-P transfer membrane (Millipore). Collagen VI α1, α2, and α3 chains were detected using the 70-XR95 polyclonal antibody (Fitzgerald Industries International). The collagen VI α1 chain was detected using a polyclonal antibody recognizing the human α1(VI) chain (H-200, Santa Cruz Biotechnology). The new collagen VI α4, α5, and α6 chains were detected using the affinity-purified antibodies described above. As a loading control, an antibody against glyceraldehyde-3-phosphate dehydrogenase was used (MAB374, Chemicon). Secondary antibodies conjugated with horseradish peroxidase were used, and bands were detected by chemiluminescence (SuperSignal West Pico, Pierce).

RESULTS

Cloning of cDNAs Coding for Three New Mouse Collagen VI Chains—In a screen of the genomic data base with collagen and matrilin sequences as queries, three genes were identified in the mouse genome that code for new VWA domain-containing collagens. Because of their homology to the α3 chain of collagen VI and their arrangement in the genome, these were designated as the α4, α5, and α6 chains of collagen VI. The corresponding cDNAs were cloned as overlapping partial clones by RT-PCR, using primers deduced from the genomic sequence, and sequenced. The cloned mouse α4 cDNA of 7084 bp (accession numbers AM231151–AM231153) contains an open reading frame of 6927 bp, encoding a protein consisting of 2309 amino acid residues preceded by a signal peptide of 22 residues, as predicted by a method using neural networks or hidden Markov models, respectively (13). The mature secreted protein has a calculated M_r of 248,389 (Fig. 1). At least nine EST clones exist that extend 207 bp in the 3′ direction and contain an ATTAAA polyadenylation signal at their 3′-ends. In addition, a partial RIKEN cDNA clone (AK159050) extends 1219 bp and also contains an ATTAAA polyadenylation signal at its 3′-end, indicating the presence of different 3′-UTRs.

The cloned mouse α5 chain cDNA of 8298 bp (accession numbers AM748256–AM748258) contains an open reading

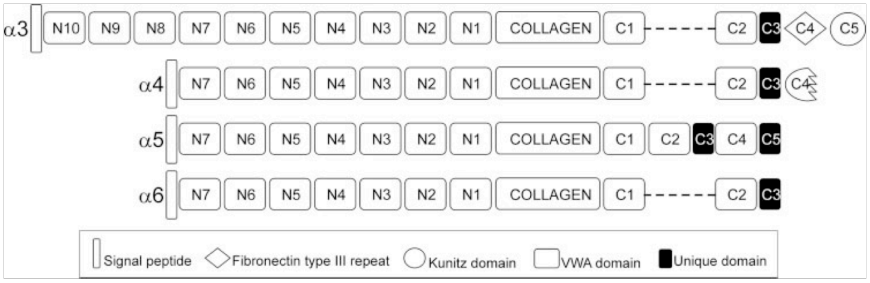

FIGURE 2. **Domain structures of the new collagen VI chains compared with the collagen VI α3 chain.** Shown are the VWA domain and the Kunitz family of serine protease inhibitors domain (Kunitz domain). The numbering of the domains is according to Chu *et al.* (8). The *dashed lines* in the collagen VI α3, α4, and α6 chains indicate the lack of duplication of the second VWA domain and the unique domain found in the collagen VI α5 chain.

frame of 7920 bp, encoding a protein consisting of 2640 amino acid residues preceded by a signal peptide of 18 residues (13). The mature secreted protein has a calculated M_r of 287,502 (Fig. 1). A partial RIKEN clone (AK134435) extends 751 bp at the 3′-end but does not contain a polyadenylation signal.

The cloned mouse collagen VI α6 chain cDNA of 7097 bp (accession numbers AM748259–AM748262) contains an open reading frame of 6795 bp, encoding a protein consisting of 2265 amino acid residues preceded by a signal peptide of 18 residues (13). The mature secreted protein has a calculated M_r of 244,260 (Fig. 1).

Domain Structure—The domain structures of the new chains are very similar to that of the collagen VI α3 chain (Fig. 2). For comparison with the already known collagen VI chains we use the nomenclature introduced by Chu *et al.* (8). The domains at the N terminus of the collagenous domain are designated with N, the domains at the C terminus of the collagenous domain with C. Numbering starts at the collagenous domain. At the N terminus all three mature proteins contain seven VWA domains (N7–N1), followed by a 336-amino acid residue long collagen triple helical domain. Toward the C terminus they have two VWA domains (C1 and C2) that are followed by a unique sequence (C3) that in the new α6 chain also represents the C-terminal end. In mouse the α4 chain carries a short stretch of 17 amino acid residues at the C-terminal end (C4) that resembles a Kunitz domain. Interestingly, when searching the genomic data bases for exons coding for a complete Kunitz domain, such a domain could be identified at this position in ortholog genes of several species. Only in mouse and rat do the sequences contain a premature stop codon, indicating that, except in rodents, a full Kunitz domain is present at the C terminus of the collagen VI α4 chain (Fig. 3*A*). In the α5 chain the C-terminal end contains a third VWA domain (C4) followed by another unique domain (C5). A major difference between the new chains and the collagen VI α3 chain is the presence of three additional VWA domains at the N-terminal end of the α3 chain. Interestingly, a splice variant of the collagen VI α3 chain (AAC23667) lacks the first, second, and fourth VWA domains and thereby, as the new chains, contains seven N-terminal VWA domains. The overall identity at the amino acid level is highest between the α5 and α6 chains (44.7%) and lowest between the α4 and α5 chains (28.0%). The overall identity of the three new chains and the α3 chain varies between 25.9 and 26.7%.

Alternative Splicing—In mouse, two different splice variants of the collagen VI α4 mRNA with premature stop codons can be deduced from EST clones. First, the ESTs AU023415 and BG068629 contain a stop codon in an alternative exon following the exon coding for the N4 domain. If translated, this transcript would yield a protein containing only the first four VWA domains. A second splice variant was detected in the three EST clones BX520360, AI427280, and W48310. Here, an alternative splice donor site in exon 35 coding for the C2 domain and an alternative splice acceptor site in exon 37 coding for the unique domain are used. Due to a shift in codon phase, the new exon codes for a different frame and contains a stop codon 101 bp downstream of the alternative splice site. If translated, this transcript would give a protein that lacks nearly one-half of the C2 domain and the unique domain. Interestingly, the alternative splice site contains a non-canonical GC-AG motif.

A RIKEN cDNA clone coding for the collagen VI α6 chain (AK054356) shows alternative splicing in the 5′-UTR, indicating the presence of two different promoters. Interestingly, due to additional alternative splicing of exon 6, a much shorter open reading frame occurs that would generate a protein containing only the first six VWA domains and lacking the seventh VWA domain, the collagenous domain, and the C-terminal non-collagenous domains.

Analysis of the Collagenous Domains—The 336-amino acid residue long collagenous domains have exactly the same size as that in the collagen VI α3 chain (Fig. 3*B*). The identity between the collagenous domain of the α3 chain and those in the α4, α5, and α6 chains is 53.3, 49.1, and 51.8%, respectively. A cysteine residue that is also present in the collagenous domain of the collagen VI α3 chain and appears to be involved in tetramer formation and stability (19) is conserved in all new chains.

The locations of the two imperfections in the Gly-Xaa-Yaa repeat found in the collagen VI α3 chain are conserved in all new chains, whereas the α5 and α6 chains have additional imperfections. In both these chains a glycine residue in a Gly-Xaa-Yaa repeat close to the C terminus of the collagenous domain is replaced by a leucine or a valine residue, respectively, introducing another imperfection. Interestingly, the position coincides with an imperfection found in the α1 and α2 chains. In addition, an imperfection is present at the center of the collagenous domains of the collagen VI α5 and α6 chains, where one or two glycine residues of Gly-Xaa-Yaa repeats are lacking, respectively.

In contrast to the collagenous domain of the collagen VI α3 chain, which contains five potentially integrin-binding RGD sequences, in each of the new chains only one RGD motif is present. In the collagen VI α4 and α6 chains the motif is found at exactly the same position where an RGD is present also in the

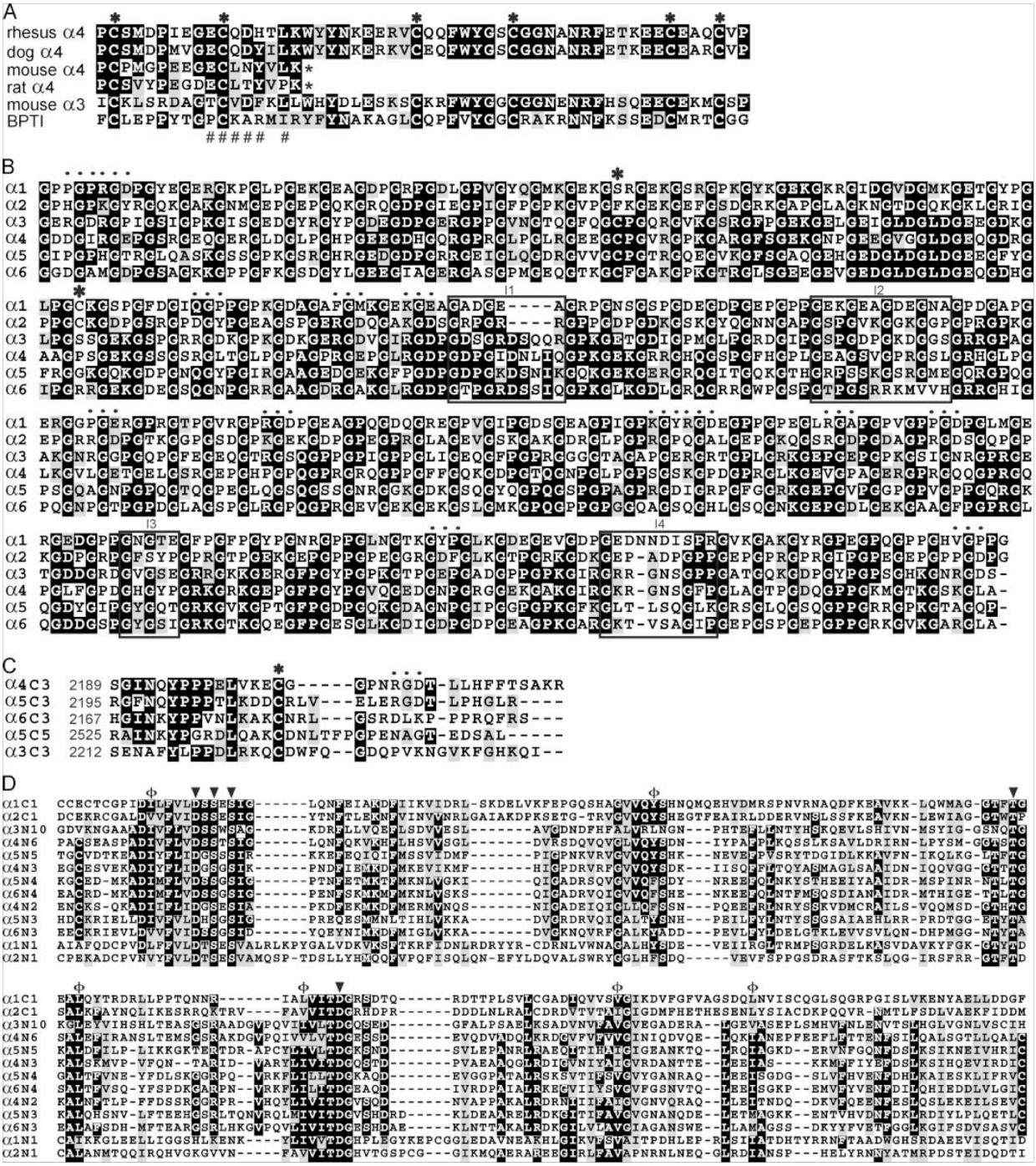

FIGURE 3. **Amino acid sequence alignment of collagen VI Kunitz domains in different species (*A*), collagenous domains from the different collagen VI chains in mouse (*B*), C-terminal parts of the unique domains in mouse (*C*), and VWA domains containing the metal ion-dependent adhesion site motif in mouse (*D*).** The sequences for the Kunitz domains of rhesus monkey, dog, and rat were deduced from genomic sequences. The sequences were aligned by CLUSTAL X using the default parameters. The residues forming the trypsin interaction site in the original bovine pancreatic trypsin inhibitor (*BPTI*) (34) are marked with a *number sign*, the cysteine residues with *asterisks*, and the RGD sequences with *dots*. Imperfections in the collagenous domains are *boxed* and numbered *I1–I4*. The conserved metal ion-dependent adhesion site (42) and the conserved hydrophobic moieties (43) are denoted with ▼ and ϕ, respectively.

collagen VI α3 chain (Fig. 3*B*). The content of proline or hydroxyproline in the *X* and *Y* positions is lower (17.4–20.5%) than in the fibril-forming collagen I α1 or collagen II α1 chains (26). N- and C-terminal of the collagenous domains several cysteine residues are present, which might form intermolecular disulfide bridges that enhance the stability of the trimeric col-

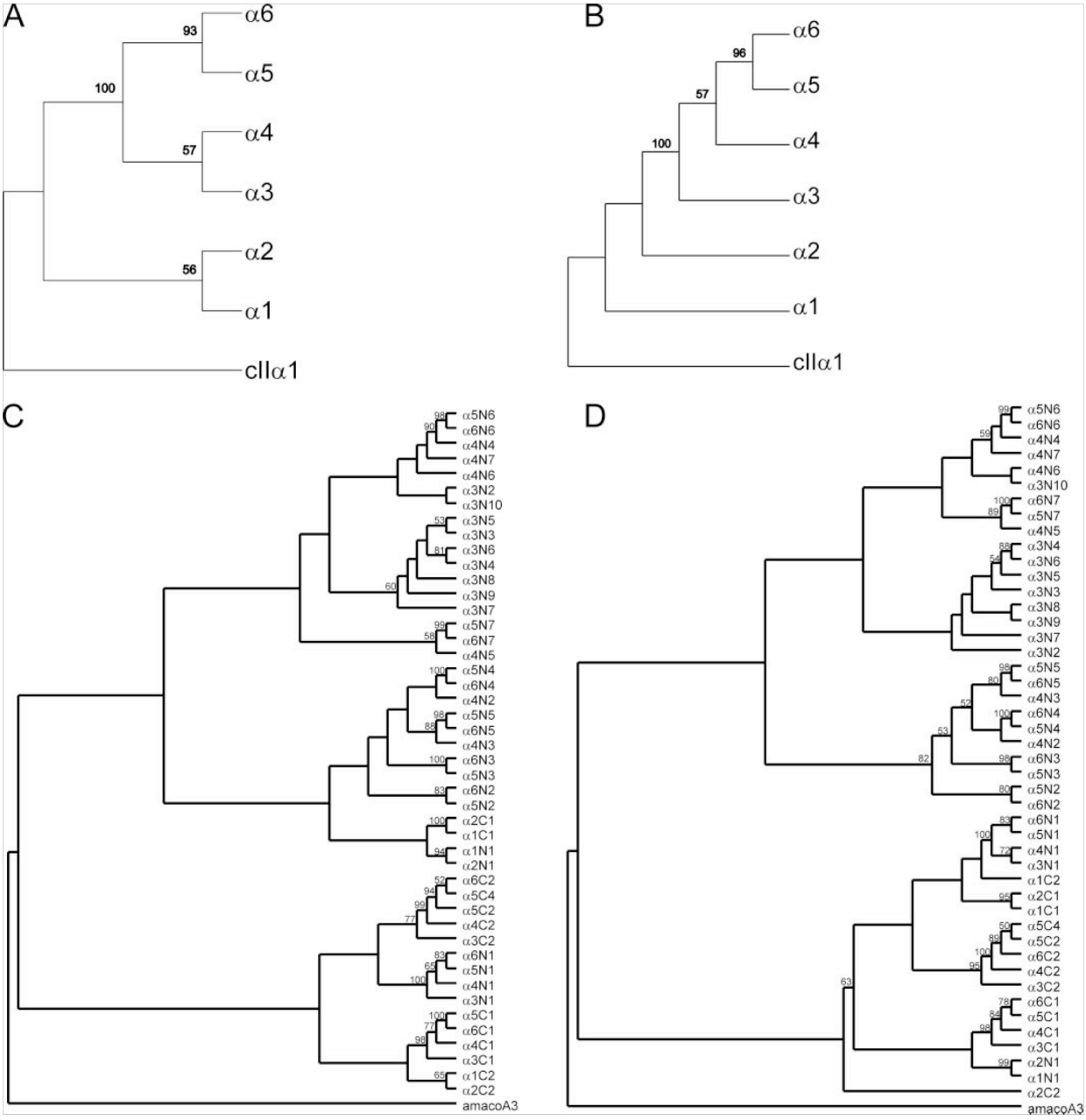

FIGURE 4. **Phylogenetic trees of the collagenous domains (*A* and *B*) and the VWA domains (*C* and *D*) of collagen VI.** The sequences from all six collagen VI chains in mouse were aligned using CLUSTAL X. The trees were constructed using the programs PROTEIN DISTANCE, NEAREST NEIGHBOUR, and CONSENSE (*A* and *C*) and PROTEIN PARSIMONY and CONSENSE (*B* and *D*) of the PHYLIP package version 3.66. Bootstrap analyses using 100 replicates were performed to show the significance. The *numbers* indicate the statistical weight of the individual branches. The collagenous domain of the collagen II α1 chain (*cIIα1*) (*A* and *B*) and the VWA3 domain of AMACO (44) (*C* and *D*) were used as outgroups.

lagens. In phylogenetic analyses using protein distance and protein parsimony, the collagenous domains of the α3, α4, α5, and α6 chains group in one clade (Fig. 4, *A* and *B*).

Analysis of the VWA Domains—Of the 28 VWA domains present in the new collagen VI chains, the metal ion-dependent adhesion site (D*X*S*X*S*X*nT*X*nD, where n represents a variable number of amino acid residues) motif, is fully conserved only in 8 (Fig. 3*D*). Sequence alignment of the VWA domains of the new chains with their counterparts present in the collagen VI α1–α3 chains highlights the homology (Fig. 3*D* and supplemental Fig. 1). The highest sequence identity between two VWA domains of the new chains is 92.1% for α5N7 and α6N7. High identity values were also obtained for the α5N4 and α6N4 (64.5%), α5N5 and α6N5 (51.9%), α5C2 and α6C3 (52.9%), α5C1 and α6C1 (50.5%), and α5N1 and α6N1 (50.3%). Among the various VWA domains found in the collagen VI α1–α3 chains, the N10

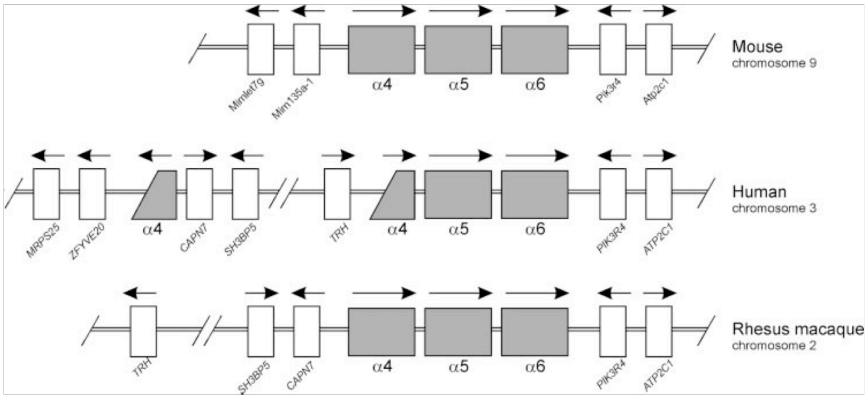

FIGURE 5. **Loci for collagen VI α4, α5, and α6 in the genomes of man, rhesus monkey, and mouse.** The orientation of the genes is indicated by *arrows*.

domain of the collagen VI α3 chain shows the highest identity value to the N7 domain of the α4 chain (39.5%). Similar identity values were obtained for α3N9 and α4N7 (34.7%) and α3C1 and α4C1 (34.5%). Identity values between the α3 chain VWA domains and α5 and α6 chain VWA domains are not higher than 28.4 and 28.9%, respectively. The identity between the VWA domains of the new chains and those of the collagen VI α1 and α2 chains is always lower than 24.0%. In phylogenetic analyses using protein distance and protein parsimony, all the VWA domains of the α5 and α6 chains pair up together (Fig. 4, *C* and *D*). The C-terminal VWA domains of the α3, α4, α5, and α6 chains group to a distinct branch in which the C1 domains are in one subbranch and the C2 domains and the C4 domain of the α5 chain are in another. Similarly, the N1 domains of the α3, α4, α5, and α6 chains all cluster together (Fig. 4, *C* and *D*).

Analysis of the Unique Domains—The unique sequences at the C-terminal end follow directly after the second C-terminal VWA domains (C2). In the collagen VI α5 chain a second unique domain is present C-terminal of the C4 domain. The unique domains are 99–111 amino acid residues long. The unique domain of the α4 chain and the first unique domain of the α5 chain as well as the second unique domain of the α5 chain and the unique domain of the α6 chain share some pairwise similarity, 31.6 and 26.1%, respectively. However, a stretch of 15 amino acid residues at the beginning of each domain is highly identical in all four unique domains and has a cysteine residue at the end (Fig. 3*C*). Interestingly, the unique sequence of the collagen VI α3 chain, C-terminal to the C2 domain, also shares some homology to the unique domains of the new chains, most clearly in the C-terminal portions, and particularly the cysteine residue is conserved (Fig. 3*C*). Interestingly, shortly after the highly homologous stretch, an RGD motif is present in both the α4 chain and the first unique domain of the α5 chain, whereas this motif is missing in the α6 chain and in the second unique domain of the α5 chain (Fig. 3*C*). In addition to the single RGD motifs present in each of the collagenous domains, these two RGD motifs are the only ones found in the new collagen VI chains. An RGD motif is lacking in the unique domain of the collagen VI α3 chain. BLAST searches with the unique sequences revealed some weak homologies to intracellular proteins like the REST corepressor 1 (α4 35/83 (42%)), ubiquitin D (α5C3 22/32 (68%)), protein-tyrosine phosphatase (α5C5, 34/71 (47%)), and dynein cytoplasmic 2 heavy chain 1 (α6 26/60 (43%)).

Structure of the Murine Collagen Col6a4-Col6a6 Genes—The new mouse collagen VI genes map to chromosome 9 (9F1) (Fig. 5). The genomic sequences are completely contained in the public data bases (NT_039477 and NW_001030918). The genes lay head to tail in tandem orientation on the minus strand. The *Pik3r4* gene and the *Mirn135a1* gene are located downstream and upstream of the new collagen genes, respectively. We identified exons by flanking consensus splice signals and by comparison with the respective cDNAs. The exon/intron organization of the three genes is very similar (Fig. 6 and supplemental Tables 2–4) regarding size, exon and intron length, and codon phase. The *Col6a4* and *Col6a5* genes are 112 kb, and the *Col6a6* gene is 104 kb long. They consist of 38, 44, and 37 exons, respectively, that code for the translated part of the mRNA (Fig. 6). The first exon in each gene completely encodes the 5′-UTR. All second exons code for the signal peptide sequence followed by six exons coding for the first six VWA domains (N7–N2), whereas the VWA domain N1 is encoded by three exons. The collagenous domains are encoded by exons 12–30. Interestingly, intron 24 of the *Col6a4* gene is a GC-AG-type intron. Exons 31 and 32 code for short spacer regions. The VWA domains C1 and C2 are encoded by exons 33/34 and 35, respectively. The structures of the three genes differ at the 3′-end. In *Col6a4* the unique sequence is encoded by two exons followed by a last exon coding for the truncated Kunitz domain and the 3′-UTR. In *Col6a6* the last two exons code for the unique domain and 3′-UTR. The more complex structure of the C-terminal end of the collagen VI α5 chain is also reflected in the *Col6a5* gene structure. The unique domain between the VWA domains C2 and C4 is encoded by two exons followed by the exon coding for the additional VWA domain C4. As in *Col6a6*, the last two exons of *Col6a5* code for the unique domain and 3′-UTR. Although there is only partial homology between the unique domains of the new collagen chains, each unique domain is encoded by two exons where the first exon is always about 95 bp and the second about 200 bp long, pointing to the likelihood of a common ancestor.

New Collagen VI Genes in Man—The orthologs of the new mouse genes map to human chromosome 3q21 (Fig. 5). The tandem orientation of the genes is conserved, but the gene coding for the α4 chain is broken into two pieces, and the 5′ region of the gene is located at 3p24.3. Only the region downstream of the new collagen VI genes, coding for *PIK3R4*, is in synteny in man and mouse. The breakpoint resembles the large scale pericentric inversion that occurred in the common ancestor of the African apes and is present in modern human chromosome 3 as well as in the chimpanzee and gorilla orthologs, but not in orangutan or Old World monkeys (27). In contrast to rhesus

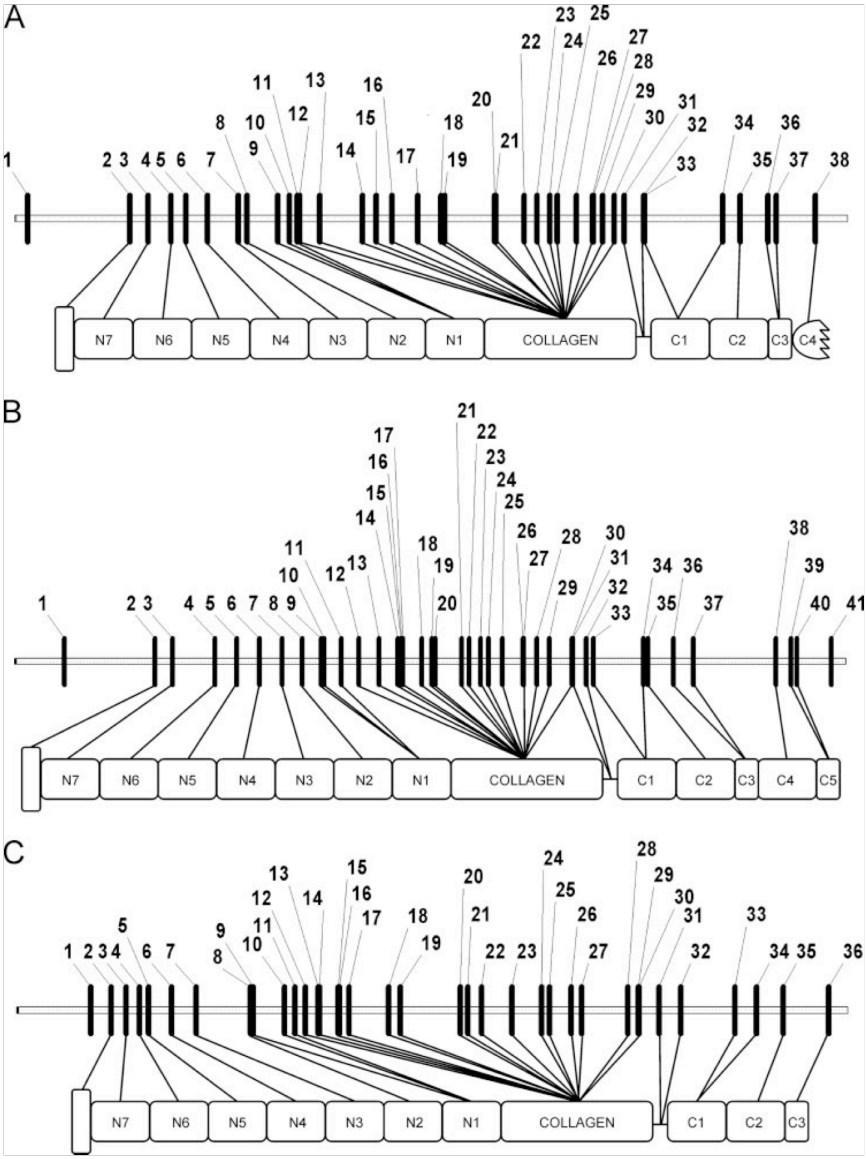

FIGURE 6. **Organization of the murine *Col6a4, Col6a5*, and *Col6a6* genes.** The *numbers* indicate the positions of exons. The protein domain structure is given below, and the corresponding exons are indicated by *lines*.

macaque, the human *COL6A4* is interrupted after the first exon coding for the collagenous domain, and EST clones for both parts of the gene can be found in the data bases. However, due to the presence of stop codons that are distributed over the sequence, both parts of the human *COL6A4* are likely to be transcribed non-processed pseudogenes. The corresponding cDNAs of the human *COL6A5* and *COL6A6* were cloned as overlapping partial clones by RT-PCR using primers deduced from the genomic sequence and sequenced (accession numbers AM774225–AM774227 and AM906078–AM906084). The human collagen VI α5 chain has an identity of 73.1% at the amino acid level to the mouse ortholog (supplemental Fig. 2). The non-identities are not evenly distributed over the sequence. A 32-amino acid long proline-rich stretch at the C terminus of C1 is missing in man, and the unique domains are highly divergent. In addition, at two positions in the C-terminal part an amino acid residue is deleted and at three positions an amino acid residue is inserted into the human α5 chain. Most of the cysteine residues are conserved, but there is an additional cysteine present in the collagenous domain of the human α5 chain. However, the cysteine codon resembles an SNP (rs1497312) leading to a non-synonymous exchange to a serine codon. The positions and sizes of the imperfections in the collagenous domain are identical to those in mouse, whereas the RGD motif in the collagenous domain of the α5 chain is lost. Instead there is a new RGD motif at the N terminus of the collagenous domain. The two RGD motifs present in the unique domain of mouse are also missing in man. Another SNP (rs11355796), which resembles the deletion of a thymidine at the C terminus forms a premature stop codon, leading to a full-length protein of 2590 residues (supplemental Fig. 2). No information is available on the population frequency, but both variants are found in the TRACES-WGS data base. Interestingly, in the alternative Celera assembly of the human genome the deletion is present, whereas the thymidine is found in the reference assembly, leading to a longer protein. In contrast to murine *Col6a5*, human *COL6A5* contains an additional intron in the 3′-UTR that leads to three different C termini by alternative splicing, thus resulting in full-length α5 chain isoforms of 2526, 2614, or 2615 amino acid residues (supplemental Fig. 2). The human collagen VI α6 chain has an identity of 83.4% at the amino acid level to the mouse ortholog, and only the last 30 amino acids at the C terminus show some differences (supplemental Fig. 3). The positions of the signal peptide cleavage site, the RGD motif, and all cysteine residues in the mature protein are completely conserved.

Interestingly, variants of the human *COL6A5* gene were recently shown to be associated with atopic dermatitis (28). The authors of that study designated the human *COL6A5* as *COL29A1*. Although not present in the original publication, the sequence was recently published in the data base (accession

number EU085556). Although in the publication the length of the protein sequence was given as 2614 amino acids, the sequence submitted to the data base is 2615 amino acids long. The reason for this difference is unclear, but the amino acid sequence is nearly completely identical with the third variant presented here (supplemental Fig. 2), the only difference being that residue 2560 is a serine residue instead of the asparagine found by us. Nevertheless, the second splice variant presented here contains 2614 amino acids. Surprisingly, the 5′-UTR region of the EU085556 contains a duplication of the 19-bp sequence GTGCGGCGCGGACCAGGGC that is not present in our sequence and is found neither in the alternative Celera assembly of the human genome nor in any of the 21 TRACE-WGS clones that cover this region but is present in the reference assembly of the human genome.

Expression of the New Mouse Collagen VI Genes—To determine the length of the new collagen VI mRNAs we performed Northern hybridization with total RNA or mRNA (Fig. 7*A*). The mRNA coding for the α6 chain was readily detected as a 9.7-kb band in total RNA derived from the lungs of newborn mice. Several messages coding for the α4 chain were detected in total RNA derived from the same source, probably indicating alternative splicing. The most prominent mRNA band had a length of 8.4 kb whereas weaker bands appeared at 11.7, 6.7, and 5.0 kb. A 9.5-kb message coding for the α5 chain was detected in purified mRNA derived from sterna of 4-week-old mice. RT-PCR was performed to screen the tissue distribution of the new collagen VI chains (Fig. 7, *B* and *C*). Products corresponding to the mRNAs for the α5 and α6 chains could be detected in lung, heart, kidney, muscle, brain, intestine, skin, femur, and sternum of newborn mice. In addition, α6 chain mRNA could be detected in calvaria. The α4 chain mRNA shows a more restricted tissue distribution and could be detected in lung, kidney, brain, intestine, skin, sternum, and weakly in calvaria (Fig. 7*B*). In adult mice, expression of the α4 chain is lost in most tissues, and RT-PCR showed a signal only in ovary and very weakly in spleen, lung, uterus, and brain. In contrast, the α5 chain is widely expressed also in adult mice, and mRNA could be detected in lung, heart, kidney, spleen, muscle, ovary, uterus, brain, skin, liver, and sternum, whereas the α6 chain expression is more restricted and could be detected in lung, heart, muscle, ovary, brain, liver, and sternum (Fig. 7*C*).

The New Collagen VI Chains Copurify with α1, α2, and α3 Chain-containing Collagen VI Prepared from Newborn Mice—If the new collagen VI chains assemble with known collagen VI chains, they should be present in conventional collagen VI preparations. Thus we isolated collagen VI from newborn mouse carcasses (25) and tested this preparation for the presence of the new chains by immunoblot. For this purpose, we generated antibodies specific for the new chains. Tagged versions of different N-terminal VWA domains were recombinantly expressed in EBNA293 cells, and the recombinant proteins were purified by affinity chromatography and used to immunize rabbits. The antisera were affinity-purified before use, and cross-reactivity among the new collagen VI chains was tested by ELISA (Fig. 8 and not shown). All three new chains were detected after reduction of the collagen VI preparation as major bands running above the 220-kDa marker (Fig. 8), consistent with the calculated molecular masses. For the collagen VI α4 and α5 chains additional lower migrating bands were detected (Fig. 8), indicating alternative splicing or proteolytic processing. The weak smear with lower mobility seen for the α4 chain (Fig. 8) could indicate the presence of non-reducible cross-linked molecules.

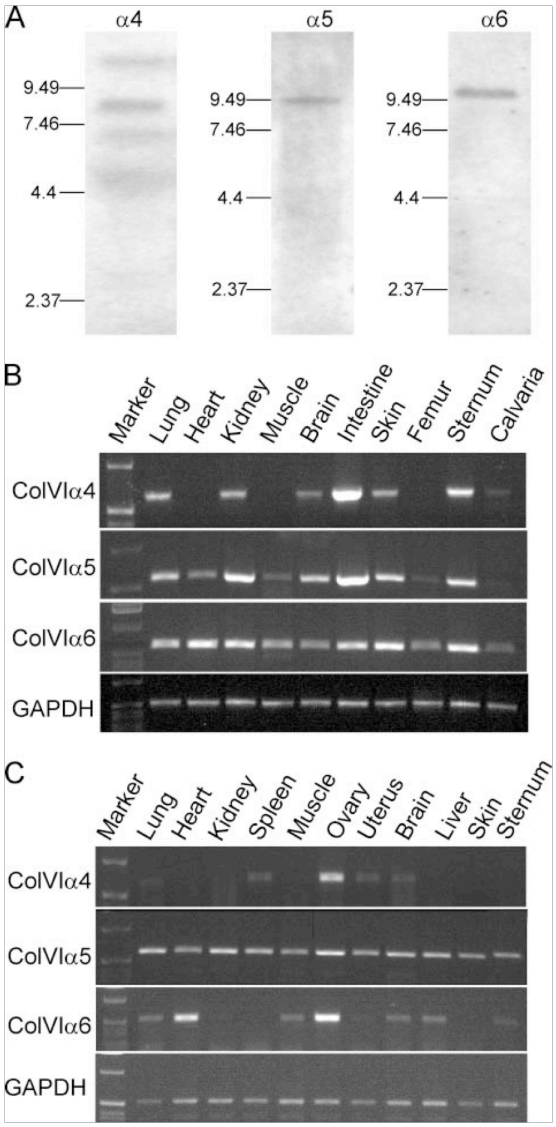

FIGURE 7. **Northern blot (*A*) and RT-PCR (*B* and *C*) analysis of the new mouse collagen VI chain mRNA species.** *A*, Northern hybridization was performed for the collagen VI α4 and α6 chains with 5 μg of total RNA from lung of newborn mice and for the α5 chain with of 1 μg of poly(A)$^+$ RNA from sternum of 4-week-old mice. Probes were generated using primers α4m8 and α4m9 for the α4 chain, α5m2 and α5m7 for the α5 chain, and α6m6 and α6m10 for the α6 chain. Position of size markers are indicated on the *left*. *B* and *C*, RT-PCR analysis was performed using primer pairs α4m6 and α4m7 for the α4 chain, α5m4 and α5m5 for the α5 chain, and α6m2 and α6m9 for the α6 chain. Template RNA was isolated from newborn (*B*) and adult mice (*C*). The 1-kb ladder from Invitrogen was used as a reference.

The Collagen VI α5 and α6 Chains, but Not the α4 Chain, Are Deposited in the Extracellular Matrix of Skeletal Muscle—Mutations in collagen VI lead to muscular dystrophies in humans,

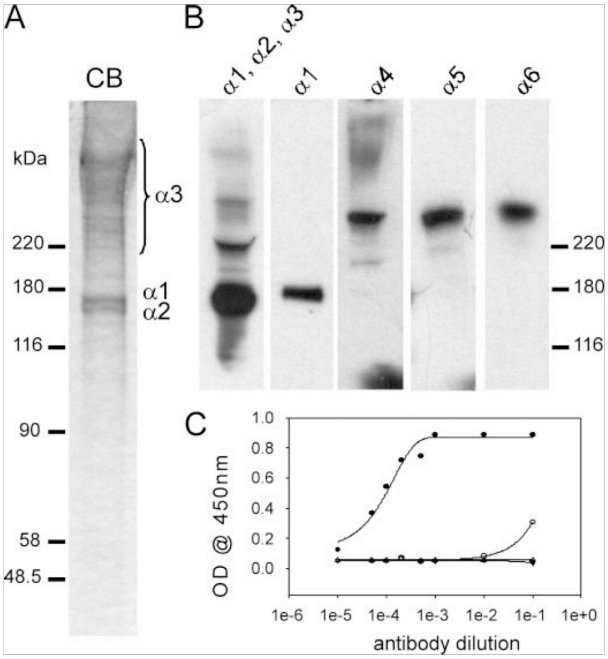

FIGURE 8. **Analysis of collagen VI purified from newborn mice (*A* and *B*) and ELISA of antibody reactivity against the collagen VI α6 chain (*C*).** Carcasses of newborn mice were extracted, and collagen VI was isolated by molecular sieve column chromatography as described previously (25). The proteins were submitted to SDS-PAGE on 4–12% polyacrylamide gradient gels under reducing conditions. *A*, Coomassie Brilliant Blue-stained gel. *B*, immunoblot of the same preparation with antibodies against collagen VI (α1, α2, α3; *lane 1*), the collagen VI α1 chain (*lane 2*), and the new collagen VI chains α4, α5, and α6 (*lanes 3–5*). *C*, reactivity of affinity-purified antibodies against the collagen VI α6 chain and lack of reactivity of antibodies against the α4 and α5 chains against the collagen VI α6 chain N2–N6 domains. ELISA plates were coated with 0.5 μg of recombinant collagen VI α6 N2–N6 protein per well, and antibodies were diluted as indicated. *Filled circles*, rabbit α6 antibody; *open circles*, rabbit α5 antibody; *filled triangles*, rabbit α4 antibody; *open triangles*, guinea pig α4 antibody. *OD*, optical density.

and mice lacking collagen VI display a myopathic phenotype affecting skeletal muscle (20). We therefore tested cryostat sections of adult mouse quadriceps femoris muscle for the expression of the new collagen VI chains (Fig. 9). By immunohistochemistry using the polyclonal antibodies, collagen VI α5 and α6 were readily detected in skeletal muscle of adult mice. As the specific antibodies against the collagen VI α4 chain did not stain skeletal muscle we tested its reactivity on sections of small intestine where this chain could be strongly detected below the mucosal layer (Fig. 9). The strong reactivity of the antibody with intestine indicates that the collagen VI α4 chain is truly absent from skeletal muscle.

The targeted interruption of the *Col6a1* gene in mouse completely abolishes the secretion of the collagen α2 and α3 chains (20), showing the need for a heterotrimeric assembly to form a functional collagen VI molecule. To determine the influence of the lack of the collagen VI α1 chain on the assembly of the new collagen VI chains we analyzed their occurrence in α1 chain-deficient mice (20). The new collagen VI chains could not be detected in quadriceps femoris of collagen VI α1 chain-deficient mice by immunohistochemistry (Fig. 9), indicating a participation of the α1 chain in the assembly of collagen VI molecules containing the new chains. The absence of the α5 and α6 chains in *Col6a1* knock-out mice was also confirmed by immunoblot analysis of diaphragm extracts (Fig. 10). For wild type mice, incubation with antibodies specific for either the collagen VI α5 or α6 chain resulted in clearly identifiable bands above 220 kDa. When the same method was applied to diaphragm from collagen VI α1 chain-deficient mice, no bands were detected, supporting the results from the immunohistochemical analysis.

DISCUSSION

We report on the identification and initial biochemical characterization of three new collagen VI chains, named collagen VI α4, α5 and α6. The mouse *Col6a4–Col6a6* genes are arranged in tandem on chromosome 9 and were numbered according to their appearance from 5′ to 3′ on the coding strand. Cloning of the cDNAs by RT-PCR and immunohistochemistry and immunoblot using antibodies raised against recombinant fragments confirmed the expression of the new collagen VI genes in mouse. These genes have previously only been incompletely annotated or incorrectly predicted by conceptual translation or gene prediction programs.

The sequences and the domain structures of the new proteins show that they represent new collagen VI chains, which probably occur as the consequence of a gene duplication of the common ancestor of the collagen VI α3 and of the new α chain genes, followed by additional duplications. The identical size of the collagenous domains of the new α chains, compared with that of the α3 chain, implies that they could substitute for the α3 chain, probably forming α1α2α4, α1α2α5, or α1α2α6 heterotrimers. The close relation between the α3 chain and the new chains is also reflected by the almost identical exon/intron organization of the portions of the respective genes encoding the collagenous domains. With the exception of the last exon, the exon sizes are the same. Alternative splicing has been reported for the α3 chain mRNA (29) leading to production of shorter protein isoforms with molecular sizes similar to those of the new chains. The collagen VI arrangement known to date is composed of α1, α2, and α3 chains that associate intracellularly in a stoichiometric ratio to form triple helical monomers. Monomers then assemble into dimers and tetramers, which are finally secreted and deposited in the extracellular matrix where they form beaded filaments by interactions of their non-collagenous domains (3). There is good evidence that the α3 chain expression is essential for the formation of functional collagen VI molecules, as human SaOS-2 cells that are deficient in α3 chain expression do not produce triple helical collagen VI (30). Although the length of the collagenous domain of the collagen VI α1 chain is also identical to that of the new chains and the α2 chain is only one amino acid residue shorter, there are other criteria that clearly show the closest relationship of the new chains with the α3 chain. First, the exact position of the cysteine residue within the collagenous domain is conserved in the α3, α4, α5, and α6 chains. In the α3 chain this cysteine appears to be involved in tetramer formation and stability (19). The α1 and α2 chains also contain a cysteine each, but these are at a different position, and they appear to be involved in the stabilization of the supercoil that is formed during antiparallel dimer forma-

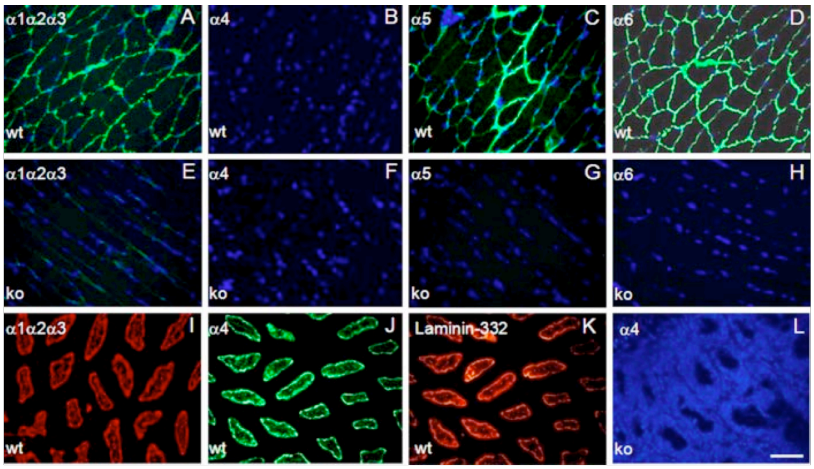

FIGURE 9. **Immunohistochemical analysis of wild type and *Col6a1* knock-out mouse.** Immunohistochemistry was performed on frozen sections from mouse quadriceps femoris muscle (*A–H*) and small intestine (*I–L*) from wild type (*wt*) (*A–D* and *I–K*) or *Col6a1* knock-out mice (*ko*) (*E–H* and *L*). Sections were incubated with the affinity-purified antibodies against the collagen VI α4 N3–N6 domain (*B*, *F*, *J*, and *L*), the collagen VI α5 N3 domain (*C* and *G*), the collagen VI α6 N2–N6 domain (*D* and *H*), human collagen VI from placenta (detecting the classical collagen VI chains α1α2α3; *A*, *E*, and *I*) and laminin 332 (*K*), followed by an AlexaFluor 488-conjugated goat anti-rabbit IgG (*green*, *A–H*), AlexaFluor 546-conjugated goat anti-rabbit IgG (*red*, *I* and *K*), or AlexaFluor 488-conjugated goat anti-guinea pig IgG (*green*, *J* and *L*). Antibodies against the classical collagen VI chains (α1α2α3) and the α5 and α6 chains, but not such against the α4 chain, strongly stained the extracellular matrix surrounding the muscle fibers of wild type (*A–D*) mice. In small intestine, antibodies against classical collagen VI (α1α2α3) (*I*) and antibodies against the collagen VI α4 chain show co-staining with those against the basement membrane marker laminin-332 (*K*). In collagen VI α1 chain-deficient mice, staining for the new collagen VI chains is absent (*L*). Nuclei were counterstained with 4′,6-diamidino-2-phenylindole (*blue*, *A–H* and *L*). The bar is 100 μm.

tion (31). Second, it has also been suggested that the supercoiled dimer is partially stabilized by ion pairs between different segments along the supercoil (32). In the α1α2α3 triple helical monomer the supercoiled part of the α1 chain carries a high negative net charge, whereas that of the α3 chain has a high positive net charge and that of the α2 is close to neutral. All three new chains carry a positive net charge that is even higher than that of the α3 chain. In addition, the positions of the two Gly-Xaa-Yaa imperfections present in the α3 chain, giving the supercoil a clearly segmented character (32), are conserved. Third, phylogenetic analyses based on the collagenous domains, using protein distance and protein parsimony methods, clusters the new chains with the collagen VI α3 chain, whereas the α1 and the α2 chains form a different branch (Fig. 4, *A* and *B*). In addition, the VWA domains C1 and C2 of the α3, α4, α5, and α6 chains also cluster in common branches (Fig. 4, *C* and *D*).

All three new chains could be detected in collagen VI preparations from newborn mouse carcasses. The Coomassie-stained gel clearly showed the distinct α1 and α2 bands and a very heterogenous distribution of bands above 220 kDa (Fig. 8*A*). By immunoblot using affinity-purified antibodies, the new chains were identified as a part of this purified collagen VI preparation (Fig. 8*B*), indicating that trimeric assemblies containing the new chains are present in tissues. Further experimental evidence for an assembly of the new chains into collagen VI came from the study of their expression in *Col6a1* knock-out mice. It was shown earlier that the absence of the collagen VI α1 chain also leads to the lack of the secretion of the α2 and α3 chains (20), indicating that the α1 chain is essential for the assembly of collagen VI molecules. The complete lack of the new chains in *Col6a1* knock-out mice clearly shows that the presence of the collagen VI α1 chain is a prerequisite also for their secretion. This observation strongly suggests that the new chains assemble in a similar way as proposed for the α1, α2, and α3 chain-containing collagen VI.

It has been shown that the N5 and the C5 domains of the collagen VI α3 chain are critical for the microfibril formation (9, 33). Based on the sequence information alone it is not clear which domains in the new chains correspond to the N5 domain of the α3 chain. In some species only the α4 chain contains a domain distinctly homologous to the α3 chain C5 domain. As in the α3 chain, this domain resembles a Kunitz domain. Interestingly, the Kunitz domain of the α4 chain is truncated in mouse and rat, but the N-terminal part, which contains the trypsin interaction site in the original bovine pancreatic trypsin inhibitor (34), is still present in the truncated molecules and could serve as an interaction module. The α5 and α6 chains lack a Kunitz domain, which may indicate differences in the assembly of α5 and α6 chain-containing microfibrils. Indeed, it will be interesting to study how collagen VI of different composition assembles. Do fibrils contain α1, α2, and only one of the four related α3, α4, α5, and α6 chains or are mixed assemblies possible? The latter alternative would lead to a very high number of possible permutations.

The ortholog human genes are present on a, in an evolutionary context, very interesting part of chromosome 3. A large pericentric inversion occurred some time after the split of Homininae and Ponginae (27). The 3′ breakpoint of the inversion is located within *COL6A4* and leads to its inactivation. Although both parts of *COL6A4* are still present and can be easily identified by their sequence, both have become transcribed non-processed pseudogenes. Thereby Homininae have become natural *COL6A4* knock-outs (Fig. 5). This raises the question of whether one of the remaining genes has taken over the function of the lost one. The major structural difference between the collagen VI α4 chain and the α5 and α6 chains is at the C terminus, where the fibronectin type III domain and the Kunitz domain occur only in the α4 chain. However, when comparing human and mouse collagen VI α5 and α6 chains, higher divergence is found at the C terminus of the α5 chain, which in addition shows alternative splicing and could represent an adaptation to a need to replace the α4 chain in Homininae.

Recently, the human *COL6A5* was associated with atopic dermatitis in a linkage study and designated *COL29A1* (28).

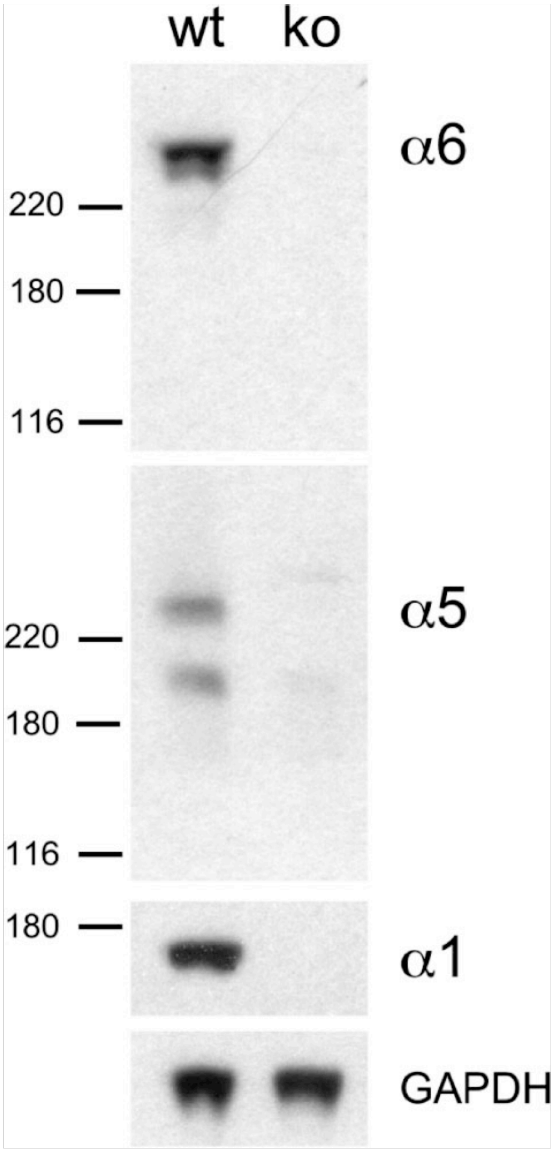

FIGURE 10. **Immunoblot analysis of collagen VI α5 and α6 chains in wild type and *Col6a1* knock-out mouse diaphragm extracts.** Diaphragm muscle of adult wild type (*wt*) and *Col6a1* knock-out mice (*ko*) were extracted with lysis buffer (see "Materials and Methods"). The proteins were submitted to SDS-PAGE with prior reduction on 4–12% polyacrylamide gradient gel, transferred to a membrane, and immunostained with specific antibodies against the collagen VI α1, α5, and α6 chains or glyceraldehyde-3-phosphate dehydrogenase (*GAPDH*).

Although neither DNA nor protein sequences were originally published, later the cDNA sequence became accessible in the data base. The protein sequence is, except for a single amino acid exchange, identical to the third potential splice variant presented here. As we have shown for mouse by RT-PCR, the collagen VI α5 chain is expressed in skin in man also (28). The expression in other tissues only partially overlaps; however intestine and lung also show expression in both species. A variety of nonsynonymous coding SNPs were described, but none could explain the association of *COL6A5* with atopic dermatitis on its own. It was therefore proposed that several variants or combinations associated with the most common haplotype of *COL6A5* are involved in the etiology of the disease. In addition, a strongly maternal transmission pattern was found, which could be due either to imprinting or to maternal effects through an interaction of the child's genotype with the maternal environment during prenatal life. Another susceptibility locus for atopic dermatitis is linked to 3p24-22 (35), which is exactly the breakpoint area where the 5′ part of the *COL6A4* pseudogene is located. It could be that the mechanism leading to atopic dermatitis is more complex and that the expression of the non-processed α4 chain pseudogenes by a yet unknown mechanism influences α5 chain expression. The maternal transmission pattern could point to such a mechanism. A number of pseudogenes have been described where gene conversion between a functional copy of a gene and a neighboring pseudogene causes disease (36). However, in the present case the mechanism is likely to be more complex.

The newly identified locus for atopic dermatitis in *COL6A5* could correlate to another susceptibility locus found on chromosome 21p21 in a Swedish population that may contain a susceptibility gene modulating the severity of atopic dermatitis especially in combination with asthma (37). Both 21p21 and 3p24 have also been described as asthma susceptibility loci (38). Interestingly, *COL6A1* and *COL6A2* are located on 21p21, which could point to a more general role of collagen VI in the development of atopic dermatitis or asthma. In contrast, there is clear evidence for the role of collagen VI in the etiology of Bethlem myopathy and Ullrich congenital muscular dystrophy. A variety of mutations in all so far known collagen VI chains have been identified (for review see Ref. 19). Interestingly, patients who have phenotypes typical of Bethlem myopathy or Ullrich congenital muscular dystrophy, but in whom mutations in the collagen VI α1, α2 and α3 chains could not be detected have been described (39–41). It is therefore tempting to speculate that mutations in the new collagen VI chains may cause muscular disease. Indeed, in mouse skeletal muscle the affinity-purified antibodies detected two of the new chains, α5 and α6, but not α4, associated with the extracellular matrix. In contrast, the α4 chain was absent from mouse muscle but detected close to the basement membrane underlying the mucosal cell layer in small intestine. This differential distribution indicates that the new chains may have tissue-specific functions allowing a modulation of collagen VI properties.

REFERENCES

1. Myllyharju, J., and Kivirikko, K. I. (2004) *Trends Genet.* **20,** 33–43
2. Veit, G., Kobbe, B., Keene, D. R., Paulsson, M., Koch, M., and Wagener, R. (2006) *J. Biol. Chem.* **281,** 3494–3504
3. Furthmayr, H., Wiedemann, H., Timpl, R., Odermatt, E., and Engel, J. (1983) *Biochem. J.* **211,** 303–311
4. Colombatti, A., Bonaldo, P., Ainger, K., Bressan, G. M., and Volpin, D. (1987) *J. Biol. Chem.* **262,** 14454–14460
5. Engvall, E., Hessle, H., and Klier, G. (1986) *J. Cell Biol.* **102,** 703–710
6. Whittaker, C. A., and Hynes, R. O. (2002) *Mol. Biol. Cell* **13,** 3369–3387
7. Chu, M. L., Pan, T. C., Conway, D., Kuo, H. J., Glanville, R. W., Timpl, R., Mann, K., and Deutzmann, R. (1989) *EMBO J.* **8,** 1939–1946
8. Chu, M. L., Zhang, R. Z., Pan, T. C., Stokes, D., Conway, D., Kuo, H. J., Glanville, R., Mayer, U., Mann, K., Deutzmann, R., and Timpl, R. (1990) *EMBO J.* **9,** 385–393

9. Fitzgerald, J., Morgelin, M., Selan, C., Wiberg, C., Keene, D. R., Lamande, S. R., and Bateman, J. F. (2001) *J. Biol. Chem.* **276,** 187–193
10. Ball, S. G., Baldock, C., Kielty, C. M., and Shuttleworth, C. A. (2001) *J. Biol. Chem.* **276,** 7422–7430
11. Ball, S., Bella, J., Kielty, C., and Shuttleworth, A. (2003) *J. Biol. Chem.* **278,** 15326–15332
12. Sipila, L., Ruotsalainen, H., Sormunen, R., Baker, N. L., Lamande, S. R., Vapola, M., Wang, C., Sado, Y., Aszodi, A., and Myllyla, R. (2007) *J. Biol. Chem.* **282,** 33381–33388
13. Bonaldo, P., Russo, V., Bucciotti, F., Doliana, R., and Colombatti, A. (1990) *Biochemistry* **29,** 1245–1254
14. Bidanset, D. J., Guidry, C., Rosenberg, L. C., Choi, H. U., Timpl, R., and Hook, M. (1992) *J. Biol. Chem.* **267,** 5250–5256
15. Brown, J. C., Golbik, R., Mann, K., and Timpl, R. (1994) *Matrix Biol.* **14,** 287–295
16. Tillet, E., Wiedemann, H., Golbik, R., Pan, T. C., Zhang, R. Z., Mann, K., Chu, M. L., and Timpl, R. (1994) *Eur. J. Biochem.* **221,** 177–185
17. Finnis, M. L., and Gibson, M. A. (1997) *J. Biol. Chem.* **272,** 22817–22823
18. Wiberg, C., Klatt, A. R., Wagener, R., Paulsson, M., Bateman, J. F., Heinegard, D., and Morgelin, M. (2003) *J. Biol. Chem.* **278,** 37698–37704
19. Lampe, A. K., and Bushby, K. M. (2005) *J. Med. Genet.* **42,** 673–685
20. Bonaldo, P., Braghetta, P., Zanetti, M., Piccolo, S., Volpin, D., and Bressan, G. M. (1998) *Hum. Mol. Genet.* **7,** 2135–2140
21. Irwin, W. A., Bergamin, N., Sabatelli, P., Reggiani, C., Megighian, A., Merlini, L., Braghetta, P., Columbaro, M., Volpin, D., Bressan, G. M., Bernardi, P., and Bonaldo, P. (2003) *Nat. Genet.* **35,** 367–371
22. Angelin, A., Tiepolo, T., Sabatelli, P., Grumati, P., Bergamin, N., Golfieri, C., Mattioli, E., Gualandi, F., Ferlini, A., Merlini, L., Maraldi, N. M., Bonaldo, P., and Bernardi, P. (2007) *Proc. Natl. Acad. Sci. U. S. A.* **104,** 991–996
23. Pfaff, M., Aumailley, M., Specks, U., Knolle, J., Zerwes, H. G., and Timpl, R. (1993) *Exp. Cell Res.* **206,** 167–176
24. Marinkovich, M. P., Lunstrum, G. P., and Burgeson, R. E. (1992) *J. Biol. Chem.* **267,** 17900–17906
25. Colombatti, A., Ainger, K., and Colizzi, F. (1989) *Matrix* **9,** 177–185
26. Persikov, A. V., Ramshaw, J. A., and Brodsky, B. (2005) *J. Biol. Chem.* **280,** 19343–19349
27. Muzny, D. M., Scherer, S. E., Kaul, R., Wang, J., Yu, J., Sudbrak, R., Buhay, C. J., Chen, R., Cree, A., Ding, Y., Dugan-Rocha, S., Gill, R., Gunaratne, P., Harris, R. A., Hawes, A. C., *et al.* (2006) *Nature* **440,** 1194–1198
28. Soderhall, C., Marenholz, I., Kerscher, T., Ruschendorf, F., Esparza-Gordillo, J., Worm, M., Gruber, C., Mayr, G., Albrecht, M., Rohde, K., Schulz, H., Wahn, U., Hubner, N., and Lee, Y. A. (2007) *PLoS Biol.* **5,** e242
29. Dziadek, M., Kazenwadel, J. S., Hendrey, J. A., Pan, T. C., Zhang, R. Z., and Chu, M. L. (2002) *Matrix Biol.* **21,** 227–241
30. Lamande, S. R., Sigalas, E., Pan, T. C., Chu, M. L., Dziadek, M., Timpl, R., and Bateman, J. F. (1998) *J. Biol. Chem.* **273,** 7423–7430
31. Chu, M. L., Conway, D., Pan, T. C., Baldwin, C., Mann, K., Deutzmann, R., and Timpl, R. (1988) *J. Biol. Chem.* **263,** 18601–18606
32. Knupp, C., and Squire, J. M. (2001) *EMBO J.* **20,** 372–376
33. Lamande, S. R., Morgelin, M., Adams, N. E., Selan, C., and Allen, J. M. (2006) *J. Biol. Chem.* **281,** 16607–16614
34. Perona, J. J., Tsu, C. A., Craik, C. S., and Fletterick, R. J. (1993) *J. Mol. Biol.* **230,** 919–933
35. Bradley, M., Soderhall, C., Luthman, H., Wahlgren, C. F., Kockum, I., and Nordenskjold, M. (2002) *Hum. Mol. Genet.* **11,** 1539–1548
36. Bischof, J. M., Chiang, A. P., Scheetz, T. E., Stone, E. M., Casavant, T. L., Sheffield, V. C., and Braun, T. A. (2006) *Hum. Mutat.* **27,** 545–552
37. Bu, L. M., Bradley, M., Soderhall, C., Wahlgren, C. F., Kockum, I., and Nordenskjold, M. (2006) *Allergy* **61,** 617–621
38. Ober, C., Cox, N. J., Abney, M., Di Rienzo, A., Lander, E. S., Changyaleket, B., Gidley, H., Kurtz, B., Lee, J., Nance, M., Pettersson, A., Prescott, J., Richardson, A., Schlenker, E., Summerhill, E., Willadsen, S., and Parry, R. (1998) *Hum. Mol. Genet.* **7,** 1393–1398
39. Baker, N. L., Morgelin, M., Peat, R., Goemans, N., North, K. N., Bateman, J. F., and Lamande, S. R. (2005) *Hum. Mol. Genet.* **14,** 279–293
40. Lampe, A. K., Dunn, D. M., von Niederhausern, A. C., Hamil, C., Aoyagi, A., Laval, S. H., Marie, S. K., Chu, M. L., Swoboda, K., Muntoni, F., Bonnemann, C. G., Flanigan, K. M., Bushby, K. M. D., and Weiss, R. B. (2005) *J. Med. Genet.* **42,** 108–120
41. Lucioli, S., Giusti, B., Mercuri, E., Vanegas, O. C., Lucarini, L., Pietroni, V., Urtizberea, A., Ben Yaou, R., de Visser, M., van der Kooi, A. J., Bonnemann, C., Iannaccone, S. T., Merlini, L., Bushby, K., Muntoni, F., Bertini, E., Chu, M. L., and Pepe, G. (2005) *Neurology* **64,** 1931–1937
42. Lee, J. O., Rieu, P., Arnaout, M. A., and Liddington, R. (1995) *Cell* **80,** 631–638
43. Perkins, S. J., Smith, K. F., Williams, S. C., Haris, P. I., Chapman, D., and Sim, R. B. (1994) *J. Mol. Biol.* **238,** 104–119
44. Sengle, G., Kobbe, B., Morgelin, M., Paulsson, M., and Wagener, R. (2003) *J. Biol. Chem.* **278,** 50240–50249

2.2 Analysis of new collagen VI chains in human skin.

ORIGINAL ARTICLE

Expression of the Collagen VI α5 and α6 Chains in Normal Human Skin and in Skin of Patients with Collagen VI-Related Myopathies

Patrizia Sabatelli[1], Sudheer K. Gara[2], Paolo Grumati[3], Anna Urciuolo[3], Francesca Gualandi[4], Rosa Curci[1], Stefano Squarzoni[1], Alessandra Zamparelli[1], Elena Martoni[4], Luciano Merlini[4], Mats Paulsson[2,5,6], Paolo Bonaldo[3] and Raimund Wagener[2]

Collagen VI is an extracellular matrix protein with critical roles in maintaining muscle and skin integrity and function. Skin abnormalities, including predisposition to keratosis pilaris and abnormal scarring, were described in Ullrich congenital muscular dystrophy (UCMD) and Bethlem myopathy (BM) patients carrying mutations in *COL6A1*, *COL6A2*, and *COL6A3* genes, whereas *COL6A5*, previously designated as *COL29A1*, was linked to atopic dermatitis. To gain insight into the function of the newly identified collagen VI α5 and α6 chains in human skin, we studied their expression and localization in normal subjects and in genetically characterized UCMD and BM patients. We found that localization of α5, and to a lesser extent α6, is restricted to the papillary dermis, where the protein mainly colocalizes with collagen fibrils. In addition, both chains were found around blood vessels. In UCMD patients with *COL6A1* or *COL6A2* mutations, immunolabeling for α5 and α6 was often altered, whereas in a UCMD and in a BM patient, each with a *COL6A3* mutation, expression of α5 and α6 was apparently unaffected, suggesting that these chains may substitute for α3, forming α1α2α5 or α1α2α6 heterotrimers.

Journal of Investigative Dermatology (2011) **131,** 99–107; doi:10.1038/jid.2010.284; published online 30 September 2010

INTRODUCTION

Collagen VI is a functionally important extracellular matrix protein expressed in many tissues, including skeletal muscle and skin. It was long considered to consist of three genetically distinct α-chains (α1, α2, α3), secreted into the extracellular matrix where they form an extended microfilamentous network. Mutations in the *COL6A1, COL6A2,* and *COL6A3* genes cause Ullrich congenital muscular dystrophy (UCMD) and Bethlem myopathy (BM). Although the muscle phenotype is predominant, various skin changes have been described in collagen VI-related disorders, including a predisposition for keratosis pilaris (follicular keratosis), abnormal scarring, such as keloids and ''cigarette paper'' scars, rough or dry skin, and striae rubrae (Pepe *et al.*, 2002; Jimenez-Mallebrera *et al.*, 2006; Lampe *et al.*, 2008; Nadeau *et al.*, 2009). In addition, a group of Indian UCMD patients shows soft velvety skin on the palms and soles that totally lack major creases and instead have fine mesh-like lines (Nalini *et al.*, 2009).

Recently, three new collagen VI chains were identified, α4, α5, and α6, that are encoded by distinct genes, *COL6A4, COL6A5,* and *COL6A6* (Fitzgerald *et al.*, 2008; Gara *et al.*, 2008). These chains are composed of seven N-terminal von Willebrand factor A domains, a collagen triple helical domain and a C-terminal non-collagenous domain containing two or three C-terminal von Willebrand factor A domains and one or two unique sequences. In addition, α4 contains a Kunitz domain. Their triple helical domains are most similar to that of α3, and, in general, the recently identified chains resemble this chain. Indeed, *Col6a1* null mice do not deposit the new chains in the extracellular matrix, showing that assembly and secretion of these requires the presence of α1 and implying that the new chains may substitute for α3, probably forming α1α2α4, α1α2α5, or α1α2α6 heterotrimers (Gara *et al.*, 2008). This is in contrast to assembly studies using transfected cells, in which only α4, but not α5 and α6, was found to be able to form heterotrimers that are secreted (Fitzgerald *et al.*, 2008). In humans, *COL6A4* is disrupted by a

[1]*Istituto Di Genetica Molecolare-CNR, Istituto Ortopedico Rizzoli, Bologna, Italy;* [2]*Center for Biochemistry, Medical Faculty, University of Cologne, Cologne, Germany;* [3]*Department of Histology, Microbiology and Medical Biotechnologies, University of Padova, Padova, Italy;* [4]*Section of Medical Genetics, Department of Experimental and Diagnostic Medicine, University of Ferrara, Ferrara, Italy;* [5]*Center for Molecular Medicine Cologne, University of Cologne, Cologne, Germany and* [6]*Cologne Excellence Cluster on Cellular Stress Responses in Aging-Associated Diseases, University of Cologne, Cologne, Germany*

Correspondence: Raimund Wagener, Institute for Biochemistry II, Medical Faculty, University of Cologne, Joseph-Stelzmann-Str. 52, Cologne D-50931, Germany. E-mail: raimund.wagener@uni-koeln.de

Abbreviations: BM, Bethlem myopathy; UMCD, Ullrich congential muscular dystrophy

Received 26 January 2010; revised 2 August 2010; accepted 16 August 2010; published online 30 September 2010

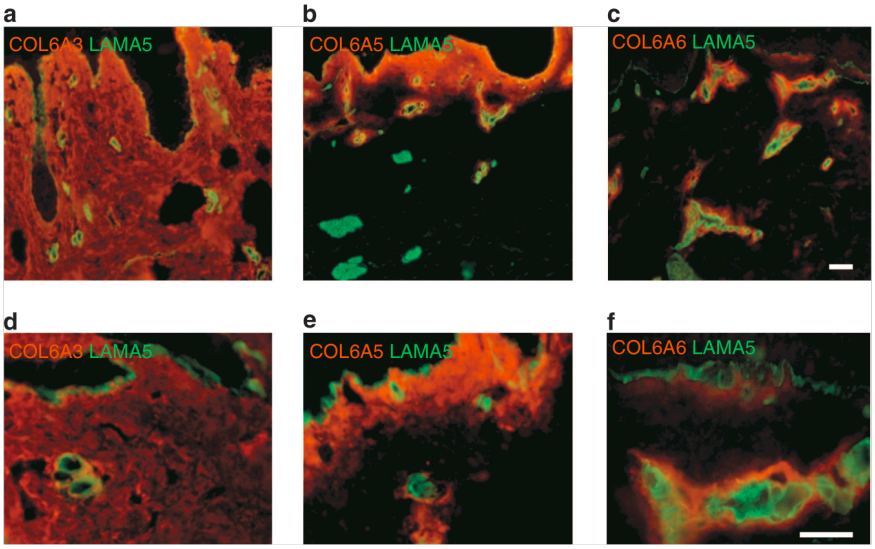

Figure 1. Collagen VI α chain distribution in normal human skin. Analysis of skin sections from a healthy donor with a mAb against collagen VI α3 (**a**, **d**) or polyclonal antibodies against collagen VI α5 (**b**, **e**) or α6 (**c**, **f**) (red). Sections were double labeled with an antibody against laminin α5 (green), as a marker of basement membranes. Collagen VI α3 shows a broad distribution in the papillary and reticular dermis, including vasculature and nerves, and hypodermis. In contrast, collagen VI α5 is localized in the papillary dermis, close to the dermal–epidermal junction, and around some vessels of the reticular dermis. α6 appears around the vessels of the papillary and reticular dermis, with a weaker and discontinuous labeling below the dermal–epidermal junction. **a**, **b**, **c** and **d**, **e**, **f** are at the same magnification. Bar = 100 μm.

chromosome break (Fitzgerald *et al.*, 2008; Gara *et al.*, 2008; Wagener *et al.*, 2009) as a consequence of a large-scale pericentric inversion on chromosome 3 and, interestingly, the 5′ end of the split gene was linked to a predisposition for osteoarthritis (Miyamoto *et al.*, 2008; Wagener *et al.*, 2009). In humans, *COL6A6* is expressed in a wide range of fetal and adult tissues, whereas *COL6A5* expression is restricted to a few sites, including lung (Fitzgerald *et al.*, 2008) and skin (Söderhäll *et al.*, 2007). The expression of the newly identified chains was yet not studied in detail, although reverse transcription-PCR revealed differences between human and mouse (Söderhäll *et al.*, 2007; Fitzgerald *et al.*, 2008; Gara *et al.*, 2008). Human α5 was found to be localized in the outer epidermis and *COL6A5* has been associated with atopic dermatitis and designated *COL29A1* (Söderhäll *et al.*, 2007). Atopic dermatitis patients were found to lack collagen VI α5 expression in the outer epidermis (Söderhäll *et al.*, 2007). This was proposed to lead to a loss of epidermal integrity that may facilitate the antigen penetration through the skin. However, in a genome-wide association study in 939 affected individuals, *COL6A5* did not show linkage to atopic dermatitis (Esparza-Gordillo *et al.*, 2009), whereas in another study a polymorphism of *COL6A5* was associated with atopy, but this association could not be consistently replicated (Castro-Giner *et al.*, 2009). To gain insight into the function of the newly identified α5 and α6 chains in human skin and their potential role in pathology, we studied their expression and deposition in normal subjects and UCMD and BM patients.

RESULTS

Collagen VI α5 and α6 show a more restricted localization pattern in human skin than the homologous α3

Immunofluorescence microscopy of normal skin sections labeled with an antibody against collagen VI α3 showed staining throughout the dermis (Figure 1a and d), whereas labeling with antibodies against collagen VI α5 and α6 revealed a more restricted localization pattern. Collagen VI α5 appeared mainly expressed at the papillary dermis (Figure 1b and e), with a more intense labeling just below the dermal–epidermal junction. Here, the expression of collagen VI α6 was much weaker and discontinuous (Figure 1c and f). In contrast, α5 and α6 were both strongly expressed around blood vessels at the interface between the papillary dermis and the reticular dermis, but not around the annexes of the deeper layers of the skin (Figure 1b and c). This pattern was confirmed by double labeling with antibodies against laminin α5, a marker for basement membranes (Figure 1). De-masking experiments revealed that the detection of the newly identified collagen VI chains in very restricted areas is not caused by a hindered accessibility of the antibodies elsewhere (Supplementary Figure S1 online). No collagen VI was detected in the epidermis, in clear contrast to the reported expression of collagen VI α5 in the outer epidermis (Söderhäll *et al.*, 2007). Immunoelectron microscopy analysis with antibodies against either collagen VI α3, α5, or α6 (Figure 2) confirmed the localization detected by immunofluorescence. In the papillary dermis, α5 and α3 colocalize with banded collagen fibrils. However, although α5 was

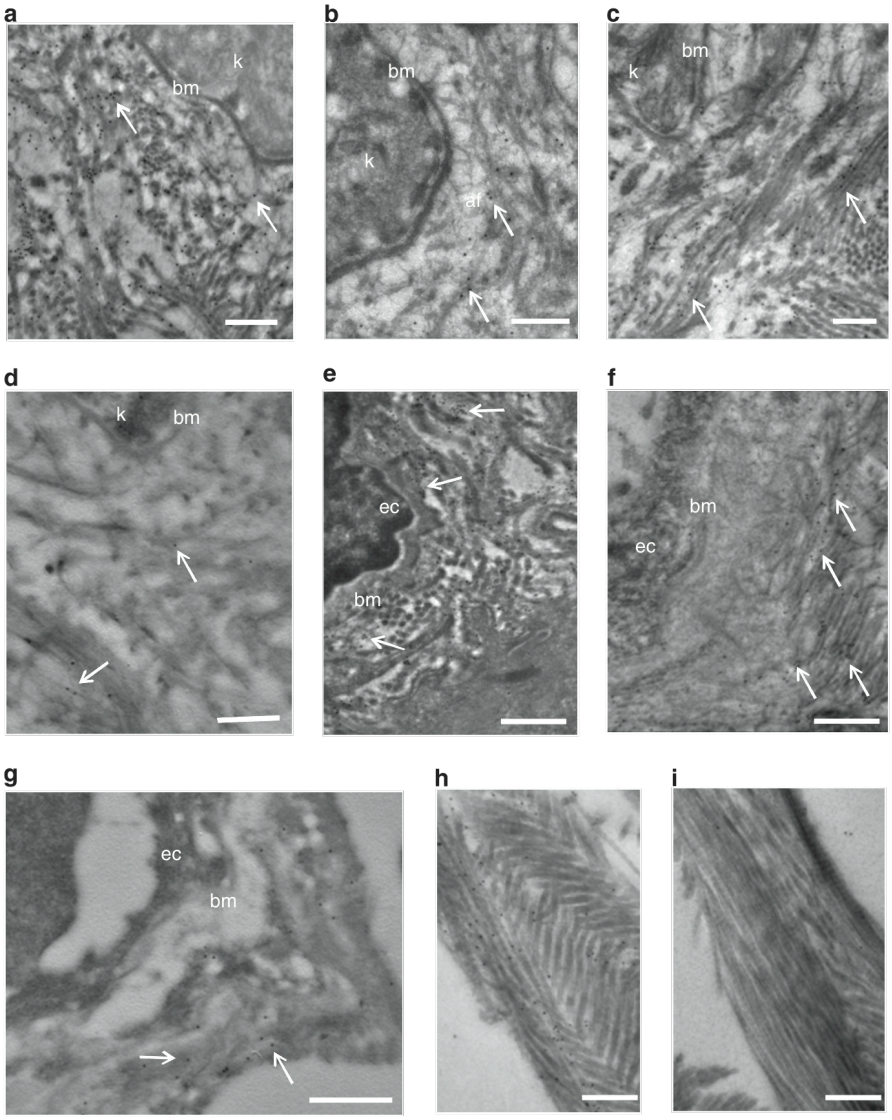

Figure 2. Ultrastructural localization of collagen VI α chains in normal human skin. (**a**–**d**) Normal papillary dermis with collagen VI α3 (**a**), α5 (**b**, **c**), and α6 (**d**) antibodies. α3 appears at collagen fibrils of the dermal–epidermal junction (arrows, **a**). α5 is associated with collagen bundles (**b**, **c**, arrows), but absent from epidermis (k), basement membrane (bm), and anchoring fibrils (af). α6 is sparse in papillary dermis (**d**, arrows). (**e**–**i**) Vessels in papillary (**e**, **f**, **g**) and collagen bundles in reticular dermis (**h**, **i**) with α3 (**e**, **h**), α5 (**f**, **i**), and α6 (**g**) antibodies. α3 is associated with collagen fibrils reaching basement membranes (**e**, arrows) and with intersecting collagen bundles (**h**); α5 and α6 with collagen bundles surrounding vessels (**f**, **g**, arrows), but not with basement membranes (**f**, **g**). α5 is absent within collagen bundles (**i**). bm, basement membrane; ec, endothelial cell. Bars = 200 nm.

clearly detected along longitudinally sectioned fibrils (Figure 2b and c), α3 was also visible in areas where fibrils were cross-sectioned (Figure 2a). None of the antibodies labeled the epidermis, the basement membrane of dermal–epidermal junctions, or anchoring plaques, which are connected to the basement membrane through anchoring filaments (Figure 2). For α6, only a weak labeling was found in the papillary dermis, where few gold particles, associated with collagen fibrils, were detected (Figure 2d). Although all chains were detected around the wall of blood vessels of the papillary dermis, these showed a different distribution (Figure 2e–i). Whereas collagen VI α5 and α6 colocalize with collagen fibril bundles surrounding vessel walls (Figure 2f and g), α3 was also detected at the vessel endothelium, together with collagen fibrils reaching the basement membrane (Figure 2e). The basement membrane underlying the endothelium was not labeled. The reticular dermis did not show labeling for α5 (Figure 2i) or α6 (not shown), whereas when labeled with the antibody against α3, bundles of collagen fibrils showed gold particles at intersections (Figure 2h).

Deposition of α5 and α6 in the skin of patients with *COL6A1*, *-A2*, and *-A3* mutations

To assess whether mutations in *COL6A1*, *COL6A2,* and *COL6A3* affect the secretion and localization of collagen VI α5 and α6, we investigated skin biopsies from six UCMD patients carrying mutations in the three genes (two in *COL6A1*, three in *COL6A2,* and one in *COL6A3*) and one BM patient with a recessive mutation in *COL6A3* (Table 1, Supplementary Table S1 online). Immunofluorescence analysis with an antibody against α3 showed a collagen VI deficiency in the skin of five patients, ranging from moderate to severe, whereas UCMD-A1b and UCMD-A2c showed normal expression (Figure 3). Interestingly, immunolabeling for α5 showed altered expression only in those patients with mutations in *COL6A1* or *COL6A2* where collagen VI α3 was also affected (Figure 4a and b). In particular, in UCMD-A1a α5 was reduced at the papillary dermis and around blood vessels (Figure 4a). The expression of α5 varied in patients carrying different compound heterozygous mutations in *COL6A2* (Table 1): while in UCMD-A2a α5 was evenly reduced, in UCMD-A2b the labeling was decreased in some areas of the papillary dermis, both at the dermal–epidermal junction and around the vessels (Figure 4a). In contrast, UCMD-A3 and BM-A3, carrying mutations in *COL6A3* (Table 1), showed α5 staining of normal intensity; however, it appeared more widely distributed in both patients and particularly in UCMD-A3 (Figure 4a). Moreover, in UCMD-A1a and UCMD-A2b, double labeling for α3 and α5 revealed ring-like deposits containing only α5 (Figure 4b). These deposits, usually detected close to the basement membrane of the dermal–epidermal junction, showed an irregular shape, and a variable diameter, ranging from 0.5 to 20 μm and were absent from normal skin. α6 was reduced in UCMD-A1a, but largely unaffected in all other patients (Figure 4c). However, it appeared more widely distributed in patients carrying mutations in *COL6A3*. Furthermore, the ring-like deposits were not detected with the antibody against α6 (not shown).

Western blot analysis of collagen VI α5 and α6 in extracts of normal and UCMD skin

Skin extracts from healthy donors and UCMD-A1a, UCMD-A2a, and UCMD-A3 were investigated by SDS–PAGE under reducing conditions using antibodies against collagen VI α3, α5, and α6 (Figure 5a). In healthy skin, both α5 and α6 were detected as major bands slightly above the 260 kDa marker, consistent with their molecular masses (Figure 5a), whereas α3 was detected migrating as two major bands below and above the 260 kDa marker. Only in UCMD patients with an altered collagen VI expression in immunohistochemistry, α3 was much fainter than in the control and in UCMD-A1a it was detected only after longer exposure. In contrast, α5 was reduced only in UCMD-A2a. However, α5 reproducibly showed a higher mobility in UCMD-A1a. The reduction of α5 in UCMD-A2a was evident with both methods, whereas the weaker signal for α5 in UCMD-A1a in immunohistochemistry was not evident in western blot. The lower molecular mass of α5 in UCMD-A1a, possibly due to abnormal processing, may make the protein more easily extractable.

***COL6A5* and *COL6A6* transcript levels are differently modified in the skin of UCMD and BM patients**

The amount of collagen VI α5 and α6 transcripts in skin biopsies from selected patients was evaluated by real-time PCR, using β-actin as a reference (Figure 5b, Table 1). Whereas levels of *COL6A5* mRNA were similar to controls or only slightly changed in UCMD-A1a, UCMD-A2a, UCMD-A2b and BM-A3, *COL6A5* mRNA levels were reduced to 20% of UCMD-A3. This indicates that the reduction of α5 seen in UCMD-A2a by immunohistochemistry and western blot is not due to transcriptional downregulation. In contrast, the reduction of *COL6A5* mRNA in UCMD-A3 did not affect expression of α5. The collagen VI α6 mRNA level was reduced to 60% of normal levels in UCMD-A3, but was significantly upregulated in UCMD-A1a and UCMD-A2a and unaffected in UCMD-A2b and BM-A3. The upregulation of *COL6A6* mRNA in UCMD-A1a and UCMD-A2a did not lead to a higher expression of the protein.

DISCUSSION

We describe the expression of the recently identified collagen VI α5 and α6 chains in human skin and its variations in the skin of patients suffering from collagen VI-related muscular dystrophies. The tissue distribution of these chains has so far not been comprehensively studied. We now show that collagen VI α5 is found in a very specific zone of the papillary dermis, just below the basement membrane. This is in clear contrast to an earlier report where collagen VI α5 (called collagen XXIX by the authors) was found to be located in the epidermis (Söderhäll *et al.*, 2007). The reason for this discrepancy is not clear. To our knowledge collagen VI has never been found in the epidermis by other authors. Generally, only a few collagens are located in the epidermis, for example, collagen XXIII (Koch *et al.*, 2006). As the lack of the new collagen VI chains in the *Col6a1* knockout mouse clearly indicates that they assemble together with α1 and, probably, α2 to form heterotrimers, an exclusive presence of collagen VI α5 in the epidermis would be surprising. The antibody that detected collagen VI α5 in epidermis was raised against a short peptide sequence and the epidermal staining could therefore be an artifact. The affinity-purified antibody used in this study was raised against a large portion of the N-terminal, non-triple helical domain of collagen VI α5 (domains N2–N6 (Gara *et al.*, 2008)). The specific staining in a narrow zone just below the basement membrane, which is reminiscent of that of matrilin-2 (Piecha *et al.*, 2002), AMACO (Gebauer *et al.*, 2009), or tenascin C (Latijnhouwers *et al.*, 2000), points to a specialized function of collagen VI α5 in this zone of the papillary dermis, which is important for the resistance to tensile stress. Nevertheless, α5 may function in the maintenance of the barrier function of the skin, as indicated by the observation of polymorphisms in *COL6A5* that were found to be linked to atopic dermatitis (Söderhäll *et al.*, 2007) or atopy (Castro-Giner *et al.*, 2009). However, the mechanism by which α5 contributes to the barrier function would be different from the earlier proposed loss of epidermal integrity in the outer epidermis of atopic dermatitis patients (Söderhäll *et al.*, 2007).

Table 1. Collagen VI mutations and phenotypic features

Patient/age at biopsy	Genomic mutation[1]	Skin phenotype	Collagen VI α3 immuno-histochemistry/ western blot	Collagen VI α5 immuno-histochemistry/ western blot	Collagen VI α5 mRNA (mean $\Delta\Delta C_t$)	Collagen VI α6 immuno-histochemistry/ western blot	Collagen VI α6 mRNA (mean $\Delta\Delta C_t$)
UCMD-A1a/ 9 years	Het COL6A1 exon 9 c.921-935 del15[2]	Rough skin, keratosis pilaris, hypertrophic scars	Moderately reduced/severely reduced	Severely reduced, ring structures/normal (higher mobility)	Normal level (0.98:1)	Severely reduced/ moderately reduced	Increased (3.93:1)
UCMD-A1b/ 11 years	Het COL6A1 exon 9 c.850 G>A[2] (Gly284Arg)	Keratosis pilaris	Not reduced/ reduced	Not reduced/ not reduced	ND	Not reduced/ increased	ND
UCMD-A2a/ 9 years	Het COL6A2 exon 12 c.1096 C>T; Het COL6A2 intron 8 c.927+5 G>A[3]	Keratosis pilaris and ''cigarette paper'' scars	Mildly reduced/ reduced	Severely reduced/ reduced	Slightly increased (1.85:1)	Normal/normal	Increased (3.55:1)
UCMD-A2b/ 9 years	Het COL6A2 intron 17 c.1459-2 A>G; het COL6A2 intron 23 c.1771-1 G>A[4]	Rough skin, keratosis pilaris	Severely reduced/ ND	Reduced, ring structures/ND	Normal level (1.23:1)	Normal/ND	Slightly increased (1.42:1)
UCMD-A2c/ 5 years	Hom COL6A2 intron 25 c.1970-9 G>A[3]	Rough skin, keratosis pilaris,	Not reduced/ND	Not reduced/ND	ND	Not reduced/ND	ND
UCMD-A3/ 9 years	Het COL6A3 intron 16 c.6210+1G>A[5]	No relevant changes (keratosis pilaris reported in other patients)[4]	Moderately reduced/reduced	Normal (widely distributed)/normal	Strongly reduced (0.19:1)	Normal/moderately reduced	Moderately reduced (0.6:1)
BM-A3/ 21 years	Hom COL6A3 exon 5 c.1393 C>T[6]	Striae rubrae, keratosis pilaris	Severely reduced/ reduced[7]	Normal/ND	Normal level (0.77:1)	Widely distributed/ ND	Slightly increased (1.49:1)

Abbreviation: ND, not determined.
[1]The DNA mutation numbering is based on complementary DNA sequence with a ''c.'' symbol before the number with +1 corresponding to the A of the ATG translation initiation codon in the respective reference sequence (COL6A1 GenBank Refseq NM_001848.2; COL6A2 GenBank Refseq NM_001849.3; COL6A3 GenBank Refseq NM_004369.2).
[2]Angelin *et al.* (2007).
[3]Martoni *et al.* (2009).
[4]Camacho Vanegas *et al.* (2001).
[5]Lampe *et al.* (2008).
[6]Demir *et al.* (2002).
[7]Squarzoni *et al.* (2006).

Most of the mutations affect the triple helical domain, except for in BM-A3 and UCMD-A2c where the N8 and C1 domains are affected (Supplementary Table S1 online). The impact of mutations in *COL6A1, COL6A2,* and *COL6A3* on the expression of collagen VI α5 and α6 in skin is diverse both at the level of transcription and translation and strongly dependent on the specific mutation (Figure 4, Table 1, Supplementary Table S1 online). This probably reflects the complex process of assembly of collagen VI microfibrils, which is prone to perturbations at different levels. As the incidence of UCMD and BM is low (0.13/100,000 and 0.77/100,000) (Norwood *et al.*, 2009), resulting in a limited access to patients, a clear genotype–phenotype correlation was not obtained. No clear correlations were found between the steady state levels of COL6A5 and COL6A6 mRNA and protein expression in selected patients. The lack of an obvious defect in secretion or assembly in the patients with mutations in collagen VI α3 (Figure 4) further indicates that the deposition of α5 or α6 is not dependent on the presence of α3 and that the new chains may instead substitute for α3 by the formation of α1α2α5 or α1α2α6-containing collagen VI molecules. Interestingly, in the UCMD-A3 and BM-A3 patients, α5 and α6 staining is more widely distributed than in normal skin. This indicates that substitution of α3 by α5 and/or α6 alters the assembly of collagen VI-containing microfibrils. The strongly reduced expression of α5 and α6 in UCMD-A1a carrying a dominant mutation in *COL6A1* matches the complete lack of the new collagen VI chains in *Col6a1* knockout mice (Gara *et al.*, 2008) and supports, in contrast to other reports (Fitzgerald *et al.*, 2008), that also human collagen VI α5 forms α1α2α5 heterotrimers. However, as seen in UCMD-A2a and -A2b that carry different compound heterozygous mutations in *COL6A2* (Table 1), it is evident that the impact on the expression of collagen VI α5 and α6 is highly dependent on the nature of the actual mutations. Interestingly, whereas the expression of α3 and α5 is clearly reduced in UCMD-A2a, α6 staining remains unaffected. Owing to the strong reduction of α2 in this patient, α2 concentration may become rate limiting in the triple helix formation. Possibly, α6 is preferred to α3 and α5 in this situation. In addition, the strong upregulation of the *COL6A6* mRNA could be responsible for this effect.

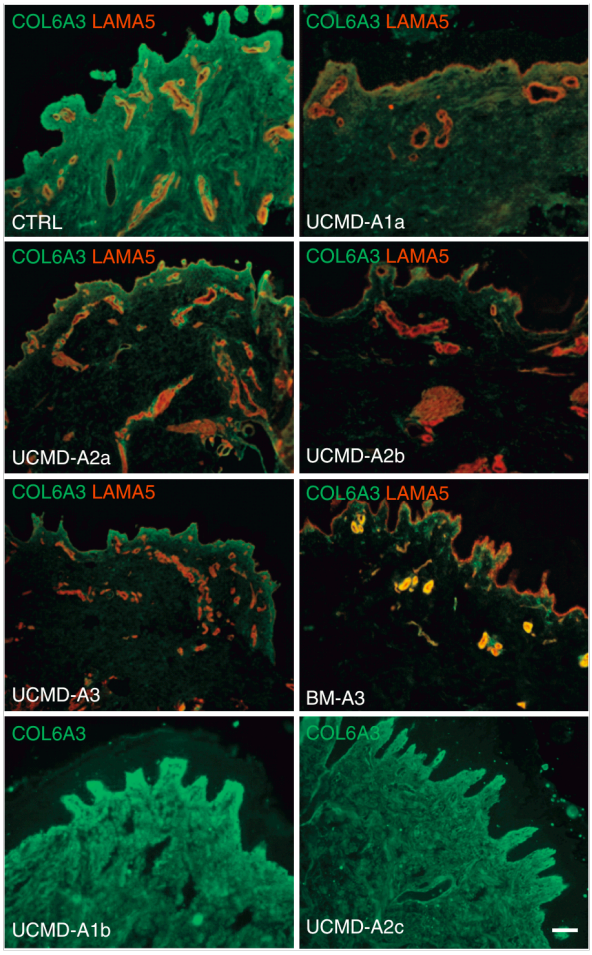

Figure 3. Collagen VI α3 chain distribution in skin of muscular dystrophy patients. Analysis of collagen VI in skin sections of six Ullrich congential muscular dystrophy (UCMD) patients carrying mutations in *COL6A1* (UCMD-A1a and UCMD-A1b), *COL6A2* (UCMD-A2a, UCMD-A2b, and UCMD-A2c), and *COL6A3* (UCMD-A3) and one Bethlem myopathy (BM) patient with a homozygous mutation in the *COL6A3* gene (BM-A3), compared with a healthy donor (CTRL). Staining was performed with antibodies against collagen VI α3 (green) and laminin α5 (red). Sections of UCMD-A1b and UCMD-A2c were only stained with antibodies against collagen VI α3. The images show a reduced expression of collagen VI α3, in four of the six patients ranging from mild (UCMD-A2a) to moderate (UCMD-A1a and UCMD-A3) or severe (UCMD-A2b and BM-A3). Bar = 100 µm.

However, it remains unclear why the strong upregulation of the *COL6A6* in UCMD-A1a is not reflected at the protein level. Similarly, in UCMD-A2b, staining for α3 and α5 is reduced and α6 is unaffected. Interestingly, as in UCMD-A1a, ring-like deposits are seen, usually close to the basement membrane of the dermal–epidermal junction (Figure 4b). These could represent aggregates of a smaller proportion of collagen VI α5, which is secreted, but not properly assembled into microfibrils. In UCMD-A1a, this may correlate with an increased mobility of collagen VI α5 in western blot (Figure 5a). The reason for the mobility change remains unclear; however, alternative splicing, alternate proteolytic processing, or an altered glycosylation could be responsible. In contrast to the other patients carrying mutations in *COL6A1* or *COL6A2*, expression of the newly identified chains is not affected in UCMD-A1b and in UCMD-A2c (Figure 4a and c), which adds to the complexity of the genotype–phenotype correlation. However, α3 is not affected (Figure 3) and it remains unclear why the formation of α1α2α3 heterotrimers is still possible. UCMD-A1b carries a heterozygous mutation in the N-terminal part of the collagenous domain (Angelin *et al.*, 2007), whereas UCMD-A2c carries a homozygous mutation in the C1 domain (Martoni *et al.*, 2009). At least in UCMD-A2c the intact collagenous domain seems to allow the assembly of α1α2α3 heterotrimers. Accordingly, the formation of α1α2α5- or α1α2α6-containing collagen VI molecules should also not be impaired if α5 or α6 substitute for α3. Nevertheless, also these two patients show a skin phenotype, which could be the consequence of secreted but malfunctioning collagen VI molecules.

The mutations in collagen VI α1, α2, and α3 that lead to muscular dystrophies cause a mitochondrial dysfunction with spontaneous apoptosis of muscle fibers. Whereas the pathogenesis of this muscular phenotype has been studied in great detail (Bernardi and Bonaldo, 2008), the etiology of the skin phenotypes in these patients is unknown. In this study we present evidence that collagen VI α5 and α6 are expressed in dermis and most likely assemble together with collagen VI α1 and α2. Therefore, a possible contribution of collagen VI α5 and α6 to the development of the skin phenotypes has to be considered. The presence of unusual extracellular aggregates of collagen VI α5 may point to a possible disease mechanism.

MATERIALS AND METHODS

Expression and purification of recombinant N-terminal collagen VI α3, α5, and α6 von Willebrand factor A domains

Complementary DNA constructs were generated by reverse transcription-PCR on human placental mRNA. For collagen VI α3 domains N1–N4 and for α5 and α6, the domains N2–N6 were chosen. Suitable primers introduced 5′-terminal *Nhe*I or *Spe*I and 3′-terminal *Bam*HI or *Xho*I restriction sites (Supplementary Table S2 online). The amplified PCR products were inserted into a modified pCEP-Pu vector (Tillet *et al.*, 1994) containing an N-terminal BM-40 signal peptide followed by a tandem strepII-tag (Finnis and Gibson, 1997). Recombinant plasmids were introduced into HEK293-EBNA cells (Invitrogen, Carlsbad, CA) using FuGENE 6 transfection reagents (Roche, Basel, Switzerland). Cells were selected with puromycin (1 µg ml^{-1}) and N-terminal tandem strepII-tagged proteins were purified from serum-containing cell culture medium using a Streptactin column (1.5 ml, IBA GmbH, Goettingen, Germany).

Preparation of antibodies against the new collagen VI chains

Purified recombinant collagen VI fragments were used to immunize rabbits and guinea-pigs. Antisera were purified by affinity chromatography on a column with antigen coupled to CNBr-activated Sepharose (GE Healthcare, Little Chalfont, Buckinghamshire, UK) (Gara *et al.*, 2008).

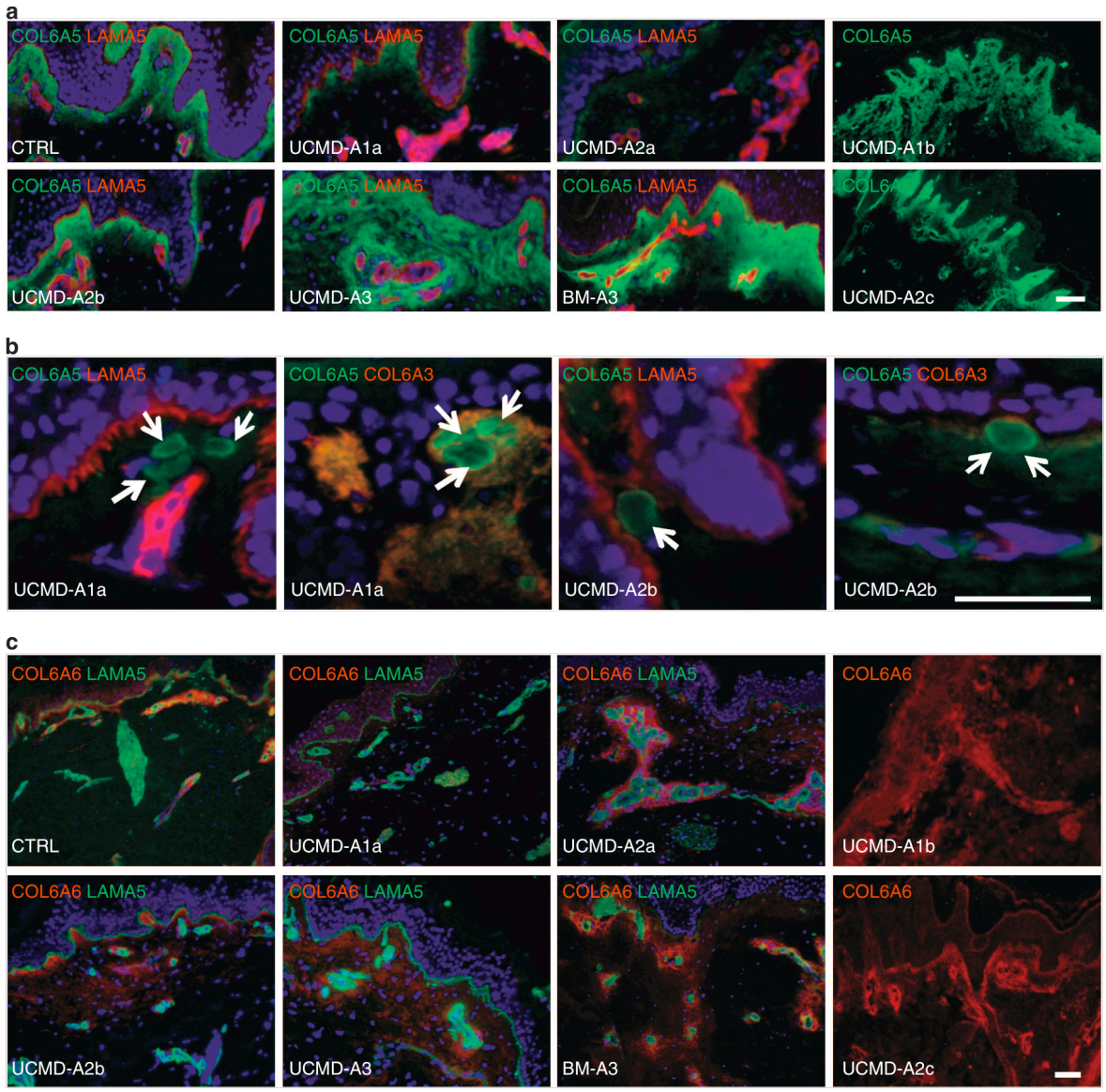

Figure 4. Collagen VI α5 and α6 chain distribution in skin of muscular dystrophy patients. (**a**) Collagen VI α5 (green) and laminin α5 (red) in skin biopsies from a normal donor (CTRL) and Ullrich congenital muscular dystrophy (UCMD) and Bethlem myopathy (BM) patients. 4,6-diamidino-2-phenylindole (blue). Collagen VI α5 is reduced in UCMD-A1a, UCMD-A2a, and UCMD-A2b, but normally expressed in the other patients. (**b**) Collagen VI α5 (green) and laminin α5 (red) or collagen VI α3 (red), in UCMD-A1a and UCMD-A2b. Ring-like deposits (arrows) positive for collagen VI α5 are seen below the epidermal–dermal basement membrane. α3 is absent within these deposits (arrows). (**c**) Collagen VI α6 (red) and laminin α5 (green). α6 is reduced in UCMD-A1a and normally expressed in UCMD-A2a. The other patients show a wide distribution of α6 in papillary dermis. Bars = 100 μm. UCMD-A1b and UCMD-A2c were not costained for laminin α5.

Patients

Skin biopsies from two healthy subjects, one BM and six UCMD patients were frozen in isopentane pre-chilled in liquid nitrogen and stored in liquid nitrogen. All patients were previously diagnosed by genetic, histochemical, and biochemical analysis, which showed mutations of the *COL6A1, COL6A2,* and *COL6A3* genes and altered collagen VI secretion and deposition in skeletal muscle and/or cultured skin fibroblasts (Table 1). All patients provided informed consent.

Western blot analysis

Frozen sections (20 μm) were prepared from skin biopsies, dissolved by incubation for 10 minutes at 70 °C in a lysis solution containing 50 mM Tris-HCl, pH 7.5, 150 mM NaCl, 10 mM $MgCl_2$, 2% SDS, 1%

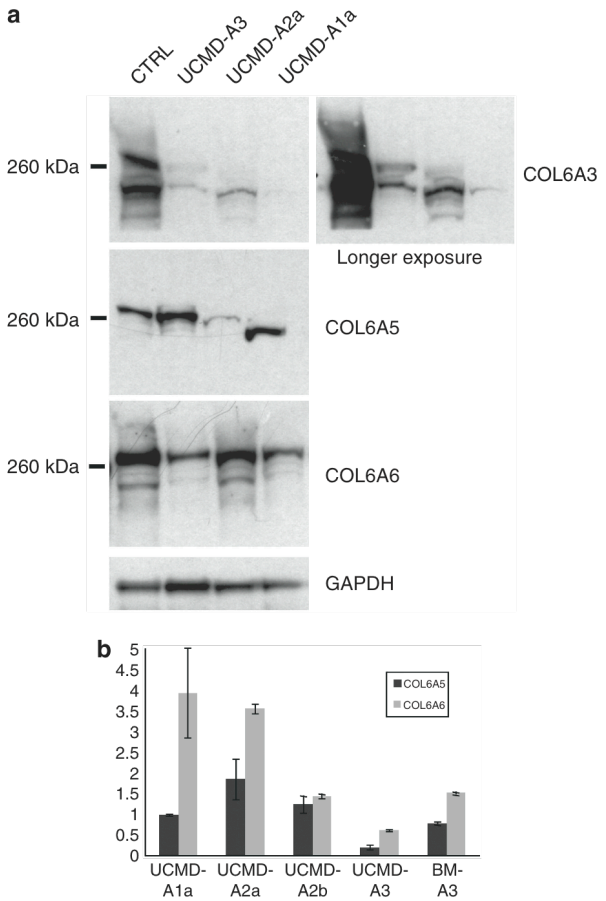

Figure 5. Collagen VI protein and mRNA expression in skin of muscular dystrophy patients. (**a**) Western blot analysis of skin extracts from a healthy control (CTRL) and the UCMD-A1a, UCMD-A2a, and UCMD-A3 patients. Proteins were separated under reducing conditions and detected with polyclonal antibodies specific for collagen VI α3, α5, and α6. For collagen VI α3, a longer exposure is shown on the right. Glyceraldehyde 3-phosphate dehydrogenase was used as a loading control. (**b**) Real-time PCR quantification of the steady-state levels of *COL6A5* and *COL6A6* mRNA transcripts in skin samples from the five UCMD/BM patients. The *COL6A5*/β-actin and *COL6A6*/β-actin ratios of control skin samples were set at 1. BM, Bethlem myopathy; UCMD, Ullrich congenital muscular dystrophy.

Triton X-100, 0.5 mM dithiothreitol, 1 mM ethylenediaminetetraacetic acid, 10% glycerol and protease inhibitors and analyzed by western blot (Gara *et al.*, 2008).

Immunofluorescence analysis

Frozen sections (7 μm) from skin of two healthy donors and one BM and six UCMD patients were incubated with an affinity-purified guinea-pig polyclonal antibody against collagen VI α5, or a monoclonal collagen VI α3 antibody (Chemicon (Billerica, MA) clone 3C4), or a rabbit polyclonal antibody against α3. For the immunofluorescence analysis of α6, frozen sections from healthy donors and patients were fixed with 2% paraformaldehyde in phosphate-buffered saline, washed in phosphate-buffered saline and permeabilized with 0.15% Triton X-100, saturated with 5% normal goat serum (Sigma, St Louis, MO) and incubated with a rabbit antibody against α6. All sections were developed with anti-rabbit or anti-guinea-pig TRITC or FITC-conjugated IgG (DAKO, Glostrup, Denmark) and double labeled with a mouse mAb against laminin α5 (Chemicon), revealed with anti-mouse FITC- or TRITC-conjugated secondary antibodies (DAKO).

Immunoelectron microscopy analysis

Skin fragments from one healthy donor were fixed in 4% paraformaldehyde in phosphate-buffered saline for 1 hour at 4 °C, washed in phosphate-buffered saline, dehydrated and embedded in London Resin White. Ultrathin sections were incubated with primary antibodies, diluted 1/10 in 20-mM Tris-buffered saline, overnight at 4 °C, followed by a 15-nm colloidal gold-conjugated anti-rabbit IgG antibody (Amersham, Little Chalfont, Buckinghamshire, UK). Sections were stained with uranyl acetate and lead citrate and observed with a Philips (Amsterdam, The Netherlands), EM400 transmission electron microscope operating at 100 kV.

Quantification of *COL6A5* and *COL6A6* transcripts by real-time PCR

Total RNA was isolated from skin sections using the RNeasy Kit (Qiagen, Hilden, Germany) and reverse transcribed using the High Capacity complementary DNA Reverse Transcription Kit (Applied Biosystems, Carlsbad, CA), as described (Merlini *et al.*, 2008). To quantify the steady-state level of *COL6A5* and *COL6A6* transcripts, TaqMan expression assays (Applied Biosystems) were used for target genes (*COL6A5 (COL29A1)*: Hs00542046_m1 exons 35-36; *COL6A6*: Hs01029204_m1 exons 12–13) and for β-actin (ACTB Endogenous Control). Real-time PCR was performed in triplicate on the Applied Biosystems Prism 7300 system, using 10 ng of complementary DNA and default parameters. Evaluation of *COL6A5* and *COL6A6* transcript levels was performed by the comparative C_t method ($\Delta\Delta C_t$ method), in at least two independent experiments. Complementary DNAs from two control skin sections were utilized as calibrators and the results were highly similar. Both skin samples were from children and thereby matching the age of the UCMD patients. For patient BM-A3, we have also performed comparison with a skin sample from an adult healthy subject, again with similar results.

CONFLICT OF INTEREST

The authors state no conflict of interest.

ACKNOWLEDGMENTS

This study was supported by the Deutsche Forschungsgemeinschaft (WA1338/2-6 and SFB 829), by the Telethon Foundation (GGP08107 and GUP08006), and by the CaRisBo Foundation, Italy. SK Gara is a member of the International Graduate School in Genetics and Functional Genomics at the University of Cologne. We are grateful to Thomas Krieg and Cornelia Mauch, Cologne, for valuable advice.

SUPPLEMENTARY MATERIAL

Supplementary material is linked to the online version of the paper at http://www.nature.com/jid

REFERENCES

Angelin A, Tiepolo T, Sabatelli P *et al.* (2007) Mitochondrial dysfunction in the pathogenesis of Ullrich congenital muscular dystrophy and prospective therapy with cyclosporins. *Proc Natl Acad Sci USA* 104:991–6

Bernardi P, Bonaldo P (2008) Dysfunction of mitochondria and sarcoplasmic reticulum in the pathogenesis of collagen VI muscular dystrophies. *Ann N Y Acad Sci* 1147:303–11

Camacho Vanegas O, Bertini E, Zhang RZ *et al.* (2001) Ullrich scleroatonic muscular dystrophy is caused by recessive mutations in collagen type VI. *Proc Natl Acad Sci USA* 98:7516–21

Castro-Giner F, Bustamante M, Ramon GJ *et al.* (2009) A pooling-based genome-wide analysis identifies new potential candidate genes for atopy in the European Community Respiratory Health Survey (ECRHS). *BMC Med Genet* 10:128

Demir E, Sabatelli P, Allamand V *et al.* (2002) Mutations in COL6A3 cause severe and mild phenotypes of Ullrich congenital muscular dystrophy. *Am J Hum Genet* 70:1446–58

Esparza-Gordillo J, Weidinger S, Folster-Holst R *et al.* (2009) A common variant on chromosome 11q13 is associated with atopic dermatitis. *Nat Genet* 41:596–601

Finnis ML, Gibson MA (1997) Microfibril-associated glycoprotein-1 (MAGP-1) binds to the pepsin-resistant domain of the alpha3(VI) chain of type VI collagen. *J Biol Chem* 272:22817–23

Fitzgerald J, Rich C, Zhou FH *et al.* (2008) Three novel collagen VI chains, α4(VI), α5(VI) and α6(VI). *J Biol Chem* 283:20170–80

Gara SK, Grumati P, Urciuolo A *et al.* (2008) Three novel collagen VI chains with high homology to the α3 chain. *J Biol Chem* 283:10658–70

Gebauer JM, Keene DR, Olsen BR *et al.* (2009) Mouse AMACO, a kidney and skin basement membrane associated molecule that mediates RGD-dependent cell attachment. *Matrix Biol* 28:456–62

Jimenez-Mallebrera C, Maioli MA, Kim J *et al.* (2006) A comparative analysis of collagen VI production in muscle, skin and fibroblasts from 14 Ullrich congenital muscular dystrophy patients with dominant and recessive COL6A mutations. *Neuromuscul Disord* 16:571–82

Koch M, Veit G, Stricker S *et al.* (2006) Expression of type XXIII collagen mRNA and protein. *J Biol Chem* 281:21546–57

Lampe AK, Zou Y, Sudano D *et al.* (2008) Exon skipping mutations in collagen VI are common and are predictive for severity and inheritance. *Hum Mutat* 29:809–22

Latijnhouwers MA, de Jongh GJ, Bergers M *et al.* (2000) Expression of tenascin-C splice variants by human skin cells. *Arch Dermatol Res* 292:446–54

Martoni E, Urciuolo A, Sabatelli P *et al.* (2009) Identification and characterization of novel collagen VI non-canonical splicing mutations causing Ullrich congenital muscular dystrophy. *Hum Mutat* 30:E662–72

Merlini L, Martoni E, Grumati P *et al.* (2008) Autosomal recessive myosclerosis myopathy is a collagen VI disorder. *Neurology* 71: 1245–53

Miyamoto Y, Shi D, Nakajima M *et al.* (2008) Common variants in DVWA on chromosome 3p24.3 are associated with susceptibility to knee osteoarthritis. *Nat Genet* 40:994–8

Nadeau A, Kinali M, Main M *et al.* (2009) Natural history of Ullrich congenital muscular dystrophy. *Neurology* 73:25–31

Nalini A, Gayathri N, Santosh V (2009) Ullrich congenital muscular dystrophy: report of nine cases from India. *Neurol India* 57:41–5

Norwood FL, Harling C, Chinnery PF *et al.* (2009) Prevalence of genetic muscle disease in Northern England: in-depth analysis of a muscle clinic population. *Brain* 132:3175–86

Pepe G, Bertini E, Bonaldo P *et al.* (2002) Bethlem myopathy (BETHLEM) and Ullrich scleroatonic muscular dystrophy: 100th ENMC international workshop, 23-24 November 2001, Naarden, The Netherlands. *Neuromuscul Disord* 12:984–93

Piecha D, Hartmann K, Kobbe B *et al.* (2002) Expression of matrilin-2 in human skin. *J Invest Dermatol* 119:38–43

Söderhäll C, Marenholz I, Kerscher T *et al.* (2007) Variants in a novel epidermal collagen gene (COL29A1) are associated with atopic dermatitis. *PLoS Biol* 5:e242

Squarzoni S, Sabatelli P, Bergamin N *et al.* (2006) Ultrastructural defects of collagen VI filaments in an Ullrich syndrome patient with loss of the α3(VI) N10-N7 domains. *J Cell Physiol* 206:160–6

Tillet E, Wiedemann H, Golbik R *et al.* (1994) Recombinant expression and structural and binding properties of α1(VI) and α2(VI) chains of human collagen type VI. *Eur J Biochem* 221:177–85

Wagener R, Gara SK, Kobbe B *et al.* (2009) The knee osteoarthritis susceptibility locus DVWA on chromosome 3p24.3 is the 5′ part of the split COL6A4 gene. *Matrix Biol* 28:307–10

3. Study of autophagy in collagen VI null mice.

Autophagy is one of the most important mechanisms maintaining the balance between anabolism and catabolism in eukaryotic cells and playing a crucial role tissue homeostasis. The process involves the degradation of either intracellular proteins, organelles or portions of cytoplasm by the lysosomal system, allowing at the same time the elimination of altered or damaged organelles and proteins, as well as the recovery of energy and metabolites during starvation or low energy supply. The starting event of autophagy is the formation of a double membrane vesicle, called autophagosome, around the protein or organelle target. Fusion of autophagosomes with lysosomes leads to the formation of a single membrane vesicle, the autolysosome, followed by degradation of the vesicle content via acidic lysosomal hydrolases (Fig. 2) (Ferraro e Cecconi, 2007; Levine e Kroemer 2008).

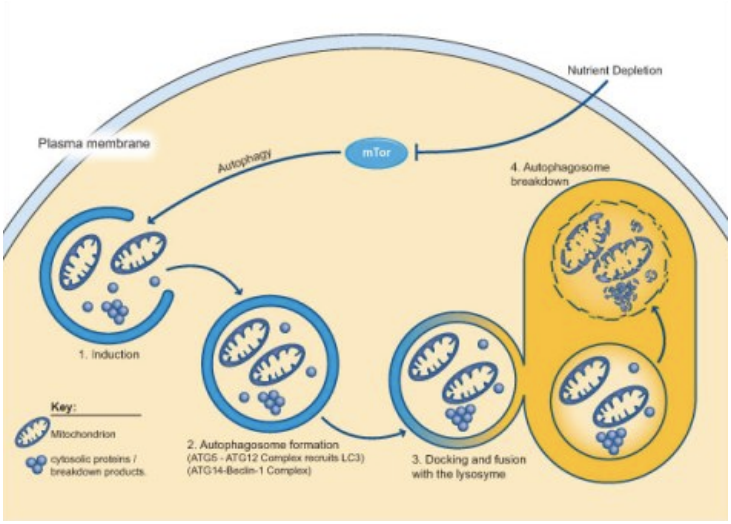

Figure 2: Authophagic process.

The main players involved in the autophagy process are encoded by a set of genes called autophagy-related genes (Atg). Most of the Atg-encoded proteins are required for the formation and maturation of autophagosomes. One of the main regulator of autophagy is mTOR, a serin-treonin kinase able to repress the process by (*i*) regulating the transcription and translation of Atg genes, and by (*ii*) modifying directly or indirectly Atg proteins.

During my PhD, I took part to a large project aimed at the understanding of molecular pathways underlying the myopathic phenotype of *Col6a1*$^{-/-}$ mice. We found that lack of collagen VI leads to an impairment of the autophagic flux in skeletal muscles. My contribution to this work was the accomplishment of part of the studies on the molecular pathways and on cell survival and apoptosis after autophagy induction.

ARTICLES

nature medicine

Autophagy is defective in collagen VI muscular dystrophies, and its reactivation rescues myofiber degeneration

Paolo Grumati[1,8], Luisa Coletto[2,8], Patrizia Sabatelli[3], Matilde Cescon[1], Alessia Angelin[4], Enrico Bertaggia[2], Bert Blaauw[5], Anna Urciuolo[1], Tania Tiepolo[1], Luciano Merlini[6], Nadir M Maraldi[3,7], Paolo Bernardi[4], Marco Sandri[2,4] & Paolo Bonaldo[1]

Autophagy is crucial in the turnover of cell components, and clearance of damaged organelles by the autophagic-lysosomal pathway is essential for tissue homeostasis. Defects of this degradative system have a role in various diseases, but little is known about autophagy in muscular dystrophies. We have previously found that muscular dystrophies linked to collagen VI deficiency show dysfunctional mitochondria and spontaneous apoptosis, leading to myofiber degeneration. Here we demonstrate that this persistence of abnormal organelles and apoptosis are caused by defective autophagy. Skeletal muscles of collagen VI–knockout (*Col6a1*$^{-/-}$) mice had impaired autophagic flux, which matched the lower induction of beclin-1 and BCL-2/adenovirus E1B–interacting protein-3 (Bnip3) and the lack of autophagosomes after starvation. Forced activation of autophagy by genetic, dietary and pharmacological approaches restored myofiber survival and ameliorated the dystrophic phenotype of *Col6a1*$^{-/-}$ mice. Furthermore, muscle biopsies from subjects with Bethlem myopathy or Ullrich congenital muscular dystrophy had reduced protein amounts of beclin-1 and Bnip3. These findings indicate that defective activation of the autophagic machinery is pathogenic in some congenital muscular dystrophies.

Macroautophagy (hereafter referred to as autophagy) is a dynamic process in which portions of cytoplasm are sequestered within double-membraned vesicles called autophagosomes and delivered to lysosomes for degradation and subsequent recycling[1–3]. The autophagic machinery is highly conserved and has key roles in tissue homeostasis, participating in the clearance of damaged organelles, misfolded proteins and pathogens[1–4]. Furthermore, autophagy is crucial for cell survival during nutrient deprivation, but it is detrimental when massively activated or inhibited[2]. Likewise, mitochondria are essential for energy conservation, but, if damaged, they become a source of proapoptotic factors and reactive oxygen species[5,6]. Selective removal of dysfunctional mitochondria via autophagy (mitophagy) is a key mechanism to not only preserve cell viability but also rejuvenate mitochondrial function[7].

Congenital muscular dystrophies represent a large and heterogeneous group of inherited muscle disorders with a severe and progressive clinical course. Mutations in any of the three genes coding for collagen VI, a major extracellular matrix protein of the endomysium of skeletal muscles, cause multiple muscle diseases, including Bethlem myopathy and Ullrich congenital muscular dystrophy (UCMD)[8]. We have previously demonstrated that muscles of *Col6a1*$^{-/-}$ mice and humans with UCMD or Bethlem myopathy have a latent mitochondrial dysfunction accompanied by ultrastructural alterations of mitochondria and the sarcoplasmic reticulum and spontaneous apoptosis of muscle fibers[9,10] (see also **Supplementary Fig. 1a**). However, in our previous study we did not uncover the reason for the occurrence of dysfunctional organelles. Here we show that the accumulation of abnormal mitochondria and sarcoplasmic reticulum is caused by a defect of autophagy and that restoration of a proper autophagic flux in *Col6a1*$^{-/-}$ muscles ameliorates these alterations.

RESULTS

Autophagy is impaired in *Col6a1*$^{-/-}$ muscles

To explore the relationship between organelle defects and muscle pathology of collagen VI muscular dystrophies *in vivo*, we examined several skeletal muscle types of *Col6a1*$^{-/-}$ mice for the main molecular pathways linked with mitochondrial function and cell survival. We chose the diaphragm and tibialis anterior as examples of oxidative and glycolytic muscles, respectively. We did not find any substantial difference between wild-type and *Col6a1*$^{-/-}$ muscles in the protein amounts of B cell leukemia/lymphoma-2 (Bcl-2), Bcl-2–associated X protein (Bax) and Bcl-X_L and in the phosphorylation of Akt, suggesting no major alterations in pro- or antiapoptotic pathways. However, the amount of the active form of AMP-activated protein kinase (AMPK) was increased in *Col6a1*$^{-/-}$ muscles (**Supplementary Fig. 1b**,**c**). AMPK acts as an energy sensor, being activated under

[1]Department of Histology, Microbiology & Medical Biotechnology, University of Padova, Padova, Italy. [2]Dulbecco Telethon Institute, Venetian Institute of Molecular Medicine, Padova, Italy. [3]Institute of Medical Genetics—National Research Council, Bologna, Italy. [4]Department of Biomedical Sciences, University of Padova, Padova, Italy. [5]Department of Human Anatomy & Physiology, University of Padova, Padova, Italy. [6]Department of Experimental and Diagnostic Medicine, University of Ferrara, Ferrara, Italy. [7]Department of Anatomical Sciences, University of Bologna, Bologna, Italy. [8]These authors contributed equally to this work. Correspondence should be addressed to P. Bonaldo (bonaldo@bio.unipd.it) or M.S. (marco.sandri@unipd.it).

Received 2 June; accepted 24 September; published online 31 October 2010; doi:10.1038/nm.2247

metabolic stress[11]. These data indicate an energy imbalance in *Col6a1*$^{-/-}$ muscles, which is readily explained by the observed mitochondrial dysfunction. Indeed, it was previously shown that *Col6a1*$^{-/-}$ flexor digitorum brevis (FDB) myofibers have an increased incidence of dysfunctional mitochondria[9]. The presence of abnormal mitochondria with disorganized cristae (**Supplementary Fig. 1d**) prompted us to check whether the autophagic system was affected. Compared to wild-type mice, muscles from *Col6a1*$^{-/-}$ mice had less of the lipidated form of microtubule-associated protein-1 light chain 3 (LC3)-II (**Fig. 1a** and **Supplementary Fig. 1e**), which is generated during autophagosome formation[1,2]. The decreased conversion of LC3-I to LC3-II suggested an alteration of basal autophagy in *Col6a1*$^{-/-}$ muscles and led us to investigate the autophagic process.

We next subjected mice to starvation for 24 h, a well-characterized stimulus able to induce the formation of autophagosomes in various organs including muscles[12]. Fasting for 24 h prompted massive autophagosome formation in wild-type but not *Col6a1*$^{-/-}$ muscles, as revealed by the appearance of LC3-positive puncta in tibialis anterior transfected with YFP-LC3 (**Supplementary Fig. 1h**) and by electron microscopy of diaphragm (**Fig. 1b**,**c**). Notably, the few autophagosomes present in *Col6a1*$^{-/-}$ diaphragm contained mitochondria with abnormal cristae (**Supplementary Fig. 1i**). Moreover, diaphragm and tibialis anterior showed reduced LC3-I to LC3-II conversion in fasted *Col6a1*$^{-/-}$ mice compared to fasted wild-type mice (**Fig. 1d** and **Supplementary Fig. 1j**). Tibialis anterior was completely resistant to autophagy induction, whereas diaphragm showed a partial LC3 conversion after 24-h starvation (**Fig. 1d**). The differential response of these two muscles probably reflects differences in metabolic properties and fiber types[12]. These results obtained with fasted mice confirm that *Col6a1*$^{-/-}$ muscles have an abnormal response to a physiological autophagic stimulus.

The decreased amount of autophagosomes and the reduced LC3 lipidation in *Col6a1*$^{-/-}$ muscles could be caused by either defective autophagy induction or excessive vesicle exhaustion. Because autophagy is a dynamically regulated process, we used a combination of *in vivo* tools for reliably monitoring the autophagic flux[13,14]. First, we used a genetic approach to knock down mRNA encoding LC3 (*Map1lc3b*) and thus inhibit autophagosome formation. To achieve this knockdown *in vivo*, we transfected adult myofibers with a bicistronic vector encoding *Map1lc3b*-targeting shRNA and GFP[15]. Knockdown of *Map1lc3b* led to a significant increase in the number of TUNEL-positive nuclei in wild-type myofibers, but it did not affect the TUNEL-positive nuclei of *Col6a1*$^{-/-}$ myofibers (**Fig. 1e**). Next, we treated mice with chloroquine[16], a lysosomal

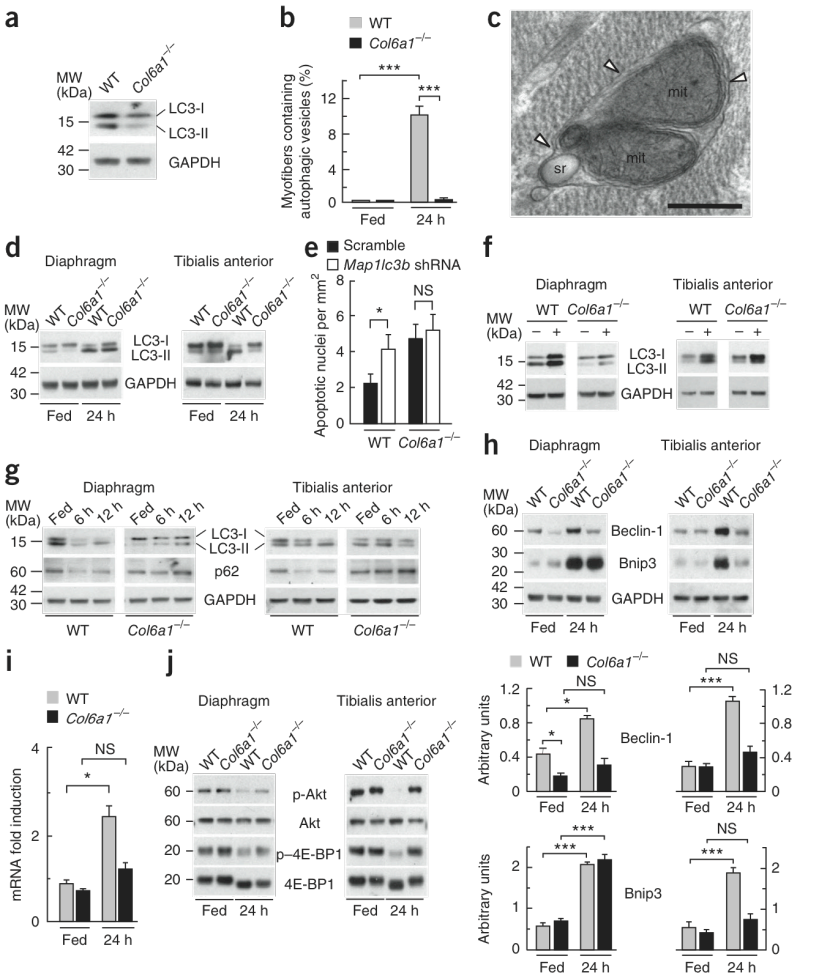

Figure 1 Autophagy is impaired in *Col6a1*$^{-/-}$ mice. (**a**) Western blot for LC3 lipidation in diaphragm of fed wild-type and *Col6a1*$^{-/-}$ mice. MW, molecular weight; WT, wild-type; GAPDH, glyceraldehyde 3-phosphate dehydrogenase. (**b**) Electron-microscopic quantification of myofibers containing autophagic vesicles in diaphragms of fed and 24-h–fasted mice (***$P < 0.001$; $n = 5$, each group). Error bars indicate s.d. (**c**) Electron micrograph of a double-membrane autophagosome (arrowheads) containing mitochondria (mit) and sarcoplasmic reticulum (sr) in diaphragms of 24-h–fasted wild-type mice. Scale bar, 400 nm. (**d**) Western blot for LC3 lipidation in diaphragm (left) and tibialis anterior (right) of fed and 24-h–fasted mice. (**e**) Quantification of TUNEL-positive nuclei in tibialis anterior transfected with vector expressing either scrambled or *Map1lc3b*-targeting shRNA (*$P <$ 0.05; NS, not significant; $n = 5$, each group). Error bars indicate s.e.m. (**f**) Western blot for LC3 lipidation in diaphragm (left) and tibialis anterior (right) of untreated mice (–) or mice treated with chloroquine diphosphate at 50 mg per kg body weight per day for 10 d (+). (**g**) Western blot for LC3 and p62 in diaphragm (left) and tibialis anterior (right) of fed, 6-h–fasted and 12-h–fasted mice. (**h**) Western blot for beclin-1 and Bnip3 in diaphragm (left) and tibialis anterior (right) of fed and 24-h–fasted mice (top) and densitometric quantification of beclin-1 (middle) and Bnip3 (bottom) (***$P < 0.001$; *$P < 0.05$; $n = 3$). Error bars indicate s.e.m. (**i**) Quantitative RT-PCR (qRT-PCR) analysis of *Bnip3* mRNA in tibialis anterior of fed and 24-h–fasted mice (*$P < 0.05$; $n = 7$). Error bars indicate s.e.m. (**j**) Western blot for Akt and 4E-BP1 phosphorylation (p-Akt and p–4E-BP1, respectively) in diaphragm (left) and tibialis anterior (right) of fed or 24-h–fasted mice.

inhibitor that blocks the degradation of autophagosome content, including LC3 (refs. 13,17), and investigated its effect on LC3 protein abundance. Chloroquine treatment led to a marked increase in LC3 bands in both diaphragm and tibialis anterior of wild-type mice, but the increase was much smaller in the corresponding samples of *Col6a1*$^{-/-}$ mice (**Fig. 1f** and **Supplementary Fig. 2a**). Finally, we assessed during fasting the variations in protein amounts of p62, a well-known substrate of the autophagy-lysosome system[13,14,18]. Both diaphragm and tibialis anterior showed a decrease in p62 during the first 6–12 h of fasting in wild-type mice but not in *Col6a1*$^{-/-}$ mice (**Fig. 1g** and **Supplementary Fig. 2b**). Together, these data show an impairment of autophagy induction in *Col6a1*$^{-/-}$ muscles, which explains their lower incidence of autophagosomes and defective LC3 lipidation.

Beclin-1 and Bnip3 are defective in *Col6a1*$^{-/-}$ muscles

Bnip3 has a key role in the autophagic removal of mitochondria[19,20], and induction of Bnip3 is crucial for autophagosome formation in muscle during starvation[15]. In contrast to the case in wild-type mice, Bnip3 protein and mRNA expression was not induced in tibialis anterior of 24-h–fasted *Col6a1*$^{-/-}$ mice (**Fig. 1h**,**i**). Conversely, diaphragm of 24-h–fasted *Col6a1*$^{-/-}$ mice showed Bnip3 induction, which matched the partial LC3 lipidation reported above (**Fig. 1h**). Other Bcl-2 family members, including Bax and Bcl-X_L, did not differ in expression between fed and fasted mice as well as between control and knockout mice, whereas Bcl-2 protein abundance was increased only in fasted *Col6a1*$^{-/-}$ tibialis anterior (**Supplementary Fig. 2e**). Bcl-2 has been shown to inhibit the autophagic function of beclin-1, a component of the class III phosphoinositide 3-kinase (PI3K) complex necessary for autophagosome formation[2,21]. Because beclin-1 plays a key part in autophagy[2], we investigated its expression in wild-type and knockout muscles. Under fed conditions, beclin-1 protein amounts were lower in *Col6a1*$^{-/-}$ diaphragm when compared to wild-type diaphragm (**Fig. 1h**). Starvation led to a marked increase of beclin-1 protein levels in both diaphragm and tibialis anterior of wild-type animals (**Fig. 1h**). Notably, the levels of mRNA encoding for beclin-1 (*Becn1*) were similar in fed and starved tibialis anterior (**Supplementary Fig. 2f**), suggesting that variations of beclin-1 levels in muscle may primarily rely on protein stability. Conversely, *Col6a1*$^{-/-}$ diaphragm and tibialis anterior did not show any substantial increase of beclin-1 protein after 24-h fasting (**Fig. 1h**). Vps34 protein, the class III PI3K of the PI3K–beclin-1 complex[1–3], was upregulated in *Col6a1*$^{-/-}$ diaphragm but not in *Col6a1*$^{-/-}$ tibialis anterior after 24-h fasting (**Supplementary Fig. 2g**,**h**). These data indicate that *Col6a1*$^{-/-}$ muscles have an imbalance of proteins actively involved in the autophagic process and suggest that complete activation of autophagy requires a proper induction of beclin-1 and Bnip3.

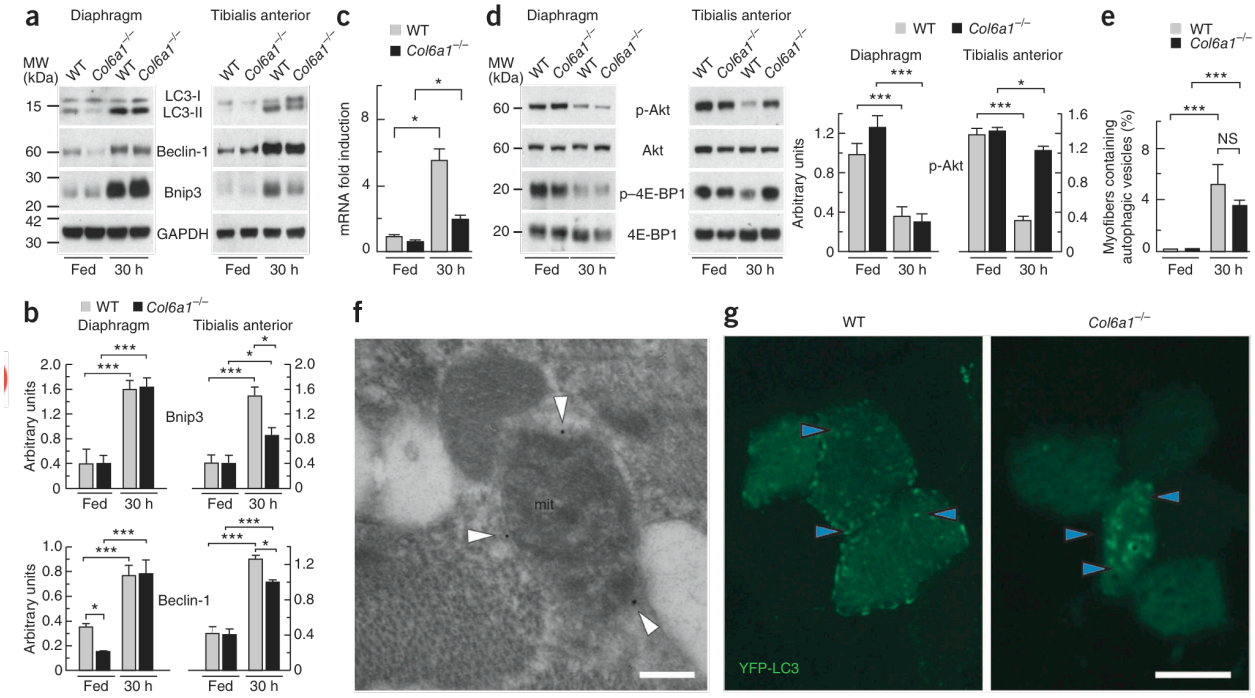

Figure 2 Prolonged starvation induces autophagy in *Col6a1*$^{-/-}$ mice. (**a**) Western blot for LC3, beclin-1 and Bnip3 in diaphragm (left) and tibialis anterior (right) of fed and 30-h–fasted mice. (**b**) Densitometric quantification of Bnip3 (top) and beclin-1 (bottom) after western blotting of diaphragm (left) and tibialis anterior (right) (***$P < 0.001$; *$P < 0.05$, $n = 3$). Error bars indicate s.e.m. (**c**) qRT-PCR analysis of *Bnip3* mRNA in tibialis anterior of fed and 30-h–fasted mice (*$P < 0.05$; $n = 7$). Error bars indicate s.e.m. (**d**) Immunoblot analysis for Akt and 4E-BP1 phosphorylation in diaphragm (left) and tibialis anterior (right) of fed and 30-h–fasted mice. The right graphs show the densitometric quantification of the western blots for p-Akt. (***$P < 0.001$; *$P < 0.05$; $n = 3$). Error bars indicate s.e.m. (**e**) Quantification of myofibers containing autophagic vesicles in diaphragms of 30-h–fasted mice (***$P < 0.001$; $n = 5$, each group). Error bars indicate s.d. (**f**) Immunogold labeling of LC3 in 30-h–fasted *Col6a1*$^{-/-}$ diaphragm. LC3 labeling (black dots marked by arrowheads) is associated with the membrane of an autophagosome containing a mitochondrion (mit). Scale bar, 300 nm. (**g**) Fluorescence microscopy of tibialis anterior cryosections from wild-type and *Col6a1*$^{-/-}$ mice transfected with YFP-LC3 and starved for 30 h. LC3 puncta (arrowheads) are indicated. Scale bar, 50 µm.

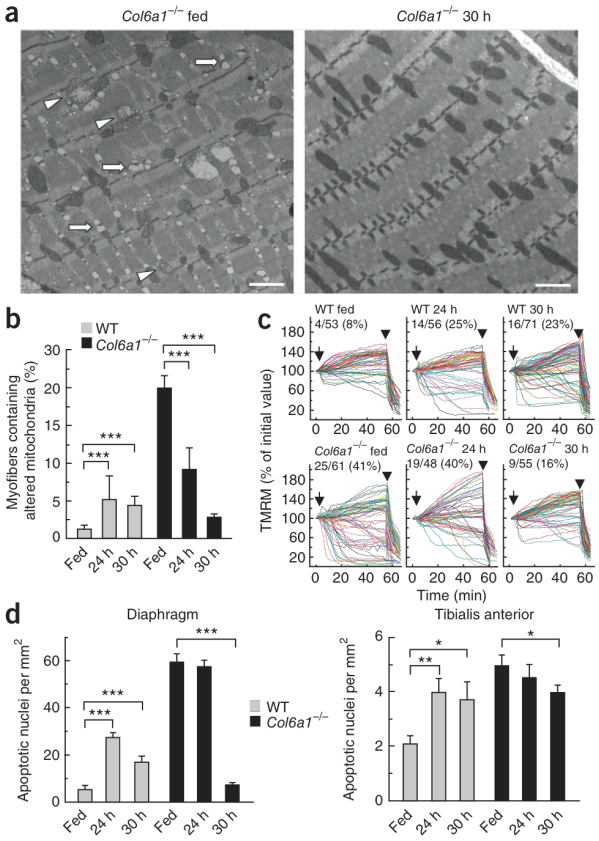

Figure 3 Induction of autophagy ameliorates the dystrophic phenotype. (**a**) Electron micrographs of diaphragm from *Col6a1*$^{-/-}$ mice in fed conditions (left) and after 30 h starvation (right). Abnormal mitochondria (arrowheads) and dilated sarcoplasmic reticulum cisternae (arrows) in myofibers of the fed *Col6a1*$^{-/-}$ mice are indicated. Scale bar, 1 μm. (**b**) Percentage of myofibers with morphologically altered mitochondria in diaphragm of fed, 24-h–fasted and 30-h–fasted mice (***$P < 0.001$; $n = 5$, each group). Error bars indicate s.d. (**c**) Mitochondrial response to oligomycin in myofibers isolated from FDB muscles of fed and fasted mice. Where indicated, 6 μM oligomycin (arrow) or 4 μM of the protonophore carbonylcyanide-*p*-trifluoromethoxyphenyl hydrazone (FCCP) (arrowhead) were added. Each trace represents the tetramethylrhodamine methyl ester (TMRM) fluorescence of a single fiber. The fraction of myofibers with depolarizing mitochondria is indicated for each condition, where fibers are considered as depolarizing when they lose more than 10% of initial value of TMRM fluorescence after oligomycin addition ($n = 5$, each group). (**d**) Quantification of TUNEL-positive nuclei in diaphragm (left) and tibialis anterior (right) of fed, 24-h–fasted and 30-h–fasted mice (***$P < 0.001$, **$P < 0.01$, *$P < 0.05$; $n = 5$, each group). Error bars indicate s.e.m.

Next, we investigated the signaling pathways involved in autophagy regulation. In skeletal muscle, autophagy and Bnip3 expression are regulated by the Akt–forkhead box protein O3 axis, a pathway that also regulates the atrophy-related ubiquitin ligase atrogin-1 (ref. 22). Similarly to Bnip3, upregulation of atrogin-1 was impaired in fasted *Col6a1*$^{-/-}$ tibialis anterior, whereas induction of muscle RING-finger protein-1, another atrophy-related ubiquitin ligase that is under nuclear factor-κB control, was unaffected (**Supplementary Fig. 2i**). These findings suggest there is abnormal Akt signaling in fasted *Col6a1*$^{-/-}$ muscles, and, indeed, starvation induced dephosphorylation of Akt in wild-type but not *Col6a1*$^{-/-}$ tibialis anterior (**Fig. 1j** and **Supplementary Fig. 2j**). In agreement with the abnormal Akt phosphorylation , the mammalian target of rapamycin pathway, which negatively regulates autophagy[2,23], remained active in fasted *Col6a1*$^{-/-}$ tibialis anterior, as indicated by the persistent phosphorylation of eukaryotic translation initiation factor 4E–binding protein-1 (4E-BP1), a downstream target of this signaling axis (**Fig. 1j**). Fasted *Col6a1*$^{-/-}$ diaphragm showed dephosphorylation of Akt and 4E-BP1, albeit to a lesser extent than starved wild-type muscles, and this explains why autophagy is partially activated in diaphragm after 24-h fasting (**Fig. 1j** and **Supplementary Fig. 2j**).

Recent studies have shown that constitutive Akt expression in wild-type muscle inhibits autophagosome formation[15]. To get further evidence of the impact of abnormal Akt signaling, we investigated the phenotype of mice expressing a muscle-specific, inducible Akt transgene, resulting in chronic Akt activation. In agreement with our findings in *Col6a1*$^{-/-}$ mice, chronic Akt activation in otherwise wild-type mice led to decreased Bnip3 and beclin-1 protein amounts and resulted in a dystrophic phenotype characterized by p62 aggregates, vacuolated fibers and centrally located myonuclei (**Supplementary Fig. 3**). These findings support a role for the persistence of Akt activation in autophagy inhibition and in the development of the dystrophic phenotype in *Col6a1*$^{-/-}$ mice.

Because 24-h fasting was not sufficient to trigger a robust Akt dephosphorylation and full activation of autophagy in *Col6a1*$^{-/-}$ muscles, we investigated whether prolonged starvation could reactivate the autophagic process and confer some beneficial effects on the dystrophic phenotype. Starvation for 30 h triggered LC3 lipidation and increased beclin-1 and Bnip3 protein amounts in both diaphragm and tibialis anterior of *Col6a1*$^{-/-}$ mice (**Fig. 2a**,**b** and **Supplementary Fig. 4a**,**b**). *Bnip3* mRNA levels were also increased by 30-h fasting, whereas *Becn1* transcripts were unaffected (**Fig. 2c** and **Supplementary Fig. 4c**). Similarly, Vps34 was induced in *Col6a1*$^{-/-}$ muscles (**Supplementary Fig. 4d**,**e**). As with 24-h fasting, Bcl-X_L and Bax expression did not change between wild-type and *Col6a1*$^{-/-}$ muscles, whereas the Bcl-2 protein amount was increased in 30-h–fasted *Col6a1*$^{-/-}$ tibialis anterior (**Supplementary Fig. 4f**). Therefore, high expression of Bcl-2 did not prevent reactivation of autophagy in *Col6a1*$^{-/-}$ mice. Prolonged starvation attenuated the differences between wild-type and *Col6a1*$^{-/-}$ muscles in the phosphorylation of Akt (**Fig. 2d**). Atrogin-1 mRNA expression was induced in 30-h–fasted *Col6a1*$^{-/-}$ mice (**Supplementary Fig. 4g**). Detection of LC3-positive vesicles by fluorescence microscopy in YFP-LC3–transfected fibers and by immunoelectron microscopy confirmed that 30-h fasting elicited substantial autophagosome formation in both wild-type and *Col6a1*$^{-/-}$ myofibers (**Fig. 2e–g** and **Supplementary Fig. 4h**).

Prolonged starvation resulted in the amelioration of myofiber abnormalities in *Col6a1*$^{-/-}$ mice (**Fig. 3a**). Indeed, *Col6a1*$^{-/-}$ diaphragms showed a significant rescue of ultrastructural alterations of mitochondria and sarcoplasmic reticulum (**Fig. 3a**,**b** and **Supplementary Fig. 4h–j**). Moreover, the percentage of FDB myofibers showing mitochondrial depolarization was substantially lower, and the amount of TUNEL-positive-nuclei in *Col6a1*$^{-/-}$ muscles became close to that of control muscles (**Fig. 3c**,**d**). Wild-type mice showed some degree of muscle alterations after fasting (**Fig. 3b–d** and **Supplementary Fig. 4h**,**j**), in keeping with the observation that excessive autophagy contributes to muscle wasting[15,24].

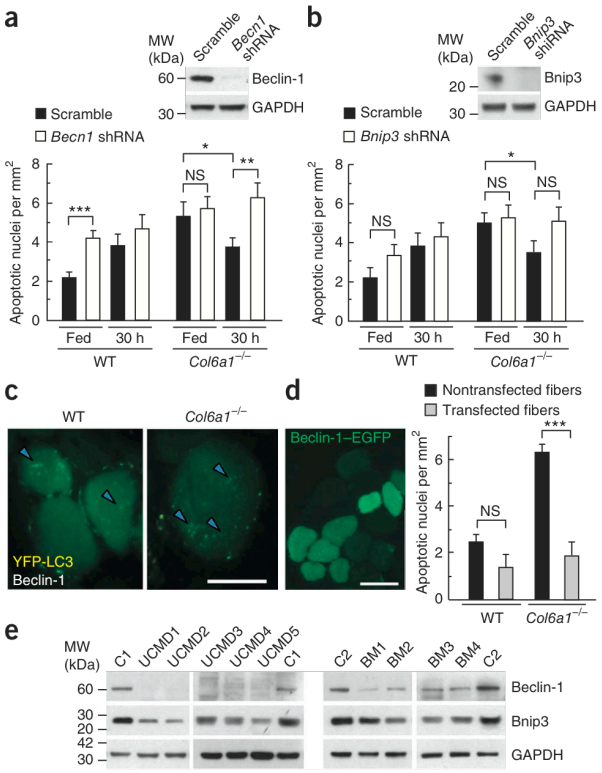

Figure 4 Beclin-1 protein abundance is decreased in muscle biopsies of subjects with UCMD or Bethlem myopathy, and its expression counteracts muscle apoptosis in *Col6a1*$^{-/-}$ mice. (**a**,**b**) Quantification of TUNEL-positive nuclei in wild-type and *Col6a1*$^{-/-}$ tibialis anterior transfected with a vector expressing scramble or *Becn1* shRNA (**a**) or *Bnip3* shRNA (**b**). Western blot confirmation of RNAi-mediated knockdown of *Becn1* and *Bnip3* in tibialis anterior of wild-type mice is included above each set of graphs (***$P < 0.001$; **$P < 0.01$; *$P < 0.05$; $n = 10$, each group). Error bars indicate s.e.m. (**c**) Fluorescence microscopy of tibialis anterior cryosections from wild-type and *Col6a1*$^{-/-}$ mice transfected with beclin-1 and YFP-LC3 expression vectors and maintained in fed condition. LC3 puncta (arrowheads) are indicated. Scale bar, 50 µm. (**d**) Right, quantification of TUNEL-positive nuclei in transfected and nontransfected myofibers of wild-type and *Col6a1*$^{-/-}$ tibialis anterior muscle after *in vivo* transfection with beclin-1–EGFP expression vector. Transfected fibers were revealed by fluorescence microscopy (left). Scale bar, 50 µm (***$P < 0.001$; $n = 10$, each group). Error bars indicate s.e.m. (**e**) Western blot for beclin-1 and Bnip3 in protein lysates of human muscle biopsies from two healthy (normal) controls (C1, C2), five individuals with UCMD (UCMD1–5) and four individuals with Bethlem myopathy (BM1–4). Data are representative of three independent experiments.

Restoration of beclin-1 ameliorates muscle phenotype

To further investigate the contribution of beclin-1 and Bnip3 in the pathogenesis of *Col6a1*$^{-/-}$ muscles, we performed *in vivo* loss-of-function experiments. Adult tibialis anterior was transfected with expression plasmids encoding shRNAs targeting *Becn1* and *Bnip3* transcripts[24]. *Becn1* knockdown for 2 weeks led to a marked increase in apoptotic nuclei in myofibers of wild-type mice and completely prevented the significant decrease of TUNEL-positive nuclei observed in 30-h–fasted *Col6a1*$^{-/-}$ mice (**Fig. 4a**). Conversely, *Bnip3* knockdown for 2 weeks did not substantially impinge on the incidence of TUNEL-positive nuclei of wild-type mice and had a minor effect on 30-h–starved *Col6a1*$^{-/-}$ mice when compared to *Becn1* knockdown (**Fig. 4b**). Together with the above findings showing that autophagy flux is impaired in *Col6a1*$^{-/-}$ muscles, these data indicate that the inefficient autophagy and subsequent muscle apoptosis observed in these mice is due to beclin-1 inhibition.

To support the pathogenetic role of beclin-1 deficiency in myofiber degeneration, we carried out *in vivo* transfection of tibialis anterior with an expression construct coding for beclin-1. Transfection of the beclin-1 construct was able to activate autophagy in both wild-type and *Col6a1*$^{-/-}$ muscles, as revealed by concurrent transfection of YFP-LC3 and formation of LC3-positive puncta (**Fig. 4c**). Moreover, beclin-1 overexpression led to a marked decrease of TUNEL-positive nuclei in myofibers of *Col6a1*$^{-/-}$ mice, whereas it did not affect wild-type muscles (**Fig. 4d**). Therefore, correction of beclin-1 levels in *Col6a1*$^{-/-}$ muscle fibers is sufficient to reactivate autophagy and thus prevent apoptotic degeneration.

To assess whether the findings obtained in the *Col6a1*-null mouse model also apply to human collagen VI disorders, we investigated muscle biopsies derived from five subjects with UCMD and four subjects with Bethlem myopathy (**Supplementary Table 1**). The amounts of both beclin-1 and Bnip3 proteins were decreased in subjects with UCMD and Bethlem myopathy when compared to healthy (normal) controls. Individuals with UCMD had very low beclin-1 levels, whereas individuals with Bethlem myopathy, whose dystrophic phenotype is milder, showed a less prominent decrease in the amount of beclin-1, which seemed closer but not identical to amounts in controls. Bnip3 protein abundance was also lower in samples from UCMD and Bethlem myopathy individuals compared to those in controls, albeit the reductions are much less prominent than that seen for beclin-1 abundance between disease samples and controls (**Fig. 4e** and **Supplementary Fig. 5a**).

Autophagy reactivation ameliorates muscle pathology

Given that prolonged starvation reactivated autophagy and blocked apoptotic degeneration in *Col6a1*$^{-/-}$ muscles, we investigated whether milder and long-lasting dietary regimens were able to activate autophagy and ameliorate muscle morphology and function. Depletion of amino acids strongly induces autophagy[25–27]. Conversely, supplementation of protein-free diets with amino acids suppresses muscle protein degradation through inhibition of autophagy[28]. To allow for a long-term response, we fed mice with a specifically designed low-protein diet (LPD) (**Supplementary Table 2**). Four weeks of LPD was able to ameliorate the dystrophic features of *Col6a1*$^{-/-}$ mice (**Fig. 5a**,**b** and **Supplementary Fig. 6**). LPD induced autophagy and did not have any significant effect on the ubiquitin-proteasome system as shown by atrogin-1 expression (**Supplementary Fig. 6c**). Diaphragm and tibialis anterior of both wild-type and *Col6a1*$^{-/-}$ LPD-fed mice showed LC3 lipidation and increased beclin-1 and Bnip3 protein amounts, consistent with the formation of autophagosomes (**Fig. 5c**,**d** and **Supplementary Fig. 6a**,**b**). Activation of autophagy by LPD led to removal of structurally abnormal organelles (**Fig. 5b** and **Supplementary Fig. 6e**). Similarly to prolonged starvation, induction of autophagy by LPD led to a marked recovery of the dystrophic alterations of *Col6a1*$^{-/-}$ mice and produced some muscle alterations in wild-type mice (**Fig. 5e**,**f** and **Supplementary Fig. 6e–g**). The percentages of myofibers showing mitochondrial depolarization and TUNEL positivity were significantly lower in LPD-fed *Col6a1*$^{-/-}$ mice compared to *Col6a1*$^{-/-}$ mice fed with normal diet and were similar to (or lower than) those observed in LPD-fed wild-type mice (**Fig. 5f** and **Supplementary Fig. 6g**). Autophagy reactivation also ameliorated the histological features of *Col6a1*$^{-/-}$ muscles, resulting in a more uniform myofiber size (**Supplementary Fig. 6h**). Moreover, long-term induction of autophagy by LPD also

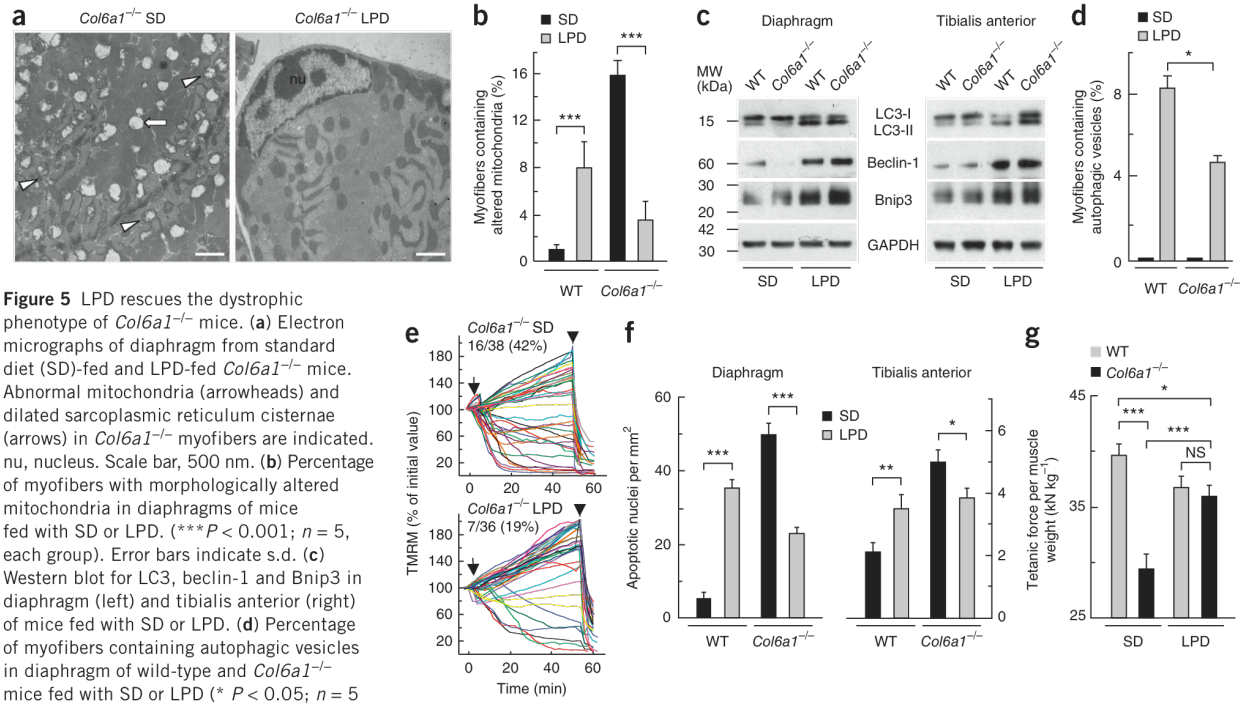

Figure 5 LPD rescues the dystrophic phenotype of *Col6a1*$^{-/-}$ mice. (**a**) Electron micrographs of diaphragm from standard diet (SD)-fed and LPD-fed *Col6a1*$^{-/-}$ mice. Abnormal mitochondria (arrowheads) and dilated sarcoplasmic reticulum cisternae (arrows) in *Col6a1*$^{-/-}$ myofibers are indicated. nu, nucleus. Scale bar, 500 nm. (**b**) Percentage of myofibers with morphologically altered mitochondria in diaphragms of mice fed with SD or LPD. (***$P < 0.001$; $n = 5$, each group). Error bars indicate s.d. (**c**) Western blot for LC3, beclin-1 and Bnip3 in diaphragm (left) and tibialis anterior (right) of mice fed with SD or LPD. (**d**) Percentage of myofibers containing autophagic vesicles in diaphragm of wild-type and *Col6a1*$^{-/-}$ mice fed with SD or LPD (* $P < 0.05$; $n = 5$ each group). Error bars indicate s.d. (**e**) Mitochondrial response to oligomycin in FDB myofibers of *Col6a1*$^{-/-}$ fed with SD or LPD. The fraction of depolarizing myofibers is provided as in **Figure 3c** ($n = 5$, each group). (**f**) Quantification of TUNEL-positive nuclei in diaphragm (left) and tibialis anterior (right) of mice fed with SD or LPD (***$P < 0.001$; **$P < 0.01$; *$P < 0.05$; $n = 5$, each group). Error bars indicate s.e.m. (**g**) *In vivo* tetanic force measurements in the gastrocnemius muscle of mice fed with SD or LPD (***$P < 0.001$; *$P < 0.05$; $n = 12$, each group). Error bars indicate s.e.m.

improved muscle strength of *Col6a1*$^{-/-}$ mice, as indicated by the significant increase of specific force measured in gastrocnemius muscle (**Fig. 5g** and **Supplementary Fig. 6i**). Thus, reactivation of autophagy by dietary approaches is sufficient to improve both morphology and function of *Col6a1*$^{-/-}$ dystrophic muscles.

Drugs inducing autophagy rescue the dystrophic phenotype

As reactivation of autophagy by dietary restriction showed a therapeutic potential in *Col6a1*$^{-/-}$ mice, we further explored this possibility with pharmacological tools. Rapamycin is a well-known inducer of autophagy that can be used for *in vivo* treatments[17]. Treatment of *Col6a1*$^{-/-}$ mice with rapamycin for 15 d decreased myofiber degeneration and removed abnormal organelles (**Fig. 6a–c** and **Supplementary Fig. 7a**). Cyclosporin A has been reported to modulate autophagy[7,29,30], and we previously demonstrated that this drug rescues the dystrophic phenotype of *Col6a1*$^{-/-}$ mice by desensitizing the mitochondrial permeability transition pore[9]. Because reactivation of autophagy in *Col6a1*$^{-/-}$ mice led to a marked amelioration of the phenotype, we investigated whether treatment with cyclosporin A would have any effect on autophagy. Notably, cyclosporin A induced autophagy in *Col6a1*$^{-/-}$ muscles, with a concomitant block of apoptotic degeneration and recovery of muscle strength (**Fig. 6d–g** and **Supplementary Fig. 7b–d**). Moreover, cylosporin A treatment restored beclin-1 and Bnip3 induction, LC3 lipidation and Akt dephosphorylation in 24-h–fasted *Col6a1*$^{-/-}$ muscles (**Fig. 6d** and **Supplementary Fig. 7e**). These data suggest that the robust beneficial effect of cyclosporin A in collagen VI–deficient mice is linked to both restoration of mitochondrial function[9] and autophagy induction.

DISCUSSION

Previous studies have shown that the muscle pathology of collagen VI–null mice and humans with UCMD or Bethlem myopathy is strictly related to ultrastructural alterations of organelles, mitochondrial dysfunction and spontaneous apoptosis in skeletal muscles[9,10]. Here we show that autophagy is impaired in *Col6a1*$^{-/-}$ muscles and that the failure of this process has a major role in the pathogenesis of the dystrophic phenotype, causing accumulation of abnormal organelles and apoptotic degeneration of muscle fibers. Forced induction of autophagy is able to reactivate the process, achieving a beneficial response in *Col6a1*$^{-/-}$ mice. Thus, prompt elimination of defective organelles is essential to protect *Col6a1*$^{-/-}$ myofibers from the harmful consequences of dysfunctional mitochondria and excessive apoptosis (**Supplementary Fig. 8a**). Indeed, accumulation of abnormal mitochondria in *Col6a1*$^{-/-}$ muscles is associated with oxidative stress and increased production of reactive oxygen species, which contribute to trigger apoptotic response[31]. Our findings indicate that a proper autophagic flux is crucial for the clearance of damaged organelles and the maintenance of muscle homeostasis. Moreover, we also point out that both defective and excessive autophagy lead to muscle degeneration, in keeping with the intricate interplay between autophagic and apoptotic pathways shown in different systems[1–3,32] (**Supplementary Fig. 8b**). In agreement with our model, muscle-specific inactivation of autophagy genes results in muscle atrophy with abnormal organelles[33,34].

In certain storage diseases and vacuolar myopathies, a reduced 'off-rate' of autophagy results from mutations of genes coding for proteins involved in lysosomal function, leading to accumulation of autophagic vesicles[1,3,35,36]. Conversely, our findings suggest that the impaired

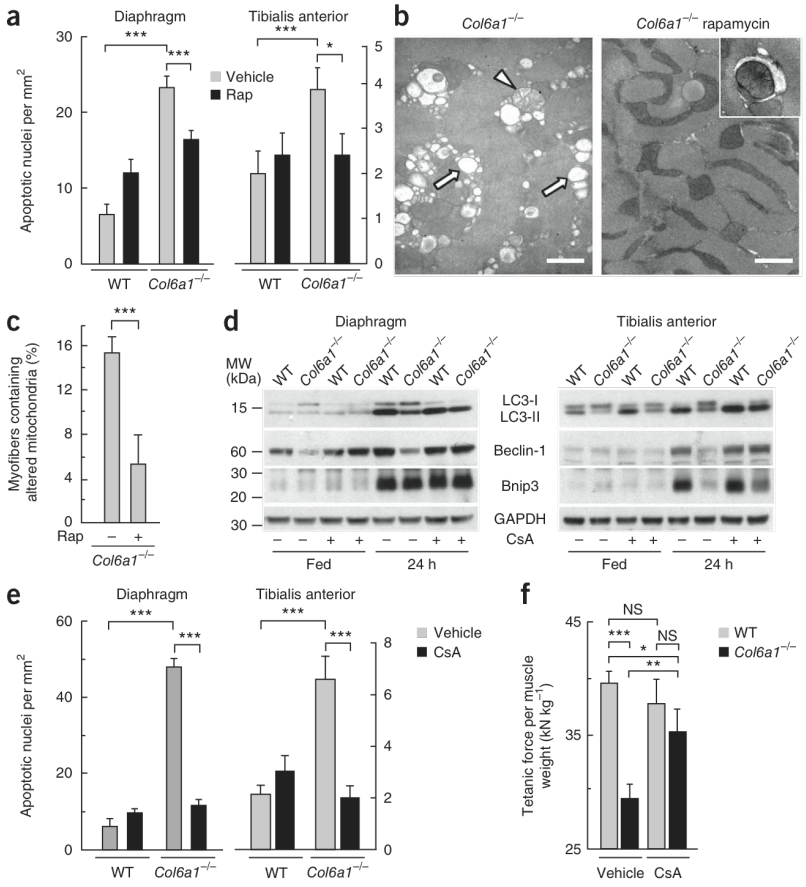

Figure 6 Pharmacological treatments induce autophagy and ameliorate the myopathic phenotype of *Col6a1*$^{-/-}$ mice. (**a**) Quantification of TUNEL-positive nuclei in diaphragm (left) and tibialis anterior (right) of wild-type and *Col6a1*$^{-/-}$ mice treated with vehicle (ethanol) or with rapamycin (Rap) for 15 d (***$P < 0.001$; *$P < 0.05$; $n = 5$, each group). Error bars indicate s.e.m. (**b**) Representative micrographs of a transverse section of diaphragm from untreated (left) and rapamycin-treated (right) *Col6a1*$^{-/-}$ mice. Abnormal mitochondria (white arrowheads) and dilated sarcoplasmic reticulum (white arrows) in the muscle of untreated mice are indicated, as is autophagosome formation in the treated mice (inset). Scale bar, 500 nm. (**c**) Percentage of myofibers with morphologically altered mitochondria in the diaphragm of *Col6a1*$^{-/-}$ mice treated with rapamycin (+) or left untreated (–) for 15 d (***$P < 0.001$; $n = 5$ each group). Error bars indicate s.d. (**d**) Western blot analysis for LC3, beclin-1 and Bnip3 in diaphragm (left) and tibialis anterior (right) of wild-type and *Col6a1*$^{-/-}$ mice treated with vehicle (olive oil) (–) or with cyclosporin A (CsA) (+) for 4 d and maintained in fed or 24-h–fasting conditions. (**e**) Quantification of TUNEL-positive nuclei in diaphragm (left) and tibialis anterior (right) of wild-type and *Col6a1*$^{-/-}$ mice treated with vehicle or with cyclosporin A for 4 d (***$P < 0.001$; $n = 4$, each group). Error bars indicate s.e.m. (**f**) *In vivo* tetanic force measurements in the gastrocnemius muscle of mice treated with vehicle or with cyclosporin A for 10 d (***$P < 0.001$; **$P < 0.01$; *$P < 0.05$; $n = 8$, each group). Error bars indicate s.e.m.

autophagic flux of collagen VI dystrophic muscles results from a decreased 'on-rate', with defective formation of autophagosomes. Indeed, we have found that amounts of two major autophagic effector proteins, beclin-1 and Bnip3, are reduced in *Col6a1*$^{-/-}$ muscles. Although Bnip3 induction is sufficient to trigger autophagy[15], our data suggest that the concomitant beclin-1 upregulation is required for a proper autophagy induction. Thus, beclin-1 seems to be necessary and sufficient for basal autophagy and for its correct induction, whereas Bnip3 is able to trigger autophagy in the presence of appropriate protein levels of beclin-1.

The demonstration that muscles of *Col6a1*$^{-/-}$ mice are characterized by inefficient autophagy has a major impact on the understanding of the pathogenesis of collagen VI muscular dystrophies. Muscle biopsies of subjects with UCMD and Bethlem myopathy show reduced protein amounts of beclin-1 and Bnip3. Notably, forced reactivation of autophagy in the mouse model by nutritional and pharmacological approaches is able to rescue the morphological and functional aspects of the dystrophic phenotype. This opens new possibilities for targeted therapeutic approaches aimed at combating muscle loss in UCMD and Bethlem myopathy that add to desensitization of the mitochondrial permeability transition pore through cyclophilin D inhibition[10,37,38].

In more general terms, our results support a view that points at the activators of autophagic process and at clearance systems as new therapeutic targets for avoiding accumulation of toxic molecules and damaged organelles in skeletal muscle. Moreover, the finding that modulation of autophagy through various nutritional and pharmacological treatments is beneficial for collagen VI dystrophic muscles paves the way for investigating autophagy defects in other muscular dystrophies.

METHODS

Methods and any associated references are available in the online version of the paper at http://www.nature.com/naturemedicine/.

Note: Supplementary information is available on the Nature Medicine website.

ACKNOWLEDGMENTS

We thank N. Bergamin for her involvement in the initial study, P. Braghetta for help with mouse manipulations, E. Rizzo and S. Castagnaro for histology, S. Cogliati for assistance with mitochondria isolation and F. Gualandi for muscle biopsies. We are grateful to N. Heintz (Rockefeller University) for supplying the beclin-1–EGFP expression construct and E. Kominami (Juntendo University School of Medicine) for the YFP-LC3 construct. This work was supported by the Telethon Foundation (GGP08107 and TCP04009), the Italian Ministry of University and Research, Association Francaise contre les Myopathies and the EU (BIO-NMD and MYOAGE).

AUTHOR CONTRIBUTIONS

P.G. performed biochemical analyses, autophagy assays, mouse treatments, analysis and interpretation of data, and contributed to manuscript preparation. L.C. carried out RNA analysis, muscle transfections, molecular biology, analysis and interpretation of data, and contributed to manuscript preparation. P.S. performed electron microscopy. M.C. performed TUNEL and histology. A.A. performed tetramethylrhodamine methyl ester (TMRM) analysis. E.B. carried out muscle transfections and mitochondria isolation. B.B. analyzed muscle mechanics. A.U. performed TUNEL analysis. T.T. genotyped and maintained mice. L.M.,

P. Bernardi and N.M.M. were involved in data analysis. P. Bonaldo and M.S. designed the study, analyzed data and wrote the paper. All authors discussed the results and commented on the manuscript.

COMPETING FINANCIAL INTERESTS
The authors declare no competing financial interests.

Published online at http://www.nature.com/naturemedicine/.
Reprints and permissions information is available online at http://npg.nature.com/reprintsandpermissions/.

1. Levine, B. & Kroemer, G. Autophagy in the pathogenesis of disease. *Cell* **132**, 27–42 (2008).
2. Maiuri, M.C., Zalckvar, E., Kimchi, A. & Kroemer, G. Self-eating and self-killing: crosstalk between autophagy and apoptosis. *Nat. Rev. Mol. Cell Biol.* **8**, 741–752 (2007).
3. Mizushima, N., Levine, B., Cuervo, A.M. & Klionsky, D.J. Autophagy fights disease through cellular self-digestion. *Nature* **451**, 1069–1075 (2008).
4. Nakai, A. *et al.* The role of autophagy in cardiomyocytes in the basal state and in response to hemodynamic stress. *Nat. Med.* **13**, 619–624 (2007).
5. Green, D.R. & Kroemer, G. The pathophysiology of mitochondrial cell death. *Science* **305**, 626–629 (2004).
6. Bernardi, P. *et al.* The mitochondrial permeability transition from in vitro artifact to disease target. *FEBS J.* **273**, 2077–2099 (2006).
7. Kim, I., Rodriguez-Enriquez, S. & Lemasters, J.J. Selective degradation of mitochondria by mitophagy. *Arch. Biochem. Biophys.* **462**, 245–253 (2007).
8. Lampe, A.K. & Bushby, K.M. Collagen VI related muscle disorders. *J. Med. Genet.* **42**, 673–685 (2005).
9. Irwin, W.A. *et al.* Mitochondrial dysfunction and apoptosis in myopathic mice with collagen VI deficiency. *Nat. Genet.* **35**, 367–371 (2003).
10. Angelin, A. *et al.* Mitochondrial dysfunction in the pathogenesis of Ullrich congenital muscular dystrophy and prospective therapy with cyclosporins. *Proc. Natl. Acad. Sci. USA* **104**, 991–996 (2007).
11. Long, Y.C. & Zierath, J.R. AMP-activated protein kinase signaling in metabolic regulation. *J. Clin. Invest.* **116**, 1776–1783 (2006).
12. Mizushima, N., Yamamoto, A., Matsui, M., Yoshimori, T. & Ohsumi, Y. *In vivo* analysis of autophagy in response to nutrient starvation using transgenic mice expressing a fluorescent autophagosome marker. *Mol. Biol. Cell* **15**, 1101–1111 (2004).
13. Mizushima, N., Yoshimori, T. & Levine, B. Methods in mammalian autophagy research. *Cell* **140**, 313–326 (2010).
14. Klionsky, D.J. *et al.* Guidelines for the use and interpretation of assays for monitoring autophagy in higher eukaryotes. *Autophagy* **4**, 151–175 (2008).
15. Mammucari, C. *et al.* FoxO3 controls autophagy in skeletal muscle *in vivo*. *Cell Metab.* **6**, 458–471 (2007).
16. Schmalbruch, H. The early changes in experimental myopathy induced by chloroquine and chlorphentermine. *J. Neuropathol. Exp. Neurol.* **39**, 65–81 (1980).
17. Rubinsztein, D.C., Gestwicki, J.E., Murphy, L.O. & Klionsky, D.J. Potential therapeutic applications of autophagy. *Nat. Rev. Drug Discov.* **6**, 304–312 (2007).
18. Bjørkøy, G. *et al.* p62/SQSTM1 forms protein aggregates degraded by autophagy and has a protective effect on huntingtin-induced cell death. *J. Cell Biol.* **171**, 603–614 (2005).
19. Hamacher-Brady, A. *et al.* Response to myocardial ischemia/reperfusion injury involves Bnip3 and autophagy. *Cell Death Differ.* **14**, 146–157 (2007).
20. Sandoval, H. *et al.* Essential role for Nix in autophagic maturation of erythroid cells. *Nature* **454**, 232–235 (2008).
21. Pattingre, S. *et al.* Bcl-2 antiapoptotic proteins inhibit beclin-1–dependent autophagy. *Cell* **122**, 927–939 (2005).
22. Sandri, M. *et al.* FoxO transcription factors induce the atrophy-related ubiquitin ligase atrogin-1 and cause skeletal muscle atrophy. *Cell* **117**, 399–412 (2004).
23. Shintani, T. & Klionsky, D.J. Autophagy in health and disease: a double-edged sword. *Science* **306**, 990–995 (2004).
24. Romanello, V. *et al.* Mitochondrial fission and remodelling contributes to muscle atrophy. *EMBO J.* **29**, 1774–1785 (2010).
25. Codogno, P. & Meijer, A.J. Autophagy and signaling: their role in cell survival and cell death. *Cell Death Differ.* **12** Suppl 2, 1509–1518 (2005).
26. Mizushima, N. Autophagy: process and function. *Genes Dev.* **21**, 2861–2873 (2007).
27. Mortimore, G.E. & Poso, A.R. Intracellular protein catabolism and its control during nutrient deprivation and supply. *Annu. Rev. Nutr.* **7**, 539–564 (1987).
28. Sugawara, T., Ito, Y., Nishizawa, N. & Nagasawa, T. Regulation of muscle protein degradation, not synthesis, by dietary leucine in rats fed a protein-deficient diet. *Amino Acids* **37**, 609–616 (2009).
29. Yoo, Y.M. & Jeung, E.B. Melatonin suppresses cyclosporine A–induced autophagy in rat pituitary GH3 cells. *J. Pineal Res.* **48**, 204–211 (2010).
30. Pallet, N. *et al.* Autophagy protects renal tubular cells against cyclosporine toxicity. *Autophagy* **4**, 783–791 (2008).
31. Menazza, S. *et al.* Oxidative stress by monoamine oxidases is causally involved in myofiber damage in muscular dystrophy. *Hum. Mol. Genet.* published online, doi:10.1093/hmg/ddq339 (17 August 2010).
32. Boya, P. *et al.* Inhibition of macroautophagy triggers apoptosis. *Mol. Cell. Biol.* **25**, 1025–1040 (2005).
33. Masiero, E. *et al.* Autophagy is required to maintain muscle mass. *Cell Metab.* **10**, 507–515 (2009).
34. Wu, J.J. *et al.* Mitochondrial dysfunction and oxidative stress mediate the physiological impairment induced by the disruption of autophagy. *Aging* **1**, 425–437 (2009).
35. Ramachandran, N. *et al.* VMA21 deficiency causes an autophagic myopathy by compromising V-ATPase activity and lysosomal acidification. *Cell* **137**, 235–246 (2009).
36. Malicdan, M.C., Noguchi, S., Nonaka, I., Saftig, P. & Nishino, I. Lysosomal myopathies: an excessive build-up in autophagosomes is too much to handle. *Neuromuscul. Disord.* **18**, 521–529 (2008).
37. Palma, E. *et al.* Genetic ablation of cyclophilin D rescues mitochondrial defects and prevents muscle apoptosis in collagen VI myopathic mice. *Hum. Mol. Genet.* **18**, 2024–2031 (2009).
38. Merlini, L. *et al.* Cyclosporin A corrects mitochondrial dysfunction and muscle apoptosis in patients with collagen VI myopathies. *Proc. Natl. Acad. Sci. USA* **105**, 5225–5229 (2008).

ONLINE METHODS

Mice. We backcrossed *Col6a1*$^{+/-}$ mice in the inbred C57BL/6J strain (Charles River) for eight generations[9]. We performed all experiments in 16- to 24-week-old mice and compared age-matched *Col6a1*$^{-/-}$ (collagen VI–null) and *Col6a1*$^{+/+}$ (wild-type) mice. We housed mice in individual cages in an environmentally controlled room (23 °C, 12-h light-dark cycle) and provided food and water *ad libitum*. For starvation experiments, we removed chow in the morning and maintained mice for 6–30 h with no food but free access to water. We fed mice with either SD (Laboratorio Dottori Piccioni) or LPD (TestDiet) (**Supplementary Table 2**). Muscle-specific inducible Akt-ER–Cre transgenic mice were previously described[15], and we achieved transgene activation by tamoxifen administration in the chow (Harlan). Mouse procedures were approved by the Ethics Committee of the University of Padova and authorized by the Italian Ministry of Health.

Drug treatments. We subjected wild-type and *Col6a1*$^{-/-}$ mice to intraperitoneal injection with either chloroquine diphosphate (50 mg per kg body weight; Sigma) every 24 h for 10 d; cyclosporine A (5 mg per kg body weight; Novartis) every 12 h for 4 d or 10 d or rapamycin (2 mg per kg body weight; LC Laboratories) every 24 h for 15 d.

Muscle *in vivo* transfection. We performed *in vivo* transfection experiments by intramuscular injection of expression plasmids in tibialis anterior followed by electroporation as previously described[22]. We used the following expression constructs: YFP-LC3 (ref. 39), beclin-1–EGFP[40] and beclin-1. For the preparation of the beclin-1 expression construct, we amplified *Becn1* cDNA by PCR from the beclin-1–EGFP plasmid using primers 5′-CTATGGAGGGGTCTAAGGC-3′ (forward) and 5′-TCACTTGTTATAGAACTGTGAGG-3′ (reverse) and cloned the amplified sequence into the HindIII and XbaI sites of the pcDNA3.1 (Invitrogen) expression vector. We carried out RNAi-mediated knockdown by transfection of shRNA constructs targeting *Map1lc3b* (ref. 15), *Bnip3* (ref. 15) and *Becn1*. For *Becn1*, we used a commercial kit containing oligonucleotides against *Becn1* target sequences and the BLOCK-IT Pol II miR RNAi expression vector (Invitrogen).

Gene expression analyses. We prepared total RNA from skeletal muscle with the Promega SV Total RNA Isolation kit. We generated cDNA products with SuperScript III reverse transcriptase (Invitrogen) and analyzed them by qRT-PCR with the QuantiTect SYBR Green PCR kit (Qiagen). We normalized all data to *Gapdh* expression. Oligonucleotide primers used for qRT-PCR are listed in **Supplementary Table 3**.

Fluorescence microscopy and transmission electron microscopy. We fixed muscle cryosections with ice-cold 4% paraformaldehyde, mounted the samples with Fluorescence Mounting Medium (DAKO) and examined them on a Leica DM5000B fluorescence microscope. For electron microscopy, we fixed and stained stretched diaphragms as previously described[9]. For statistical analysis, we studied at least 1,000 muscle fibers, obtained from two levels of three different tissue blocks for each diaphragm. We considered positive fibers presenting at least one mitochondrion with abnormal cristae or a portion of dilated sarcoplasmic reticulum. We performed immunoelectron microscopy according to previously published protocols[41]. We etched ultrathin sections with 3% sodium alcholate, treated them with 10% H_2O_2 and incubated them overnight with LC3-specific antibody (LB 100-2220, Novus Biologicals). We visualized the antibody binding by incubation with 15-nm colloidal gold-conjugated secondary antibody (Amersham).

Western blotting. We pulverized mouse frozen muscles and human muscle biopsies by grinding in liquid nitrogen, and we lysed and immunoblotted the samples as previously described[22]. When needed, we stripped and reprobed membranes. We used antibodies from Cell Signaling Technologies specific for the following proteins: 4E-BP1 (9452), phospho–4E-BP1 (Thr37 and Thr46) (2855), AMPK (2532), phospho-AMPK (Thr172) (2531), Akt (9272), phospho-Akt (Ser473) (4058), Bcl-X_L (2764), beclin-1 (3738), caspase-3 (9665), caspase-9 (9504), LC3 (2775), S6 (2212), phospho-S6 (Ser240 and Ser244) (2215). Antibodies to Bnip3 (B7931) and Vps34 (V9764) were from Sigma. Antibodies to Bax (sc-493) and TOM20 (sc-11415) were from Santa Cruz. Antibodies to Bcl-2 (610539) and calnexin (610523) were from BD Transduction Laboratories. Antibody to p62 (GP62-C) was from Progen. Antibody to GAPDH (MAB374) was from Chemicon International. We performed western blots in at least three independent experiments. We carried out densitometric quantification by the ImageJ software (US National Institutes of Health).

Isolation of skeletal myofibers and measure of mitochondrial membrane potential. We isolated muscle fibers from FDB muscle, and we measured mitochondrial membrane potential by epifluorescence microscopy on the basis of the accumulation of TMRM fluorescence, as previously described[9,37]. We considered fibers as depolarizing when they lost more than 10% of the initial value of TMRM fluorescence. We performed imaging with a Zeiss Axiovert 100 TV inverted microscope equipped with a 12-bit digital cooled charge-coupled device camera (Micromax, Princeton Instruments). We analyzed the data with MetaFluor imaging software (Universal Imaging).

Terminal deoxynucleotidyl transferase dUTP nick end labeling. We prepared sections (7-µm thick) from diaphragm, after fixation with 4% paraformaldehyde and paraffin embedding, and from tibialis anterior muscles frozen in isopentane. We performed TUNEL assays with the ApopTag peroxidase *in situ* apoptosis detection system (Chemicon)[9,37]. For transfected muscles, we determined the number of TUNEL-positive nuclei in randomly selected fields by considering, separately, transfected and nontransfected fibers.

Muscle mechanics. We carried out *in vivo* determination of force and contraction kinetics of gastrocnemius muscle as previously described[42].

Human samples. We froze muscle biopsies of children and adults in isopentane. Details on subjects included in the study are provided in **Supplementary Table 1**. All subjects provided informed consent and were previously diagnosed with UCMD and Bethlem myopathy according to the criteria of the European NeuroMuscular Center[43] and by genetic analysis, which showed mutations in any of the *COL6A1*, *COL6A2* and *COL6A3* genes.

Statistical analyses. We expressed data as means ± s.e.m. or as means ± s.d. We determined statistical significance by unequal variance Student's *t* test (for TUNEL assay), equal variance Student's *t* test (for qRT-PCR and muscle mechanics) and Mann-Whitney test (for electron microscopy). A *P* value of less than 0.05 was considered statistically significant.

39. Tanida, I. *et al.* HsAtg4B/HsApg4B/autophagin-1 cleaves the carboxyl termini of three human Atg8 homologues and delipidates microtubule-associated protein light chain 3– and GABAA receptor-associated protein–phospholipid conjugates. *J. Biol. Chem.* **279**, 36268–36276 (2004).
40. Zhong, Y. *et al.* Distinct regulation of autophagic activity by Atg14L and Rubicon associated with beclin-1–phosphatidylinositol-3-kinase complex. *Nat. Cell Biol.* **11**, 468–476 (2009).
41. Degrassi, A. *et al.* Transfer of HIV-1 to human tonsillar stromal cells following cocultivation with infected lymphocytes. *AIDS Res. Hum. Retroviruses* **10**, 675–682 (1994).
42. Blaauw, B. *et al.* Akt activation prevents the force drop induced by eccentric contractions in dystrophin-deficient skeletal muscle. *Hum. Mol. Genet.* **17**, 3686–3696 (2008).
43. Pepe, G. *et al.* Bethlem myopathy (BETHLEM) and Ullrich scleroatonic muscular dystrophy: 100th ENMC international workshop, 23–24 November 2001, Naarden, The Netherlands. *Neuromuscul. Disord.* **12**, 984–993 (2002).

Angelin A, Tiepolo T, Sabatelli P, Grumati P, Bergamin N, Golfieri C, Mattioli E, Gualandi F, Ferlini A, Merlini L, Maraldi NM, Bonaldo P & Bernardi P (2007). Mitochondrial dysfunction in the pathogenesis of Ullrich congenital muscular dystrophy and prospective therapy with cyclosporins. *Proc Natl Acad Sci USA*; 104, 991–996.

Backingham M (2001). Skeletal muscle formation in vertebrates. *Curr Opin Genet Dev*; 11(4):440-8.

Baker NL, Morgelin M, Peat R, Goemans N, North KN, Bateman JF &Lamande SR (2005). Dominant collagen VI mutations are a common cause of Ullrich congenital muscular dystrophy. *Hum Mol Genet*; 14, 279–293.

Benchaouir R, Meregalli M, Farini A, D'Antona G, Belicchi M, Goyenvalle A, Battistelli M, Bresolin N, Bottinelli R, Garcia L, Torrente Y (2007). Restoration of human dystrophin following transplantation of exon-skipping-engineered DMD patient stem cells into dystrophic mice. *Cell Stem Cell*;1(6):646–657.

Bethlem J &Wijngaarden GK (1976). Benign myopathy, with autosomal dominant inheritance. A report on three pedigrees. *Brain*; 99, 91–100.

Bernardi P, Petronilli V, Di Lisa F, Forte M (2001). A mitochondria perspective on cell death. *Trend Biochem. Sci*; 26, 112-117.

Bonaldo P, Russo V, Bucciotti F, Bressan GM &Colombatti A (1989). Alpha 1 chain of chick type VI collagen. The complete cDNA sequence reveals a hybrid molecule made of one short collagen and three von Willebrand factor type A–like domains. *J Biol Chem*; 264, 5575–5580.

Bonaldo P, Russo V, Bucciotti F, Doliana R &Colombatti A (1990). Structural and functional features of the alpha 3 chain indicate a bridging role for chicken collagen VI in connective tissues. *Biochemistry*; 29, 1245–1254.

Bonaldo P, Braghetta P, Zanetti M, Piccolo S, Volpin D, Bressan GM (1998). Collagen VI deficiency induces early onset myopathy in the mouse: an animal model for Bethlem myopathy. *Human Molecular Genetics*; 7, 2135-2140.

Braghetta P, Ferrari A, Fabbro C, Bizzotto D, Volpin D, Bonaldo P, Bressan GM (2008). An enhancer required for transcription of the Col6a1 gene in muscle connective tissue is induced by signals released from muscle cells. *Exp Cell Res*; 314(19), 3508-18.

Brack AS, Conboy IM, Conboy MJ, Shen J, Rando TA (2008). A temporal switch from notch to Wnt signaling in muscle stem cells is necessary for normal adult myogenesis. *Cell Stem Cell*;

2(1):50-9.

Burg MA, Tillet E, Timpl R &Stallcup WB (1996). Binding of the NG2 proteoglycan to type VI collagen and other extracellular matrix molecules. *J Biol Chem*; 271, 26110–26116.

Camacho Vanegas O, Bertini E, Zhang RZ, Petrini S, Minosse C, Sabatelli P, Giusti B, Chu ML &Pepe G (2001). Ullrich scleroatonic muscular dystrophy is caused by recessive mutations in collagen type VI. *Proc Natl Acad Sci USA*; 98, 7516–7521.

Campbell K.P., and Stull J.T. (2003). Skeletal muscle basement membrane-sarcolemma-cytoskeleton interaction minireview series. *J. Biol. Chem;* 278, 12599-12600.

Camargo FD, Green R, Capetanaki Y, Jackson KA, Goodell MA (2003). Single hematopoietic stem cells generate skeletal muscle through myeloid intermediates. *Nat Med*; 9(12):1520–1527.

Castets P, Bertrand AT, Beuvin M, Ferry A, Le Grand F, Castets M, Chazot G, Rederstorff M, Krol A, Lescure A, Romero NB, Guicheney P, Allamand V (2010). Satellite cell loss and impaired muscle regeneration in selenoprotein N deficiency. *Hum Mol Genet.*

Cerletti M, Jurga S, Witczak CA, Hirshman MF, Shadrach JL, Goodyear LJ, Wagers AJ (2008). Highly efficient, functional engraftment of skeletal muscle stem cells in dystrophic muscles. *Cell*; 134(1):37-47.

Charge SB and Rudnicki MA (2006). Cellular and molecular regulation of muscle regeneration. Physiol Rev; 84: 209-238.

Chu ML, Zhang RZ, Pan TC, Stokes D, Conway D, Kuo HJ, Glanville R, Mayer U, Mann K, Deutzmann R &Timpl R (1990). Mosaic structure of globular domains in the human type VI collagen alpha 3 chain: similarity to von Willebrand factor, fibronectin, actin, salivary proteins and aprotinin type protease inhibitors. *EMBO J*; 9, 385–393

Collins CA, Olsen I, Zammit PS, Heslop L, Petrie A, Partridge TA, Morgan JE (2005). Stem cell function, self-renewal, and behavioral heterogeneity of cells from the adult muscle satellite cell niche. *Cell*; 122(2):289-301.

Colombatti A, Bonaldo P, Ainger K, Bressan GM &Volpin D (1987). Biosynthesis of chick type VI collagen. I. Intracellular assembly and molecular structure. *J Biol Chem*; 262, 14454–14460.

Colombatti A & Bonaldo P (1987). Biosynthesis of chick type VI collagen. II. Processing and secretion in fibroblasts and smooth muscle cells. *J Biol Chem*; 262, 14461–14466.

Colombatti A, Mucignat MT & Bonaldo P (1995). Secretion and matrix assembly of recombinant type VI collagen. *J Biol Chem*; 270, 13105–13111.

Colombatti A & Bonaldo P (1991). The superfamily of proteins with von Willebrand factor type A–like domains: one theme common to components of extracellular matrix, hemostasis, cellular adhesion, and defense mechanisms. *Blood*; 77, 2305–2315.

Conboy IM, Rando TA (2002). The regulation of Notch signaling controls satellite cell activation and cell fate determination in postnatal myogenesis. *Dev Cell*; 3:397–409.

Conboy IM, Conboy MJ, Wagers AJ, Girma ER, Weissman IL, Rando TA (2005). Rejuvenation of aged progenitor cells by exposure to a young systemic environment. *Nature*; 433:760–764.

Conboy MY, Karasov AO, Rando TA (2007). High incidence of non-random template strand segregation and asymmetric fate determination in dividing stem cells and their progeny. *PLos Biol*; 5(5): e 102.

Corbel SY, Lee A, Yi L, Duenas J, Brazelton TR, Blau HM, Rossi FM (2003). Contribution of hematopoietic stem cells to skeletal muscle. *Nat Med*;9(12):1528–1532.

Cornelison DD, Filla MS, Stanley HM, Rapraeger AC, Olwin BB (2001). Syndecan-3 and syndecan-4 specifically mark skeletal muscle satellite cells and are implicated in satellite cell maintenance and muscle regeneration. *Dev Biol*; 239(1):79-94.

Cosgrove BD, Sacco A, Gilbert PM, Blau HM (2009). A home away from home: challenges and opportunities in engineering in vitro muscle satellite cell niches. *Differentiation*; 78(2-3):185-94. Review.

Delfini MC, Hirsinger E, Pourquie O, and Duprez D (2000). Delta 1-activated notch inhibits muscle differentiation without affecting Myf5 and Pax3 expression in chick limb myogenesis. *Development*; 127: 5213-5224.

Demir E, Sabatelli P, Allamand V, Ferreiro A, Moghadaszadeh B, Makrelouf M, Topaloglu H, Echenne B, Merlini L &Guicheney P (2002). Mutations in COL6A3 cause severe and mild phenotypes of Ullrich congenital muscular dystrophy. *Am J Hum Genet*; 70, 1446–1458.

DiMario J, Buffinger N, Yamada S, Strohman RC (1989). Fibroblast growth factor in the extracellular matrix of dystrophic (mdx) mouse muscle. *Science*; 244(4905):688-90.

Doliana R, Bonaldo P &Colombatti A (1990). Multiple forms of chicken alpha 3(VI) collagen chain generated by alternative splicing in type A repeated domains. *J Cell Biol*; 111, 2197–2205.

Durbeej M and Campbell KP (2002). Muscular dystrophies involving the dystrophin-glycoprotein complex: an overview of current mouse models. *Current Opinion in Genetics & Development*; 12, 349- 361.

Engler AJ, Sen S, Sweeney HL, Discher DE (2006). Matrix elasticity directs stem cell lineage specification. *Cell*; 126:677–689.

Ferraro E and Cecconi F (2007). Autophagic and apoptotic response to stress signals in mammalian cells. *Archives of Biochemistry and Biophysics*; 462, 210-219.

Floss T, Arnold HH, Braun T (1997). A role of FGF-6 in skeletal muscle regeneration. *Genes Dev*; 11(6): 2040-2051.

Forte M, Bernardi P (2005). Genetic dissection of the permeability transition pore. *J Bioenerg Biomembr*; 37. 121-8.

Fuchs E, Tumbar T and Guasch G (2004). Socializing with their neighbors: stem cell and their niche. *Cell*; 116:769-778.

Gang EJ, Darabi R, Bosnakovski D, Xu Z, Kamm KE, Kyba M, Perlingeiro RC (2009). Engraftment of mesenchymal stem cells into dystrophin-deficient mice is not accompanied by functional recovery. *Exp Cell Res*;315(15):2624–2636.

Gara SK, Grumati P, Urciuolo A, Bonaldo P, Kobbe B, Koch M, Paulsson M, Wagener R (2008). Three novel collagen VI chains with high homology to the alpha 3 chain. *J. Biol. Chem*; 283, 10658-10670.

Gao Y, Kostrominova TY, Faulkner JA, Wineman AS (2008). Age-related changes in the mechanical properties of the epimysium in skeletal muscles of rats. *J Biomech*; 41:465–469.

Georgia S, Soliz R, Li M, Zhang P, Bhushan A (2006). p57 and Hes1 coordinate cell cycle exit with self-renewal of pancreatic progenitors. *Dev Biol*; 298(1):22-31.

Gilbert PM, Havenstrite KL, Magnusson KE, Sacco A, Leonardi NA, Kraft P, Nguyen NK, Thrun S, Lutolf MP, Blau HM (2010). Substrate elasticity regulates skeletal muscle stem cell self-renewal in culture. *Science*; 329(5995):1078-81.

Golding JP, Calderbank E, Partridge TA, Beauchamp JR (2007). Skeletal muscle stem cells express anti-apoptotic ErbB receptors during activation from quiescence. *Exp Cell Res*; 313(2):341-56.

Grumati P, Coletto L, Sabatelli P, Cescon M, Angelin A, Berteggia E, Blaauw B, Urciuolo A, Tiepolo T, Merlini L, Maraldi N, Bernardi P, Sandri M, Bonaldo P (2010). Autophagy is detective in collagen VI muscolar dystrophies, and its reactivation rescues myofiber degeneration. *Nature Medicine*.

Guglieri M, Magri F, Comi GP (2005). Molecular etiopathogenesis of limb girdle muscular and congenital muscular dystrophies: boundaries and contiguities. *Clin Chim Acta*; 361(1-2):54-79.

Guilak F, Cohen DM, Estes BT, Gimble JM, Liedtke W, Chen CS (2009). Control of stem cell fate by physical interactions with the extracellular matrix. *Cell Stem Cell*; 5:17–26.

Gussoni E, Pavlath GK, Lanctot AM, Sharma KR, Miller RG, Steinman L, Blau HM (1992). Normal dystrophin transcripts detected in Duchenne muscular dystrophy patients after myoblast transplantation. *Nature*; 356(6368):435–438.

Gussoni E, Bennett RR, Muskiewicz KR, Meyerrose T, Nolta JA, Gilgoff I, Stein J, Chan YM, Lidov HG, Bönnemann CG, Von Moers A, Morris GE, Den Dunnen JT, Chamberlain JS, Kunkel LM, Weinberg K (2002). Long-term persistence of donor nuclei in a Duchenne muscular dystrophy patient receiving bone marrow transplantation. *J Clin Invest*; 110(6):807–814.

Huard J, Roy R, Bouchard JP, Malouin F, Richards CL, Tremblay JP (1992). Human myoblast transplantation between immunohistocompatible donors and recipients produces immune reactions. *Transplant Proc*; 24(6):3049–3051.

Irintchev A, Zeschnigk M, Starzinski-Powitz A, Wernig A (1994). Expression pattern of M-cadherin in normal, denervated, and regenerating mouse muscles. *Dev Dyn*; 199:326–337.

Irwin WA, Bergamin N, Sabatelli P, Reggiani C, Megighian A, Merlini L, Braghetta P, Columbaro M, Volpin D, Bressan GM, Bernardi P &Bonaldo P (2003). Mitochondrial dysfunction and apoptosis in myopathic mice with collagen VI deficiency. *Nat Genet*; 35, 267–271.

Jenniskens GJ, Veerkamp JH, van Kuppevelt TH (2006). Heparan sulfates in skeletal muscle development and physiology. *J Cell Physiol*;206(2):283-94. Review.

Jöbsis GJ, Keizers H, Vreijling JP, de Visser M, Speer MC, Wolterman RA, Baas F &Bolhuis PA

(1996). Type VI collagen mutations in Bethlem myopathy, an autosomal dominant myopathy with contractures. *Nat Genet* 14, 113–115.

Jöbsis GJ, Boers JM, Barth PG &de VM (1999). Bethlem myopathy: a slowly progressive congenital muscular dystrophy with contractures. *Brain*; 122 (Pt 4), 649–655.

Kadi F & Thornell LE (2000). Concomitant increases in myonuclear and satellite cell content in female trapezius muscle following strength training. *Histochem Cell Biol*; 113, 99–103.

Karalaki M, Fili S, Philippou A, Koutsilieris M (2009). Muscle regeneration: cellular and molecular events. *In Vivo*;23(5):779-96. Review.

Karpati G, Ajdukovic D, Arnold D, Gledhill RB, Guttmann R, Holland P, Koch PA, Shoubridge E, Spence D, Vanasse M, et al. (1993). Myoblast transfer in Duchenne muscular dystrophy. *Ann Neurol*; 34(1):8–17.

Keene DR, Engvall E &Glanville RW (1988). Ultrastructure of type VI collagen in human skin and cartilage suggests an anchoring function for this filamentous network. *J Cell Biol*; 107, 1995–2006.

Kopan R, nye JS, and Weintraub H (1994). The intracellular domain of mouse Notch: a constitutively activated repressor of myogenesis direct at the basic helix-loop-helix region of MyoD. *Development.*; 120:2385-2396.

Kuang S, Charge SB, Seale P, Huh M, Rudnicki MA (2006). Distinct roles of Pax7 and Pax3 in adult regenerative myogenesis. *J Cell Biol*; 172(1): 103-113.

Kuang S, Kuroda K, La Grand F, Rudnicki MA (2007). Asymmetric self-renewal and commitment of satellite stem cells in muscle. *Cell*; 129(5): 215-228.

Kuang S, Gillespie MA and Rudnicki MA (2008). Niche regulation of muscle satellite cell self-renewal and differentiation. *Cell Stem Cell*; 2:22–31.

Kuang W, Xu H, Vilquin JT, Engvall E (1999). Activation of the lama2 gene in muscle regeneration: abortive regeneration in laminin alpha2-deficiency. *Lab Invest*; 79 1601–1613.

Kuo HJ, Maslen CL, Keene DR and Glanville RW (1997). Type VI collagen anchors endothelial basement membranes by interacting with type IV collagen. *J. Biol. Chem;* 272, 26522-26529.

Lampe AK & Bushby KM (2005). Collagen VI related muscle disorders. *J Med Genet*; 42, 673–685.

Langsdorf A, Do AT, Kusche-Gullberg M, Emerson CP Jr, Ai X (2007). Sulfs are regulators of growth factor signaling for satellite cell differentiation and muscle regeneration. *Dev Biol*; 311(2):464-77.

Law PK, Goodwin TG, Fang QW, Chen M, Li HJ, Florendo JA, Kirby DS (1991). Myoblast transfer therapy for Duchenne muscular dystrophy. *Acta Paediatr Jpn*; 33(2):206–215.

Law PK, Goodwin TG, Fang Q, Duggirala V, Larkin C, Florendo JA, Kirby DS, Deering MB, Li HJ, Chen M, et al. (1992). Feasibility, safety, and efficacy of myoblast transfer therapy on Duchenne muscular dystrophy boys. *Cell Transplant*; 1(2-3):235–244.

Le Grand F, Jones AE, Seale V, Scime A, Rudnicki MA (2009). Wnt7a activates the planar cell polarity pathway to drive the symmetric expansion of satellite stem cells. *Cell Stem Cell*; 4(6):535–547

Lescaudrom L, Peltekian E, Fontaine-Perus J, Paulin D, Zampieri M, Garcia L and Parrish E (1999). Blood borne macrophages are essential for the triggering of muscle regeneration following muscle transplant. *Neuromuscul Disord*; 9: 72-80.

Levine B and Kroemer G (2008). Autophagy in the pathogenesis of disease. *Cell*; 132, 27-42.

Liu Y, Labosky PA (2008). Regulation of embryonic stem cell self-renewal and pluripotency by Foxd3. *Stem Cells*; 26(10):2475-84.

Lopez JI, Mouw JK, Weaver VM (2008). Biomechanical regulation of cell orientation and fate. *Oncogene*; 27:6981–6993.

Machida S, Booth FW (2004). Insulin-like growth factor 1 and muscle growth: implication for satellite cell proliferation. *Proc Nutr Soc*; 63(2):337-40. Review.

Mauro A. Satellite cells of skeletal muscle fibers (1961). *J Biophys Biochem Cytol*; 9:493-495.

Meliga E, Strem BM, Duckers HJ, Serruys PW (2007). Adipose-derived cells. Cell Transplant;16(9):963–970.

Mendell JR, Kissel JT, Amato AA, King W, Signore L, Prior TW, Sahenk Z, Benson S, McAndrew PE, Rice R, et al. (1995). Myoblast transfer in the treatment of Duchenne's muscular dystrophy. *N Engl J Med*; 333(13):832–838.

Merlini L, Morandi L, Granata C &Ballestrazzi A (1994). Bethlem myopathy: early–onset benign autosomal dominant myopathy with contractures. Description of two new families. *Neuromuscul Disord*; 4, 503–511.

Merlini L, Angelin A, Tiepolo T, Braghetta P, Sabatelli P, Zamparelli A, Ferlini A, Maraldi NM, Bonaldo P, Bernardi P (2008a). Cyclosporin A corrects mitochondrial dysfunction and muscle apoptosis in patients with collagen VI myopathies. *Proc. Natl. Acad. Sci. USA*; 105(13):5225-9.

Merlini L, Martoni E, Grumati P, Sabatelli P, Squarzoni S, Urciuolo A, Ferlini A, Gualandi F, Bonaldo P (2008b). Autosomal recessive myosclerosis myopathy is acollagen VI disorder. *Neurology*, 71(16), 1245-53.

McCormick KM & Thomas DP (1992). Exercise-induced satellite cell activation in senescent soleus muscle. *J Appl Physiol*; 72, 888–893.

McClung JM, Davis JM and Carson JA (2007). Ovarian hormone status and skeletal muscle inflammation during recovery from disuse in rat. *Exp Physiol*; 92: 219-232.

McKinney-Freeman SL, Jackson KA, Camargo FD, Ferrari G, Mavilio F, Goodell MA (2002). Muscle-derived hematopoietic stem cells are hematopoietic in origin. *Proc Natl Acad Sci USA*; 99(3):1341–1346.

Midwood KS and Salter DM (2001). NG2/HMPG modulation of human articular chondrocyte adhesion to type VI collagen is lost in osteoarthritis. *J. Pathol;* 195, 631-635.

Miller RG, Sharma KR, Pavlath GK, Gussoni E, Mynhier M, Lanctot AM, Greco CM, Steinman L, Blau HM (1997). Myoblast implantation in Duchenne muscular dystrophy: the San Francisco study. *Muscle Nerve*; 20(4):469–478.

Moore KA and Lemischke IR (2006). Stem cells and their niches. *Science*; 309: 2064-2067.

Molgo J, Colasantei C, Adams DS and Jaimovich E (2004). IP3 receptors and Ca^{+} signals in adult skeletal muscle satellite cells in situ. *Biol Res*; 37: 635-639.

Montarras D, Morgan J, Collins C, Relaix F, Zaffran S, Cumano A, Partridge T, Buckingham M (2005). Direct isolation of satellite cells for skeletal muscle regeneration. *Science*; 309(5743):2064-7

Morandi L, Bernasconi P, Gebbia M, Mora M, Crosti F, Mantegazza R, Cornelio F (1995). Lack of mRNA and dystrophin expression in DMD patients three months after myoblast transfer. *Neuromuscul Disord*; 5(4):291–295.

Morgan JE and Zammit PS (2010). Direct effects of the pathogenic mutation on satellite cell function in muscular dystrophy. *Exp Cell Res*; 316(18):3100-8. Review

Morrison SJ and Kimble J (2006). Asymmetric and symmetric stem-cell divisions in development and cancer. *Nature*; 441(7097):1068-74.

Musarò A (2005). Growth factor anhancement of muscle regeneration: a central role of IGF-1. *Arch Ital Biol*; 143(3-4): 243-248.

Nanda A, Carson-Walter EB, Seaman S, Barber TD, Stampfl J, Singh S, Vogelstein B, Kinzler KW, St Croix B (2004).TEM8 interacts with the cleaved C5 domain of collagen alpha 3(VI). *Cancer Res*; 64,817- 20.

Neumeyer AM, Cros D, McKenna-Yasek D, Zawadzka A, Hoffman EP, Pegoraro E, Hunter RG, Munsat TL, Brown RH Jr (1998). Pilot study of myoblast transfer in the treatment of Becker muscular dystrophy. *Neurology*; 51(2):589–592.

Ono Y, Gnocchi V, Zammit P and Nagatomi R (2009). Presenilin-1 acts via Id1 to regulate the function of muscle satellite cells in a g-secretase-indipendent manner. *J Cell Scien*; 122(Pt 24):4427-38.

Pan TC, Zhang RZ, Sudano DG, Marie SK, Bonnemann CG &Chu ML (2003). New molecular mechanism for Ullrich congenital muscular dystrophy: a heterozygous in–frame deletion in the COL6A1 gene causes a severe phenotype. *Am J Hum Genet*; 73, 355–369.

Pfaff M, Aumailley M, Specks U, Knolle J, Zerwes HG &Timpl R (1993). Integrin and Arg–Gly–Asp dependence of cell adhesion to the native and unfolded triple helix of collagen type VI. *Exp Cell Res*; 206, 167–176.

Pisconti A, Cornelison DD, Olguín HC, Antwine TL, Olwin BB (2010). Syndecan-3 and Notch cooperate in regulating adult myogenesis. *J Cell Biol*; 190(3):427-41.

Ratajczak MZ, Majka M, Kucia M, Drukala J, Pietrzkowski Z, Peiper S, Janowska-Wieczorek A (2003). Expression of functional CXCR4 by muscle satellite cells and secretion of SDF-1 by muscle-derived fibroblasts is associated with the presence of both muscle progenitors in bone marrow and hematopoietic stem/progenitor cells in muscles. *Stem Cells*; 21:363–371.

Relaix F, Montarras D, Zaffran S, Gayraud-Morel B, Rocancourt D, Tajbakhsh S, Mansouri A, Cumano A, Buckingham M (2006). Pax3 and Pax7 have distinct and overlapping functions in adult muscle progenitors cells. *J Cell Biol*; 172(1): 91-102.

Sabatelli P, Bonaldo P, Lattanzi G, Braghetta P, Bergamin N, Capanni C, Mattioli E, Columbaro M, Ognibene A, Pepe G, Bertini E, Merlini L, Maraldi NM &Squarzoni S (2001). Collagen VI deficiency affects the organization of fibronectin in the extracellular matrix of cultured

fibroblasts. *Matrix Biol*; 20, 475–486.

Sabatelli P, Gara SK, Grumati P, Urciuolo A, Gualandi F, Curci R, Squarzoni S, Zamparelli A, Martoni E, Merlini L, Paulsson M, Bonaldo P, Wagener R (2010). "Expression of the Collagen VI α5 and α6 Chains in Normal Human Skin and in Skin of Patients with Collagen VI-Related Myopathies." *Invest Dermatol*; 131(1):99-107.

Sacco A, Doyonnas R, Kraft P, Vitorovic S, Blau HM (2008). Self-renewal and expansion of single transplanted muscle stem cells. *Nature*; 456(7221):502-6.

Sambasivan R, Tajbakhsh S (2007). Skeletal muscle stem cells birth and properties. *Semin Cell Dev Biol*; 18(6): 870-882.

Sampaolesi M, Torrente Y, Innocenzi A, Tonlorenzi R, D'Antona G, Pellegrino MA, Barresi R, Bresolin N, De Angelis MG, Campbell KP, Bottinelli R, Cossu G (2003). Cell therapy of alpha-sarcoglycan null dystrophic mice through intra-arterial delivery of mesoangioblasts. *Science*;301(5632):487–492.

Sasaki T, Hohenester E, Zhang RZ, Gotta S, Speer MC, Tandan R, Timpl R &Chu ML (2000). A Bethlem myopathy Gly to Glu mutation in the von Willebrand factor A domain N2 of the collagen alpha3(VI) chain interferes with protein folding. *FASEB J*; 14, 761–768.

Sanes J.R. (2003). The basement membrane/basal lamina of skeletal muscle. *J. Biol. Chem*; 278, 12601-04.

Sacco A, Mourkioti F, Tran R, Choi J, Llewellyn M, Kraft P, Shkreli M, Delp S, Pomerantz JH, Artandi SE, Blau HM (2010). Short Telomeres and Stem Cell Exhaustion Model Duchenne Muscular Dystrophy in mdx/mTR Mice. *Cell*; 143(7):1059-71.

Scacheri PC, Gillanders EM, Subramony SH, Vedanarayanan V, Crowe CA, Thakore N, Bingler M &Hoffman EP (2002). Novel mutations in collagen VI genes: expansion of the Bethlem myopathy phenotype. *Neurology*; 58, 593–602.

ScaddenDT (2006). The stem-cell niche as an entity of action. *Nature*; 441: 1075-1079.

Sherwood RI, Christensen JL, Conboy IM, Conboy MJ, Rando TA, Weissman IL, Wagers AJ (2004). Isolation of adult mouse myogenic progenitors: functional heterogeneity of cells within and engrafting skeletal muscle. *Cell*; 119:543–554.

Skuk D, Goulet M, Tremblay JP (2006). Use of repeating dispensers to increase the efficiency of the intramuscular myogenic cell injection procedure. *Cell Transplant*; 15(7):659–663.

Söderhäll C, Marenholz I, Kerscher T, Rüschendorf F, Esparza-Gordillo J, Worm M, Gruber C, Mayr G, Albrecht M, Rohde K, Schulz H, Wahn U, Hubner N, Lee YA (2007). Variants in a novel epidermal collagen gene (COL29A1) are associated with atopic dermatitis. *PLoS Biol*; 5(9):e242.

Snow MH (1977). Myogenic cell formation in regenerating rat skeletal muscle injured by mincing. II. An autoradiographic study. *Anat Rec*; 188: 201-217.

Shi X, Garry DJ (2006). Muscle stem cells in development, regeneration, and disease. *Gen Dev*; 20(13): 1692-1708.

Shinin V, Gayraud-Morel B, Gomes D, Tajbakhsh S (2006). Asymmetric division and cosegreration of template DNA strands in adult muscle satellite cells. *Nat Cell Biol*; 8(7): 677-687.

Spalding KL, Bhardwaj RD, Buchholz BA, Druid H, and Frisen J (2005). Retrospective birth dating of cells in humans. *Cell*; 122:133-143.

Squarzoni S, Sabatelli P, Bergamin N, Guicheney P, Demir E, Merlini L, Lattanzi G, Ognibene A, Capanni C, Mattioli E, Columbaro M, Bonaldo P &Maraldi NM (2006). Ultrastructural defects of collagen VI filaments in an Ullrich syndrome patient with loss of the alpha3(VI) N10–N7 domains. *J Cell Physiol*; 206, 160–166.

Stallcup WB (2002). The NG2 proteoglycan: past insights and future prospects. *Journal of Neurocytology*; 31, 423-435.

Tajbakhsh S, Bober E, Babinet C, Pournin S, Arnold H, Buckingham M. (1996). Gene targeting the myf-5 locus with nlacZ reveals expression of this myogenic factor in mature skeletal muscle fibers as well as early embryonic muscle. *Dev Dyn*; 206(3): 291-300.

Tatsumi R, Anderson JE, Nevoret CJ, Halevy O, Allen RE (1998). HGF/SF is present in normal adult skeletal muscle and is capable of activating satellite cells. *Dev Biol*; 194(1): 114-128.

Tatsumi R, Liu X, Pulido A, Morales M, Sakata T, Dial S, Hattori A, Ikeuchi Y and Allen RE (2006). Satellite cell activation in stretched skeletal muscle and the role of nitric oxide and hepatocyte growth factor. *Am J Physiol Cell Physiol*; 290: C1487-1494.

Tedesco S, Dellavalle A, Diaz-Manera J, Messina G and Cossu G (2010). Repairing skeletal muscle: regenerative potential of skeletal muscle stem cells. *J Clinic Inv*; 120(1):11-9.

Timpl R. (1996). Macromolecular organization of basement membranes. *Current Opinion in Cell Biology*; 8, 618-624.

Torrente Y, Belicchi M, Sampaolesi M, Pisati F, Meregalli M, D'Antona G, Tonlorenzi R, Porretti L, Gavina M, Mamchaoui K, Pellegrino MA, Furling D, Mouly V, Butler-Browne GS, Bottinelli R, Cossu G, Bresolin N (2004). Human circulating AC133(+) stem cells restore dystrophin expression and ameliorate function in dystrophic skeletal muscle. *J Clin Invest*; 114(2):182–195.

Tremblay JP, Malouin F, Roy R, Huard J, Bouchard JP, Satoh A, Richards CL (1993). Results of a triple blind clinical study of myoblast transplantations without immunosuppressive treatment in young boys with Duchenne muscular dystrophy. *Cell Transplant*; 2(2):99–112.

White RB, Biérinx AS, Gnocchi VF, Zammit PS (2010). Dynamics of muscle fibre growth during postnatal mouse development. *BMC Dev Biol*; 10:21.

Wozniak AC, Anderson JE (2007). Nitric oxide-dependence of satellite stem cell activation and quiescence on normal skeletal muscle. *Dev Dyn*; 236(1): 240-250

Zammit PS, Heslop L, Hudon V, Rosenblatt JD, Tajbakhsh S, Buckingham ME, Beauchamp JR, Partridge TA (2002). Kinetics of myoblast proliferation show that resident satellite cells are competent to fully regenerate skeletal muscl efibers. *Exp Cell Res*; 281(1): 39-49.

Zammit PS, Golding, JP, Nagata, Y, Hudon, V, Partridge, TA, and Beauchamp, JR (2004). Muscle satellite cells adopt divergent fates: a mechanism for self-renewal? *J Cell Biol*; 166(3): 347-357.

Zammit PS, Partridge TA & Yablonka-Reuveni Z (2006). The skeletal muscle satellite cell: the stem cell that came in from the cold. *J Histochem Cytochem*; 54: 1177-1191.

Zammit PS, Relaix F, Nagata Y, Ruiz AP, Collins CA, Partridge TA, Beauchamp JR (2006). Pax7 and myogenic progression in skeletal muscle satellite cells. *J Cell Sci*; 119(pt9): 1824-1832.

Zamzami N, Kroemer G (2001). The mitochondrion in apoptosis: how Pandora's box opens. *Nat Rev Mol Cell Biol*; 2, 67-71.

Zhang RZ, Sabatelli P, Pan TC, Squarzoni S, Mattioli E, Bertini E, Pepe G &Chu ML (2002). Effects on collagen VI mRNA stability and microfibrillar assembly of three COL6A2 mutations in two families with Ullrich congenital muscular dystrophy. *J Biol Chem*; 277, 43557–43564.

Zou Y, Zhang RZ, Sabatelli P, Chu ML, Bönnemann CG (2008). Muscle interstitial fibroblasts are the main source of collagen VI synthesis in skeletal muscle: implications for congenital muscular dystrophy types Ullrich and Bethlem. *J Neuropathol Exp Neurol*; 67(2):144-54